Estimation and dynamic longitudinal control of an electric vehicle with in-wheel electric motors

Marcel-Stefan Geamanu

ÉCOLE DOCTORALE: STITS

Laboratoire des Signaux et Systèmes, SUPELEC
Département Contrôle, IFPEN

DISCIPLINE PHYSIQUE

THÈSE DE DOCTORAT

soutenue le 30/09/2013

par

Marcel-Stefan GEAMANU

Estimation and Dynamic Longitudinal Control of an Electric Vehicle with In-wheel Electric Motors

Directeurs de thèse: Hugues MOUNIER - Professeur (L2S)
Gilles CORDE - Chef de département (IFPEN)

Jury :

President :	Dorothée NORMAND-CYROT	-	Directeur de recherche (L2S)
Rapporteurs :	Dominique MEIZEL	-	Professeur (ENSIL)
	Fatihcan ATAY	-	Professeur (MPG)
Examinateurs :	Michel FLIESS	-	Professeur (LIX)
	Brigitte D'ANDREA-NOVEL	-	Professeur (MINES)
Membres invités :	Silviu-Iulian NICULESCU	-	Directeur (L2S)
	Arben CELA	-	Professeur (ESIEE)
	Guénaël LE SOLLIEC	-	Ingénieur recherche (IFPEN)

Acknowledgments

I am deeply grateful to Professor Hugues Mounier for introducing me to the field of Vehicle Dynamics and Control and for his patience when I started working on this thesis. His advice and comments regarding my work were always helpful and enlarged my vision in the field of Automatics. At the same time, I would like to express my gratitude to Professor Silviu-Iulian Niculescu for his constructive comments and advice regarding all the scientific papers that I submitted. I would also like to thank Professor Arben Cela for the detailed analysis of my work and his helpful remarks, that brought precision and finesse into my research. Last, but not least, I would like to thank Mr. Gilles Corde and Mr. Guénaël Le Solliec for the support during my thesis research. Their implication and useful propositions helped me develop and enlarge my knowledge as engineer.

As well, I am grateful for the promptitude to my requests from the part of all cited above. Their availability to help me in my research was decisive regarding the timing of the proposed objectives.

I would like to thank my parents Constanta and Tenel Geamanu for their love, support and confidence in me. They helped me go through this period with ease and comfort. Also, I am grateful for the persistence and encouragements of my girlfriend Denisa Iacobescu, who helped me focus on this important phase of my life.

List of Abbreviations

$2WD$	Two Wheel Drive
$4WD$	Four Wheel Drive
ABS	Anti-lock Brake System
ASR	All Wheel Drive
AWD	Anti-Slip Regulation
CM	Center of Mass
EBD	Electronic Brake-force Distribution
ECU	Electronic Control Unit
EMF	Electro-Motive Force
ESP	Electronic Stability Program
EV	Electric vehicle
$FSMC$	Fuzzy Sliding-mode Control
HEV	Hybrid Electric Vehicle
HIL	Hardware In the Loop
ICE	Internal Combustion Engine
LQG	Linear Quadratic Gaussian
MFC	Model Following Control
$MTTE$	Maximum Transmissible Torque Estimation
$NPID$	Non-linear Proportional Integrator Derivative
ODE	Ordinary Differential Equation
PI	Proportional Integrator
PID	Proportional Integrator Derivative
SIL	Software In the Loop
$SISO$	Single Input Single Output
SSG	Start-Stop Group
TCS	Traction Control System
XBS	Extended Braking Stiffness
ZEV	Zero-Emission Vehicle

Nomenclature

λ	Longitudinal slip ratio
V_x	Longitudinal vehicle speed (m/s)
μ_x	Longitudinal friction
$\mu_{x_{max}}$	Maximum longitudinal friction
F_{aero}	Longitudinal aerodynamic drag force (N)
F_x	Longitudinal tire force (N)
F_z	Normal force on the tire (N)
R_x	Force due to rolling resistance (N)
T	Wheel torque (Nm)
ω	Angular wheel speed (rad/s)
r_e	Effective tire radius (m)
m	Quarter vehicle mass (Kg)
I	Wheel moment of inertia $(Kg * m^2)$
ρ	Air density (Kg/m^3)
C_d	Aerodynamic drag coefficient
C_r	Rolling resistance coefficient
ϕ	Suspended mass pitch angle (rad)
M	Total mass of the vehicle (Kg)
m_w	Individual wheel mass (Kg)
l_i	Distance from the center of gravity to the axles (m)
c	Suspension damping coefficient (Nm)
k	Suspension spring coefficient (N)
C_r	Rolling resistance coefficient
G_s	Suspended center of mass
G_u	Unsuspended center of mass
h_0	Distance from G_s to the ground (m)
K_x	Longitudinal stiffness coefficient
α	Adaptation parameter

List of Figures

List of Tables

Contents

Résumé

Chapitre 1: Introduction générale

L'objectif principal de cette thèse est l'étude de l'exploitation de systèmes moteurs-roues (machines électriques intégrées à la roue) pour le contrôle de la dynamique véhicule. Cette thèse est issue d'un co-financement (numéro 186-654, 2010-2013) entre le Laboratoire des Signaux et Systèmes (CNRS) et l'Institut Français du Pétrole et Énergies Nouvelles (IFPEN). Elle a été initiée par IFPEN à la suite du projet VelRoue financé par l'ADEME et ayant comme partenaires Renault et Michelin. L'objectif du projet était de concevoir une nouvelle architecture hybride pour véhicules utilitaires composée d'un GMP thermique traditionnel sur le train avant et de moteurs-roue sur le train arrière. Cette architecture permet un roulage urbain en mode électrique et extra-urbain en mode thermique, avec récupération de l'énergie sur le train arrière en cas de freinage.

Les avantages apportés par l'utilisation du moteur électrique sont avérés et de nouvelles techniques de contrôle sont développées pour optimiser son utilisation. Les lois de contrôle basent généralement sur la grandeur principale du moteur électrique: le couple transmis, qui peut être mesuré via le courant consommé. Une autre caractéristique importante du moteur électrique est son temps de réponse, avec le fait qu'il peut produire des couples négatifs, pour ralentir le véhicule, tout en stockant l'énergie. La nouveauté du présent travail est de considérer le moteur-roue électrique comme seul signal de contrôle dans des phases d'accélération et des phases de ralentissement, simplifiant l'architecture de la conception du véhicule et des lois de contrôle. Pour répondre à la demande conducteur tout en préservant un comportement sain du véhicule, des stratégies d'estimation de la limite d'adhérence seront présentées. En fonction de cette adhérence maximale disponible entre la route et les pneus, un couple adéquat sera calculé pour assurer un comportement stable dans des phases d'accélération aussi bien que que des freinage. L'aspect critique étudié dans ce travail est la non-linéarité des caractéristiques d'interaction entre la route et le pneu et la complexité de son estimation dans des conditions variables. La stratégie d'estimation devra détecter tous les changements d'adhérence de route et la loi de contrôle calculée devra maintenir la stabilité véhicule même lorsque la friction maximale change. Certaines formes de

perturbation et de bruit seront également prises en compte afin de tester la robustesse des approches d'estimation et de contrôle proposés.

En terme de sécurité active, le contrôle longitudinal d'un véhicule est d'importance majeure. C'est une tâche complexe qui exige la connaissance de certains paramètres instantanés comme le couple du moteur ou le couple transmis à la roue, l'accélération du châssis, l'accélération angulaire de la roue ou l'adhérence de la route sur laquelle le véhicule se déplace. L'estimation des ces paramètres est donc déterminante dans la construction d'un contrôleur qui garantit un comportement latéral et longitudinal stable du véhicule. Parmi les systèmes de sécurité active les plus importants en phase d'accélération, le système de contrôle de traction (TCS) rétablit la traction si les roues commencent à patiner et le programme de stabilité électronique (ESP)intervient pour prévenir une perte menaçante du contrôle latéral du véhicule. Dans le cas du freinage, le système décisif est le système d'anti-blocage (ou ABS), qui empêche le blocage des roues. On peut trouver d'autres systèmes embarqués, comme le système de distribution de force de freinage électronique (EBD), qui assure une distribution optimale de la force de freinage transmise aux roues, pour éviter de déraper et assure un ralentissement stable du véhicule.

Tous ces systèmes contribuent à une meilleure contrôlabilité du véhicule dans des situations critiques comme le freinage d'urgence ou l'accélération sur des revêtements glissants. Ils interprètent les signaux des divers capteurs pour réaliser des estimations des grandeurs caractéristiques et nécessaires aux algorithmes de contrôle. Les systèmes embarqués qui fournissent les estimations doivent être robustes aux bruits de mesure et aux perturbations. A fortiori, ces calculs doivent être faits en temps réel, donc une complexité réduite et une réponse rapide de la loi de contrôle sont nécessaires. Enfin, l'environnement dans lequel le véhicule fonctionne est dynamique, les caractéristiques d'adhérence peuvent varier en fonction de l'état de la route et de la météo. Ainsi, on ne peut prévoir les réactions du conducteur pouvant influencer la réponse globale du véhicule dans des situations d'urgence. Le contrôleur devrait prendre en compte tous ces aspects pour préserver un comportement stable du véhicule. Bien que le contrôle latéral du véhicule présente une importance majeure dans la stabilité globale du véhicule, le présent travail est concentré sur le contrôle longitudinal du véhicule, puisqu'il représente le point de départ de la dynamique véhicule.

Analyse longitudinale de la dynamique du véhicule

L'interaction entre le pneu et la route sur laquelle se déplace le véhicule a une influence cruciale sur le comportement du véhicule pendant l'accélération ou le freinage. La réponse du véhicule aux demandes du conducteur (la direction, l'accélération ou le freinage) dépend donc de manière critique de l'adhérence du pneu à la route. La force de friction entre les roues et la route est fortement variable, en fonction de nombreux facteurs comme les conditions météorologiques (des températures chaudes, la pluie, la neige ou la glace), le type de revêtement (asphalte, pavé, graviers, etc), voir la présence d'autres corps (graisse, boue, eau, etc). Des tests expérimentaux ont montré que la friction longitudinale (appelée μ_x) peut être modélisée comme une fonction du taux de glissement longitudinal (λ), pour des conditions de route différentes, comme indiqué dans la Figure 1.

Le taux de glissement longitudinal peut être défini comme [13]:

$$\lambda = \frac{V_\omega - V_x}{\max(V_\omega, V_x)}, \tag{1}$$

avec V_ω la vitesse linéaire de la roue et V_x la vitesse du véhicule.

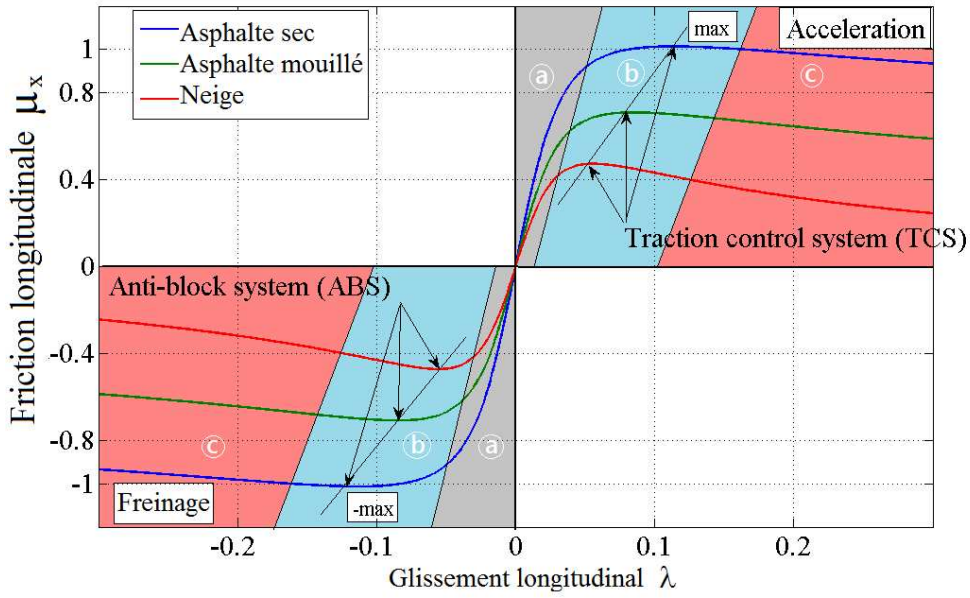

Figure 1: Adhérence typique entre la surface de route et les pneus, comme fonction du glissement longitudinal (modèle de Pacejka [73]).

Les courbes montrées en Figure 1 présentent trois zones visibles d'intérêt :

- La première zone est appelée zone de "pseudo-glissement", ou "zone linéaire" (zone ⓐ de la Figure 1). Dans cette zone, le glissement de la roue est faible et stable.

- La deuxième zone est celle où le seuil "max" est atteint (la zone ⓑ de la Figure 1). Après dépassement de ce seuil, les valeurs de $\mu_x(\lambda)$ entrent dans la zone non-linéaire.

- La troisième zone est appelée "la zone de glissement" ou "zone non-linéaire" des courbes (la zone ⓒ de la Figure 1). En accélération, la force n'est plus suffisamment transmise à la route, le glissement diverge et la roue accélère, causant le patinage incontrôlable de la roue et la perte de traction. A l'inverse en freinage, la roue se bloque.

Pendant l'accélération, $V_\omega > V_x$, il existe donc une force de friction imposée aux roues dans la direction du mouvement ($\lambda > 0$). Cette force de friction, aussi connue sous le nom de force de traction, est fonction de l'adhérence entre le pneu et la surface de la route et contribue au mouvement du véhicule. Cependant, si le taux de glissement excède une valeur maximale comme indiqué en Figure 1, la roue commence à tourner bien plus rapidement que la vitesse du centre de gravité de véhicule et la traction est donc perdue. Ceci est la zone de fonctionnement du TCS, sa tâche principale étant de conserver des valeurs de μ_x inférieures à la valeur "max" illustrée en Figure 1.

Pendant le freinage, des forces extérieures sont appliquées à la roue pour que la vitesse linéaire de roue soit inférieure à la vitesse du véhicule, par exemple, $\lambda < 0$. Il existe donc une force de freinage, qui s'est oppose au mouvement, causant le ralentissement du véhicule. Comme dans le cas d'accélération, si le ratio de glissement passe par une valeur "-max", comme indiqué en Figure 1, la vitesse de roue diminuera jusqu'au blocage complet, causant la perte d'adhérence. La tâche principale de l'ABS est donc d'assurer que les valeurs de $-\mu_x$ restent plus grandes que la valeur "-max", pour empêcher le blocage de la roue.

La non-linéarité de l'adhérence engendre une certaine complexité des algorithmes de contrôle. Pour préserver un comportement stable du véhicule dans des manœuvres typiques, le contrôle doit donc garder les valeurs instantanées de friction pour rester dans l'intervalle $[0, |\max|]$. Durant des manœuvres d'urgence, où les valeurs de friction excèdent le seuil "max", le contrôle doit pouvoir diminuer la force de traction ou de

freinage jusqu'à retrouver une adhérence stable entre la roue et le sol et donc, un comportement stable du véhicule.

Analyse d'impact de l'électrification du véhicule

Un véhicule électrique (EV) utilise un ou plusieurs moteurs électriques pour la propulsion. Ces moteurs peuvent être situés au centre du véhicule et fournir via un système de transmission la puissance aux roues, ou, placés directement aux roues avec l'utilisation de moteurs-roues. L'avantage le plus marquant des moteurs électriques est un temps de réponse rapide. Un autre avantage clé est le freinage régénératif, c'est-à-dire leur capacité de récupérer l'énergie normalement perdue pendant le freinage, pour la stocker. En outre, dans le cas des moteurs-roue, ils peuvent être contrôlés indépendamment, apportant de nouvelles possibilités de contrôle de véhicule.

Les moteurs-roue constituent le système de propulsion/freinage unique pour le véhicule électrique étudié. Comparés à un véhicule thermique conventionnel, les moteurs électriques au sein des roues ont quelques avantages importants:

- ils produisent un couple important aux basses vitesses,
- ils ont une haute puissance instantanée,
- les valeurs du couple sont facilement reproductibles,
- ils ont un temps de réponse rapide,
- ils offrent la possibilité d'un freinage régénératif.

Les nouveaux moteurs électriques aux roues fournissent même plus de possibilités pour la sécurité active et le contrôle de trajectoire, puisqu'ils peuvent fournir un couple de freinage sur les roues plus rapidement que les freins conventionnels. En outre, des informations importantes incluant la vitesse angulaire de la roue et le couple peuvent être estimées plus facilement en mesurant le courant électrique passant par le moteur.

Comparé au design d'un véhicule électrique conventionnel avec un moteur placé au centre, le design du moteur-roue a certains avantages. La premier avantage de l'électrification dans la roue est que les véhicules peuvent être contrôlés via un système de type "drive-by-wire". Les voitures avec contrôle électronique des freins et d'accélération fournissent plus d'horizons pour la dynamique du véhicule comme:

- la régulation de vitesse, où le véhicule peut maintenir une distance donnée par rapport à un véhicule en avant,
- l'évitement de collision, où le véhicule peut automatiquement freiner pour éviter une collision,
- l'aide au freinage d'urgence, où le véhicule détecte un arrêt d'urgence et applique le freinage maximal,
- des différentiels actifs, où la vitesse de roue individuelle est ajustée en réponse à d'autres demandes,
- le freinage différencié actif, où l'effort de freinage de roue individuel est ajusté en temps réel pour maintenir la stabilité de véhicule.

Tandis que certaines de ces caractéristiques ont commencé à apparaître comme des options pour quelques véhicules avec moteur à combustion interne, des freins ABS facultatifs peuvent augmenter considérablement le coût d'un modèle de base. Comme les moteurs-roue freinent et accélèrent un véhicule avec un seul système électrique/électronique, beaucoup de fonctions peuvent être ajoutées comme des mises à jour logicielles plutôt que d'installer des systèmes supplémentaires. Ceci devrait mener à des systèmes de sécurité dynamiques actifs moins chers pour les véhicules équipés de moteur-roue. En éliminant la transmission mécanique incluant les boîtes de vitesse et différentiels, on arrive à une réduction significative des poids et des coûts, diminuant en même temps l'impact du produit sur l'environnement.

Étant donné tous les aspects présentés ci-dessus, la présence d'un actionneur unique en accélération et en freinage pourrait faciliter la tâche de contrôle qui réalise le TCS et l'ABS. Un actionneur unique signifie un seul temps de réponse pour les deux cas et les deux tâches pourraient être corrélées dans une tâche unique: le contrôle du couple à la roue. Le temps de réponse rapide d'un moteur-roue permet d'utiliser des techniques de contrôle avancées qui limiteront directement le couple aux roues en fonction de l'adhérence disponible. Pour cela, des techniques d'estimation seront étudiées, pour calculer notamment la limite de friction. Ces valeurs seront utilisées par la stratégie de contrôle pour calculer un couple adéquat à appliquer aux roues, afin de maintenir l'adhérence en accélération ou freinage tout en répondant à la demande conducteur. De plus, des cas extrêmes de variations rapides de la limite d'adhérence seront étudiés pour vérifier la robustesse des méthodes de contrôle proposées. De même, des scénarios

plus réalistes seront testés, comme l'accélération brusque, le véhicule partant à vitesse nulle, ou des manœuvres de freinage d'urgence à haute vitesse avec changement des conditions de route. Les simulations prendront en compte divers perturbations et des bruits de mesure. Le but final est d'avoir une estimation robuste et une technique de contrôle qui fera face à toutes les perturbations possibles. Les simulations seront effectuées dans l'environnement Matlab/Simulink.

Chapitre 2: Modélisation

La modélisation est le processus d'élaboration d'un modèle, qui est une représentation de l'architecture et du fonctionnement du système [56]. Un des buts d'un modèle est la possibilité de prédire l'effet de changements sur le système. D'une part, un modèle devrait être une approximation proche du système réel et intégrer la plupart de ses caractéristiques notables. D'autre part, il ne devrait pas être trop complexe afin d'être traitable mathématiquement ou numériquement.

Dans ce qui suit, nous avons considéré un modèle de véhicule simple à une roue, ainsi qu'un modèle plus complet à quatre roues motrices. Ensuite, pour représenter le système véhicule dans des environnements réalistes, un modèle d'interaction entre la route et le pneu à été pris en compte, puisqu'il définit le comportement de l'adhérence du véhicule sous différents profils de vitesse. Ceci est le cœur de la problématique de contrôle dynamique du véhicule et un modèle de friction de pneu réaliste est nécessaire pour obtenir les résultats de simulation appropriés du comportement dynamique du véhicule. D'une part, un modèle de véhicule représentatif doit être configuré pour respecter des exigences d'analyse et d'autre part, on doit considérer un modèle de conducteur, afin de simuler les actions de ce dernier. Le modèle de conducteur aidera à simuler un suivi de profil de vitesse, la production des couples de freinage et des forces d'accélération.

Le modele de vehicule à une roue

Le point de départ de notre méthodologie de recherche est celui du modèle de véhicule à une roue. C'est un modèle simple, pourtant tout à fait suffisant pour représenter la roue et la dynamique du véhicule et fournir une bonne base de départ pour les stratégies de contrôle et d'estimation. Une vue longitudinale du modèle est présentée en Figure 2.

Les équations globales du système incluant le véhicule et la dynamique de roue

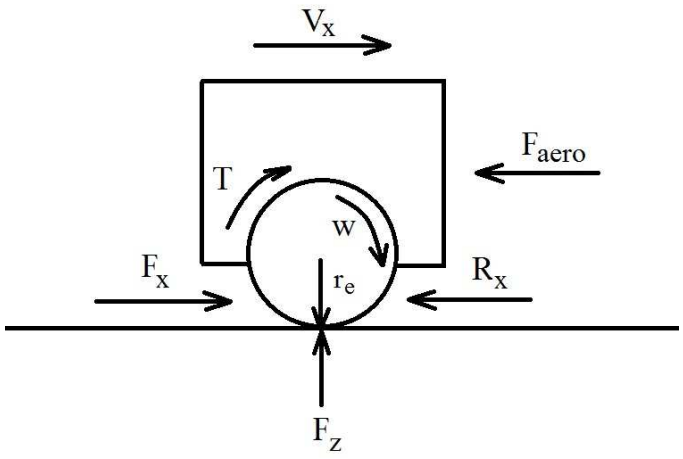

Figure 2: Modele de vehicule à une roue.

peuvent être écrites comme suit [75, 38]:

$$m\dot{V}_x = F_x - F_{aero}, \tag{2}$$

$$I\dot{\omega} = T - r_e F_x - R_x, \tag{3}$$

$$F_x = \mu(\lambda) F_z, \tag{4}$$

$$F_z = mg, \tag{5}$$

$$\lambda = \frac{r_e\omega - V_x}{\max(r_e\omega, V_x)}. \tag{6}$$

Les variables utilisées dans les equations du modèle sont définies comme suit:

- m- la masse du véhicule.
- $\dot{V}_x$- l'accélération longitudinale du châssis.
- F_x- la force longitudinale de traction.
- $F_{aero} = (\rho C_d V_x^2)/2$- la force aérodynamique longitudinale avec: ρ la densité d'air, C_d le coefficient aérodynamique longitudinal et V_x la vitesse longitudinale du châssis.
- I- l'inertie de la roue.
- T- le couple de traction/freinage.
- r_e- le rayon effectif de roue.

- $R_x = mgC_r$- la force de résistance au roulement avec: m la masse du véhicule, g l'accélération gravitationnelle et C_r le coefficient de résistance au roulement.
- μ- la friction longitudinale.
- λ- le taux de glissement longitudinal.
- F_z- la force normale.
- ω- la vitesse angulaire de roue.

Dans ce modèle, la dynamique de véhicule est représentée par l'équation (2), ayant fait la supposition que la pente de la route est nulle. La dynamique de roue est décrite dans l'équation (3), avec une force de résistance au roulement constante. Les roues sont supposées être toujours en contact avec le sol et le centre de la roue est supposé être à une distance r_e constante du sol. Il ne prend donc pas en compte la déformation du pneu mais ce serait augmenter la complexité du modèle pour un résultat négligeable [98]. En conséquence, les forces pneumatique verticales sont supposées être perpendiculaires en dessous du centre de roue. On considère également la force normale sur le pneu constante dans l'équation (5), puisqu'aucun système de suspension n'a été pris en compte. La friction entre le pneu et la surface de route est représentée par le terme $\mu(\lambda)$ dans l'équation (4). Son expression est une fonction du taux de glissement longitudinal, représenté par l'équation (6, donc bien que ceci soit un modèle simpliste, il représente bien la dynamique principale qui influence le comportement dynamique longitudinal du véhicule, comme le glissement de la roue en accélération ou le dérapage de roue dans le ralentissement, comme indiqué dans la Figure 3. Les autres variations pourront donc etre considérés comme des perturbations sur le système. Il nous permettra de développer les stratégies d'estimation de la friction maximale et de calculer les lois de commande adéquates pour réaliser le contrôle longitudinal de la roue. Avec ce modèle simple, nous validerons la robustesse de nos approches qui seront mises en œuvre sur un modèle de véhicule à quatre roues.

Le modèle du conducteur

Nous considérons ici un modèle basique de conducteur. Il simulera les actions du conducteur (l'accélération, le freinage) dans les différentes études de cas réalistes. Les demandes du conducteur peuvent être traduites en des profils de vitesse de référence

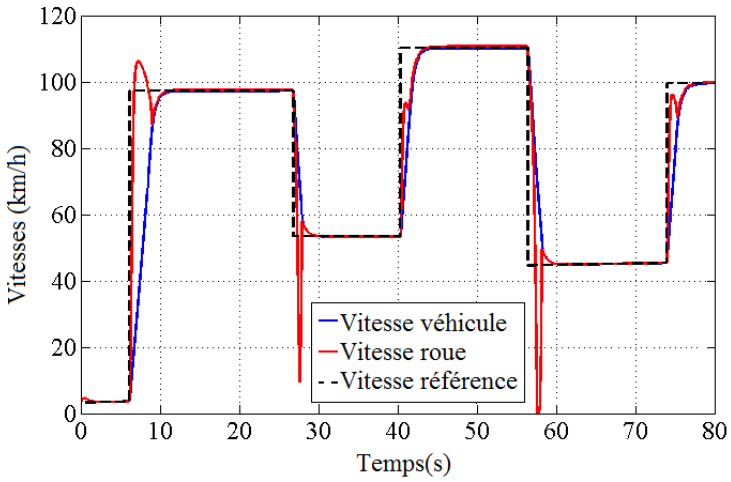

Figure 3: Comportement du modèle dans des phases d'accélération et de freinage.

à suivre. Par exemple, un appui brutal sur la pédale d'accélération se traduit par une consigne de type échelon de vitesse. Ces demandes seront transformées en consignes de couple, qui sont transmises à la roue. Le modèle de conducteur est ici considéré comme un contrôleur par platitude utilisé pour suivre un profil de vitesse de référence, fournissant les couples nécessaires, dans le cas où le glissement est négligé.

Pour calculer les couples adéquats au suivi d'une vitesse de référence, une configuration fondée sur la platitude est mise en place. La platitude est une propriété qui étend la contrôlabilité des systèmes linéaires aux systèmes dynamiques non-linéaires. Nous montrerons que V_x est une sortie plate pour ce modèle de véhicule. À cette fin, les variables de système doivent être exprimées en fonction de V_x et de ses dérivées. L'expression finale du contrôleur fondé sur la platitude est la suivante:

$$T_{flat} = r_e(F_{aero} + \frac{1}{r_e}R_x + mPI_{out} + m\dot{V}_{x_{ref}}). \tag{7}$$

Le contrôleur PI_{out} est construit avec une fonctionnalité de type anti-emballement, avec $\nu = V_{x_{ref}} - V_x$ et u_{min}, u_{max} étant les limites de couple du moteur électrique. L'expression de la sortie du contrôleur PI_{out} est donnée dans l'algorithme 1.

Le modèle d'interaction pneu-route

L'influence de la friction sur la dynamique longitudinale est difficile à quantifier puisqu'elle dépend de nombreux facteurs. Pour une meilleure compréhension de ce

Algorithme 1: Contrôleur PI avec anti-emballement.

---

if $((\nu \geqslant 0)$ and $(PI_{out} \geqslant u_{max}))$ or $((\nu \leqslant 0)$ and $(PI_{out} \leqslant u_{min})$
$\quad PI_{out_{t_k}} = K_p \nu_{t_k} + K_i (\int \nu)_{t_{k-1}} dt$
else
$\quad PI_{out_{t_k}} = K_p \nu_{t_k} + K_i (\int \nu)_{t_k} dt,$

---

phénomène, il est utile de regarder d'abord de plus près la formule Pacejka [73], qui est une formule empirique mais les résultats font référence dans la littérature comme étant la plus représentative de la réalité. La formule de Pacejka donne une expression de la force de friction longitudinale F_x. Les entrées statiques du modèle sont représentées par le termes b_n (qui ont des valeurs fixées selon le type du pneu) et les entrées dynamiques sont la force normale F_z et le taux de glissement longitudinal λ. La forme finale de F_x peut être écrite comme suit:

$$F_x = D \sin(C \arctan(B\lambda - E(B\lambda - \arctan(B\lambda)))) \tag{8}$$

Les expressions pour le calcul de B, C, D et E sont :

- $B = \frac{(b_3 F_z^2 + b_4 F_z) e^{-b_5 F_z}}{CD}$.
- $C = b_0$.
- $D = (b_1 F_z + b_2) F_z$.
- $E = b_6 F_z^2 + b_7 F_z + b_8$.

La friction longitudinale entre la route et le pneu (μ_x), modélisée par une fonction de Pacejka est illustrée en Figure 2.4.

Comme on peut le voir, il y a des différences importantes en fonction des conditions de route. Le sommet de chaque courbe diffère d'un type de surface de route à un autre, aussi bien que la valeur du taux de glissement longitudinal correspondant à ce sommet. Ainsi, par exemple, pour une surface de route sèche, le sommet de la courbe est approximativement à $\mu_x = 1$ et la valeur du taux de glissement correspondante est $\lambda = 0.1$. Sur une surface avec un petite adhérence, la valeur maximale pour μ_x est atteinte pour $\lambda = 0.05$.

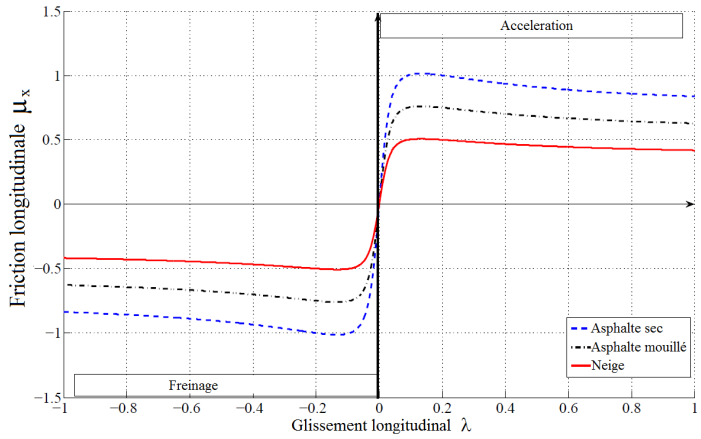

Figure 4: Courbes de Pacejka modelisant la friction longitudinale.

Le modèle dynamique de Pacejka

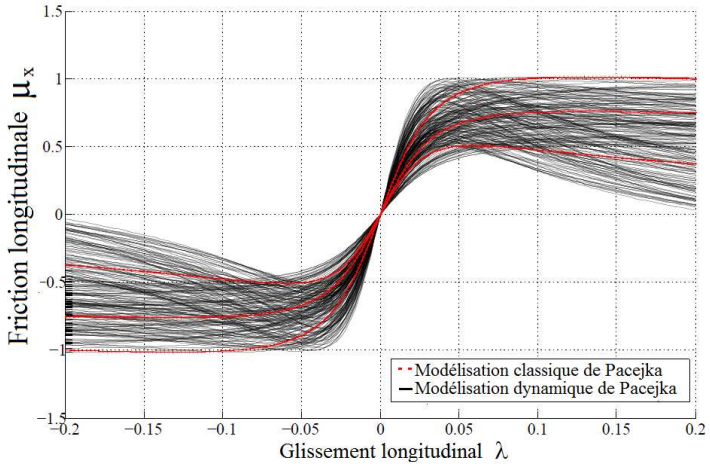

Figure 5: Modélisation réaliste des courbes de Pacejka.

Au lieu des courbes modélisées par Pacejka, dans des environnements réels nous trouvons des nuages de points dont la position peut varier d'un instant d'échantillonnage à un autre [77, 30]. Au lieu donc de considérer seulement trois courbes théoriques modélisant les principaux types de surfaces de route (sec, humide et neigeuse), nous les interprétons comme variant continuellement pendant la manœuvre de conduite. Cette approche donnera une modélisation plus réaliste des conditions de route et permettra d'avoir une meilleure vue des résultats de la méthode proposée dans cet environnement.

Chapitre 3: Estimation de paramètres

Tout modèle contient des paramètres modifiant son comportement et des variables dont il permet de prédire l'évolution. Dans quelques cas ces paramètres ou variables peuvent être mesurés directement, comme par exemple, la vitesse de rotation des roues. Dans d'autres cas, les paramètres d'intérêt doivent être estimés en utilisant des équations du modèle.

Les véhicules électriques ont un avantage majeur comparés aux véhicules thermiques, en cela que la valeur instantanée du couple transmis aux roues est disponible *en ligne* en mesurant le courant moteur. Puisque le moteur électrique est placé directement sur les roues, les calculs de la friction instantanée peuvent être accomplis à partir de l'équation (3). Ceci est la nouveauté de notre travail, puisque l'on considère que le seul actionneur pour accélérer et ralentir le véhicule est le moteur électrique à la roue. Le temps de réponse est minime et il peut être indépendamment contrôlé, apportant la possibilité d'appliquer les nouvelles techniques de contrôle qui dépendent directement de la friction disponible. Nous avons donc considéré aucun frein hydraulique dans les simulations, sachant que le moteur électrique utilisé est assez puissant pour fournir des couples de freinage suffisants. On considère également deux variables importantes: la vitesse angulaire de la roue (ω) et la vitesse longitudinale du véhicule (V_x). Notez, cependant, que le calcul de V_x venant d'accéléromètres n'est pas direct (les signaux venant de ces capteurs sont très bruités et doivent être intégrés, d'où un problème d'évaluation de la condition initiale; voir [66] pour un estimateur simple et pourtant efficace de V_x).

A partir de ces trois variables T, ω et V_x, les calculs seront effectués pour évaluer tous les paramètres nécessaires pour les lois de contrôle appliquées aux roues. A partir d'une estimation de la friction maximale, des techniques de contrôle différentes seront élaborées pour réaliser un comportement de roue linéaire dans des situations d'urgence, représentant le but final du présent travail.

Nous avons utilisé l'équation (3) du modèle pour évaluer la friction longitudinale instantanée. Remplaçant l'équation (4) dans l'équation (3), l'expression pour μ_x est alors:

$$\mu_x = \frac{1}{r_e F_z}(T - I\dot{\omega} - R_x). \tag{9}$$

Le calcul du taux de glissement longitudinal peut également être obtenu directe-

ment par le biais de l'équation suivante:

$$\lambda = \frac{r_e\omega - V_x}{\max(r_e\omega, V_x)}. \tag{10}$$

Pour la construction finale de l'estimateur de l'adhérence maximale, nous allons utiliser un terme d'une importance significative, pour la pente des courbes de friction. Il s'agit de l'une des variables les plus importantes pour le développement futur de la stratégie d'estimation, nommée XBS. Cette dernière est définie comme la dérivée de la friction par rapport au taux de glissement longitudinal [17]:

$$XBS(t) = \frac{d\mu_x}{d\lambda} = \frac{\dot{\mu}_x}{\dot{\lambda}}. \tag{11}$$

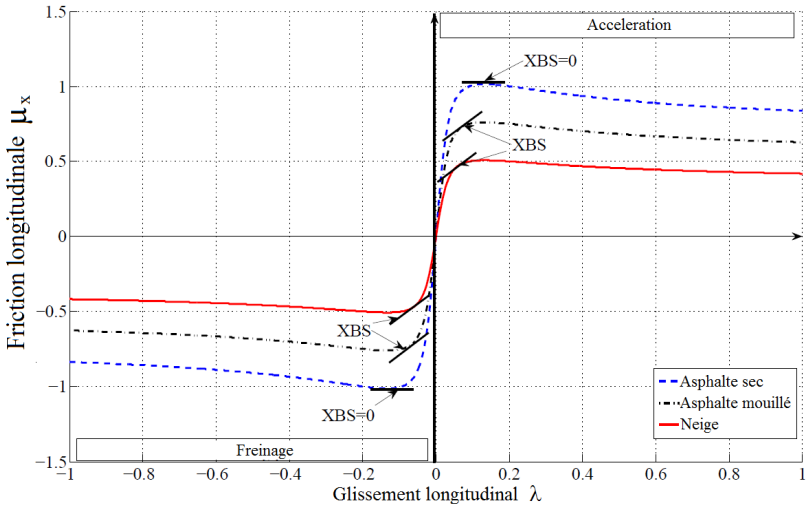

Figure 6: La définition de XBS selon [17].

Cette variable fournit des informations sur la friction instantanée. Si la pente est positive (XBS$>$ 0), alors μ_x est situé dans la zone stable des courbes, autrement si la pente est négative, μ_x est situé dans la zone instable, après le sommet. Lorsque XBS$=$ 0, la valeur de la friction est maximale et donc, la traction ou la force de freinage est maximale. Ceci est la raison pour laquelle cette variable est souvent utilisée, comportant des informations importantes sur le point critique des courbes de friction (le sommet où XBS$=$ 0).

Estimation de l'adhérence maximale

Pour estimer la friction maximale disponible nous nous sommes servi des propriétés du modèle de Dugoff [75]. Le modèle de Dugoff possède une caractéristique intéressante, supposant une distribution de pression verticale uniforme sur la surface de contact de pneu: il a un comportement monotone, comme illustré en Figure 7. Ceci est une simplification comparée à la pression parabolique plus réaliste du modèle de Pacejka. Cependant, les forces longitudinales dans le modèle de Dugoff sont exprimées en fonction de la friction maximale; de là, l'intérêt d'estimation des paramètres Dugoff pour obtenir une estimation de la friction maximale.

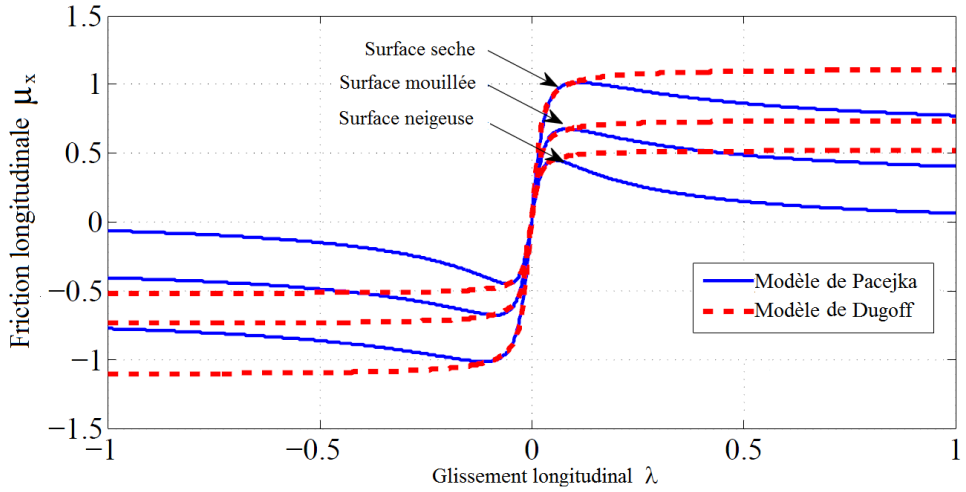

Figure 7: Caractéristiques de friction comparées sur les courbes de Pacejka et Dugoff.

Dans le modèle de Dugoff, les efforts longitudinaux sont modélisée comme suit:

$$F_x^D = \alpha f(\tau) K_x \lambda. \tag{12}$$

Où $f(\tau)$ est:

$$f(\tau) = \begin{cases} (2-\tau)\tau, & \tau < 1 \\ 1, & \tau \geqslant 1 \end{cases}, \quad \tau = \frac{\alpha \mu_{x_{max}} F_z}{2|K_x \lambda|}. \tag{13}$$

Dans cette formulation, les deux paramètres clé sont K_x et α. Le paramètre K_x est la pente des courbes $\mu_x - \lambda$ (ou $F_x - \lambda$) dans la région linéaire et il a un impact

sur la forme des courbes (cf. Figure 8).

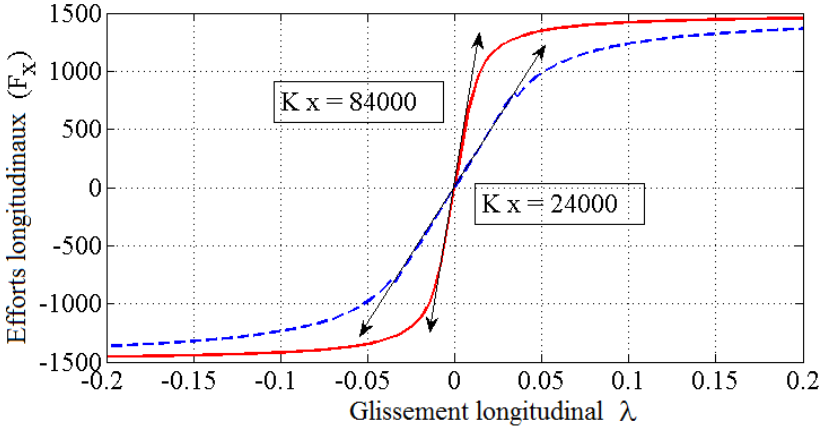

Figure 8: L'impact de K_x sur les courbes de Dugoff.

L'autre paramètre clé est un facteur de pondération entre le modèle de Dugoff et le modèle de Pacejka qui permet de positionner le point d'intersection entre les courbes correspondantes au maximum de la courbe du modèle de Pacejka (cf. Figure 9).

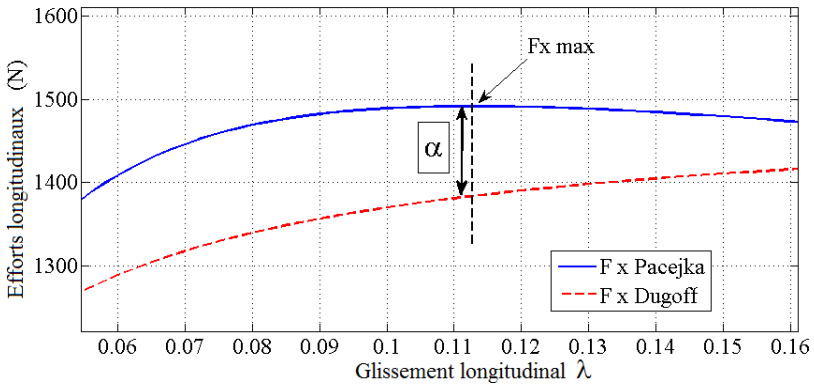

Figure 9: Le paramètre de pondération α.

Si ces deux paramètres sont bien estimés, nous obtenons le résultat illustré en Figure 10, signifiant que la pente de la courbe du modèle de Dugoff correspondra à la pente de la courbe du modèle de Pacejka.

La Figure 11 récapitule l'estimation des deux paramètres clés K_x et α.

Considérons ensuite le cas de la région non-linéaire de $f(\tau)$, c'est-à-dire $f(\tau) =$

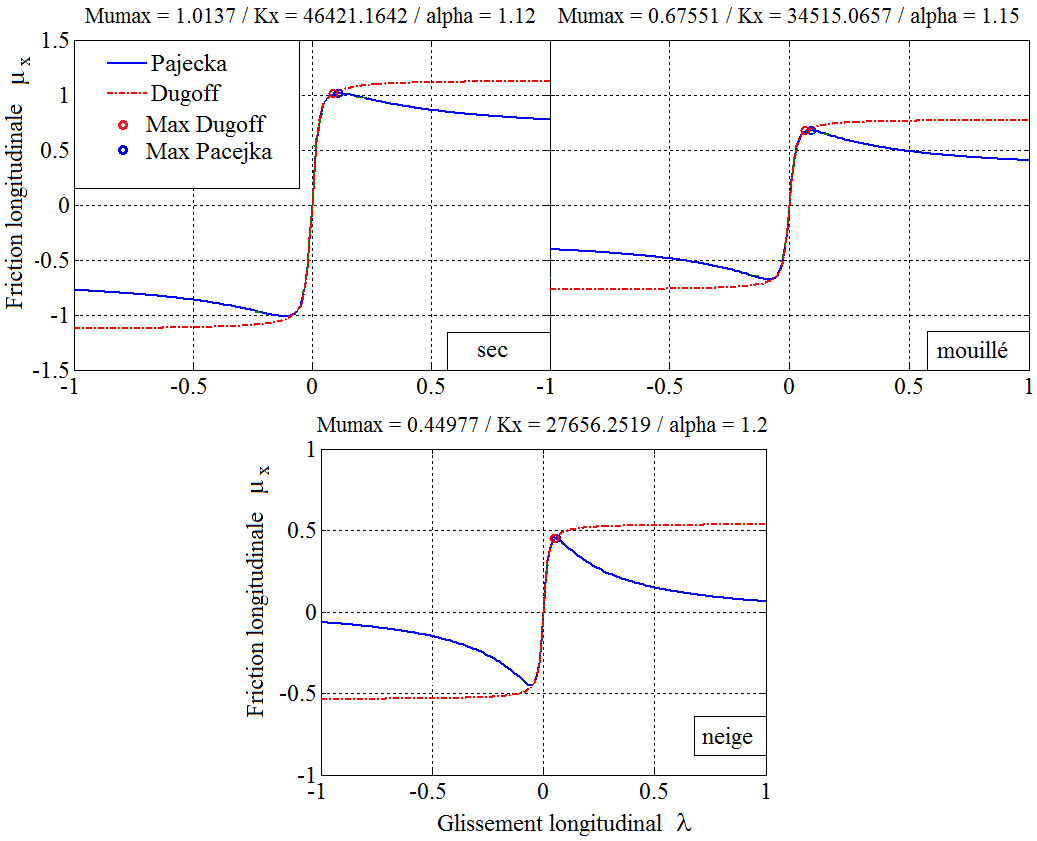

Figure 10: Estimation exacte de α et K_x sur le modèle de Dugoff comparé au modèle de Pacejka.

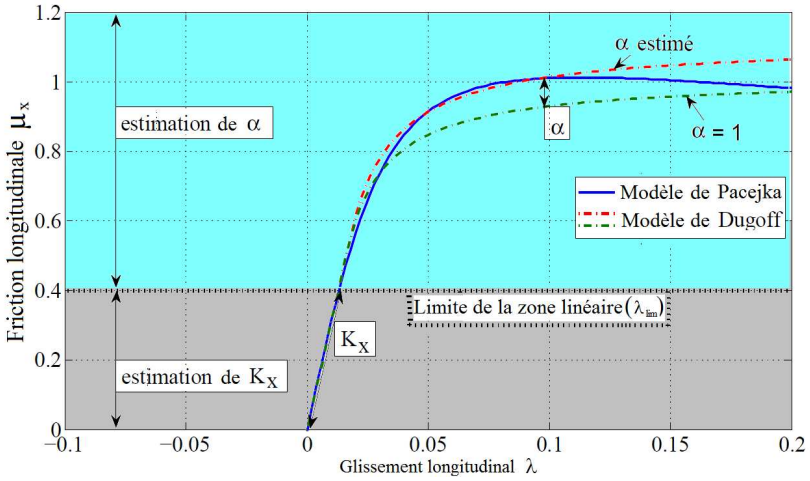

Figure 11: Vue graphique du processus d'estimation de α et de K_x.

$(2-\tau)\tau$. Les efforts longitudinaux peuvent être exprimés comme suit:

$$F_x^D = \left(2 - \frac{\alpha\mu_{x_{max}}F_z}{2|K_x\lambda|}\right)\frac{\alpha\mu_{x_{max}}F_z}{2|K_x\lambda|}K_x\lambda. \tag{14}$$

Cette expression peut être récrite comme équation algébrique en la friction maximale:

$$\alpha^2\mu_{x_{max}}^2F_z^2 - 4\alpha\mu_{x_{max}}|K_x\lambda|F_z + 4|K_x\lambda|F_x^D = 0, \tag{15}$$

avec les deux solutions:

$$\mu_{x_{max}} = \frac{2\alpha(|K_x\lambda| \pm \sqrt{K_x\lambda(K_x\lambda - F_x^D)})}{F_z}. \tag{16}$$

Le signe entre les deux termes du numérateur est '+' quand $\lambda \geqslant 0$ et '−' quand $\lambda < 0$. Ayant obtenu aussi des estimations de K_x et de α, nous proposons un algorithme qui calcule la friction maximale:

Algorithme 2: Calcul de $\mu_{x_{max}}$.

---

if $(|\lambda| > \lambda_{lim}\ )$
  $\mu_{x_{max}}^D(t_k) = \frac{2\alpha(|K_x\lambda(t_k)| \pm \sqrt{K_x\lambda(t_k)(K_x\lambda(t_k) - F_x(t_k))})}{F_z}$
else
  $\mu_{x_{max}}^D(t_k) = \mu_{x_{max}}^D(t_{k-1})$

Chapitre 4: Contrôle

Le but de ce chapitre est d'élaborer des lois de commande qui préserve l'adhérence longitudinale de la roue, indépendamment du comportement du conducteur (accélération brusque ou freinage d'urgence) et des conditions de route (humide, sèche ou neigeuse), et c'est en utilisant comme actionneur unique le couple fourni par les moteurs électriques aux roues. Le moteur électrique que nous utilisons sur cette application à une puissance maximale de 39 kW et un couple maximal de 34.2 Nm. Il transmet son couple via une démultiplication de rapport R=17, donnant un couple total de freinage/accélération de 581.4 Nm par roue. Ce couple est suffisant pour freiner le véhicule dans des manœuvres d'urgence, et ne nécessite donc aucun frein hydraulique. Néanmoins, dans un véhicule réel le freinage hydraulique devrait être considéré, puisqu'une saturation de charge de la batterie qui fournit l'énergie électrique aux moteurs pourrait signifier qu'aucun couple négatif ne puisse être produit par le moteur. Donc, un système hydraulique doit être préservé dans un design de véhicule doté des moteurs électriques aux roues. Dans ce travail, nous n'avons pas considéré cet aspect, nous nous sommes attachés à montrer qu'avec uniquement les moteurs électriques, il est possible de préserver un comportement stable de la roue et du véhicule.

La première étape de cette stratégie est d'estimer "en ligne", en utilisant les caractéristiques du modèle de pneu de Dugoff, la friction maximale entre la roue et la route décrite dans le Chapitre 3. La deuxième étape est d'appliquer une commande qui conserve la friction longitudinale instantanée à sa valeur maximale.

La nouveauté du présent travail consiste en l'utilisation du moteur électrique comme seul actionneur en accélération et freinage, pour fournir couples nécessaires pour accomplir les fonctions de TCS et d'ABS. Les moteurs roue fournissent plus de possibilités pour la sécurité active et le contrôle de trajectoire. Ces moteurs ont une latence très basse et peuvent fournir un couple de freinage sur les roues plus rapidement que des freins hydrauliques conventionnels. Dans la configuration classique avec moteur thermique, l'estimation des forces de friction de roue est problématique, en raison d'un manque d'estimation fiable du couple produit par le moteur et transmis aux roues. Avec un moteur électrique, grâce à la connaissance du couple transmis calculé à partir du courant mesuré, on peut évaluer les forces de friction aux roues. Contrairement aux stratégies existantes, plutôt conservatrices, décrites dans [13, 15, 36], qui contrôlent directement le glissement sur une consigne fixe, le moteur électrique permet

d'appliquer un contrôle directement sur la friction, en considérant les conditions de route. Le maintien de la friction sous son sommet en accélération ou freinage, permettra de conserver la stabilité du véhicule tout en optimisant la récupération d'énergie en freinage.

Commande en boucle ouverte par saturation du couple

Ce contrôle en boucle ouverte saturera le couple demandé par le conducteur à une valeur de couple maximale, calculée à partir de l'équation dynamique de la roue (3):

$$I\dot{\omega} = T - r_e F_x - R_x. \tag{17}$$

En remplaçant F_x par l'équation (4), on obtient l'expression du couple T suivante:

$$T = I\dot{\omega} + r_e \mu_x F_z + R_x. \tag{18}$$

Et le couple de saturation prenant en compte la friction maximale estimée est:

$$T_{sat} = I\dot{\omega} + r_e \mu_{x_{max}} F_z + R_x. \tag{19}$$

Le couple obtenu avec la formule ci-dessus, limitera le couple demandé par le conducteur en cas de glissement, après un *algorithme d'activation* décrit comme suit:

Algorithme 3: Activation de la loi de commande.

---

if $|\lambda| \leqslant \|\lambda_{lim}|$
  $T_{wheel} = T_{flat}$
else
  if $\lambda > 0$
    $T_{wheel} = \min(T_{flat}, T_{sat})$
    else $T_{wheel} = \max(T_{flat}, T_{sat})$

Tant que nous sommes dans la zone linéaire des courbes de friction, délimitée par λ_{lim}, le couple appliqué T_{wheel} est égal au couple venant des demandes du conducteur. Ici, nous sommes dans la zone pseudo-glissante comme indiqué en Figure 1, donc dans la zone stable. Une fois que le seuil λ_{lim} est dépassé, la valeur minimale entre le couple

saturé et le couple conducteur sera appliqué en accélération et la valeur maximale en freinage. De cette façon, le couple saturé limitera toujours le couple venant du conducteur, ce qui évitera le blocage des roues ou le patinage.

Maintenant analysons la réponse de système avec une caractéristique d'adhérence variable, en appliquant le contrôle en boucle ouverte. On peut voir que le maximum de la friction modélisé est atteint dans tous les cas, même si cette valeur maximale varie dans le temps (la Figure 13). Des oscillations apparaissent en transitoire le temps que l'algorithme d'adaptation du paramètre α converge. Néanmoins, lorsque ce dernier a convergé, un suivi stable de la friction maximale est réalisé.

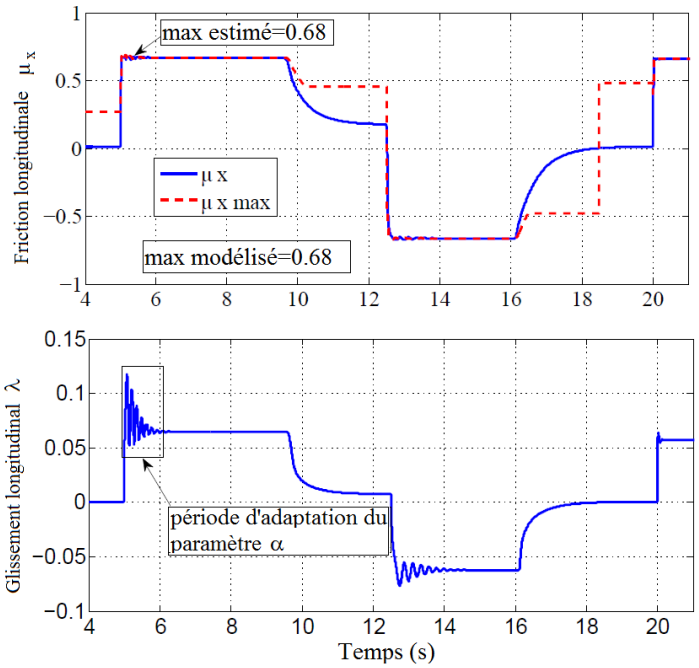

Figure 12: Estimation précise de la friction maximale.

En appliquant la même stratégie de commande sur le modèle dynamique de Pacejka présenté dans le Chapitre 2, nous obtenons les résultats en termes de suivi de friction maximale illustrées en Figure 14.

Nous pouvons constater que, malgré la variation de la friction maximale, la méthode d'estimation fournit une valeur fiable pour $\mu_{x_{max}}$. Le $\mu_{x_{controlle}}$ de la Figure 14 montre que la friction instantanée n'excède jamais le maximum de la valeur estimée, accomplissant donc le but recherché. La grande variation de paramètres du modèle de Pacejka se rapproche de situations réelles, donnant des estimations qui ne restent plus

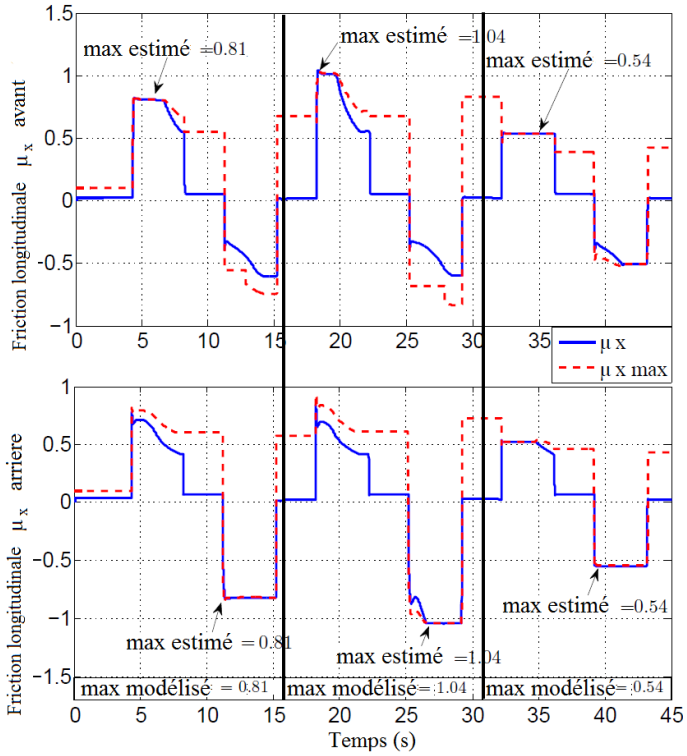

Figure 13: Estimation précise de la friction maximale sur route avec $\mu_{x_{max}}$ variable.

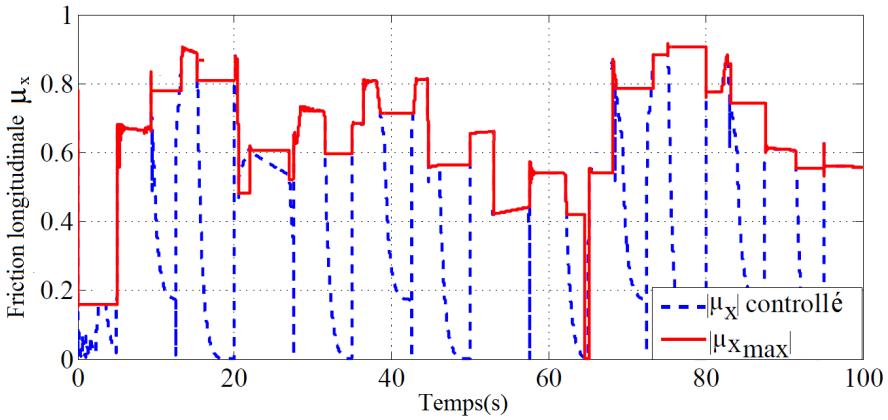

Figure 14: Suivi de friction maximale avec modélisation dynamique de conditions de route.

seulement une courbe, mais s'étalent sur des multiples courbes, comme indiqué en la Figure 15.

La commande en boucle ouverte peut suffire dans le cas idéal, où les perturbations

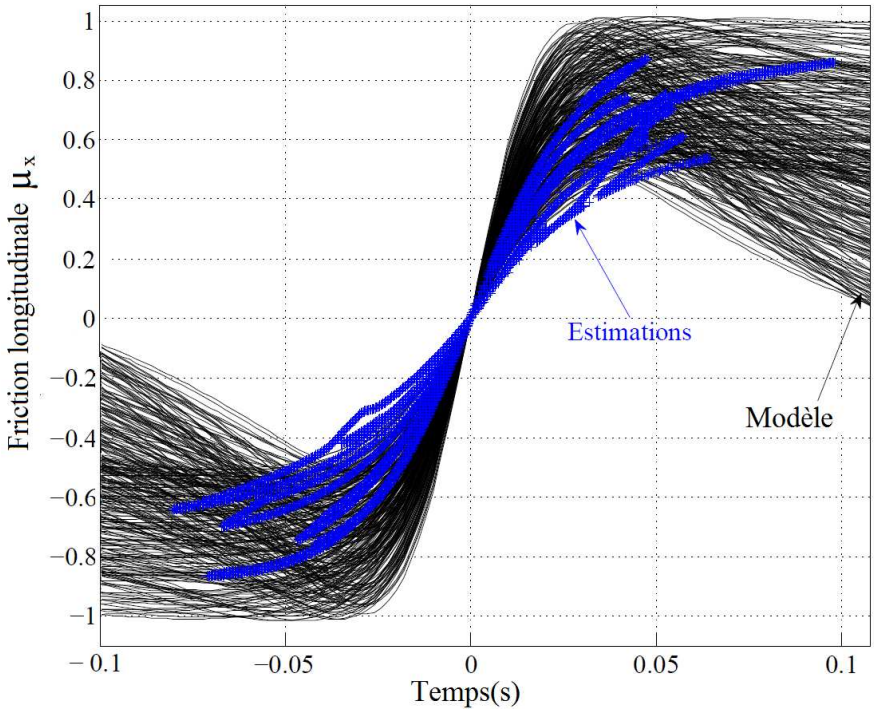

Figure 15: Estimation et contrôle de la friction sur des conditions de route variables.

et le bruit ne sont pas présents. Une loi de commande en boucle fermée permettra d'obtenir la robustesse du contrôle, atténuant l'effet des perturbations et du bruit de mesure.

Commande en boucle fermée par modes glissants

Puisque nous disposons de la friction maximale et de la friction instantanée, l'objectif lors de situations d'urgence (freinage ou accélération brusques), sera de préserver la friction au niveau de son maximale qui sera donc la consigne. Pour cette loi de commande évidente est donc $S = \mu_{x_{max}} - \mu_x$.

Le contrôle par modes glissants est alors défini comme:

$$T_{sliding} = T_{eq} + sign(S)T_{sm}, \tag{20}$$

Pour notre modèle de véhicule l'expression finale de la commande appliquée sera:

$$T_{sliding} = I\dot{\omega} + r_e F_z \mu_{x_{max}} + R_x + sign(S) \int (Sk_2)dt. \tag{21}$$

L'activation de la commande se fera de la même manière que pour le cas du contrôle en boucle ouverte. Ces algorithmes d'activation définissent une zone de "sécurité" dans laquelle nous permettons au couple venant du conducteur d'être appliqué à la roue du véhicule, sachant que pour ces valeurs de λ nous sommes au début des courbes de $\mu - \lambda$ et ainsi dans la zone linéaire stable.

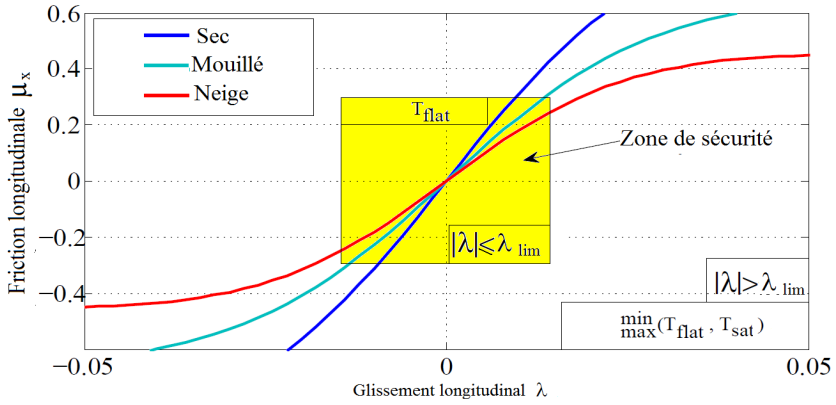

Figure 16: Zone de sécurité (zone pseudo-linéaire de courbes $\mu - \lambda$).

Commande sans modèle en boucle fermée

Le contrôle sans modèle doit conserver la friction instantanée μ_x à sa valeur maximale $\mu_{x_{max}}$. Ici, nous utilisons le couple de roue T pour contrôler la friction instantanée μ_x. Ceci mènera à l'expression suivante pour l'expression de la commande:

$$T = \frac{1}{\beta}\left[-\hat{F} - k_1 e - k_2 \int e\right], \qquad \hat{F} = \hat{\dot{\mu}}_x - \beta(t_k)T(t_k), \qquad e = \mu_x - \mu_{x_{max}}. \quad (22)$$

avec $\mu_{x_{max}}$ la friction de référence, $\hat{\dot{\mu}}$ une estimation de la dérivée de μ_x, $T(t_k)$ une valeur précédente de T (une approximation de T), $\beta = -\dfrac{r_e V_x \frac{d\mu_x}{d\lambda}}{I \max(r_e^2\omega^2, V_x^2)}$ et F incluant les parties négligées.

Nous définissons $\varepsilon = |\mu_{x_{max}}| - |\mu_x| \geqslant k$ comme notre loi de déclenchement. L'activation de la loi de commande suivra l'algorithme suivant:

Algorithme 4 : Activation de la loi de commande.

---

if $|\varepsilon| \geqslant k$
  $T_{wheel} = T_{driver}$
else
  $T_{wheel} = T_{model\,free}$

Comparaison entre les commandes par modes glissants et sans modèle

Dans ce cas, une accélération et une manœuvre de freinage brusques sont simulées sur une route sèche ($\mu_{x_{max}} = 1$). L'application des techniques de contrôle sur ce scénario donne les résultats illustrés en comparaison en Figure 17 et Figure 18. Dans

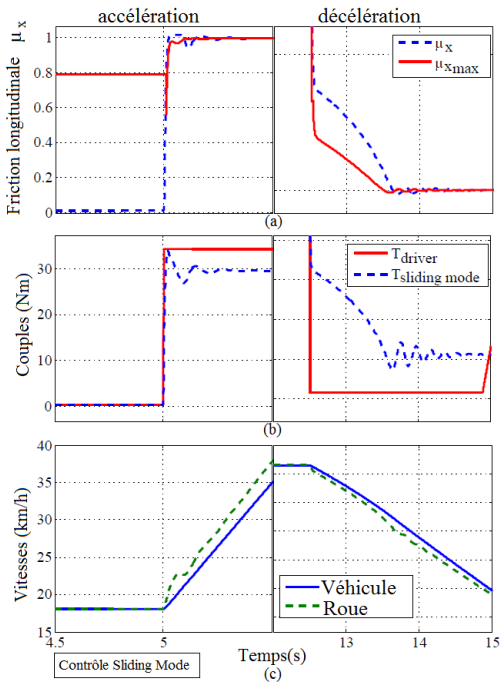

Figure 17: Commande par modes glissants sans perturbation.

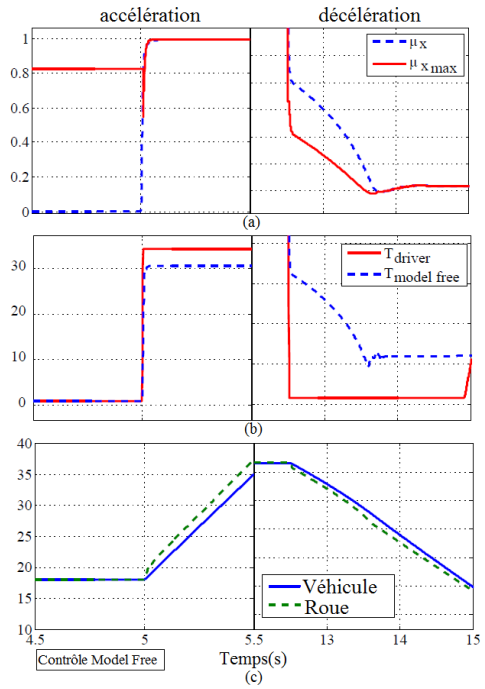

Figure 18: Commande sans modèle sans perturbation.

les deux cas la friction maximale est suivie, pourtant avec moins d'oscillations dans le cas de commande sans modèle (la Figure 18 .(a) comparée à la Figure 17 .(a)). Ceci aboutit à une réponse de couple plus stable dans le cas de commande sans modèle (la Figure 18 .(b)) comparée à la commande par modes glissants (la Figure 17 .(b)). Par

conséquent, le couple transmis donne un comportement de roue plus stable dans le cas de commande sans modèle (la Figure 18 .(c)), améliorant la stabilité du véhicule et le confort des passagers.

Dans des environnements réalistes, des perturbations peuvent surgir. On peut considérer ces perturbations comme une variation de la friction maximale.

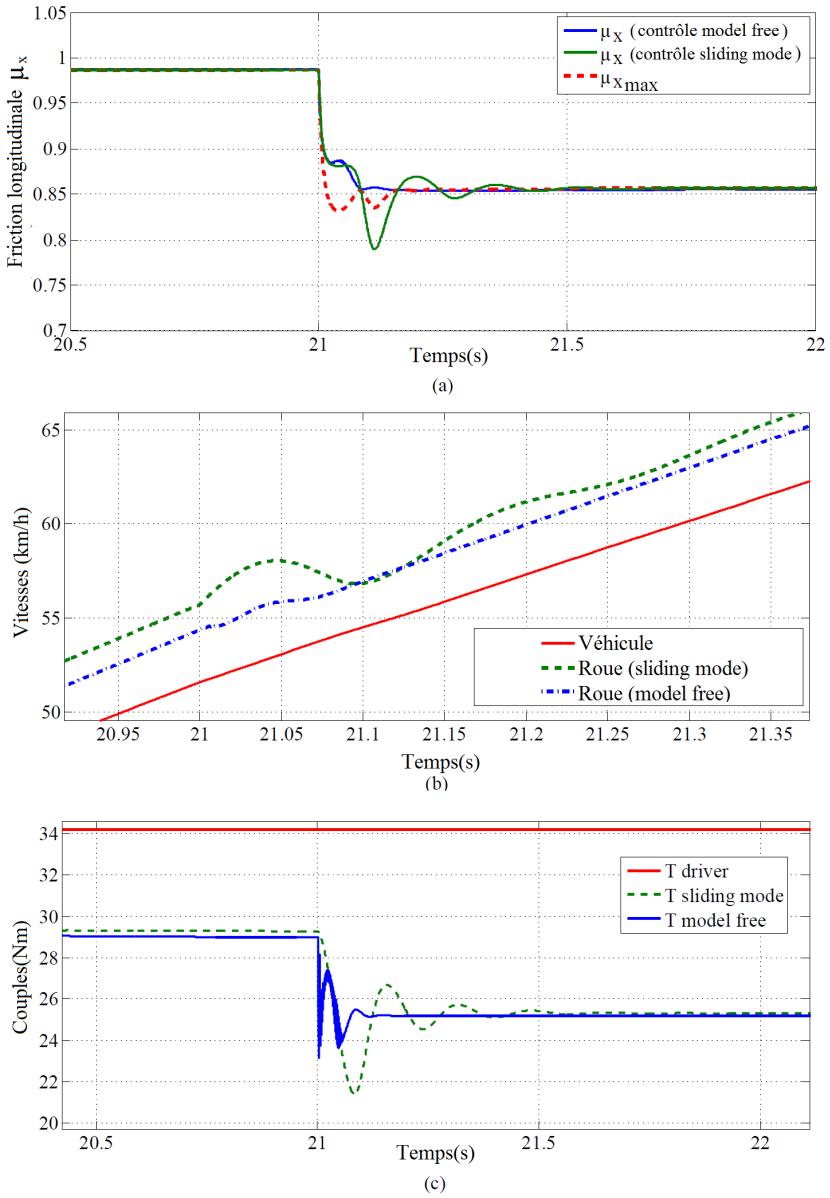

Figure 19: Comparaison entre les lois de commande en présence de perturbation.

Dans ce deuxième scénario, une perturbation est simulée apparaître à l'instant

de simulation t=21s, changeant la friction maximale de sa valeur initiale 1 à 0.85. Dans un environnement réaliste, ceci pourrait être considéré comme une transition d'une route sèche à une humide. Malgré la perturbation, le contrôle devrait pouvoir continuellement suivre la friction maximale de référence. On montre les résultats en Figure 19.

Chapitre 5: Conclusions générales et perspectives

Cette thèse résume les contributions principales sur l'analyse, l'estimation et la commande de la dynamique de véhicule pour un véhicule équipé de moteurs électriques aux roues. Notre attention s'est concentrée sur l'estimation de la friction maximale entre le pneu et la surface de la route et sur la commande appliquée pour réaliser un comportement de roue stable. Seule la dynamique longitudinale est considérée dans ce travail.

Une problématique des véhicules à moteurs à combustion interne est le manque d'informations précises et rapides sur les couples transmis. A contrario, un des avantages des moteurs électriques à la roue est la connaissance précise du couple transmis. Cette caractéristique a été exploitée via l'équation dynamique de la roue pour estimer la friction longitudinale instantanée entre le pneu et la route. D'autres paramètres d'intérêt comme le taux de glissement longitudinal ou les forces normales sur les pneus ont été facilement estimés avec la connaissance du couple de roue. Néanmoins, la friction instantanée n'est pas suffisante pour réaliser le contrôle longitudinal. Une nouvelle approche pour estimer l'adhérence maximale est donc présentée. Elle est basée sur l'inversibilité du modèle de Dugoff et une adaptation en ligne de ses paramètres, avec des résultats satisfaisants même dans des conditions de route variables.

Différentes techniques de commande ont été utilisées pour réaliser le contrôle longitudinal de la roue. Disposant d'estimations pour la friction instantanée et la friction maximale, une manière évidente de commander la dynamique de roue dans des situations d'urgence est de maintenir la friction instantanée à sa valeur disponible maximale. Cette nouvelle approche est appelée suivi de friction maximale et n'est possible que par l'utilisation de moteurs électriques aux roues. Les techniques de commande standard ne permettent pas le contrôle direct de la friction et reposent sur un contrôle direct du glissement sur un seuil fixe conservateur. La nouvelle approche présentée dans cette thèse se fonde sur un algorithme d'activation qui active le suivi de friction maximale

lorsqu'il est nécessaire, c'est-à-dire dans le cas de freinage d'urgence ou des manœuvres d'accélération brusques, quand la friction instantanée s'approche du maximum disponible. Le suivi de la friction instantanée à son maximum permet une dynamique de roue stable et linéaire tant en accélération que lors les phases de freinage. Les techniques fondées sur la commande par modes glissants et sans modèle ont été testées dans cette thèse. La commande sans modèle s'est avérée être plus efficace en termes de suivi de friction maximale, la réalisation d'un suivi de référence plus rapide, avec moins d'oscillations transmises à la roue. Ceci apporte un comportement plus stable en accélération et en freinage. La nouvelle idée présentée dans cette thèse est que le moteur électrique à la roue peut être utilisé comme unique actionneur dans l'accélération et les phases de freinage, lorsqu'il est assez puissant pour fournir les couples nécessaires.

Les perturbations et le bruit peuvent affecter les deux processus d'estimation et de commande. Étant donné que le véhicule fonctionne dans des environnement en plein air, des perturbations peut surgir aisément. Nous avons considéré un changement de l'adhérence de route comme une perturbation et des tests de simulation ont été conduits pour illustrer le comportement des stratégies d'estimation et de commande. Les deux techniques de commande testées se sont avérées être efficaces, avec un avantage pour la commande sans modèle, qui réalise de meilleurs résultats en termes de suivi de friction maximale et de temps de réponse. Les erreurs sur le modèle et le bruit affectant les paramètres importants ont été aussi simulés. Les résultats ont prouvé la robustesse des deux techniques de commande. Même dans des cas où le bruit est présent, la friction maximale a été bien suivie, accomplissant l'objectif final des lois de commande. Ces situations ont été poussées à l'extrême intentionnellement pour tester le comportement de l'étape d'estimation et de commande dans des situations limites. L'estimation et le contrôle se sont avérés être robustes dans le cas de changement de conditions d'adhérence de route aussi bien que dans des scénarios avec perturbations et bruit. Quelques scénarios "réalistes" ont été aussi testés en simulation, pour compléter tous les scénarios possibles qui peuvent surgir dans les environnements réels.

Perspectives

Le moteur électrique à la roue fournit plus de possibilités de contrôle du couple transmis à la roue, étant placé proche de celle ci. Une de ses caractéristiques clés est un temps de réponse court et une génération de couple presque instantanée. Pour un

véhicule équipé de quatre moteurs électriques aux roues, une stratégie de contrôle avancée peut être prévue. Chaque roue peut être commandée et le couple adéquat est fourni selon la friction maximale estimée. Le contrôle latéral du véhicule peut être alors amélioré en ajustant simplement les couples transmis aux roues. Des techniques de supervision peuvent également être mises en place pour optimiser la distribution entre les roues tout en préservant le comportement dynamique du véhicule.

Pour répondre au besoin croissant de la mobilité en réduisant massivement les émissions de CO2, l'électrification des véhicules devient essentielle. L'utilisation du moteur électrique à la roue comme un actionneur unique permet la récupération d'énergie dans les phases de freinage, mais il doit être bien coordonné avec le système de véhicule global et particulièrement avec le système de freinage hydraulique pour réaliser le cahier des charges de sécurité. Le maintien de la friction instantanée à son maximum disponible en freinant signifie une régénération d'énergie maximale. Les algorithmes d'optimisation corrélés avec un superviseur global peuvent être configurés comme cela est déjà réalisé en [48]. Les algorithmes proposés permettent l'adaptation du couple des moteurs électriques, gardant le freinage optimal et sûr sans utiliser des actionneurs hydrauliques classiques pour la correction de la dynamique.

General introduction

The main objective of the present thesis focuses on the integration of the in-wheel electric motors into the conception and control of road vehicles. The present thesis is the subject of the grant 186-654 (2010-2013) between the Laboratory of Signals and Systems (L2S-CNRS) and the French Institute of Petrol and New Energies (IFPEN). The thesis work has originally started from a vehicular electrification project, equipped with in-wheel electric motors at the rear axle, to obtain a full electric urban use and a standard extra-urban use with energy recovery at the rear axle in braking phases.

The standard internal combustion engines have the disadvantage that complex estimation techniques are necessary to compute the instantaneous engine torque. At the same time, the actuators that control the braking system have some delays due to the hydraulic and mechanical circuits. These aspects represent the primary motivation for the introduction and study of the integration of the electric motor as unique propelling source for the vehicle.

The advantages brought by the use of the electric motor are revealed and new techniques of control are set up to maximize its novelty. Control laws are constructed starting from the key feature of the electric motor, which is the fact that the torque transmitted at the wheel can be measured, depending on the current that passes through the motor. Another important feature of the electric motor is its response time, the independent control, as well as the fact that it can produce negative torques, in generator mode, to help decelerate the vehicle and store energy at the same time. Therefore, the novelty of the present work is that the in-wheel electric motor is considered to be the only control actuator signal in acceleration and deceleration phases, simplifying the architecture of the design of the vehicle and of the control laws. The control laws are focused on simplicity and rapidity in order to generate the torques which are transmitted at the wheels. To compute the adequate torques, estimation strategies are set up to produce a reliable maximum friction estimation. Function of this maximum adherence available at the contact between the road and the tires, an adequate torque will be computed in order to achieve a stable wheel behavior in acceleration as well as in deceleration phases. The critical issue that was studied in this work was the non-linearity of the tire-road interaction characteristics and its complexity to estimate when it varies. The estimation strategy will have to detect all changes in the road-surface adherence and the computed control law should maintain

the stability of the wheel even when the maximum friction changes. Perturbations and noise are also treated in order to test the robustness of the proposed estimation and control approaches.

All the characteristics presented above can be summarized and regarded as a response to a specification demand concerning the use of the electric motor as well as the rapidity and simplicity of the control laws:

- the electric motor is the only actuator to accelerate and decelerate the vehicle,
- the electric motor must provide the achievement of anti-slip and anti-skid functions,
- estimation of the maximum friction due to the knowledge of the transmitted wheel torque,
- robustness of the estimation in variable environment,
- the control law must be simple and rapid in terms of friction tracking,
- the control must be robust to perturbation, model errors and measurement noise.

The outline of the thesis is structured in five main chapters, organized as follows:

In **Chapter 1** vehicle dynamics is presented along with the context in which the thesis is placed. The main vehicular safety functions with their existing controllers along with some main vehicle propulsion architectures are discussed. The in-wheel electric motor system and its advantages influencing vehicle dynamics are also introduced here.

In **Chapter 2** the focal point is the modeling of the vehicle dynamics discussed on one wheel and four wheel vehicle model. A simple driver model used to simulate realistic driver's actions is also shown in chapter two. The third important aspect discussed here is the tire road interaction model and its influence on the longitudinal dynamics. A new approach of dynamic modeling the road conditions is described. The results shown in this chapter are related to the paper of the author [25].

Chapter 3 presents the advantages brought by the use of the in-wheel electric motor. Its characteristics are utilized in order to estimate the parameters of interest which will form the estimation and the control strategies. A new approach to estimate

the maximum available friction is described in this chapter. The results are part of author's published papers [26] and [27], and its collaboration in the paper [48].

In **Chapter 4** the attention is focused on different control techniques that are applied in order to achieve a stable longitudinal vehicular control. These techniques take advantage of the rapidity in terms of response time of the in-wheel electric motor. Some realistic case study scenarios are presented. The results shown in this chapter belong to author's papers [28], [29] and [96].

Finally, **Chapter 5** presents the concluding remarks of this thesis and some future perspectives.

A list of publications submitted/accepted to various conferences and journals completes this introduction.

Submitted journal papers

- M.S. Geamanu, A. Cela, H. Mounier, S.I. Niculescu, G. Le Solliec, *Tire-road friction estimation and longitudinal control for electric vehicles*. Submitted to International Journal on Control, Automation and Systems, May 2012.

- J. Wang, M.S. Geamanu, A. Cela, H. Mounier, S.I. Niculescu, *Event driven model free control and comparison with standard approaches in motion controls*. Submitted to: IEEE Transactions on Control System Technology, February 2013.

Published international conference papers

- M.S. Geamanu, A. Cela, H. Mounier, S.I. Niculescu, G. Le Solliec, *Road condition estimation and longitudinal control for electric vehicles*, International Conference on Control, Automation and Systems, Gyeonggi-do, South Korea, 2011.

- M.S. Geamanu, A. Cela, H. Mounier, S.I. Niculescu, G. Le Solliec, *Longitudinal Control for an All-Electric Vehicle*, International Electric Vehicle Conference, Greenville, South Carolina, USA, 2012.

- M.S. Geamanu, A. Cela, H. Mounier, S.I. Niculescu, G. Le Solliec, *Maximum friction estimation and longitudinal control for a full in-wheel electric motor*

vehicle, International Conference on Control, Automation and Systems, Jeju, South Korea, 2012.

- M.S. Geamanu, A. Cela, H. Mounier, S.I. Niculescu, G. Le Solliec, *Adherence control for electric vehicles on varying road conditions*, Mediterranean Conference on Control and Automation, Platanias-Chania, Crete, 2013.

- G. Le Solliec, A. Chasse, M.S. Geamanu, *Regenerative braking optimization and wheel slip control for a vehicle with in-wheel motors*, 7th IFAC Symposium on Advances in Automotive Control, Tokyo, Japan, 2013.

- J. Wang, M.S. Geamanu, A. Cela, H. Mounier, S.I. Niculescu, *Event driven model free control for quad-rotor*, IEEE Multiconference on Systems and Control, Hyderabad, India, 2013.

Chapter 1

Vehicle dynamics control issues and motivation

Contents

1.1 Introduction

The dynamic behavior of road vehicles can be analyzed with several approaches. This can be regarded as a simple spring mass system, through a three-degree of freedom

bicycle model, to a large degree of complexity using a multi-body system simulation package. As computational speed has increased and software user interfaces have also improved, commercial packages have become widely used in industry for rapidly evaluating hundreds of test conditions much faster than real time. Vehicle models can be simulated with advanced controller designs provided as software in the loop (SIL) with controller design software such as Matlab/Simulink, or with physical hardware in the loop (HIL).

Vehicle motions are due to the forces generated between the tires and road, and therefore the tire model is an essential part of the model. The tire model must produce realistic forces during braking, acceleration, cornering, and combinations, on a range of surface conditions. Many tire-road interaction models are in use and most of them are semi-empirical, such as the Pacejka model [73]. Other models are also utilized, such as Dugoff tire model [75], with a simpler approach to model the maximum friction, or Burckhardt tire model [8], which has a velocity dependency. In the past, many simplifications were necessary in order to get real-time performance with reasonable graphics. However, improvements in computational speed have combined with interest in realistic physics, leading to complex driving simulators.

In terms of active vehicular safety, achieving longitudinal control is an aspect of major importance. It is a complex task that requires the knowledge of many instantaneous parameters as the transmitted engine or motor torque to the wheel, the chassis acceleration, the wheel angular acceleration or the adhesive coefficient of the road on which the vehicle is moving. Deriving a good estimation of these parameters is a dominant factor in the obtainment of a controller that guarantees a stable lateral and longitudinal behavior of the vehicle, along with passenger comfort. Among the most important active safety systems in acceleration, we can name the traction control system (TCS), which restores traction if driven wheels begin to spin and the electronic stability program (ESP), which intervenes to avert an impending loss of the lateral vehicle control. In deceleration, the decisive system is the anti-lock braking system (ABS), that allows the wheels to continue interacting in a tractive manner with the road surface as directed by driver steering inputs while braking, preventing the wheels from locking up. One can find other vehicle embedded systems like the electronic brake-force distribution system (EBD), which ensure an optimal distribution of the brake force transmitted to the wheels in order to avoid skidding, and consequently, a stable deceleration of the vehicle.

All these systems contribute to a better handling of the vehicle in critical situations such as sudden hard braking or acceleration on slippery road surfaces, cornering combined with braking or acceleration, offering an improvement in terms of active safety and assisted driving. Active safety systems use an understanding of the state of the vehicle to both avoid and minimize the effects of a crash. They interpret signals from various sensors to help the driver control the vehicle. To achieve usable estimations of various parameters, the embedded systems that provide the estimations have to be robust to noisy measurements or perturbations. At the same time, the computation of control laws that achieve specific safety functions, has to be made in real-time, therefore a reduced complexity and a fast response of the control law is needed. In addition, the environment on which the vehicle operates is subject to continuous variation. Longitudinal friction can vary from one sample time to another and is hard to be predicted, adding complexity to the control task. As well, driver's actions cannot be anticipated and can influence the overall vehicle response in critical situations. The controller should take into account all these aspects to achieve a stable behavior of the vehicle. Even though the lateral control of the vehicle presents a major importance in overall vehicle stability, the present work is focused on the longitudinal control of the vehicle, since it represents the starting point in order to achieve a stable vehicle comportment. Therefore, the ABS (longitudinal braking phases) and TCS (longitudinal acceleration phases) functions of the vehicle safety will be discussed in the following.

1.2 Vehicle propulsion system architecture

There exist a certain number of vehicle propulsion architectures, such as vehicles propelled by internal combustion engines (ICE vehicles), electrically powered vehicles (EV), and architectures that combine these configurations (hybrid electric vehicles, or HEVs). The most common architecture is the ICE configuration (see Figure 1.1) and contains the engine placed centrally and the mechanical power supplied by the motor transmitted to the wheels via a gearbox and transmission components. A reservoir allows the storage of fuel required for operating the engine, while a battery charged by an alternator driven by the engine, supplies the electrical current necessary to the vehicle components. The torque can be transmitted only at two of the wheels, giving a two wheel drive vehicle (2WD), or at all four of them, giving a four wheel drive or all-wheel drive vehicle (4WD or AWD).

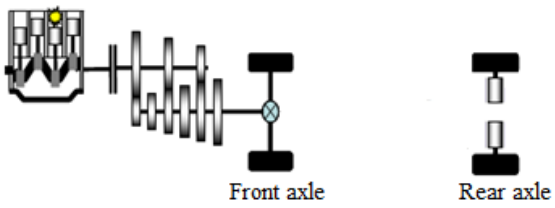

Figure 1.1: Example of internal combustion vehicle architecture [74].

A hybrid electric vehicle (HEV) combines a conventional internal combustion engine (ICE) propulsion system with an electric propulsion system. The presence of the electric powertrain is intended to achieve either better fuel economy than a conventional vehicle or better performance. There are a variety of HEV types, and the degree to which they function as EVs varies as well. Some varieties of HEVs use their internal combustion engine to generate electricity by spinning an electrical generator (this combination is known as a motor-generator), to either recharge their batteries or to directly power the electric drive motors. Many HEVs reduce idle emissions by shutting down the ICE at idle and restarting it when needed; this is known as a start-stop system. A vehicle configuration placed between the ICE vehicle and the full electric vehicle is presented in Figure 1.2. This architecture contains the following components:

- an internal combustion engine at the front axle,
- an electric motor at the rear axle,
- a start-stop group.

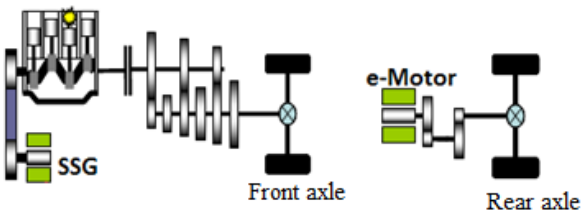

Figure 1.2: Example of hybrid vehicle configuration [74].

Another hybrid configuration is the so-called "bi-mode" vehicle as shown in Figure 1.3, which combines the two types of propulsion systems as following:

- extra-urban use, propelled by the ICE and electric assistance (start, boost),
- urban use zero-emission vehicle (ZEV) propelled only by the in-wheel electric motors.

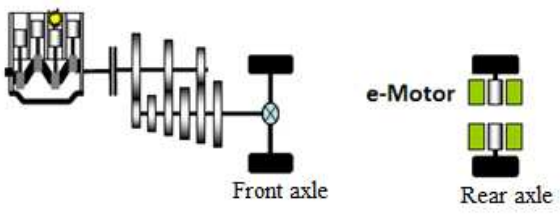

Figure 1.3: Example of bi-mode vehicle configuration [74].

The full electrification of the vehicle contains only electric motors that propel the vehicle. These vehicles are called "battery electric vehicles" or "all-electric vehicles" and use rechargeable batteries, placed on board of the vehicles, to provide the necessary power for propulsion. The architecture, shown in Figure 1.9, uses 4 in-wheel electric motors to generate the traction forces, that can also be used as generators in order to help the braking system, or even more, to fully replace it (Brake-by-wire system).

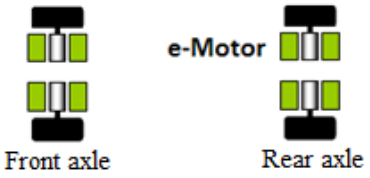

Figure 1.4: Example of in-wheel electric vehicle architecture [74].

1.3 Longitudinal vehicle dynamics analysis

The interaction between the tire and the surface of the road on which the vehicle is moving has a crucial influence on vehicle's behavior during acceleration, braking or cornering maneuvers. The vehicle response to the driver's inputs (steering, acceleration or braking) depends on a critical factor which is the adherence between the tire and the road surface. The friction between the wheels and the road is subject to

variation, its values changing due to numerous factors such as the weather conditions (hot temperatures, rain, snow or ice), road maintenance, type of the pavement (asphalt, concrete or cobblestone) and the presence and composition of the third body (grease, mud, water, leaves, sand, snow, etc.), a thin film between the tire and the ground. Experimental testing showed that longitudinal friction (called μ_x) can be crudely modeled as a function of the longitudinal wheel slip ratio (λ) for different road surface conditions, as shown in Figure 1.5.

The longitudinal slip ratio may be defined as [13]:

$$\lambda = \frac{V_\omega - V_x}{\max(V_\omega, V_x)}, \tag{1.1}$$

where V_ω denotes the linear speed of the wheel and V_x is the vehicle speed.

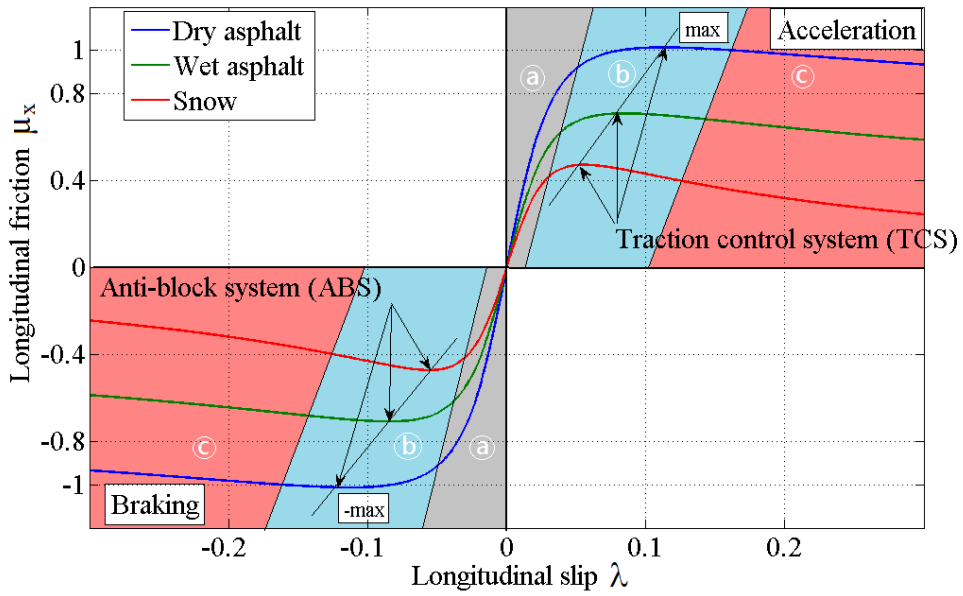

Figure 1.5: Typical adhesion characteristics between road surface and tires, as a function of the slip ratio and road surface conditions (according to Pacejka modeling [73]).

The curves shown in Figure 1.5 present three visible zones of interest:

- The first zone of the curves is called the "pseudo-sliding zone" or "linear zone" (zone ⓐ shown in Figure 1.5). In this zone, the values of λ are low, giving a stable behavior of the wheel.
- The second zone is where the "max" threshold is found (zone ⓑ in Figure 1.5).

Afer exceeding this threshold, the values of $\mu_x(\lambda)$ enter in the non-linear zone.

- The third zone is called the "sliding zone" or the "non-linear zone" of the curves (zone ⓒ in Figure 1.5). Here, the linear speed of the wheels is much bigger than the vehicle speed in acceleration phase (causing uncontrollable wheel spin and traction loss), or much smaller in braking phase (causing wheel block and skid).

During acceleration, $V_\omega > V_x$, therefore there exists a friction force on the wheels in the direction of the forward motion ($\lambda > 0$). This friction force, also known as traction force, is caused by the slip between the tire and the road surface and contributes to the forward motion of the vehicle. However, if the slip ratio exceeds a maximum value as shown in Figure 1.5, the wheel starts to spin considerably faster than the vehicle speed and therefore traction is lost. This is the working area of the TCS, its main task being to keep the values of μ_x smaller than the "max" value shown in Figure 1.5.

During braking, external forces are applied to the wheel so that the linear speed of the wheel is lower than vehicle's speed, e.g., $\lambda < 0$. Therefore there exists a braking force, which is opposite to the forward motion, causing the vehicle to decelerate. As in the acceleration case, if the slip ratio passes through a "-max" value as shown in Figure 1.5, the wheels speed will be smaller than the vehicle speed until complete lock-up, causing the loss of adherence. Therefore, the main task of the ABS is to keep the values of $-\mu_x$ bigger than the "-max" value, to prevent the wheel lock.

The non-linearity of the adherence problem gives the complexity of the control algorithm task. In order to achieve a stable behavior of the vehicle in typical vehicle maneuvers, the control must manage the friction values to stay in the interval [0, |max|]. In emergency maneuvers, where the friction values exceed the "max" threshold, the control has to be able to bring back back its values, guaranteeing maximum grip and therefore stable wheel and vehicle behavior.

ABS and TCS controllers pose unique challenges to the designer:

- for optimal performance, the controller must operate at an unstable equilibrium point;
- depending on road conditions, the maximum braking/traction torque may vary over a wide range;
- the tire slippage measurement signal, crucial for controller performance, is both highly uncertain and noisy;

- on rough roads, the tire slip ratio varies widely and rapidly due to tire bouncing;
- the braking system contains transportation delays which limit the control system bandwidth.

Furthermore, the decisive influencing factor in the functioning of the ABS and TCS is the friction between the tires and the road surface. It is an unknown parameter and thus needs to be estimated. In the classical ICE configuration, the estimation of the wheel friction forces is problematic, due to the lack of a reliable estimation of the torque transmitted to the wheels. Therefore, a better knowledge of this transmitted torque should lead to a more precise control, and consequently to an improved active safety. The system complexity is increased since ABS and TCS use different actuators for their functioning. These have different dynamics with different response times, with possible influence on overall vehicle response. With the introduction of the electric motors, one can envisage the achievement of both ABS and TCS functions with the torque provided by the motor. These important functions will depend only on the dynamics of the electric motor, improving response time and providing the possibility for advanced control techniques. A description of the functioning of ABS and TCS is detailed in the following.

1.4 Background on ABS system

1.4.1 Brief ABS system overview

The ABS system prevents the wheels to block in case of sudden hard braking requirements coming from the driver, maintaining wheel steer-ability in critical situations.

Four main components constitute the ABS system, as shown in Figure 1.6: speed sensors, valves, a pump, and a controller.

- speed sensors: the anti-lock braking system needs some way of knowing when a wheel is about to lock up. The speed sensors, which are located at each wheel, or in some cases in the differential, provide this information.
- valves: there is a valve in the brake line of each brake controlled by the ABS. On some systems, the valve has three positions:
  - position one, the valve is open; pressure from the master cylinder is passed right through to the brake.

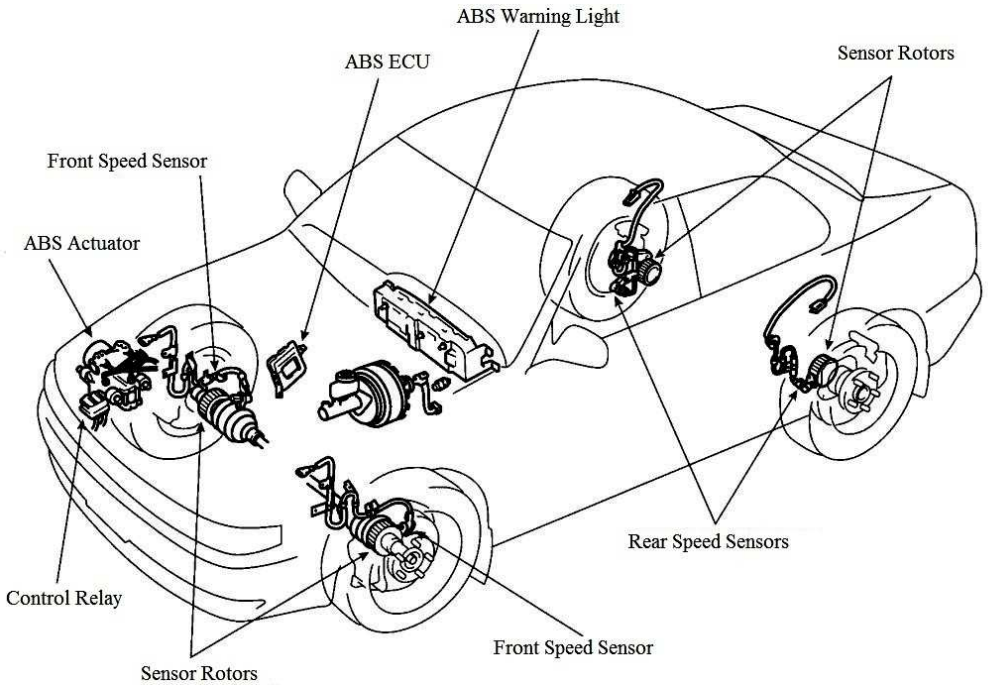

Figure 1.6: Standard ABS control system on a ICE vehicle according to [7].

  - position two, the valve blocks the line, isolating that brake from the master cylinder. This prevents the pressure from rising further, should the driver push the brake pedal harder.
  - position three, the valve releases some of the pressure from the brake.

- pumps: since the valve is able to release pressure from the brakes, there has to be some way to put that pressure back. This is what the pump does; when a valve reduces the pressure in a line, the pump is there to get the pressure back up.

- controller: the controller is an ECU type unit in the car which receives information from each individual wheel speed sensor. In turn, if a wheel loses traction, the signal is sent to the controller, the controller will then limit the brake-force and activate the ABS modulator which actuates the braking valves on and off.

The ECU constantly monitors the rotational speed of each wheel; if it detects a wheel rotating significantly slower than the others, a condition indicative of impending wheel lock, it actuates the valves to reduce hydraulic pressure to the brake at the

affected wheel, thus reducing the braking force on that wheel; the wheel then turns faster. Conversely, if the ECU detects a wheel turning significantly faster than the others, brake hydraulic pressure to the wheel is increased so the braking force is reapplied, slowing down the wheel. This process is repeated continuously and can be detected by the driver via brake pedal pulsation. Some anti-lock systems can apply or release braking pressure 16 times per second.

The limitations in classical ABS are mainly the delays that are due to the hydraulics and the solenoids that take part in the braking maneuver. In average, the solenoids and the hydraulic braking system have around 150 milliseconds of delay (the time it takes for the hydraulics and solenoids to reach the desired set point): 50 milliseconds of dead time and 100 ms of response time. The pulsations of a functioning ABS can impact the comfort of the passengers as well as the optimality of the braking power.

1.4.2 Existing controllers

The basis of ABS system is to monitor carefully the operating conditions of the wheels and adjust the applied braking torque. As shown in Figure 1.7, the ABS is typically designed to keep the tires operating within a desired range of slip. This will prevent the wheel from locking thus maintain steering and vehicle stability.

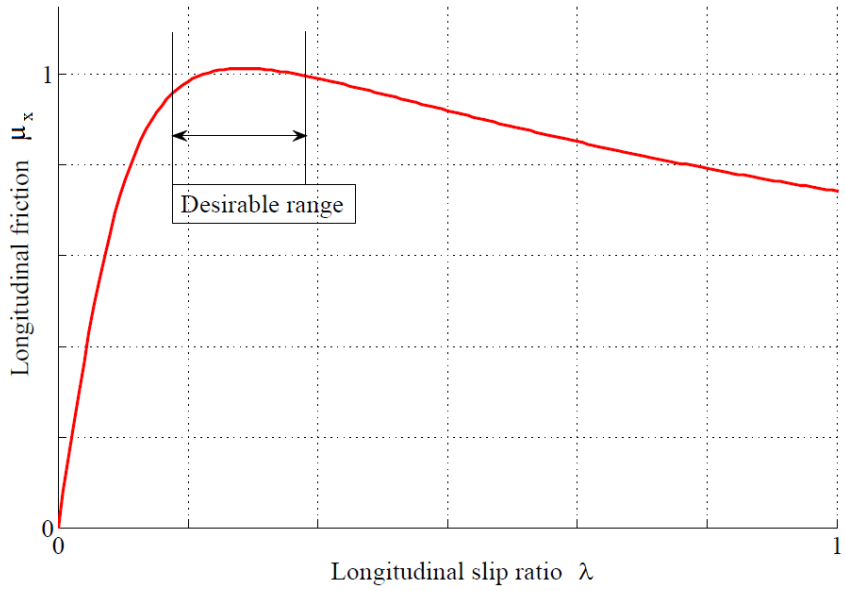

Figure 1.7: ABS system desirable working range.

In typical ABS, a bang-bang (on-off) controller is used, being a very common and inexpensive way to control a system. The bang-bang controller successfully regulate braking torque and ensure that the wheel will never lock-up, ensuring that the vehicle can maintain steering and yaw stability during braking as shown in Figure 1.8.

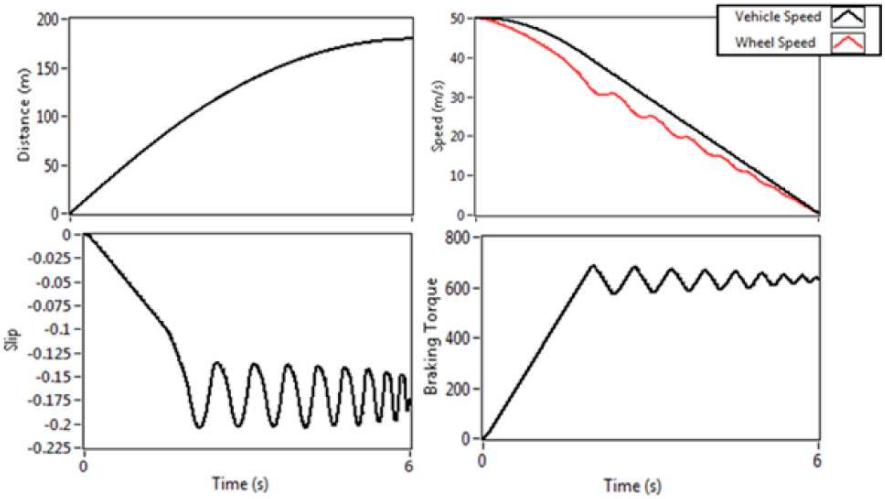

Figure 1.8: ABS braking simulation results according to [54].

As can be seen, oscillations [2] of the longitudinal slip ratio arise with this type of controller. To tackle the non-linear problem of the ABS control, researchers have employed various control approaches such as the soft computing. One classical approach is based on the PID control, used to improve the performance of the ABS, as shown in [84]. The PID controller is simple in design but there is a clear limitation in its performance. It does not posses enough robustness for practical implementation. For solving this problem, [39] applied a new Nonlinear PID (NPID) control algorithm. The NPID algorithm combines the advantages of robust control and easy tuning. Simulation results at various situations show that NPID controller has shorter stopping distance and better velocity performance than the conventional PID controller and a loop-shaping controller.

The optimal control of nonlinear system such as ABS is one of the most challenging and difficult subjects in control theory. In [87] a nonlinear output feedback control law is proposed for active braking control systems. The design is performed via Lyapunov-based methods and its effectiveness is assessed via simulations on a vehicle simulator. The change in the road conditions implies a continuous adaptation in controller parameter. In order to solve this issue, an adaptive control- Lyapunov

approach is suggested by [23] and similar ideas are pursued in [103], where a robust adaptive wheel slip controller is presented and in [100], where a dynamical tire road friction model is used to control the vehicle in emergency braking situations.

In [90], the authors developed the anti-lock braking control system integrated with active suspensions applied to a quarter car model by employing the nonlinear back-stepping design schemes. In emergency, although the braking distance can be reduced by the control torque from disk/drum brakes, the braking time and distance can be further improved if the normal force generated from active suspension systems is considered simultaneously.

Other results have been published coupling the ABS problem and the sliding-mode control. In [11], a design of sliding-mode controllers under the assumption of knowing the optimal value of the target slip was introduced. A problem of concern here is the lack of direct slip measurements. In [42] a sliding-mode controller is proposed to regulate the wheel slip, depending on the vehicle forward velocity. The proposed controller anticipates the upcoming values of wheel slip and takes the necessary action to keep the wheel slip at the desired value. The performance of the control algorithm as applied to a quarter vehicle is evaluated through simulations and experimental studies that include sudden changes in road conditions. The oscillation with the neighborhood of the switching surface cause chattering. Chattering is undesirable, since it involves extremely high control actuator activity, and furthermore may excite high-frequency dynamics and therefore it must be reduced (or eliminated) for the controller to perform properly.

In [91] an approach is presented to incorporate the wheel slip constraint a priori into control design so that the skidding can be avoided. A wheel torque and wheel steering control structure is proposed to transform the original problem to that of state regulation with input constraint. For the transformed problem, a low-and-high gain technique is applied to construct the constrained controller and to enhance the use of the wheel slip under constraint. Simulations show that the proposed control scheme, during tracking on a snow road, is capable of limiting the wheel slip, and has a satisfactory co-ordination between wheel torque and wheel steering.

Fuzzy logic control has been proposed to tackle the ABS problem for the unknown environmental parameters. In [99] an anti-lock brake system modeling is presented along with a fuzzy control method and in [45] a method for fuzzy learning control for ABS is shown.

However, the large amount of fuzzy rules makes the analysis complex. Some researchers have proposed fuzzy control design methods based on the sliding-mode control scheme. These approaches are referred to as fuzzy sliding-mode control (FSMC) design methods [92], called intelligent control in [51].

ABS control is a highly a nonlinear control problem due to the complicated relationship between friction and slip. Another impediment in this control problem is that the linear velocity of the wheel is not directly measurable and has to be estimated. Friction between the road and tire is also not measurable or may need complex sensors (dynamo-metric sensors).

However, all the strategies presented above rely weather on fixed thresholds of the longitudinal slip ratio, or are based on complex estimation algorithms and control laws, making them unsuitable for application in embedded systems. The main challenge in ABS control system is to find the optimal slip ratio and to control the wheel slip at this point, independently of the variation of the road conditions. This aspect could be achieved if, for example, the torque transmitted at the wheel is measurable and has a fast response time.

1.5 Background on TCS system

1.5.1 Brief TCS system overview

Traction control system operates in the case of vehicle acceleration and prevents the spin of the wheel if the driver's inputs require a significant acceleration. The TCS, also known as anti-slip regulation (ASR), is typically a secondary function of the anti-lock braking system (ABS) on production motor vehicles, designed to prevent loss of traction of driven road wheels. Intervention consists of one or more of the following:

- reduce or suppress spark sequences to one or more cylinders.
- reduce fuel supply to one or more cylinders.
- apply a brake force at one or more wheels.
- close the throttle, if the vehicle is fitted with drive by wire throttle.
- in turbo-charged vehicles, actuate a boost control solenoid to reduce boost and therefore engine power.

The basic idea behind the need of a traction control system is the difference between traction of different wheels evidencing apparent loss of road grip that compromise steering control and stability of vehicles. Difference in slip may occur due to turning of a vehicle or different varying road conditions for different wheels. In modern vehicles, traction control systems utilize the same wheel speed sensors employed by the anti-lock braking system. These sensors measure differences in rotational speed to determine if the wheels that are receiving power have lost traction. Delay of the actuators is also considerable in the functioning of TCS, from 100 milliseconds up to a few seconds. All the aspects presented above make the ABS and TCS functions a complex task that demands high computational cost and manifold embedded systems.

1.5.2 Existing controllers

For the TCS control problem, there are also many approaches utilized by researchers. In [40], a slip controller is proposed which uses the brake and the throttle actuators simultaneously. To avoid measurement problems and get a simple structure, the brake controller is designed using a Lyapunov redesign method and the throttle controller is designed using multiple sliding mode control. Through the hybrid use of brake and throttle controllers, the vehicle is insensitive to the variation of the vehicle mass, brake gain and road condition and can achieve required acceleration performance.

In [86], a sliding mode controller design for traction control systems is presented. In [49], two different control algorithms are presented for adaptive vehicle traction control, which includes wheel slip control, optimal time control, anti-spin acceleration and anti-skid control, and longitudinal platoon control. The two control algorithms are respectively based on adaptive fuzzy logic control and sliding mode control with on-line road condition estimation. The controllers both result in improved performance, compared with standard fuzzy logic control and standard sliding mode control which do not have adaptive algorithms.

As in the case of ABS control system, the main challenge for achieving TCS control is to find an optimal slip ratio for which the friction characteristics are not exceeding the maximum available. Fixed thresholds of the slip ratio are inefficient in the case of road condition variation. Therefore, an adaptive estimation technique has to be set up, in order to estimate in real-time the maximum friction. Electric motors [3] bring many advantages such as the information about the transmitted wheel torque. With the knowledge of the wheel dynamics and the transmitted torque, advanced estimation

techniques can provide the estimation of the maximum friction. The main advantages brought by the use of the electric motors are detailed in the following.

1.6 Vehicle electrification impact analysis

1.6.1 Powertrain architecture

An electric vehicle (EV), also referred to as an electric drive vehicle, uses one or more electric motors or traction motors for propulsion [4]. These motors can be conventionally placed centrally and deliver via a transmission system the power at the wheels, or, directly at the wheels with the use of newly introduced in-wheels motors. The most distinct advantage of an EV is the quick and precise torque response of the electric motors [5]. Another key advantage of electric EVs is regenerative braking, i.e. their ability to recover energy normally lost during braking as electricity can be restored to the on-board battery or to the electrical grid. Furthermore, the motors can be controlled independently, bringing new possibilities of advanced vehicular control [61].

1.6.2 In-wheel motor system

Figure 1.9: An example of in-wheel electric motor system [67].

In-wheel electric motors can operate in two modes [9]:

- as motor, converting electrical energy taken from a source (electric generator, battery, fuel cell) into mechanical energy used to propel the vehicle.

- as generator, converting the mechanical energy taken from a motor (ICE, the wheels during vehicle braking, etc..) in electrical energy used for charging the battery.

The in-wheel motors constitute the unique propulsion/deceleration system for the studied electric vehicle. Compared with ICE [**?**], in-wheel electric motors have some important advantages:

- they produce a high torque at low speeds.
- they have a high instant power and a high power density.
- torque values are easily reproducible.
- they provide a fast torque response.
- they provide the possibility for regenerative braking.

These characteristics ensure good dynamic performance and provide the possibility to estimate the driving or braking forces between tires and road surfaces in real time [35], which contributes a great deal to the application of new TCS/ABS control strategies based on road condition estimation [34].

The new in-wheel motors provide even more possibilities for active safety and trajectory control, since they are able to provide a braking torque on the wheels faster than conventional brakes which are normally used for this purpose. A further merit of a 4 in-wheel-motor driven electric vehicle (4WD EV) is that the driving/braking torque of each wheel is independently adjustable due to small but powerful motors, which can be housed in vehicle wheel assemblies. Besides, important information including wheel angular velocity and torque can be achieved much easier by measuring the electric current passing through the motor.

Compared with the conventional electric vehicle design [59] with one motor situated centrally driving two/four wheels by axles, the wheel motor arrangement has certain advantages. The first novelty of in-wheel electrification is that the vehicles can be controlled via a so-called ”drive-by-wire” system. Cars with electronic control of brakes and acceleration provide more opportunities for computerized vehicle dynamics such as:

- active cruise control, where the vehicle can maintain a given distance from a vehicle ahead.

- collision avoidance, where the vehicle can automatically brake to avoid a collision.
- emergency brake assist, where the vehicle senses an emergency stop and applies maximum braking.
- active software differentials, where individual wheel speed is adjusted in response to other inputs.
- active brake bias, where individual wheel brake effort is adjusted in real time to maintain vehicle stability.
- brake steer, where individual wheel brake bias is adjusted to assist steering.

While some of these features have started to appear as options for some internal combustion engine vehicles, optional ABS brakes can increase considerably the cost of a base model. As wheel motors brake and accelerate a vehicle with a single solid state electric/electronic system, many of the above features can be added as software upgrades rather than requiring additional systems/hardware to be installed. This should lead to cheaper active dynamic safety systems for wheel motor equipped road vehicles.

Eliminating mechanical transmission including gearboxes, differentials, drive shafts and axles, provides a significant weight and manufacturing cost saving, while also decreasing the environmental impact of the product.

1.6.3 Existing controllers

Based on these remarkable advantages, a couple of advanced motion controllers have been developed, in order to improve the handling and stability of a 4WD EV. The main problem in achieving a good ABS and TCS control is that friction between the road surface and the tire is unknown, leading to a higher complexity in the design of the controller. Anti-skid, or ABS control problem for the electric vehicles has been under research since many years now. In [52], an anti-skid controller with PI regulator for EV without speed sensor is proposed to prevent the slip between tire and road. When skid occurs, the equivalent inertia of the EV system will change, and the acceleration of the wheels will also change. A back EMF observer is constructed to acquire the information of speed as well as the acceleration. Then, a dynamic model error observer is setup using the back EMF signal to regulate the torque (current) command, and keep

the status of EV within a safe area. The simulations and experiment presented in the paper prove that the torque reduction of the speed sensor-less controller can prevent the skid phenomenon effectively, especially in the process of accelerating control.

Anti-skid control for electric vehicles was also studied in [79]. Here, the electric motor response was compared to ABS system response. Simulation results pointed out that feedback gain could not be high enough to prevent the rapid change of wheel velocity, if the actuator's delay is considerable. The delay in the hydraulic brake system seems to be such a limitation. Electric motor's torque response is much faster, therefore, more effective ABS-like system will be available. Thus, the ABS in the electric vehicle should be actuated by the electric motor.

For the traction control problem, the Model Following Control (MFC) approaches which do not need information on chassis velocity or acceleration sensors, are proposed in [80], where the advantages of the electric motor are shown, in [78],where a yaw moment stabilization for small electric vehicles is presentet, and in [24], where a motion stabilization control of electric vehicle under snowy conditions based on yaw-moment observer is described.

In these systems, the controllers only make use of torque and wheel rotation as input variables for calculation. Fewer sensors contribute not only to lower costs, but also to increase reliability and independence from driving conditions, which are the most outstanding features of this class of control systems. Nevertheless, these control designs based on compensation have to consider the worst stability case to decide the compensation gain, which impairs the performance of anti-slip control. Furthermore, gain tuning for some specific tire-road conditions also limits the practicability of this method. Recently, the MTTE approach [102] that requires neither chassis velocity nor information about tire-road conditions further upgrades the anti-slip performance of electric vehicles. In this system, use is only made of the torque reference and of the wheel rotation speed to estimate the maximum transmissible torque to the road surface; then the estimated torque is applied for anti-slip control implementation. This approach also shows its benefits for vehicle mass-perturbed operation. Since a human being is involved in the operation of a vehicle, the total mass potentially varies with different drivers and passengers.

Sliding-mode controller design for optimal slip control of electric vehicles based on fuzzy vehicle velocity estimation logic is presented in [72]. Here, the simulations and experiments indicate that a sliding mode controller for the wheel slip works well to

track a given desired wheel slip ratio. The disadvantage of the method it that it utilizes a fixed threshold for the wheel slip regulation, not taking into account the various road adhesion changes. An adaptive controller design for TCS control was presented in [76], but due to complex algorithms and numerous parameters, the convergence time of the estimations is significant and could affect the proper response of the traction control system.

Given all the aspects presented above, the presence of an unique actuator in acceleration and deceleration phases, could facilitate the control task that achieves TCS and ABS functions. One actuator means only one response time for both cases, therefore the two tasks could be correlated into a sole task: wheel control. Adding the fast response time of hub-wheels can provide advanced control techniques that are applied directly at the wheels as function of the available friction.

Even if the electric motors are used for the control approaches presented above, none of them estimate the maximum friction. They are still based on standard wheel slip regulation, and do not fully consider the advantages of the wheel electrification. Therefore, a maximum friction estimation technique and the adequate control techniques are the main focus of the present work.

1.7 A new approach for dynamic longitudinal estimation and control

The final objective is to accomplish a full longitudinal control of an electric vehicle equipped with 4 in-wheel motors, traveling in varying road conditions and with various acceleration constraints or speed requirements provided by the driver. Therefore, the controller will have to be able to maintain a stable behavior of the vehicle and to adapt to the varying travel conditions and driver requirements. The attention will be focused on the major advantages that the in-wheel electric motor brings to improve the development of the control commands necessary to obtain lateral and longitudinal control of the vehicle. The fast response and the reproducibility provided by the electric motor will be utilized as a starting point in estimating the friction forces between the wheels and the road surface. It will allow to apply a control as function of the maximum available friction, having as control input the electric motor torque. With the capabilities of the electric motors to provide equally a braking torque (generator mode) and a traction torque (motor mode), with the possible over-sizing

of the generated torque, simulations will be made in both acceleration and braking phases using as ***unique*** actuator the instantaneous electric motor torque. Therefore, the only control command actuator will be the in-wheel motor torque, with an optimal distribution of the torques to the wheels, e.g., smaller torques will be sent to the wheels which have small adherence with the surface, and greater torques to the wheels with good grip on the surface. To optimize the performance of such system, we want to study the coupling between high-level layers of estimation/control and the so-called low-level layers of torque distribution management. The overall system should be flexible and adaptable at various environmental changes.

For this purpose, different estimation techniques will be studied in order to achieve usable maximum friction values. These values will be used by the control strategy which will compute an adequate torque to be applied at the wheels, in order to maintain grip in acceleration or deceleration. Moreover, the extreme cases of rapid friction variation will be studied in order to verify the robustness of the proposed control methods. Likewise, more *realistic* scenarios will be tested, such as hard acceleration started from zero vehicle speed, or hard braking maneuvers at high speeds with varying road surface conditions. At the same time, simulations will be carried on the case where perturbation arise or noise is propagated on different system variables. The final goal is to have a robust estimation and control technique that will cope with all possible perturbations that can arise in computations or the continuous variation of the road surface adhesion. Simulations will be carried out in Matlab/Simulink environment.

Chapter 2

Modeling

Contents

2.1 Overview

Generally, modeling is categorized in qualitative modeling and quantitative modeling [81]. Qualitative methods [6] produce information only on the particular cases studied, and any more general conclusions are only hypotheses [47]. Quantitative methods can be used to verify which of such hypotheses are true [46]. Qualitative modeling concerns representation and reasoning about continuous aspects of entities and systems in a symbolic, human-like manner [21]. Qualitative mathematics formalizes notions of quantity and relationships at a more abstract level of detail [22] than mathematics as traditionally used in science and engineering [93]. Quantitative modeling requires selecting and identifying relevant aspects of a system and to use mathematical models to quantify them [55]. Using quantitative methods, it is possible to give precise and testable expression to qualitative ideas [14].

Generally, a model is a representation of the architecture and functioning of some system of interest [56]. A model is similar to but simpler than the system it represents. One of the purposes of a model is to enable the possibility to predict the effect of changes to the system. On the one hand, a model should be a close approximation of the real system and integrate most of its notable features. On the other hand, it should not have a high degree of complexity in order to be understood and experiment with it. A good model is a trade-off between realism and simplicity. The complexity of a model is recommended to increase iteratively in order to make the simulation process easy to assimilate. An important issue in modeling is model validity. Model validation techniques include simulating the model under known input conditions and comparing model output with system output. Generally, a model intended for a simulation study is a mathematical model developed with the help of simulation software. Mathematical model classifications include deterministic (input and output variables are fixed values) or stochastic (at least one of the input or output variables is probabilistic); static (time is not taken into account) or dynamic (time-varying interactions among variables are taken into account). Typically, simulation models are stochastic and dynamic.

A simulation of a system is the operation of a model of the system in different environments with different initial conditions or under perturbation. The model can be reconfigured and experimented with, in order to obtain the desired results. The operation of the model can be studied, and hence, properties concerning the behavior of the actual system or its subsystem can be inferred. Simulation is a tool to evaluate the performance of a system, existing or proposed, under different configurations of interest and over specific periods of real time. Simulation is used before an existing system is altered or a new system built, to reduce the chances of failure to meet specifications, to eliminate unforeseen constraints, to prevent under or over-utilization of resources, and to optimize system performance.

According to practitioners, simulation modeling and analysis is one of the most frequently used operations research techniques. Simulation modeling and analysis makes it possible to:

- Obtain a better understanding of the system by developing a mathematical model of a system of interest, and observing the system's functioning in detail over long periods of time;

- Test hypotheses about the system for feasibility;

- Compress time to observe certain phenomena over long periods of time or expand time to observe a complex phenomenon in detail;
- Study the effects of certain changes on the operation of a system by altering the system's model or introducing perturbations into the model; this can be done without disrupting the real system and significantly reduces the risk of experimenting with the real system;
- Experiment with new or unknown situations about which only weak information is available;
- Identify the "driving" variables - ones that performance measures are most sensitive to - and the inter-relationships among them;
- Use multiple performance metrics for analyzing system configurations;

Our model of interest is the road vehicle. Two main philosophies are used to model road vehicles:

- forward model (or driver driven),
- backward model (or vehicle driven).

In a forward-looking model, the driver model will send an acceleration demand or brake pedal demand to the different powertrain and component controllers (e.g., in ICE configuration: throttle for engine, displacement for clutch, gear number for transmission, or mechanical braking for wheels) in order to follow the desired vehicle speed profile. The driver model will then modify its command depending upon how close the profile is followed. As components react as in reality to the commands, we can implement advanced component models, take into account transient effects (such as engine starting, clutch engagement/disengagement, or shifting), or develop realistic control strategies that would be later implemented in real-time applications.

By contrast, in a backward-looking model, the desired vehicle speed goes from the vehicle model back to the engine to finally find out how each component should be used to follow the speed cycle. Because of this model organization, quasi-steady models can only be used and realistic control cannot be developed. Consequently, transient effects cannot be taken into account. Backward models are usually used to define trends while forward looking models allow selection of powertrain configurations, technologies as well as development of controls that will later be implemented in

the vehicles. Simulation tools, more specifically forward-looking models which target specific vehicles, are widely used in the industry to properly address the component interactions that affect fuel consumption and performance. With systems becoming increasingly complex, predicting the effect of combining several systems is becoming a difficult task due to the non-linearity of some phenomena (e.g. the interaction between the tire and the road surface).

To completely represent a vehicular system in realistic environments, a tire-road interaction model has to be taken into account, since it defines vehicle's behavior in different adherence combined with speed profiles scenarios. This is the core of the problematic of vehicular dynamic control, and a realistic tire friction model is needed in order to obtain proper simulation results of the vehicle dynamic behavior. On one hand, a representative vehicle model has to be set up to meet analysis requirements, and on the other, a driver model needs to be considered, to simulate realistic driver's actions. The driver model will help simulate a speed profile tracking, generating the braking and the acceleration forces, as well as other secondary functions as passenger comfort. The considered vehicle model is a simulation-oriented model, its equations retaining the important aspects in the wheel dynamics and neglecting secondary parameters. Its purpose is to isolate the wheel dynamics and tire-road friction characteristics from other vehicle sub-systems, in order to highlight the innovation of the use of in-wheel electric motors.

2.2 Vehicle model description

2.2.1 One wheel vehicle model

The starting point of our research methodology is the one wheeled vehicle model. It is a simple, yet quite sufficient model to represent the wheel and vehicle dynamics and to provide a good starting basis for the estimation and control strategies. A graphical longitudinal view of the model is presented in Figure 2.1.

The overall system equations including the vehicle and wheel dynamics can be

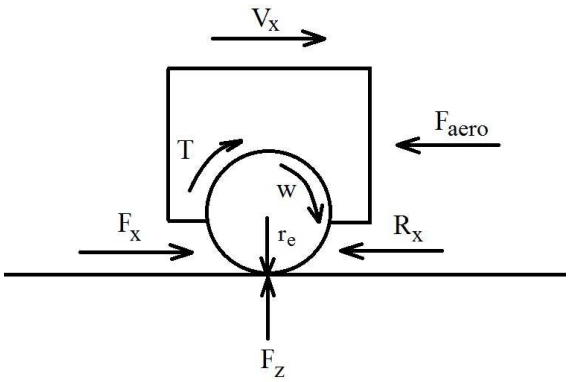

Figure 2.1: One wheel vehicle model.

written as follows [75, 38]:

$$m\dot{V}_x = F_x - F_{aero}, \tag{2.1}$$

$$I\dot{\omega} = T - r_e F_x - R_x, \tag{2.2}$$

$$F_z = mg, \tag{2.3}$$

$$F_x = \mu(\lambda) F_z, \tag{2.4}$$

$$\lambda = \frac{r_e\omega - V_x}{\max(r_e\omega, V_x)}. \tag{2.5}$$

In this model, the vehicle dynamics is represented by equation (2.1), having made the assumption that the slope of the road is equal to zero. Here, F_x is the traction or braking force and $F_{aero} = (\rho C_d V_x^2)/2$ is the aerodynamic drag force as function of the air density $\rho = 1.3kg/m^3$, the aerodynamic drag coefficient $C_d = 0.32$ and the square of the chassis velocity V_x^2.

The wheel dynamics is described in equation (2.2), with the rolling resistance force $R_x = mgC_r$, considered constant. The term C_r defines the rolling resistance coefficient and is set to $C_r = 0.01$. In order to avoid a contact problem, the wheels are assumed to be always in contact with the ground. A further simplification is that the wheel center is assumed to always stay at the same distance r_e perpendicular to the ground. This is of course not accurate, but because of uncertain wheel geometries and elastic properties any other model would not be much more accurate while just increasing the complexity [98]. As a result of this simplification, the tire forces are assumed to attack perpendicularly below the wheel center. Since these forces have a

quite complicated distributed area in reality, this assumption is as good as any other for small angles. In equation (2.2) an important assumption is made, being that the transmitted wheel torque T is measurable due to the use of the in-wheel electric motor.

The normal force on the tire is considered constant in this model (equation (2.3)), since no suspension system was taken into account. The friction between the tire and the road surface is represented by the term $\mu(\lambda)$ in equation (2.4). Its expression is function of the longitudinal slip ratio, represented by equation (2.5). Longitudinal slip ratio is the amount of slip between the the wheel and the road surface when traction or braking force is applied.

Even though this is a simplistic model, it represents all the important dynamics that can influence the dynamic behavior of the vehicle, such as wheel slip in acceleration or wheel skid in deceleration, as shown in Figure 2.2. It will help in the development of the maximum friction estimation and to design the adequate control laws in order to achieve wheel slip and skid control. A four-wheeled vehicle model used to extend longitudinal vehicle dynamics is described in the following.

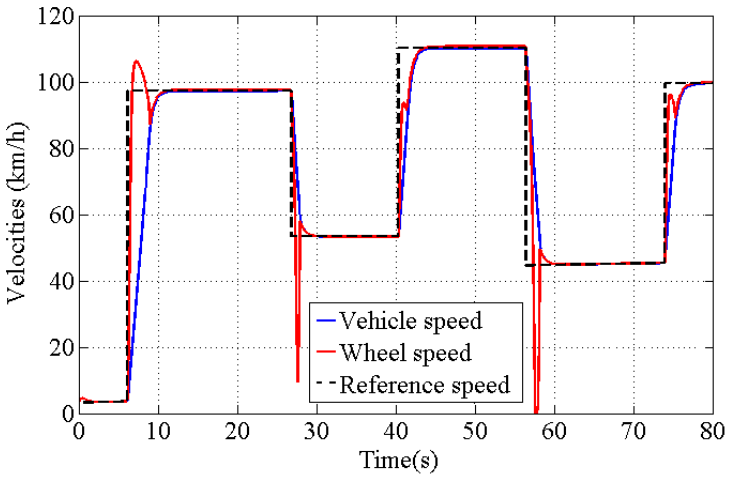

Figure 2.2: Model behavior in acceleration and braking phases.

2.2.2 Four wheels vehicle model

Four-wheeled vehicle model is introduced to take into consideration the load transfer that occurs during braking or acceleration dynamics. This model extends the one-

wheeled vehicle model, solely longitudinal dynamics being considered. The full four-wheeled vehicle model is described in [98]. Simplifications were made to this model to cope with simulation demands. The four wheeled mechanical model consists of the main vehicle mass to which the four wheels are attached via a suspension system [98]. The main body u can theoretically assume any position in space and has therefore 6 degrees of freedom, 3 for position and 3 for orientation. The position is represented by the coordinates x y and z of its center of mass in an inertial reference frame A as shown in the figures 2.3 and 2.4.

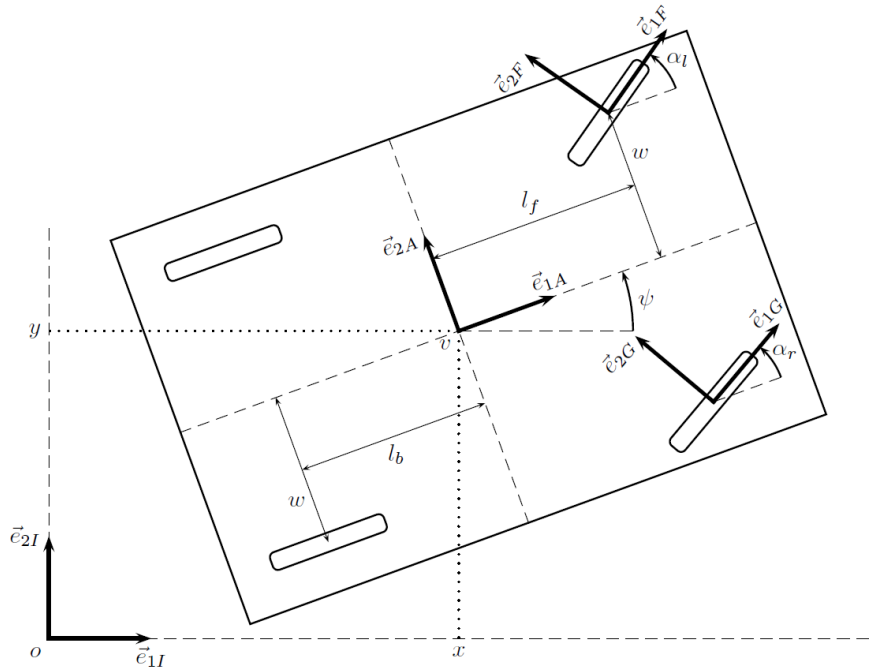

Figure 2.3: Top view of the described model (no roll and pitch) according to [98].

The orientation leaves the center of mass position unchanged and is represented by a commonly used set of Euler-angles which consist of three elementary rotations performed one after another. The first rotation is by the angle ψ around the z-axis $\overrightarrow{e}_{3I}$ of the inertial reference frame. This rotation is called the yaw rotation and is shown in Figure 2.3.

The second rotation is by the angle θ around the negative x-axis $-\overrightarrow{e}_{1A}$ of the first frame A as shown in figure 2.4. This rotation is called the roll rotation.

The third rotation is by the pitch angle ϕ around the negative y-axis $-\overrightarrow{e}_{2B}$ of the second frame B as depicted in figure 2.5. Note that this pitch angle is defined positive when the front of the vehicle goes up. This leads to the reference frame C which is

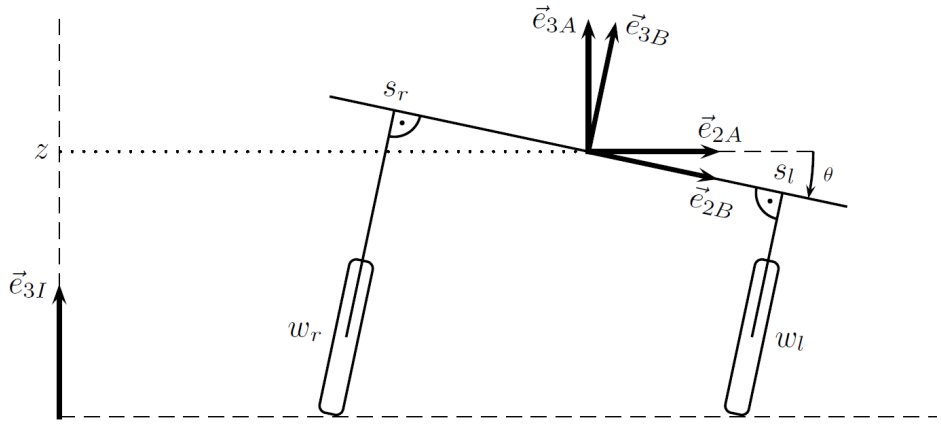

Figure 2.4: Front view of the described model (no pitch) according to [98].

attached to the main vehicle body.

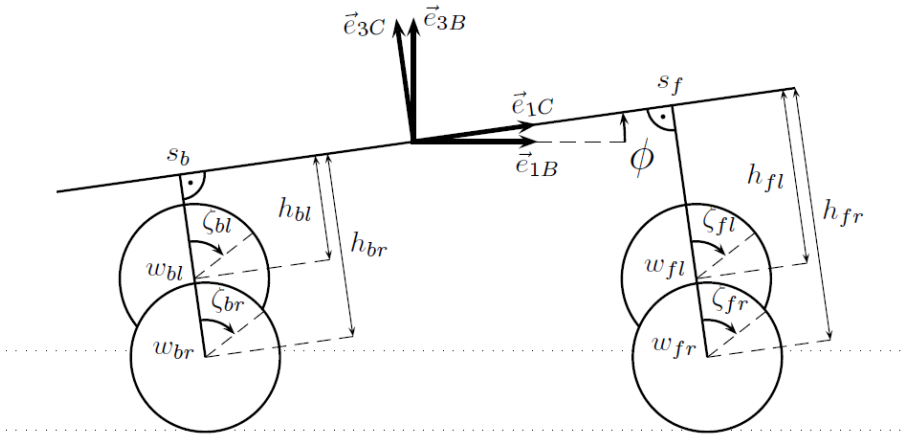

Figure 2.5: Suspension of the described model according to [98].

Each wheel is modeled as having its own suspension, which consists of a linear prismatic joint with one degree of freedom, and a spring-damper system affixed to that joint. No mass is associated with the suspension part, but if necessary, it can be approximated by adding its mass to the wheel mass and its inertia with respect to the wheel center to the inertia of the vehicle body. Additionally, the two front wheels can each be steered by an individual steering angle α_l and α_r, which can later be calculated from a single steering angle.

The system equations are found by using the Lagrangian approach [75]. The min-

imal coordinates for the four wheeled model are $q = (x, y, z, \phi, \omega_i)$. Since we are interested in building a longitudinal control of the vehicle modeled as shown above, the yaw and roll motions and the steering angles are not taken into account. Therefore, the complete model can be viewed as a bicycle model, as shown in Figure 2.6. The system inputs are the four combined motor/brake torques T_i acting on the wheels.

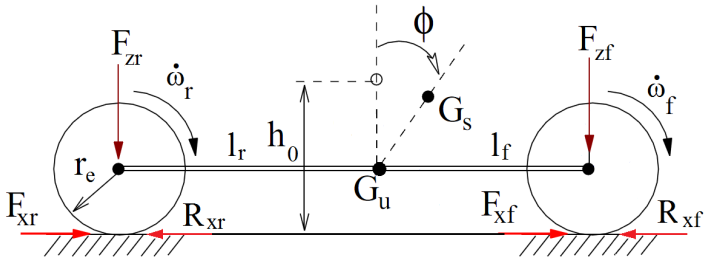

Figure 2.6: Side view of the described model according to [98].

Here, G_s and G_u are respectively the centers of gravity of the suspended and unsuspended mass, l_f and l_r are the distances from the center of mass to the front and rear axle and ϕ is the pitch angle. The suspension dynamics are taken into account, with the associated load transfer that arises when the vehicle is accelerating or braking. The forces that act on each pair of wheels are shown in Figure 2.6. The overall system equations including the vehicle, wheel and load transfer dynamics can be written as follows:

$$M\dot{V}_x = F_x - F_{aero}, \tag{2.6}$$

$$I\dot{\omega}_i = T_i - r_e F_{x_i} - C_r F_{z_i}, \tag{2.7}$$

$$F_x = \sum_{i=1}^{4} F_{xi}, \tag{2.8}$$

$$F_{x_i} = \mu_{x_i}(\lambda) F_{z_i}, \tag{2.9}$$

$$F_{z_i} = m_{w_i} g - k(l_i \phi - h_0) - c l_i \dot{\phi}. \tag{2.10}$$

$$\tag{2.11}$$

Here, l_i is distance from the center of gravity to the axles (m) and the indexes are $i = fl, fr, bl, br$ with the signification: fl=front left, fr=front right, bl=back left and br=back right.

The suspended mass is connected to the unsuspended mass and assumed to be

allowed to rotate by the pitch angle ϕ. The center of mass G_s of the suspended mass is assumed to be at a distance h from its rotational axis as shown in Figure 2.7 and lies directly above the center of mass G_u of the unsuspended mass for $\phi = 0$. Additionally there is a spring-damper combination located at each of the two wheels as seen in Figure 2.7 which forms the suspension of the system. This model does not correspond to most real systems as usually each wheel has a suspension on its own. However, such a model is fine for a first approximation as it shows a very similar behavior to a real system. This model does not yet include any form of friction to the ground,

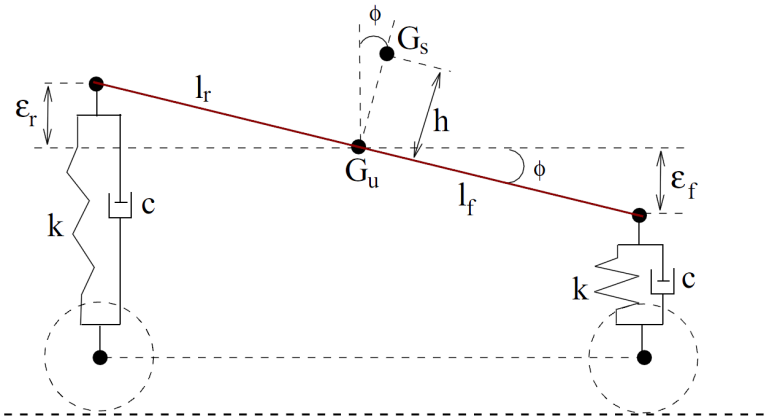

Figure 2.7: Side view of the model, showing the simplified suspension according to [98].

which is instead represented by the external forces F_{xf} and F_{xr}. These forces have to be calculated using an additional friction model for which a Pacejka formula is used as described in section 2.4.

For the suspension, a linear spring-damper system is assumed so the suspension force is simply $F_s = -k(h_w - h_{0w}) - c\dot{h}_w$. Note that the parameter h_{0w} is the unsprung vertical distance between the wheel-center and vehicle's CM and therefore differs by a constant from the unsprung suspension length. The term h_w is vertical distance from the vehicle reference frame from the CM to the center of each wheel, i.e. the displacement of each suspension. The resulting generalized suspension force is therefore:

$$f_{s,w} = -\left(\frac{\partial h_w}{\partial q}\right)^T (k(h_{lf} - h_{lf,0}) + c\dot{h}_w). \tag{2.12}$$

2.3 Flatness-based driver model

The human factor (driver behavior) plays an important role in future automotive technologies aimed at both improving traffic safety and preserving the environment. The latest vehicles, equipped with rich sensors, and connected to the Internet are now making possible the analysis of driver's behavior. In the present work, driver's actions are represented by reference speed profiles, obtained by the inversion of the vehicle dynamics equation.

Drivers have specific habits when operating a road vehicle. Their driving styles differs in how they hit the gas and brake pedals, how they turn the steering wheel, and how much distance they keep to follow a vehicle safely and comfortably. In [69], driving behaviors are modeled as car-following and pedal operation patterns. The relationship between following distance and velocity mapped into a two-dimensional space is modeled for each driver with an optimal velocity model approximated by a nonlinear function or with a statistical method. The work [82] presents the development of the modeling and recognition of human driving behavior based on a stochastic model. First, a parameter estimation algorithm for the model with multiple measured input-output sequences is developed based on the expectation-maximization algorithm. Second, the developed parameter estimation algorithm is applied to driving data with the focus being on driver's collision avoidance behavior.

Our interest in modeling a driver's behavior is much more simple than the approaches presented above. In order to apply different control techniques on to the vehicle model, a basic driver model is considered. It will simulate the driver's actions (acceleration, braking) in different realistic case studies. Driver's requirements can be translated in different reference speed profiles, as, for example, a hard push of the acceleration pedal signifies a sudden high speed tracking demand. Therefore, its demands will result in different torque demands, that are transmitted to the wheel. These torque demands translate into reference speed values to track. The most suitable strategy in trajectory tracking is the so-called "flatness" theory [57]. Hence, the driver model is in fact regarded as a flatness-based controller used to track a reference speed profile, providing the necessary torques to accelerate or brake the vehicle.

2.3.0.1 Brief differential flatness recall [70]

A non-linear system is called differentially *flat* [94] is there exists a collection $y = (y_1, ..., y_m)$ (where m is the number of independent inputs in the system) of functions, called a *flat output*, with the following three properties:

1. The components of y can be expressed in terms of the system variables z via differential relations of the type

$$y_i = P_i(z, ..., z^{(\rho_i)}) \tag{2.13}$$

for $i = 1, ..., m$

2. The components of y are differentially independent, i.e. they are not related by any (non-trivial) differential equation

$$Q(y, ..., y^{(\alpha)}) = 0. \tag{2.14}$$

3. Every variable z_i used to describe the system, for instance states or inputs, is directly expressed from y using only differentiation. In other words, any such z_i satisfies a relation of the type

$$z_i = R(y, ..., y^{(\gamma)}) \tag{2.15}$$

The third property yields a simple solution to the problem of tracking the collection of reference trajectories $y_r(t) = (y_{1_r}(t), ..., y_{m_r}(t))$. The second property ensures that the different components of $y_r(t)$ can be chosen independently.

This notion can also be defined, for the case of systems with a state $\mathbf{x}$ and controls $\mathbf{u}$ by

Definition 1. *The system*

$$\dot{\boldsymbol{x}} = f(\boldsymbol{x}, \boldsymbol{u}) \tag{2.16}$$

with $\boldsymbol{x} \varepsilon \boldsymbol{R}^n$ *and* $\boldsymbol{u} \varepsilon \boldsymbol{R}^m$ *is differentially flat [71] if there exists a set of variables, called flat output,*

$$\boldsymbol{y} = h(\boldsymbol{x}, \boldsymbol{u}, \dot{\boldsymbol{u}}, ..., \boldsymbol{u}^{(r)}), \quad \boldsymbol{y} \varepsilon \boldsymbol{R}^m, \, r \varepsilon \boldsymbol{N} \tag{2.17}$$

such that

$$\boldsymbol{x} = A(\boldsymbol{y}, \dot{\boldsymbol{y}}, ..., \boldsymbol{y}^{(q_x)}) \tag{2.18}$$

$$\boldsymbol{u} = B(\boldsymbol{y}, \dot{\boldsymbol{y}}, ..., \boldsymbol{y}^{(q_u)}) \tag{2.19}$$

with q an integer, and such that the system equations

$$\frac{dA}{dt}(\boldsymbol{y}, \dot{\boldsymbol{y}}, ..., \boldsymbol{y}^{(q+1)}) = f(A(\boldsymbol{y}, \dot{\boldsymbol{y}}, ..., \boldsymbol{y}^{(q)}), B(\boldsymbol{y}, \dot{\boldsymbol{y}}, ..., \boldsymbol{y}^{(q+1)})) \tag{2.20}$$

are identically satisfied.

2.3.0.2 Application to a driver model

To compute the adequate torques in order to follow a reference speed, a flatness-based speed tracking scheme is set up. Flatness is a system property which extends the linear systems controllability to nonlinear dynamical systems. We will use flatness theory to show that V_x is a flat output for the vehicle model. For this purpose, system variables have to be expressed as function of V_x and its derivatives.

From equation (2.5) of the longitudinal slip ratio we pull the expression of the wheel angular speed as function of V_x:

$$\omega = \frac{1}{r_e}(V_x + \lambda \max(r_e\omega, V_x)). \tag{2.21}$$

Therefore, the derivative of the wheel angular speed is:

$$\dot{\omega} = \frac{1}{r_e}(\dot{V}_x + \dot{\lambda} \max(r_e\omega, V_x) + \lambda \dot{\max}(r_e\omega, V_x)). \tag{2.22}$$

To take into consideration the case where $r_e\omega = V_x$ and to compute its derivative, the function *max* is approximated, in the neighborhood of $|r_e\omega - V_x| < \eta$, with:

$$\max(r_e\omega, V_x) \approx g * \max(r_e\omega, V_x). \tag{2.23}$$

where g is an impulse Dirac delta function and $\eta = 0.01$.
The traction or braking force F_x is expressed as function of $\dot{V}_x$ and V_x from equation

(2.1), replacing also the aerodynamic drag force by its expression $F_{aero} = \frac{1}{2}\rho C_d V_x^2$:

$$F_x = m\dot{V}_x + \frac{1}{2}\rho C_d V_x^2. \tag{2.24}$$

Finally, the traction of braking torque applied at the wheel is expressed as function of V_x and its derivative, replacing the expressions for $\dot{\omega}$ and F_x in the wheel dynamics equation 2.2:

$$T = \frac{I}{r_e}(\dot{V}_x + \dot{\lambda}\max(r_e\omega, V_x) + \lambda\dot{\max}(r_e\omega, V_x)) + r_e(m\dot{V}_x + \frac{1}{2}\rho C_d V_x^2) + R_x. \tag{2.25}$$

All system variables were written as function of V_x and its first order derivative, a fact that proves that V_x is a flat output of our system. Therefore, a flatness-based reference tracking scheme can be developed. We have shown that the vehicle model is trivially flat [57], with V_x being a flat output. Making the (physically sound) assumption that the wheel dynamics is fast compared to the car body one, the model (2.1)-(2.5) reduces to:

$$m\dot{V}_x = \frac{1}{r_e}(T - R_x) - F_{aero}. \tag{2.26}$$

A linearizing transformation with new input u is given by $T = r_e(F_{aero} + \frac{1}{r_e}R_x + mu)$, yielding the trivial dynamics $\dot{V}_x = u$. An PI controller with anti-windup is then chosen for u:

$$u = PI_{out} + \dot{V}_{x_{ref}}. \tag{2.27}$$

The final expression for the flatness-based controller is:

$$T_{flat} = r_e(F_{aero} + \frac{1}{r_e}R_x + mPI_{out} + m\dot{V}_{x_{ref}}). \tag{2.28}$$

The "anti-windup" reacts when the control reaches the limits of the actuator, thereupon the integral term could increase indefinitely. A combination of conditional integration and calculation of the output of the integrator as a function of the controller output PI is used here. When the PI output goes out of the electric motor torque limitations range, the integral term stops charging. The output of the PI controller is shown in algorithm 1 (with $\nu = V_{x_{ref}} - V_x$ and u_{min}, u_{max} being the torque ranges of

the electric motor).

Table 2.1: Algorithm 1: PI controller with anti-windup.

---

if $((\nu \geqslant 0)$ and $(PI_{out} \geqslant u_{max}))$ or $((\nu \leqslant 0)$ and $(PI_{out} \leqslant u_{min})$

$$PI_{out_{t_k}} = K_p \nu_{t_k} + K_i (\int \nu)_{t_{k-1}} dt$$

else

$$PI_{out_{t_k}} = K_p \nu_{t_k} + K_i (\int \nu)_{t_k} dt,$$

The purpose of driver model is to provide the input torque to track the $V_{x_{ref}}$ trajectory, independently of the fact that the latter could induce slip or not. For example, for a given speed profile, the driver model will generate the torque signal (T_{driver}) presented in Figure 2.8 in order to track it.

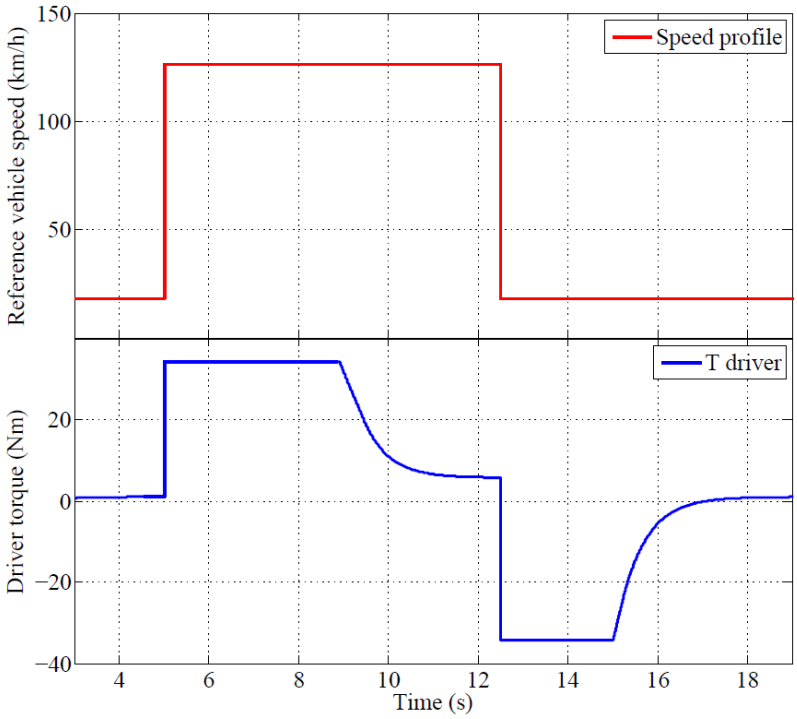

Figure 2.8: Torque demand generated by the driver model.

2.4 Tire-road interaction model

The influence of the friction on the longitudinal dynamics is hard to quantify since it depends on numerous factors which are not easily separable. For a better understanding of this phenomenon, it is helpful to first look closer at the Pacejka formula [73], which is an empirical formula whose results are usually close to the reality.

2.4.1 Standard Pacejka model

The Pacejka formula [73] calculates the longitudinal tire force F_x. The static input is the b_n coefficients (which have fixed values depending on the type of the tire), and the dynamic input is load or the normal force F_z and the longitudinal slip ratio λ. The final form of F_x can be written as follows:

$$F_x = D\sin(C\arctan(B\lambda - E(B\lambda - \arctan(B\lambda)))) \tag{2.29}$$

The B, C, D and E variables are computed as follows :

- $D = (b_1F_z + b_2)F_z$ (the peak value of the curve)
- $C = b_0$ (the shape factor determines the shape of the peak)
- $B = \frac{(b_3F_z^2 + b_4F_z)e^{-b_5F_z}}{CD}$
- $E = b_6F_z^2 + b_7F_z + b_8$

Some interpretations of the Pacejka coefficients are the following:

- D is the maximum force the tire can generate, at its peak performance.
- BCD is the longitudinal stiffness of the tire.
- $\arctan(BCD)$ gives the angle of the curve where it passes through the origin. This is a stiffness indicator as well. The curve usually has the following shape: linear from the origin, peaking (at height D), then gradually coming down again as shown in figure 2.9
- b_1 is the load sensitivity, while b_2 is the constant friction.

Table 2.2: Pacejka parameters reference values.

Parameter	Dry road	Wet road	Snowy road
b_0	1.5699	1.40	1.45
b_1	-25.63	-20.5	-15.5
b_2	1305	1000	700
b_3	6.825	6.825	6.825
b_4	395.69	395.69	395.69
b_5	0	0	0
b_6	0.0034	0.0034	0.0034
b_7	-0.0082	-0.0082	-0.0082
b_8	0.6565	0.6565	0.6565

The constant parameters $b_0 - b_8$ have fixed values depending of the tire and the road conditions. In Table 2.2 are shown the considered reference values of the Pacejka parameters for the three main types of roads: dry, wet and snowy.

From the equation (2.4) of the vehicle model, one can see that the friction μ_x is the ratio between the longitudinal force F_x calculated as above, and the normal force on the tire. So, the longitudinal friction between the road and the tire (μ_x), modeled by a Pacejka function of the longitudinal slip (λ) has the form shown in Figure 2.9.

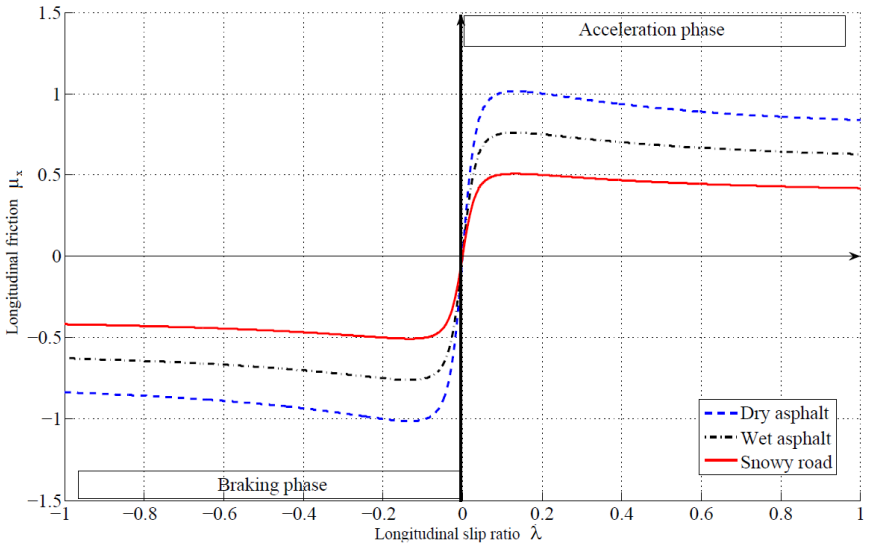

Figure 2.9: Pacejka curves modeling the friction.

As can be seen, there are different curves for different road surface conditions. The peak of each curve differs from one type of road surface to another, as well as the

value of the slip ratio corresponding to that peak. So, for example, for a dry road surface, the peak of the curve is approximately at $\mu_x = 1$, and the values of the slip ratio at which it reaches this value is $\lambda = 0.1$. On a surface with a small friction, the peak value for μ_x is reached at $\lambda = 0.05$. Therefore, different road surfaces imply different peak values for the friction at different slip ratios, giving the complexity of the interaction between the wheel and the road.

Of course, these are theoretical curves, the real peak values may differ for different types of surfaces (cobblestone, asphalt, etc.), but having roughly the same shape as shown in Figure 2.9. The curves have an interesting characteristic, regarding the force applied at the wheels and the traction that is obtained. If the traction force applied at the wheels give a friction smaller than the peak value, then we have a good grip on to the surface. However, once the peak value is exceeded, applying more force will only lead to less traction and more wheel slip. The phenomenon is shown in Figure 2.10, for the acceleration and braking phases. Once the peak of the friction curves is exceeded, applying the traction torque will induce an excessive spin of the wheels. This is the reason why traction control and anti-lock systems are such complex systems and require adaptation at the road surface conditions, in order to achieve good grip between the wheel and the surface.

2.4.2 Dynamic Pacejka model

Instead of the curves modeled by Pacejka, in real environments we find a cloud of points whose position can vary from a sample time to another for the same road conditions [77, 30], as shown in Figure 2.11.

Therefore, instead of considering only three theoretical curves modeling the main types of road surfaces (dry, wet and snowy), we interpret them as continuously varying during the driving maneuver. This approach will give a more realistic modeling of the road surface conditions and will allow to have a better view of the results of the proposed method in this environment.

In Pacejka formula, parameters C and D have the most noticeable influence on the curves. One interpretation of the Pacejka coefficients is the following:

- C represents the behavior of the curves once the maximum value is exceeded . A small C will be translated in a small slope of the curve after its peak. This parameter has also an influence on the slope of the pseudo-linear segment of the curves, as shown in Figure 2.12.

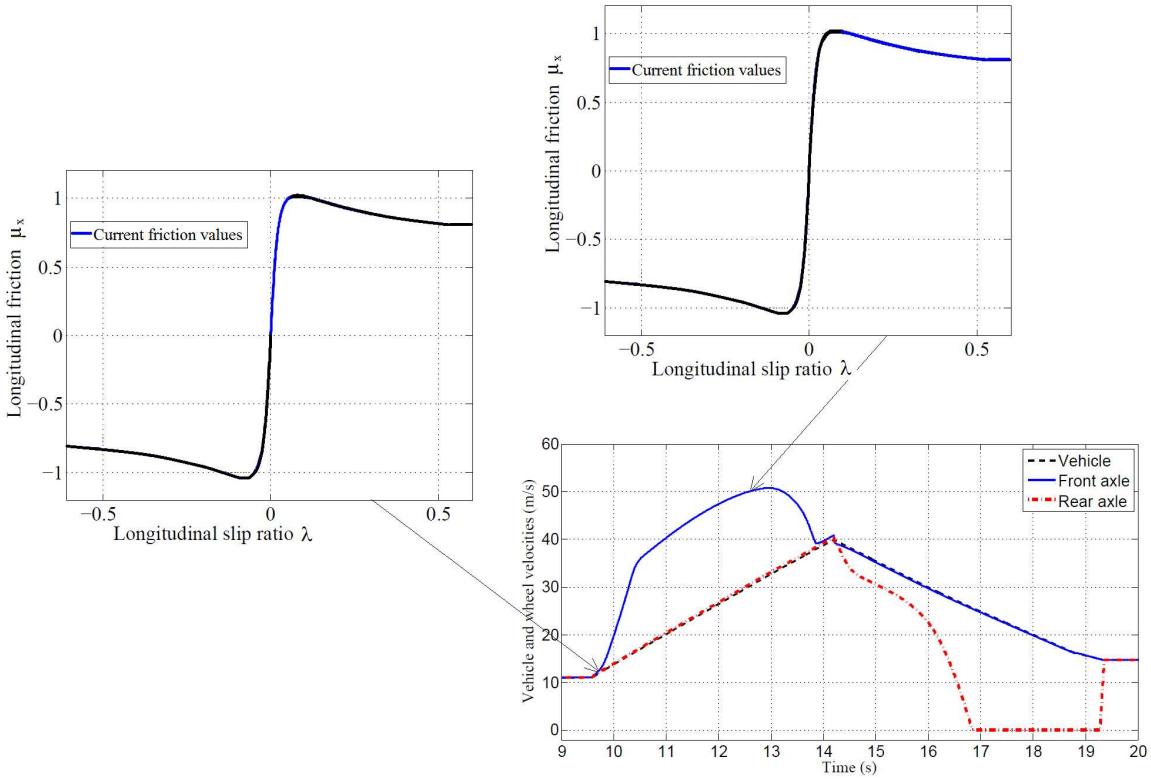

Figure 2.10: Nonlinear behavior of the friction curves.

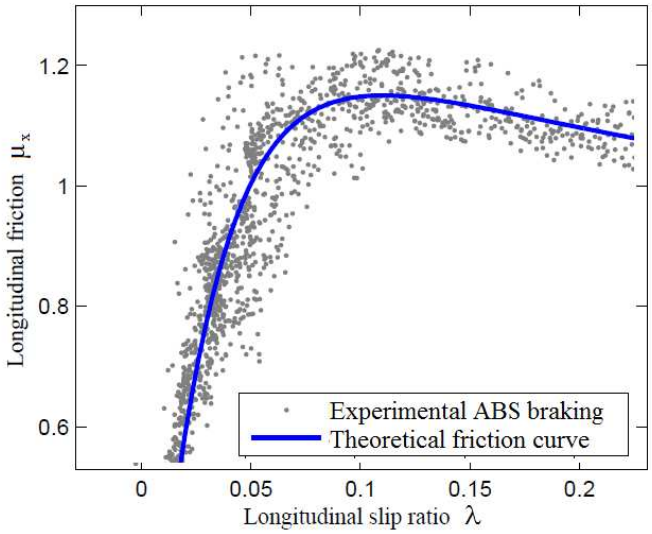

Figure 2.11: Experimental friction estimation according to [30].

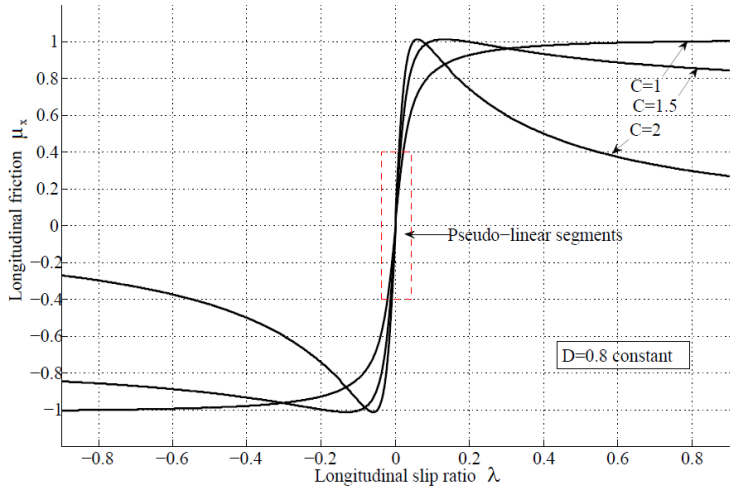

Figure 2.12: Parameter C influence on the friction curves.

- D is the maximum force the tire can generate, at its peak performance, influencing also the slope of the pseudo-linear segments of the curves, as shown in Figure 2.13.

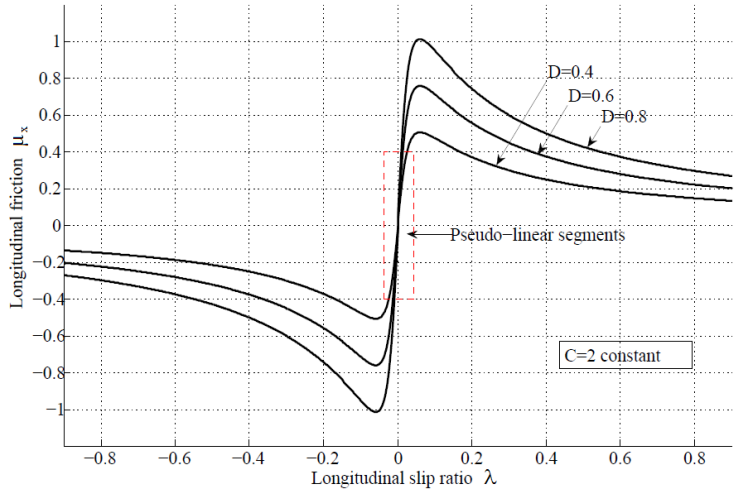

Figure 2.13: Parameter D influence on the friction curves.

The friction between the wheels and the road is subject to variation, its values changing due to numerous factors as the weather conditions (hot temperatures, rain, snow or ice), road maintenance and type of the pavement (asphalt, concrete or cobblestone). So, instead of using fixed parameters in the computation of C and D, we can consider them as time-varying in order to model the variation of road conditions in real situ-

ations. To model this variation, we have summed up parameters C and D into one single variable which gives the state of the road, called X_r. Modeling C and D into one single variable represents the realistic case of the friction variation. Therefore, X_r will vary between [0..1], giving a maximum adherence when it is close to 1 (simulating a dry asphalt road for example), and a small adherence when it is close to 0 (simulating a snowy or icy road), but will take into account all the other adherences in between, modeled as a continuous variation of C and D. Parameters C and D will have the following expressions:

$$C = X_r + k_c \tag{2.30}$$

$$D = \frac{k_{d_1}}{X_r + k_{d_2}} + X_r k_{d_3} \tag{2.31}$$

with $k_c, k_{d_1}, k_{d_2}, k_{d_3}$ being design parameters. Therefore, Pacejka formula will be rewritten as follows:

$$F_x = \left(\frac{k_{d_1}}{X_r + k_{d_2}} + X_r k_{d_3}\right) \sin((X_r + k_c) \arctan(B\lambda - E(B\lambda - \arctan(B\lambda)))) \tag{2.32}$$

Therefore, the variable X_r will give us the state of the road surface and we can use it to model a continuous variation of the road surface condition. This will yield a more realistic approach of Pacejka curves, regarded as multiple time-varying curves, as shown in Figure 2.14. Here we pass through snowy roads with $\mu_{x_{max}} = 0.4 \sim 0.5$ and rainy roads with $\mu_{x_{max}} = 0.7 \sim 0.8$ towards dry roads with $\mu_{x_{max}} = 0.9 \sim 1$. Nevertheless, the curves between these values are also taken into account, giving an approach to model road conditions closer to reality.

Let us note the maximum available friction with $\mu_{x_{max}}$, representing the peak value of the curves shown in Figure 2.9. Here we pass through snowy roads with $\mu_{x_{max}} = 0.4 \sim 0.5$ and rainy roads with $\mu_{x_{max}} = 0.7 \sim 0.8$ towards dry roads with $\mu_{x_{max}} = 0.9 \sim 1$. Nevertheless, the curves between these values are also taken into account, giving an approach to model road conditions closer to reality.

The use of the variable X_r for the computation of parameters C and D of Pacejka model brings a continuous modeling of the state of the road. Slow variation of the adherence can be easily simulated as shown in Figure 2.15 as well as rapid changes of the road conditions.

At the same time, the simulation of a slow variation of the adherence fits the

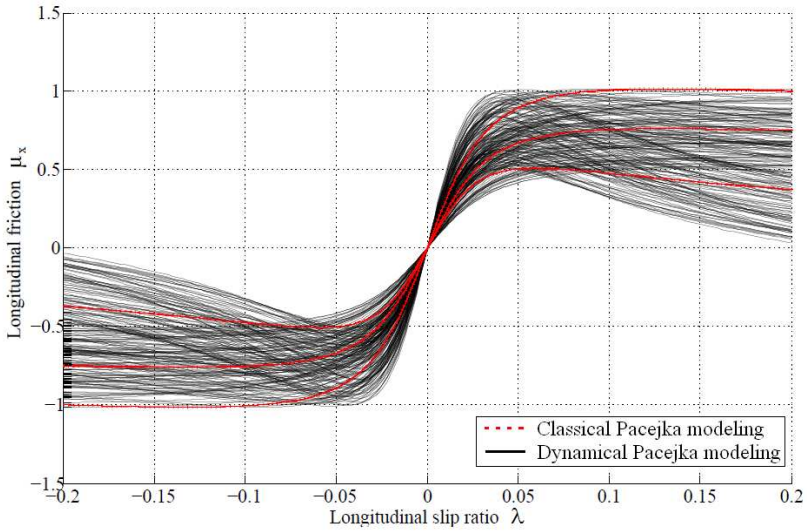

Figure 2.14: Realistic modelling of Pacejka curves.

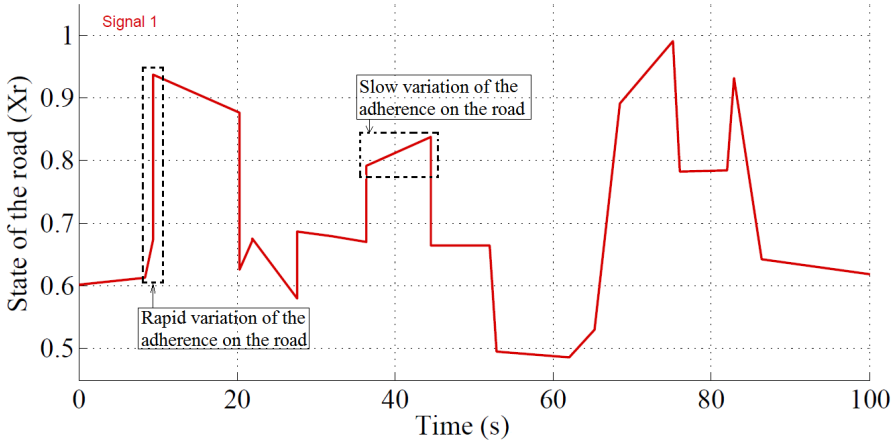

Figure 2.15: Time evolution of the state of the road and its variation.

majority of real situations, as the friction changes in a continuous manner (rain or snow take a certain amount of time to influence the friction of the road surface). Even though rapid changes of the adherence can arise in much less situations (such as passing over a puddle or a icy patch on the road), they are also taken into account and simulated accordingly as shown in Figure 2.15.

Chapter 3

Parameter estimations

Contents

Estimation theory [41] deals with estimating the values of parameters based on measured/empirical data. The parameters describe an underlying physical setting in such a way that their value affects the distribution of the measured data. An estimator attempts to approximate the unknown parameters using the measurements [33]. In estimation theory, two approaches are generally considered [95]:

- the probabilistic approach assumes that the measured data is random with probability distribution dependent on the parameters of interest [43].
- The set-membership approach [68] assumes that the measured data vector belongs to a set which depends on the parameter vector.

Many times in practice one has a model to describe specific phenomena, but the model contains parameters which alter its behavior. In some cases, these parameters can be measured directly, for example, measuring the speed of rotation of the wheels. In other occasions, the parameters of interest must be estimated starting from mathematical equations of the model [58]. Parameter estimation provides the necessary tools for the mathematical modeling of certain phenomenon. Variables and constants appearing in the models can be estimated, therefore the problem can be regarded as a study of inverse problems. Parameter estimation can be related to four optimization problems:

- criterion: the choice of the best function to optimize;
- estimation: the optimization of the chosen function;
- design: optimal design to obtain the best parameter estimates;
- modeling: the determination of the mathematical model which best describes the system from which data are collected.

Non-linear state estimation and some related topics, like parametric estimation, fault diagnosis, and perturbation attenuation, are tackled in [20] via a new methodology in numerical differentiation. Parameter estimation in vehicle dynamics [**?**, 33] is a complex task which yields an estimate of some variables that are not measurable. This is the case of longitudinal friction, known as μ_x, as described in section 2.4.1, which uses for its computation information about the transmitted wheel torque or wheel angular speed [1]. In addition, the control should use the maximum available friction, i.e. the peak of Pacejka curves shown in Figure 2.9, therefore more complexity is added in the overall scheme. This is the main reason why most actual control strategies use the longitudinal slip ratio, λ, as control variable and a fixed threshold as described in [13, 15, 36]. The use of in-wheel electric motors should provide the possibility of conceiving control strategies that are based directly on the maximum longitudinal friction, and not on fixed thresholds, yielding a new perspective on active safety.

Our estimation strategy follows a step-by-step process in order to compute the maximum available friction between the tire and the road. It starts with the estimation of the slopes of the friction curves, followed by the estimation of the instantaneous longitudinal friction, the longitudinal slip ratio and the load transfer. It will take advantage of the characteristics of Dugoff tire model to estimate the peak of the curves modeled by Pacejka.

3.1 The use of in-wheel electric motors

In-wheel electric motor system has a major advantage in comparison with standard ICE vehicles, being that we can have a instantaneous value of the torque transmitted at the wheels by measuring the current that passes through the motor. Since the electric motor is placed close the wheel, computations of the instantaneous friction can be accomplished starting from equation (2.2) of the one-wheeled vehicle model. This brings the novelty in our work, since the only actuator to accelerate and decelerate the vehicle is considered to be the in-wheel electric motor. It has small response time and it can be independently controlled, bringing the possibility to apply new control techniques that depend directly on the available friction. Therefore, no hydraulic brakes were considered in simulations, knowing that the in-wheel electric motor that is utilized is powerful enough to provide sufficient braking torques (e.g. 40kW). Two important variables are also considered known in this work: the wheel angular speed (ω) and the vehicle longitudinal speed (V_x), since nowadays odometers and accelerometers can accurately provide this information. Note, however, that the computation of V_x from accelerometers is not direct (signals coming from these sensors are very noisy, and have to be integrated, wherefrom an initial condition estimation problem; see [66] for a simple, yet effective estimator of V_x). Standard control approaches rely on a global estimation of V_x which yields a global traction force F_x and consequently a global longitudinal friction [88]. With the in-wheel electric motor we use each individual wheel speed to compute the individual friction at the wheels, which provides the possibility of independent wheel control.

Starting with the three variables that are supposed as known, T, ω and V_x, computations will be carried out in order to estimate necessary parameters to be utilized by the control strategy to apply adequate control laws at the wheels. These parameters are:

- the longitudinal slip ratio, λ,
- the instantaneous longitudinal friction, μ_x,
- the normal force, F_z.

Next, with the vehicle and wheel dynamics modeling and the advantages brought by the in-wheel electric motor, estimation techniques will be set up to provide a reliable

maximum friction estimation, called $\mu_{x_{max}}$. Starting from the latter estimation, different control techniques will be set up to achieve linear wheel behavior in emergency situations, representing the final goal of the present work. An important parameter that will be used in the estimation of $\mu_{x_{max}}$ will be the slope of the friction curves, which is an indicator of whether the maximum value of the curves was exceeded or not. This parameter is called the extended braking stiffness, or XBS, and its computation is described in [17].

3.2 Direct estimation of the parameters of interest

The in-wheel electric motors provide the knowledge of the instantaneous transmitted wheel torque by measuring the current that passes through the motor. Therefore we took advantage of equation (2.2) of the one wheel vehicle model, in order to estimate the instantaneous longitudinal friction. Replacing equation (2.4) in equation (2.2), the expression for μ_x is then:

$$\mu_x = \frac{1}{r_e F_z}(T - I\dot{\omega} - R_x). \tag{3.1}$$

The estimation process of the instantaneous friction compared to its modeled values is shown in Figure 3.1.

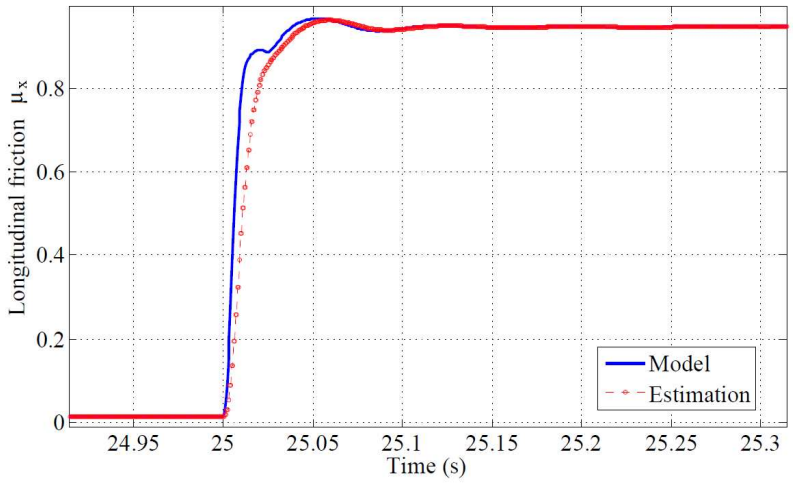

Figure 3.1: Longitudinal friction estimation.

Using the wheel acceleration to estimate the instantaneous friction is more reliable

than using the vehicle speed estimation, knowing that, in most cases, signals coming from accelerometers can carry much more noise than odometers ($\dot{\omega}$ in equation (3.1)) and integration of noisy signals can be problematic [18].

The computation of the longitudinal slip ratio can also be obtained directly by the use of the following equation:

$$\lambda = \frac{r_e\omega - V_x}{\max(r_e\omega, V_x)}. \tag{3.2}$$

The estimation of the instantaneous longitudinal slip ratio compared to the modeled value is shown in Figure 3.2.

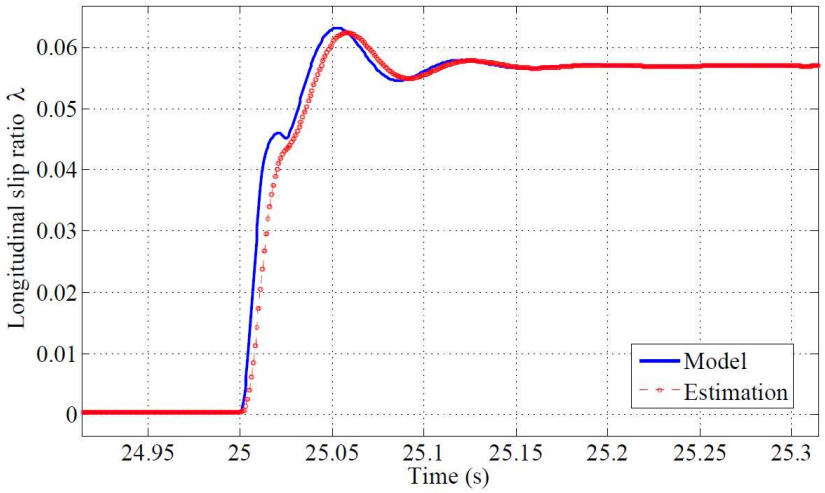

Figure 3.2: Longitudinal slip ratio estimation.

In Figure 3.3, a typical time evolution for the longitudinal friction and longitudinal slip ratio, is presented. The estimation of the parameters is conducted on the four wheeled vehicle model to show their evolution in standard acceleration and braking phases.

Nevertheless, an instantaneous friction estimation is not sufficient to achieve a control of the wheel dynamics, therefore a maximum friction estimation $\mu_{x_{max}}$ is needed. On the four-wheeled vehicle model, in order to estimate $\mu_{x_{max}}$, information about the normal forces on the wheels is also needed. This information cannot be measured directly, and we need to estimate it. Due to the suspension system, in acceleration or braking phases a phenomenon called *load transfer* arises, giving a bigger load on the rear wheels in acceleration and on the front wheels in deceleration. When a car is

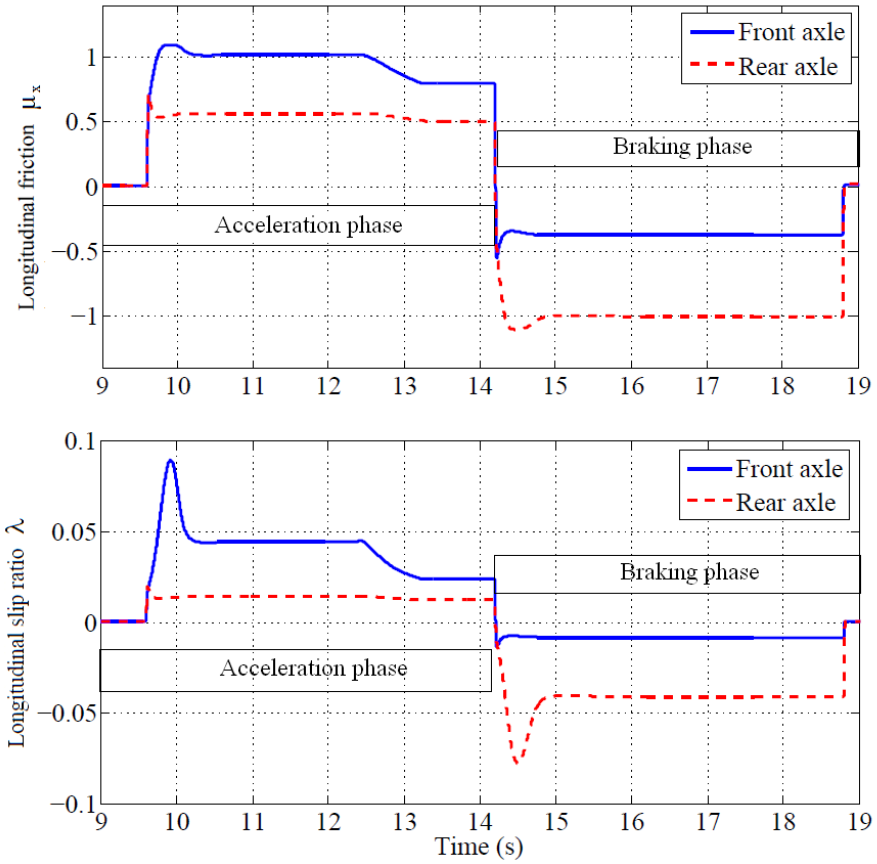

Figure 3.3: Longitudinal friction and slip ratio in acceleration and braking phases.

accelerating on a level road, the vertical forces under the front and rear wheels are[38]:

$$F_{zf} = \frac{1}{2}mg\frac{l_r}{l_f + l_r} - \frac{1}{2}mg\frac{h_0}{l_f + l_r}\frac{\dot{V}_x}{g}, \tag{3.3}$$

$$F_{zr} = \frac{1}{2}mg\frac{l_f}{l_f + l_r} + \frac{1}{2}mg\frac{h_0}{l_f + l_r}\frac{\dot{V}_x}{g}. \tag{3.4}$$

The first terms, $\frac{1}{2}mg\frac{l_r}{l_f+l_r}$ and $\frac{1}{2}mg\frac{l_f}{l_f+l_r}$, are called static parts, coming from the static weight distribution (static position of the center of gravity) and the second terms, $\pm\frac{1}{2}mg\frac{h_0}{l_f+l_r}\frac{\dot{V}_x}{g}$, are called dynamic parts of the normal forces, coming from the dynamic mass transfer in acceleration or deceleration (with $\dot{V}_x$ being the chassis longitudinal acceleration).

When the vehicle is braking, the dynamic part becomes significant in the front of the vehicle, giving a larger load in the front of the vehicle, and a smaller one in the

back, and vice-versa in acceleration, as shown in Figure 3.4.

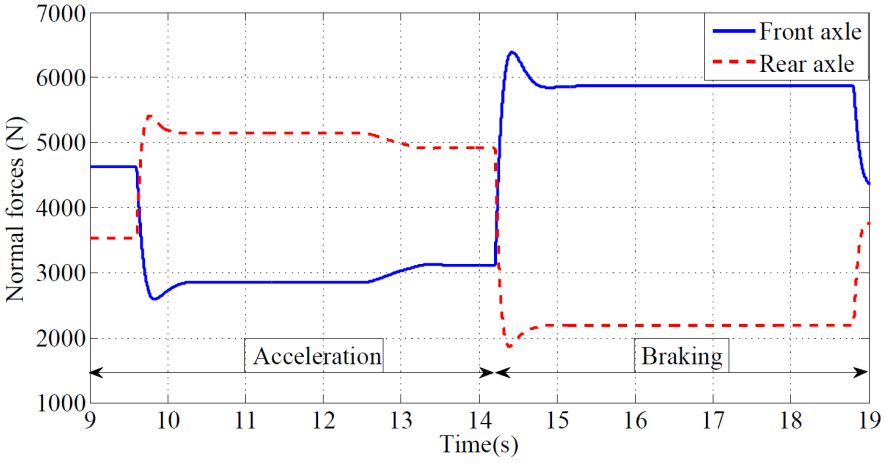

Figure 3.4: Load transfer in acceleration and braking phases.

As stated before, the instantaneous friction is not sufficient in order to obtain a maximum friction estimation. This is a more complex process and to achieve it, a required estimation is that of the slope of the friction characteristics, the extended braking stiffness. In our strategy this wont be considered a control parameter, but a secondary parameter used in the adaptation process of the weighting parameter between Dugoff and Pacejka models (see section 3.4.2).

3.3 Extended braking stiffness (XBS) estimation

An important variable in the future development of the estimation strategy, even though is not considered as a control variable, is the so-called *extended braking stiffness* (XBS). The computation of this variable is filtered with a first-order filter, which induces a loss in terms of dynamics, but not with decisive impact on its final purpose, being considered as a secondary variable. The XBS is defined as the derivative of the friction with respect to slip ratio [17]:

$$XBS(t) = \frac{d\mu_x}{d\lambda} = \frac{\dot{\mu}_x}{\dot{\lambda}}. \tag{3.5}$$

This parameter indicates the slope of the friction curves $\mu_x(\lambda)$ and can provide information about the instantaneous friction. If the slope is positive (XBS>0) , then

μ_x is placed in the stable zone of the curves, otherwise if the slope is negative, μ_x is placed in the unstable zone of the curves, after the peak. When XBS=0, the friction is at the peak of the curves, meaning that at this point we have maximum friction value and therefore maximum traction or braking force. This is the reason why this parameter is often used, carrying important information about the critical point of the friction curves (the peak where XBS=0).

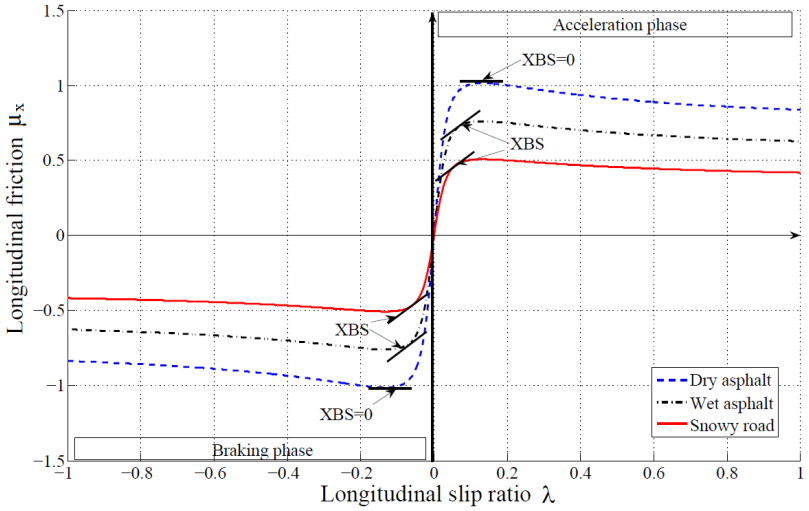

Figure 3.5: XBS definition according to [17].

The interest in having a knowledge about the slope of the friction curves is obvious, since starting from this information, an eventual controller can use it, allowing more torque to be transmitted at the wheel or not, in function of XBS value. However, deriving a good estimation of this parameter is not obvious. Firstly, we need to have an information about the instantaneous friction, which sometimes cannot be achieved (in the case of the ICE vehicles). Secondly, for the longitudinal slip ratio, the knowledge of the chassis velocity (V_x), and of the wheel angular velocity (ω) is required. Adding that XBS is calculated as the ratio between the derivatives of the friction and the slip ratio, and the derivatives are sensitive to noise, we can see that there are plenty of constraints and difficulties in the obtainment of the XBS estimation. Nevertheless, this is not a control variable in our control strategy, but a variable used for the adaptation of a Dugoff model parameter, therefore a filtering stage is taken into account.

3.4 Estimation of the maximum friction $\mu_{x_{max}}$

3.4.1 Existent solutions

Numerous static and dynamic tire force models have been developed in order to achieve accurate simulation of the evolution of the friction forces ([10, 73, 85, 101]). However, extensive testing is needed to determine all the parameters of those analytic models. In addition, the parameters vary in real-time for different potential tires, tire pressure or wear state.

Nevertheless, many approaches tried to use analytic techniques to determine the friction from the tire force models. Simplified models have been coupled with vehicle and wheel dynamics to generate different observations and filtering techniques: [16] used fuzzy logic techniques; [53, 89] developed different least-squares methods; [12, 31, 50, 83] used several kinds of nonlinear asymptotic observers. The majority of them try to obtain a reliable tire effort estimate and afterwards, the maximum tire friction value, by fitting different types of polynomial functions. Unfortunately, these approaches are either based on hypotheses that are too restrictive (only longitudinal dynamics situations for example), or they concentrate their efforts on precise estimation of the tire forces, not going in depth into the estimation of the maximum friction.

For the estimation of the maximum friction the approach called "diagnosis-based" presented in [17] tends to take advantage of numerical algorithms to be able to detect dangerous zones (the non linear zones of the curves before arriving at the peak as shown in Figure 3.5) in a reliable way. Once the entrance in the non linear zone is detected, a simple tire behavior model will help in deriving a good estimation of the maximum friction. In this strategy, some important parameters are fixed, being computed "off-line" and they not change during simulation. The weakness of the method is that these parameters stay fixed and their values influence the estimation process. In order to obtain a more robust estimation of the maximum friction, an "on-line" estimation of these parameters is required.

3.4.2 Dugoff tire model

Dugoff tire model has an interesting feature, assuming a uniform vertical pressure distribution on the tire contact patch. This means it has a monotone behavior, i.e. the F_x peak never appears as seen in Figure 3.6. This is a simplification compared to the more realistic parabolic pressure assumed in Pacejka model. However, Dygoff

model is invertible and the longitudinal forces are directly related to the maximum friction in linear equations, hence the interest to estimate Dugoff parameters in order to obtain a maximum friction estimation.

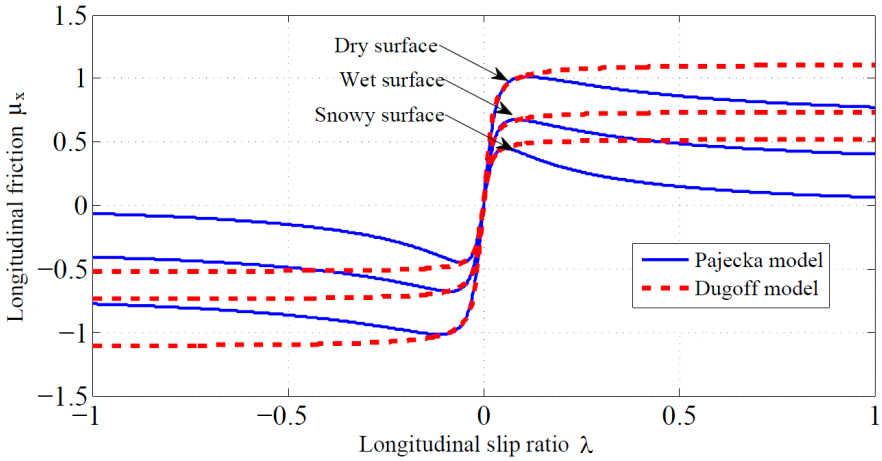

Figure 3.6: Friction characteristics compared on Pacejka and Dugoff curves.

In Dugoff's tire-model, longitudinal efforts are modeled as follows:

$$F_x^D = \alpha f(\tau) K_x \lambda. \tag{3.6}$$

with α being a weighting factor and $f(\tau)$ a piecewise function:

$$f(\tau) = \begin{cases} (2-\tau)\tau, & \tau < 1 \\ 1, & \tau \geqslant 1 \end{cases}, \quad \tau = \frac{\alpha \mu_{x_{max}} F_z}{2|K_x \lambda|}. \tag{3.7}$$

It is not difficult to see that $\mu_{x_{max}}$ can be expressed in terms of four a priori known variables F_x, F_z, λ, K_x. The $\mu_x - \lambda$ characteristics have two specific regions. The first one is linear and its limit is given by $\tau = 1$, therefore, when its values are below 1, we are in the non linear region. In the linear region, the longitudinal efforts are calculated as $F_x^D = K_x \lambda$. Therefore, the values for K_x can be derived in the linear region of the friction curves ($f(\tau) = 1$):

$$K_x = \frac{F_x}{\lambda}. \tag{3.8}$$

The longitudinal stiffness parameter K_x is in fact the slope of the $\mu_x - \lambda$ curves (or

$F_x - \lambda$ curves) in the linear region and impacts on the shape of the curves (see Figure 4.9).

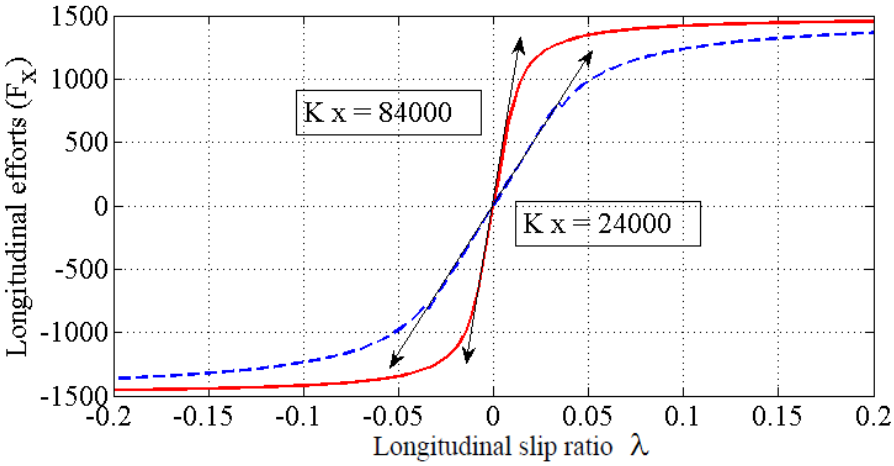

Figure 3.7: Impact of K_x on the friction curves based on Dugoff model.

As observed in "off-line" computations, Dugoff tire model saturates at a different level than Pacejka tire model. It is in fact the weighting factor between Dugoff and Pacejka models, denoted α, that drives Dugoff model to cross through Pacejka model exactly in the peak of the curve (Figure 3.8). The weighting factor α is derived in the

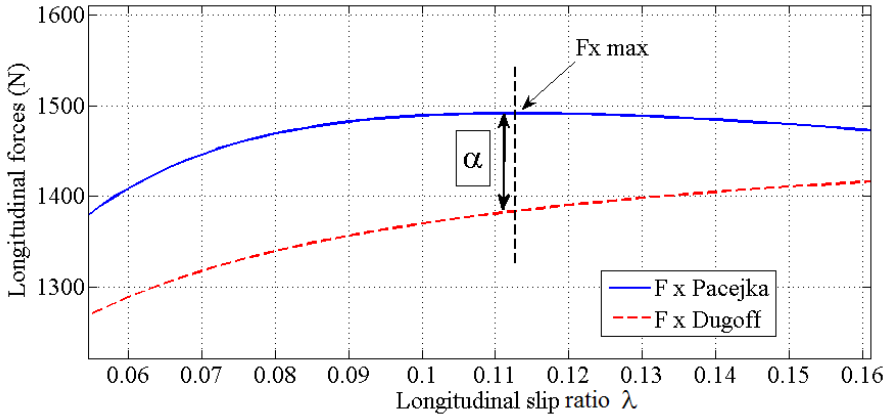

Figure 3.8: Weighting parameter α at the peak of longitudinal efforts built with Pacejka and Dugoff models.

non linear zone of $\mu - \lambda$ characteristics. However, the estimation of this parameter is more difficult, since its value can be calculated only at the peak of the $\mu - \lambda$ curve.

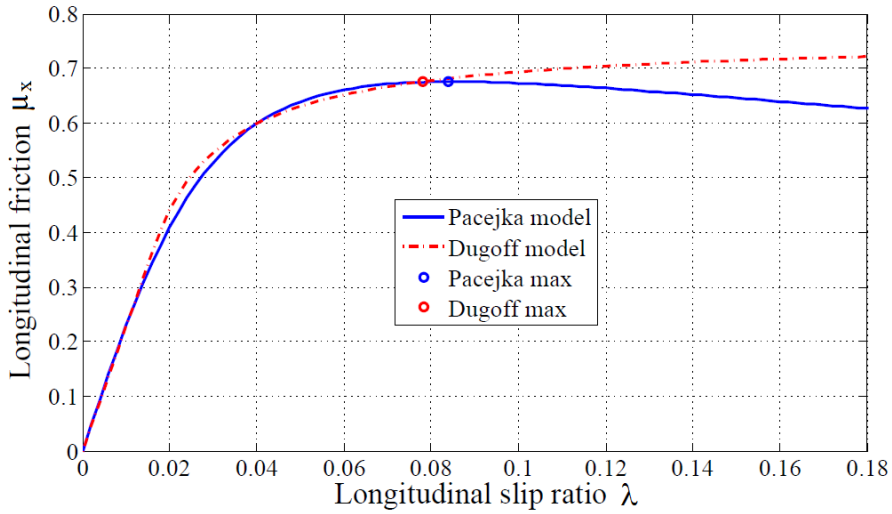

Figure 3.9: Weighted and normal Dugoff evolutions compared to Pacejka model.

The shape and peak value of the friction curves $\mu_x(\lambda)$ are influenced by the longitudinal stiffness coefficient (K_x) and by the weighting factor (α). As K_x influences the slope of the linear zone of the curves, with an impact also on start of the non-linear zone, α gives the place where the peak of the Dugoff curves corresponds to the peak of Pacejka curves. Therefore, the knowledge of these two parameters is very important in achieving a weighted Dugoff curve that is similar to Pacejka curve until its peak. An underestimation of the K_x parameter can induce wrong shapes of the curves, as shown in Figure 3.10.

In the left side of Figure 3.10 the behavior of the curves with an underestimation on a dry road is shown, and in the right side, for a wet road. The impact of K_x is more clear on the wet road, where a wrong value for this parameter gives a shape of the curve with the peak already on the non-linear zone of Pacejka curves.

As for α, if this parameter is underestimated, the peak of the Dugoff curve will exceed the peak of the Pacejka curve, as shown in Figure 3.11.

If these two parameters are well estimated, then we will obtain the result shown in Figure 4.1, meaning that the slope of Dugoff curves will match the slope of Pacejka curves and in addition, the peak of the weighted Dugoff curve will be close to the Pacejka peak.

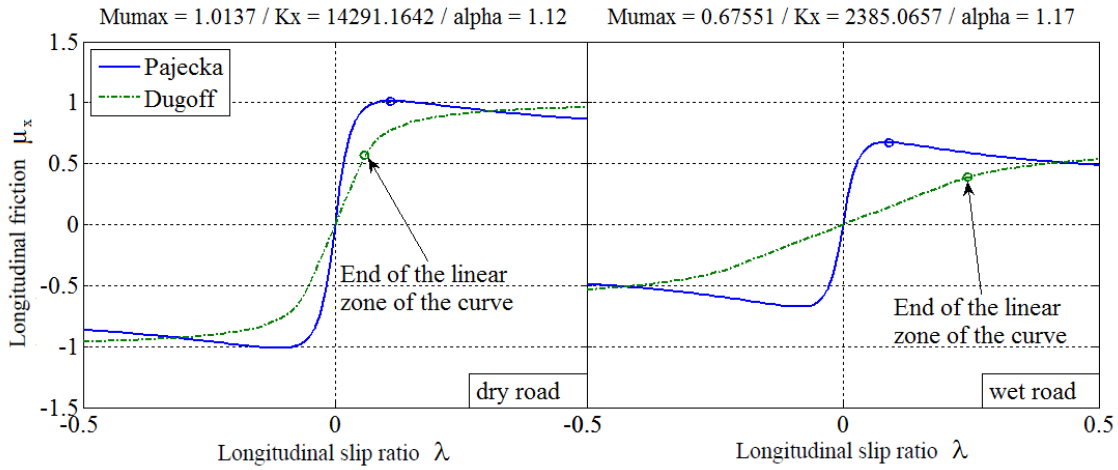

Figure 3.10: Underestimation of K_x and its impact on Dugoff model compared to Pacejka model.

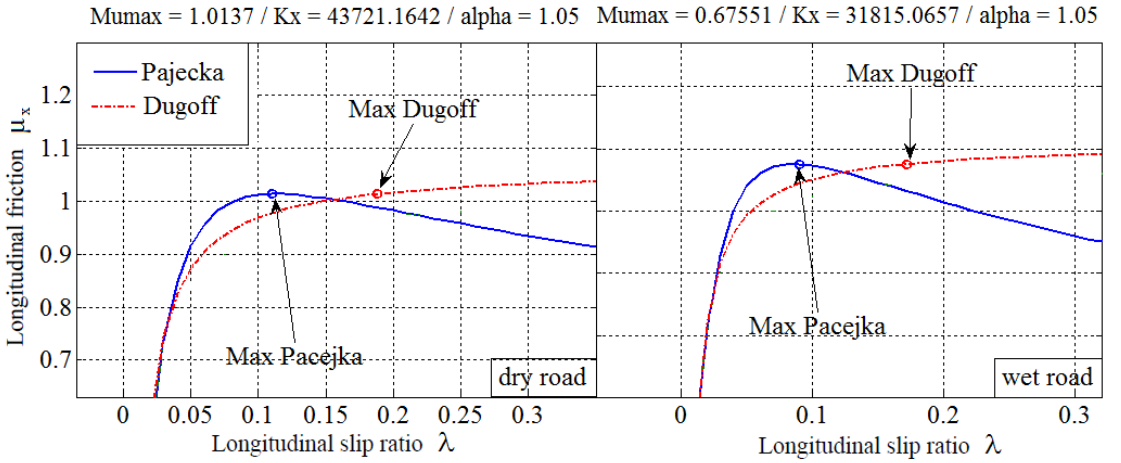

Figure 3.11: Underestimation of α and its impact on Dugoff model compared to Pacejka model.

3.4.3 Maximum friction solution based on Dugoff model

This approach is based on the fact that the Dugoff tire model is more explicit and simple than the Pacejka model. It has two key parameters, described in the previous section: K_x and α which are used in the obtainment of the maximum friction. For the longitudinal stiffness coefficient K_x, on the pseudo-linear segments of Pacejka model, we have derived its different values for different types of road surface conditions and

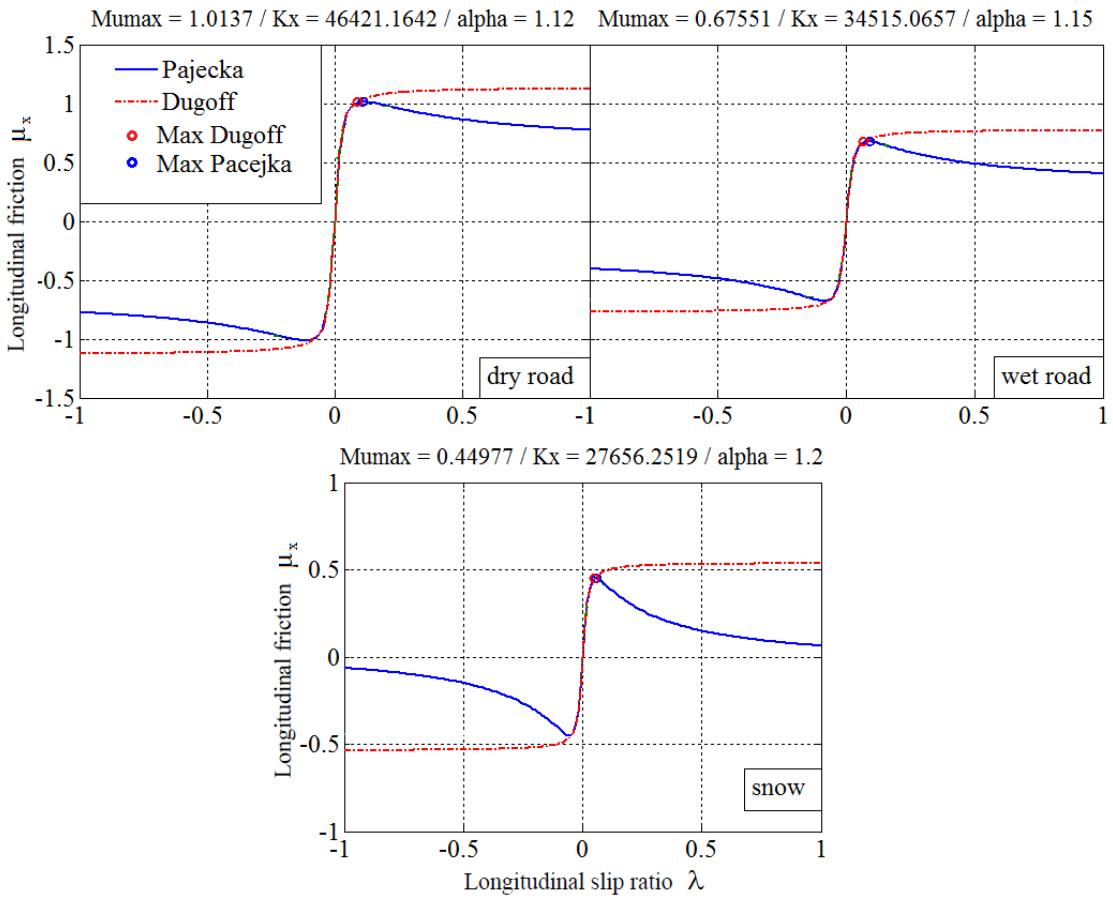

Figure 3.12: Good estimation of α and K_x on Dugoff model compared to Pacejka model.

we have obtained K_x=47000 for a dry road ($\mu_{x_{max}} = 1$), K_x=34500 for a wet road ($\mu_{x_{max}} = 0.7$) and K_x=27600 for a snowy road ($\mu_{x_{max}} = 0.4$). To estimate K_x, a simple approach was used, a first order filter being applied on equation (3.8). The filter permits to keep a history of the preceding values of the parameter as the friction changes. The evolution for the estimated values and of the model values is shown in Figure 3.13.

In the non linear region of the curves, longitudinal efforts are calculated as:

$$F_x^D = \alpha(2-\tau)\tau K_x \lambda. \tag{3.9}$$

Knowing that $\tau = (\alpha \mu_{x_{max}} F_z)/(2|K_x\lambda|)$, we can calculate the limit value for the

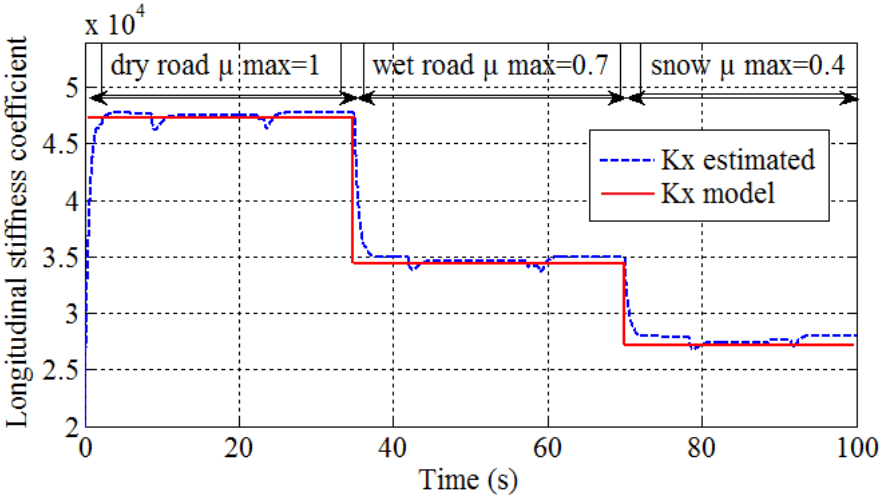

Figure 3.13: Longitudinal stiffness parameter K_x and its values for different adherence.

longitudinal slip after which we enter in the non linear region :

$$|\lambda_{lim}| = \frac{\alpha \mu_{x_{max}} F_z}{2|K_x|}. \tag{3.10}$$

Hence, if $|\lambda| \leqslant \lambda_{lim}$, we are in the linear region of the curves, otherwise we are in the non linear one.

For the second parameter, α, we have also derived its different values at the peak of the Pacejka model for different types of adherence and we have obtained α=1.12 for a dry road ($\mu_{x_{max}} = 1$), α=1.15 for a wet road ($\mu_{x_{max}} = 0.7$) and α=1.2 for a snowy road ($\mu_{x_{max}} = 0.4$). As it can be observed, α hardly varies from one type of road to another. An algorithm that takes advantage of the previous XBS estimation is designed to adapt α as the friction curve changes. The initial value of α starts with a mean value of $\alpha_{init} = 1.1$ computed "off-line". Next, as the friction curve changes, the parameter adapts its value following the next algorithm:

We proposed an algorithm that calculates the estimation of α and Figure 3.14 shows that it reaches the values calculated ”off-line” as the friction changes.

The following figure summarizes the estimation of the two key parameters K_x and α and shows exactly where their estimation process takes places on the characteristics:

Next, let us take the non linear region case of the $f(\tau)$ function, i.e. $f(\tau) = (2-\tau)\tau$.

Table 3.1: Algorithm 2: α adaptation algorithm.

---

if $(|\lambda| \geqslant \lambda_{lim}$)
  i=1 (ADAPT ON)
    if $XBS_{min} - XBS_{[-max;max]} \geqslant 0$
      $\alpha = \int (XBS_{min} - XBS)_{[-max;max]} k_{up} i$
    else
      $\alpha = \int (XBS_{min} - XBS)_{[-max;max]} k_{down} i$
else
  i=0 (ADAPT OFF)

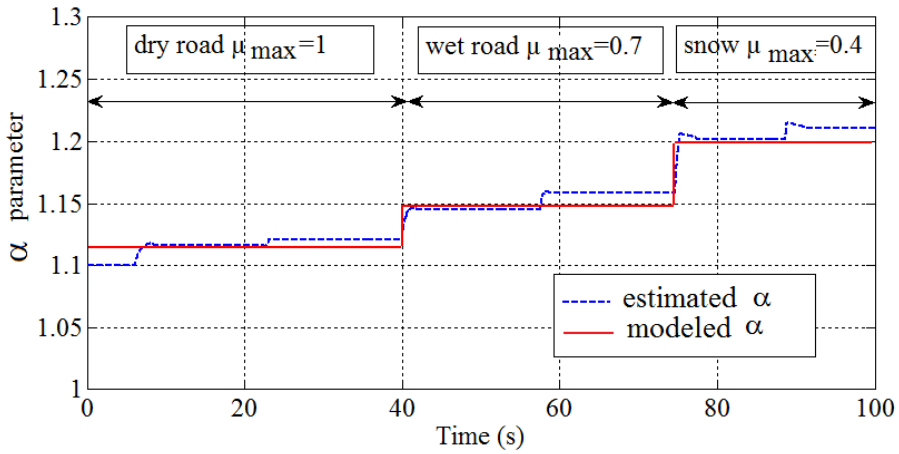

Figure 3.14: Estimation of parameter α following the adaptation algorithm 2.

Then, the longitudinal efforts can be expressed as follows:

$$F_x^D = \left(2 - \frac{\alpha \mu_{x_{max}} F_z}{2|K_x \lambda|}\right) \frac{\alpha \mu_{x_{max}} F_z}{2|K_x \lambda|} K_x \lambda. \tag{3.11}$$

This expression can be rewritten as a second algebraic equation of the maximum friction:

$$\alpha^2 \mu_{x_{max}}^2 F_z^2 - 4\alpha \mu_{x_{max}} |K_x \lambda| F_z + 4|K_x \lambda| F_x^D = 0, \tag{3.12}$$

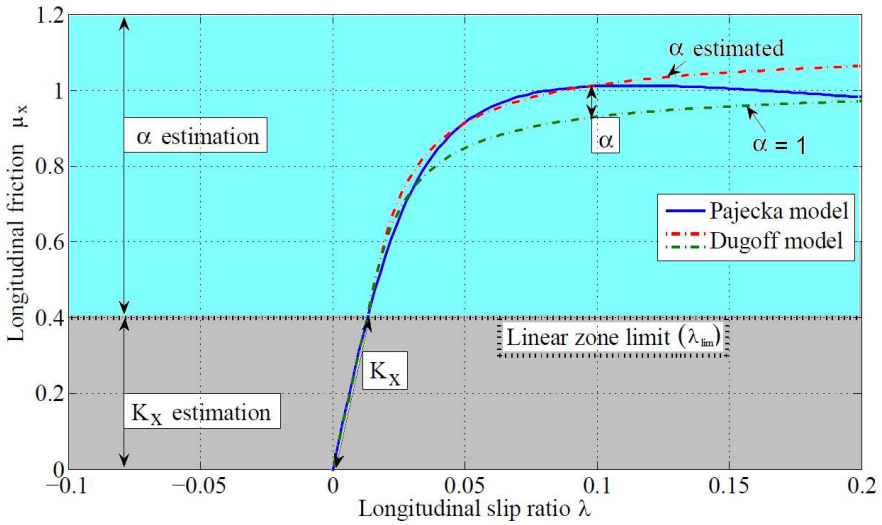

Figure 3.15: α and K_x graphical view of the estimation process.

whose two solutions are:

$$\mu_{x_{max}} = \frac{2\alpha(|K_x\lambda| \pm \sqrt{K_x\lambda(K_x\lambda - F_x^D)})}{F_z}. \tag{3.13}$$

The sign between the two terms of the numerator is '+' when $\lambda \geqslant 0$ and '-' when $\lambda < 0$. Having also the estimates of K_x and α, we propose an algorithm that computes the maximum friction as shown in algorithm 3.

Table 3.2: Algorithm 3: $\mu_{x_{max}}$ computation.

---

if $(|\lambda| > \lambda_{lim}\ )$

$\quad \mu^D_{x_{max}}(t_k) = \frac{2\alpha(|K_x\lambda(t_k)| \pm \sqrt{K_x\lambda(t_k)(K_x\lambda(t_k) - F_x(t_k))})}{F_z}$

else

$\quad \mu^D_{x_{max}}(t_k) = \mu^D_{x_{max}}(t_{k-1})$

With this algorithm, the maximum available friction is computed in order to be transmitted to the control stage, which will bring the instantaneous friction at its maximum value in emergency maneuvers like hard acceleration or hard braking. Keeping the instantaneous friction at its maximum available value will yield a stable wheel behavior (neither wheel lock nor wheel spin), achieving stable overall vehicle dynamics.

3.5 Longitudinal dynamics analysis

Vehicle response to driver's requirements is strongly influenced by the adhesion between the tire and the road surface. The grip may vary from very low adhesion surfaces (snowy or icy roads with $\mu_{x_{max}} \leq 0.3$) to high adhesion surfaces (dry asphalt can arrive up until $\mu_{x_{max}} = 1.2$). Friction turns out to have a major influence on the longitudinal dynamics of the vehicle even at a very small variation. The following analysis will prove this statement.

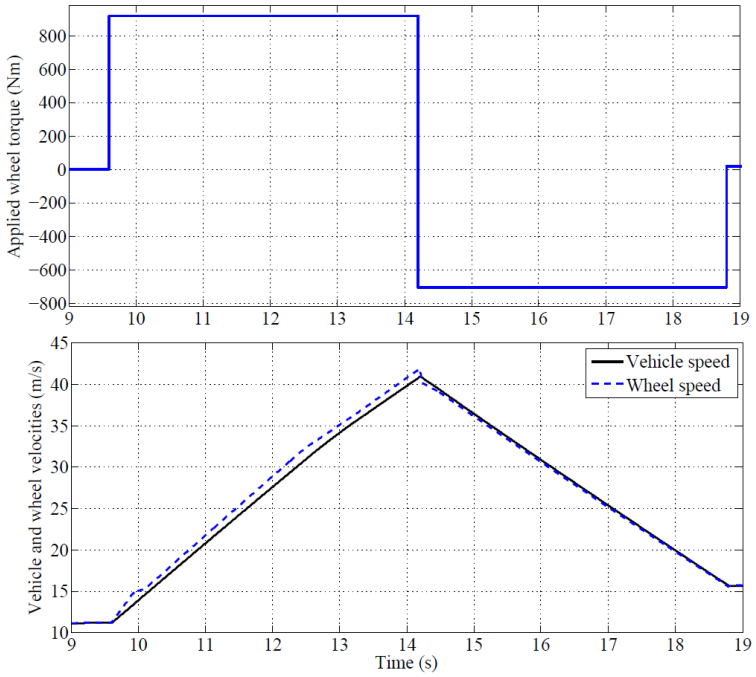

Figure 3.16: Torque input and vehicle response.

In a first step, we want to see the time evolution for different parameters in the case of a hard acceleration demanded by the driver, followed by a hard braking maneuver. Driver's requirement of a hard acceleration can be translated as a high torque input for the overall system. The torque transmitted at the wheel is untainted and its effect on the vehicle behavior is shown in Figure 3.16.

As we can see, the wheels maintain their grip on to the road surface, giving a stable acceleration and deceleration of the vehicle. This is because the longitudinal friction as function of the longitudinal slip ratio is placed on the friction curve before its peak. This means we are still in the stable pseudo-sliding zone of the friction curves, where

the wheels do not slip in acceleration or skid in braking phases. This is shown in Figure 3.17.

On the same figure, one can see that the maximum friction has been simulated to be at approximately 1.085. This corresponds to a dry road surface. The wheels do not lose the grip and accelerate the vehicle in a stable manner to 40 m/s. Then, the vehicle decelerates without skidding.

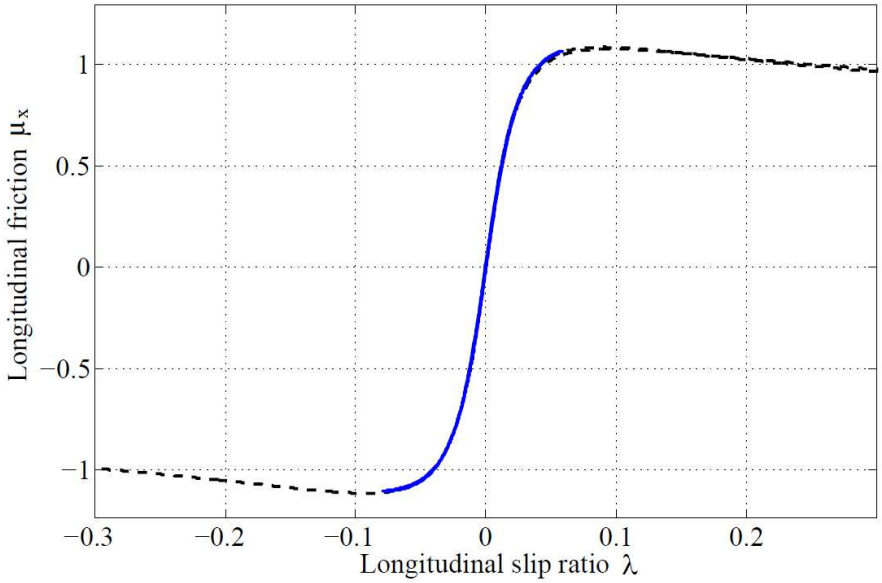

Figure 3.17: Longitudinal friction values shown on Pacejka curves.

The same torque input has been simulated on the full four-wheeled vehicle model and applied at each wheel. The values for the friction and the longitudinal slip are shown in Figure 3.18. Having a closer look on the friction curves, one can see that they have different values for the front and the back wheels. This happens because of the load transfer which arises in acceleration as well as in braking phases. The friction is larger in the front of the vehicle in acceleration, and smaller in the back, and vice-versa in braking. The same phenomenon arises for the longitudinal slip values.

The load transfer can be seen in Figure 3.19. In acceleration, the load, or the normal force is bigger in the back of the vehicle, and smaller in the front. The normal force will be bigger in the front of the vehicle when it decelerates, and smaller in its back.

This simple simulation shows that as long as the friction stays in the pseudo-sliding zone of the characteristics, a linear and stable wheel acceleration and deceleration is

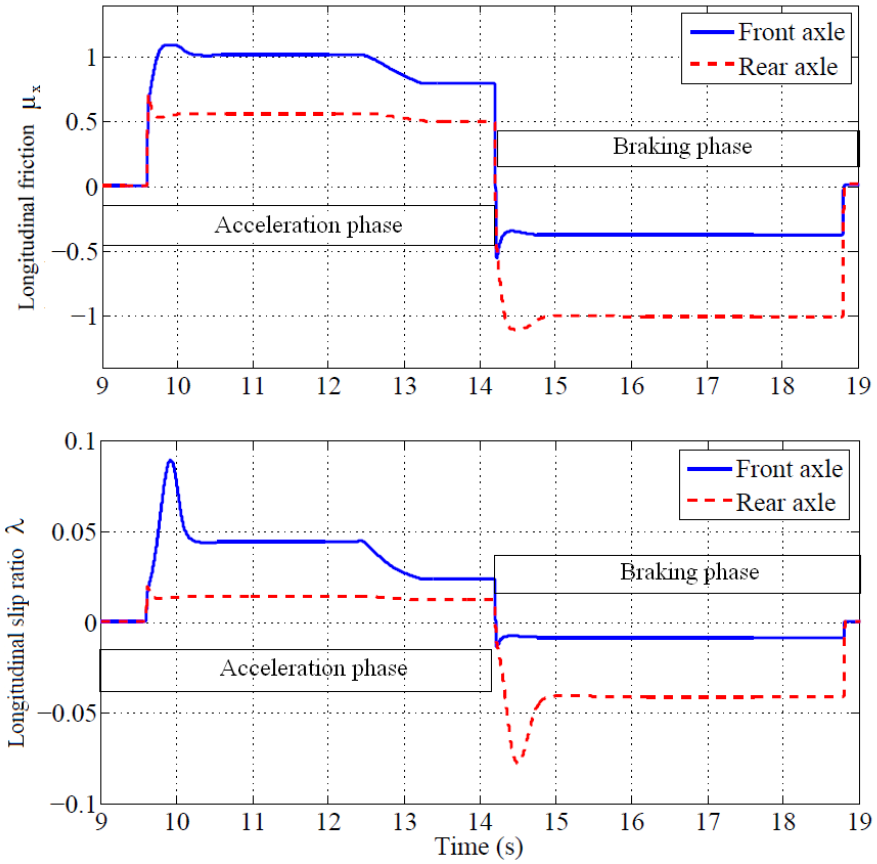

Figure 3.18: Longitudinal friction values for the front and back axles.

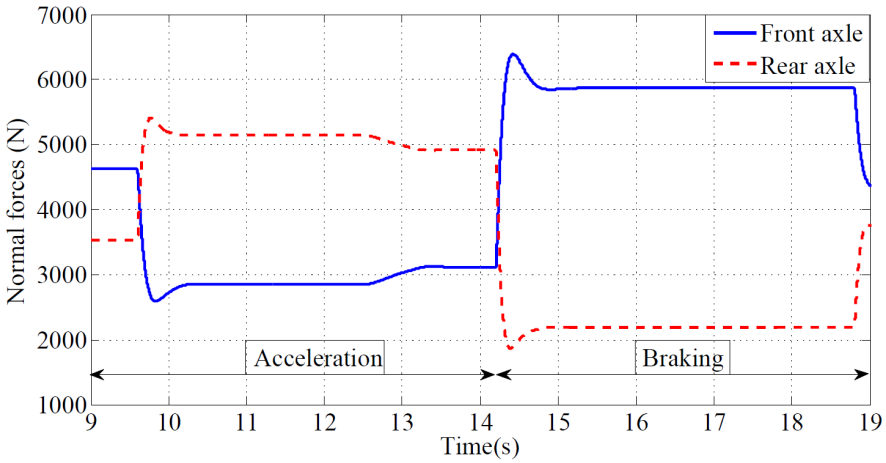

Figure 3.19: Load transfer in acceleration and braking phases.

achieved. The overall vehicle response is now tested on a road with a smaller $\mu_{x_{max}}$ (set to be at 1.02). The same amount of torque is applied as before, untainted to all four wheels of the vehicle. In Figure 3.20, one can see vehicle and wheel evolutions with a traction force applied, followed by a braking one.

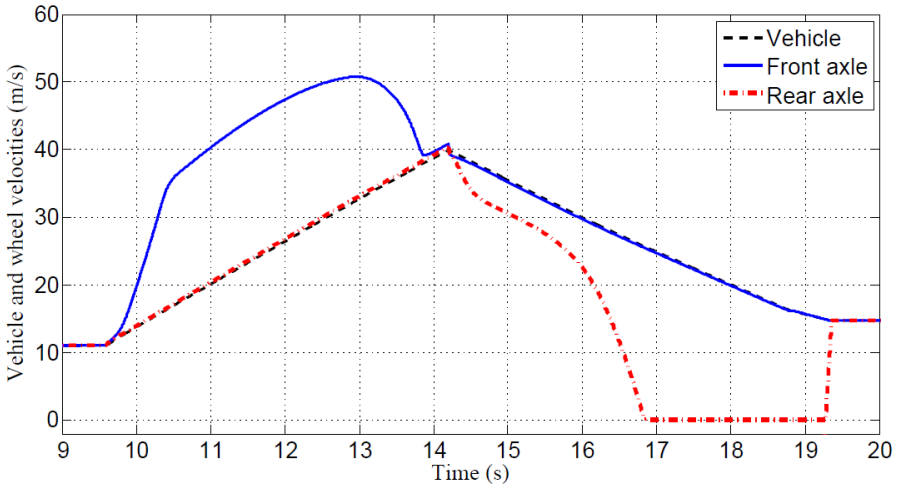

Figure 3.20: Vehicle and wheel velocities on a road with $\mu_{x_{max}} = 1.02$.

Giving a smaller friction, in acceleration, the front wheels lose their grip and start slipping, because the friction values passed the peak of Pacejka curves and entered in the unstable zone *"c"*, where more torque applied will only give more wheel slip. The friction values on the curve of Pacejka are shown in Figure 3.21.

In acceleration phase, the front wheels are spinning uncontrollably and in braking phase, the back wheels achieve complete lock-up, therefore the value of the longitudinal slip ratio becomes -1.

The difference between the maximum friction simulated on the first test, and the second one is 0.06. So, a small variation of the friction can induce totally different vehicle and wheel responses. This happens because of the non linearity of the friction curves. If the friction stays before the peak, the torque applied will lead to grip on the road. Once exceeded, the torque applied will only lead to wheel spin or wheel block, losing the grip on the road.

Therefore, an active controller to be able to adapt at the change of the road surface adhesion, is mandatory. It has to detect the maximum friction on which the vehicle is moving, so it can transmit to the wheels the maximum torque that maintains the grip on the road. The estimation stage can be complex, since one has to derive a good

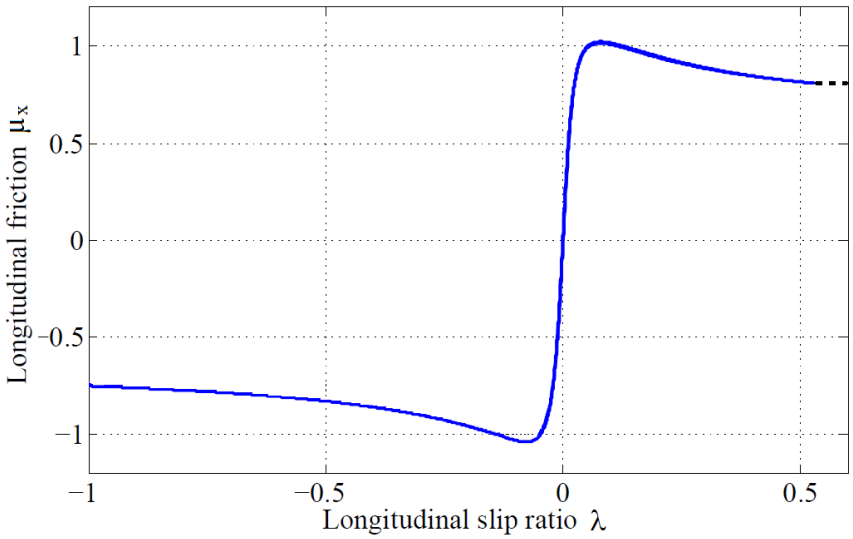

Figure 3.21: Friction values shown on Pacejka curves.

estimation of the normal force on the tire (F_z) and the friction force (F_x). The presence of the electric motors can simplify this task by providing an instant knowledge of the transmitted torque to the wheels.

3.5.1 Analysis of system behavior without model parameter adaptation (fixed values for α and K_x)

In the following tests, parameters α and K_x will stay fixed, showing their influence on maximum friction computation. In a first test, α and K_x will be overestimated at a fixed value of 1.3 and respectively 40000, for a wet road scenario, where their off-line calculated values should have been 1.17 and respectively 34500. The parameters will keep these values fixed on this test. The result is shown in Figure 3.22.

The result is the same with the one where $\mu_{x_{max}}$ value was fixed and underestimated. If, on the other hand, parameters are underestimated, the result will be opposite, giving an overestimation of $\mu_{x_{max}}$. In this test parameters will stay fixed at $\alpha = 1.08$ and $K_x = 30000$. This will induce oscillations in the final value, that will grow in amplitude and width, as shown in Figure 3.23.

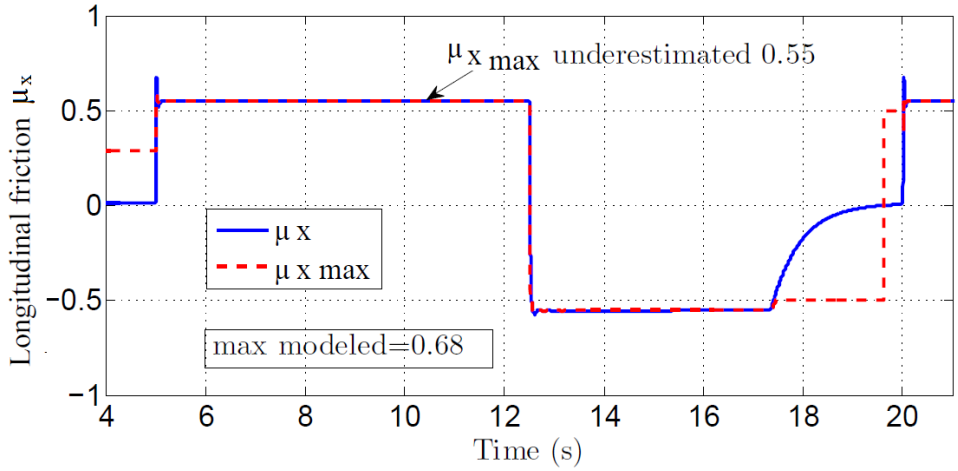

Figure 3.22: Fixed values of α and K_x that lead to the underestimation of $\mu_{x_{max}}$.

3.5.2 Adaptation of α parameter

Even when the maximum friction is overestimated, this model has a stabilizing effect around the maximum friction value. This is due to the α adaptation algorithm, which searches the maximum, even if its estimated value is exceeded.

While XBS values are bigger than XBS_{min}, meaning that we are still in the linear stable zone before the peak, α will decrease and the maximum friction will increase until it will exceed the peak. Then, once XBS becomes negative, α will start to increase (algorithm 2), and μ_{max} will decrease, entering again in the linear zone before the peak, and making XBS once again positive. This process continues and the oscillations are increasingly smaller as shown in Figure 3.25, until a stabilized value for μ_{max} is achieved.

Now lets analyze system response when the adaptation algorithm of parameter α is enabled on a time-varying road surface adhesion characteristic. One can see that the maximum modeled value of the friction is reached in all cases, even if this maximum value varies in time (Figure 3.26). There is a transient time where oscillations arise due to the slow adaptation of α. Nevertheless, when the parameter is adapted, a linear tracking of the maximum friction is achieved.

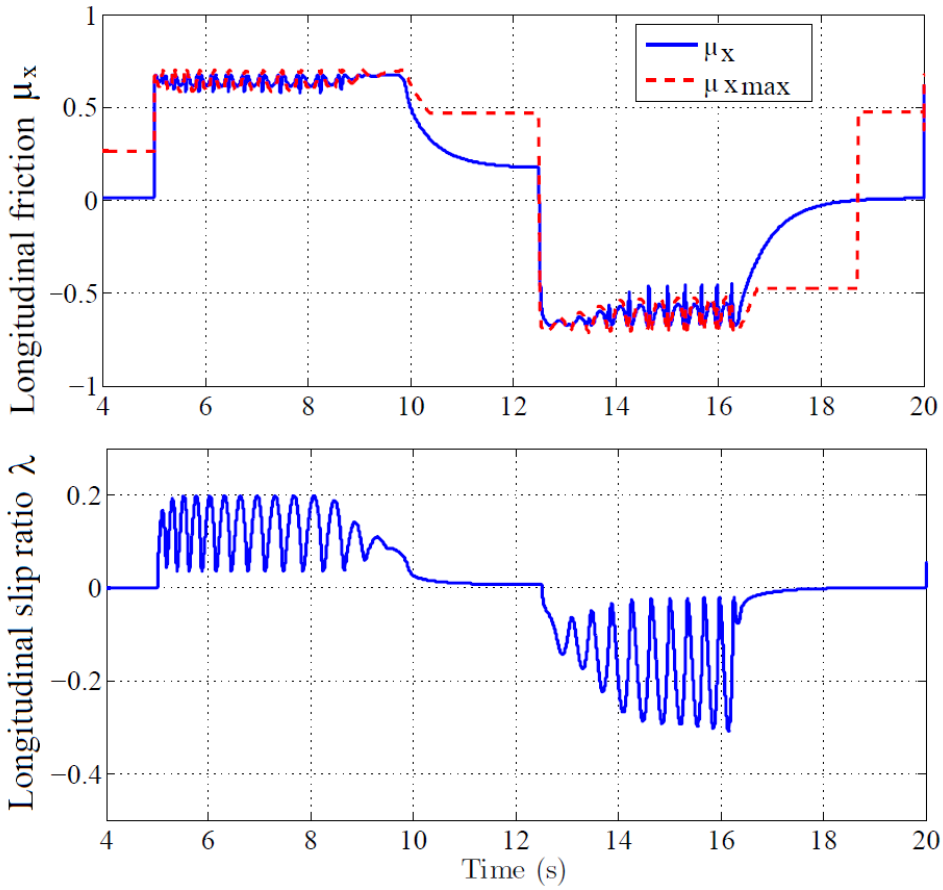

Figure 3.23: Overestimation of maximum friction.

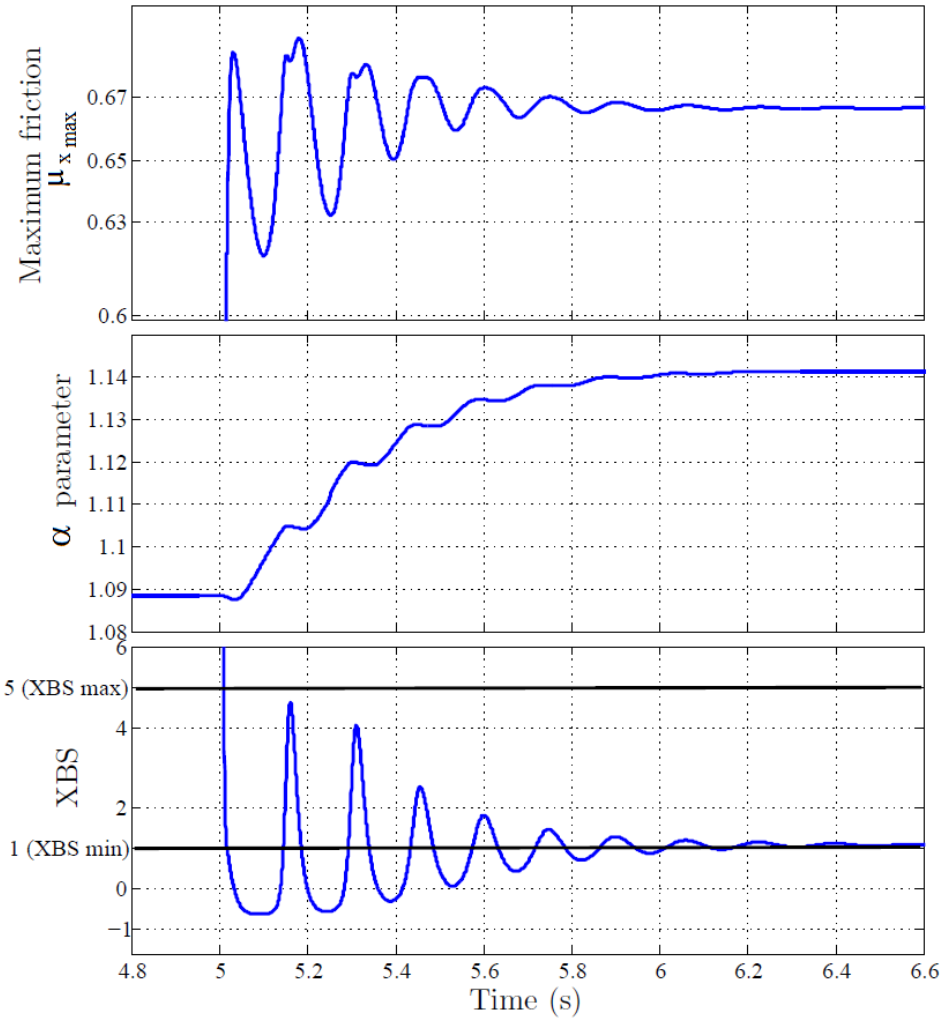

Figure 3.24: Stabilizing effect of the estimation strategy.

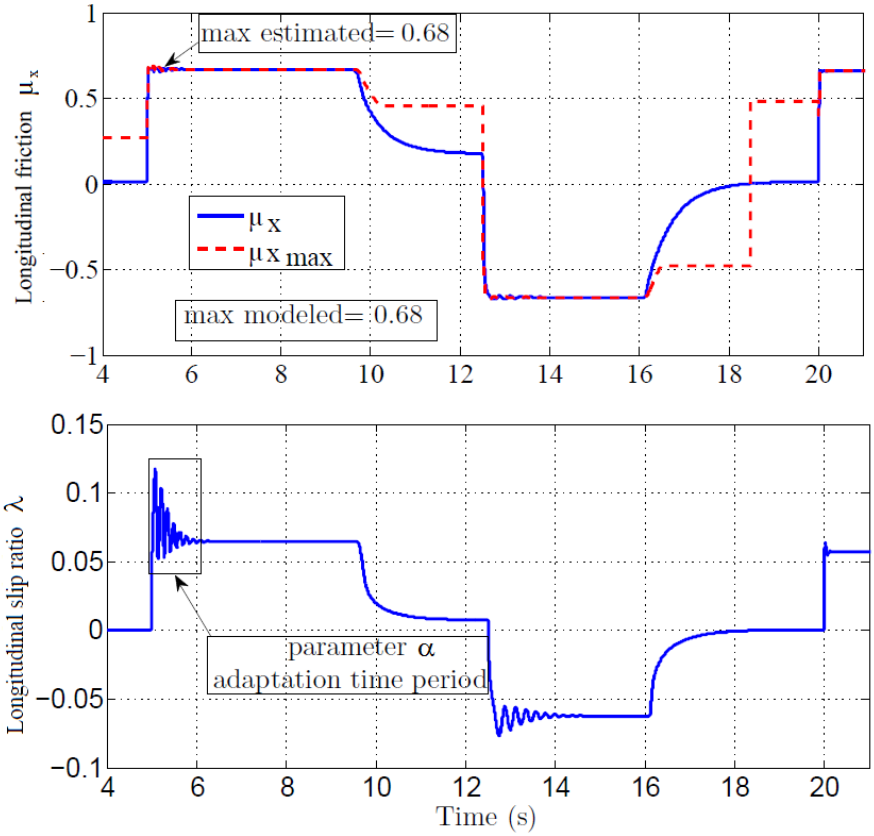

Figure 3.25: Accurate estimation of maximum friction.

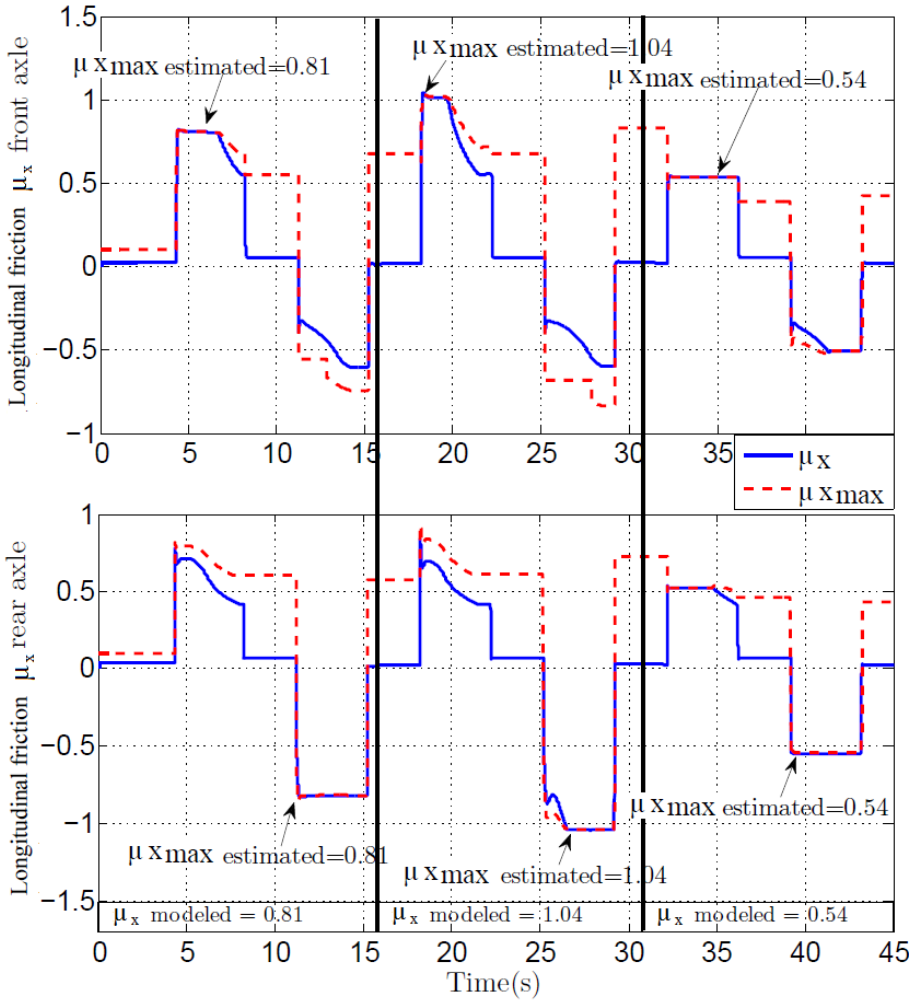

Figure 3.26: Accurate estimation of maximum friction on time-varying $\mu_{x_{max}}$.

Chapter 4

Control

Contents

4.1 Overview

The usual objective of control theory is to calculate solutions for the proper corrective action from the controller that result in system stability, that is, the system will hold the set point and not oscillate around it. A summarized list of some of the main control techniques is:

- Adaptive control uses on-line identification of the process parameters, or modification of controller gains, thereby obtaining strong robustness properties. Adaptive controls were applied for the first time in the aerospace industry in the 1950s, and have found particular success in that field.

- Hierarchical control system is a type of control system in which a set of devices and governing software is arranged in a hierarchical tree. When the links in the tree are implemented by a computer network, then that hierarchical control system is also a form of networked control system.

- Intelligent control uses various computing approaches like neural networks, Bayesian probability, fuzzy logic, machine learning, evolutionary computation and genetic algorithms to control a dynamic system.

- Optimal control is a particular control technique in which the control signal optimizes a certain cost index. Two optimal control design methods have been widely used in industrial applications, as it has been shown they can guarantee closed-loop stability. These are Model Predictive Control (MPC) and linear-quadratic-Gaussian control (LQG). The former can more explicitly take into account constraints on the signals in the system, which is an important feature in many industrial processes. However, the optimal control structure in MPC is only a means to achieve such a result, as it does not optimize a true performance index of the closed-loop control system. Together with PID controllers, MPC systems are the most widely used control technique in process control.

- Robust control deals explicitly with uncertainty in its approach to controller design. Controllers designed using robust control methods tend to be able to cope with small differences between the true system and the nominal model used for design. The early methods of Bode and others were fairly robust; the state-space methods invented in the 1960s and 1970s were sometimes found to lack robustness. A modern example of a robust control technique is H-infinity loop-shaping developed by Duncan McFarlane and Keith Glover. Robust methods aim to achieve robust performance and/or stability in the presence of small modeling errors.

- Stochastic control deals with control design with uncertainty in the model. In typical stochastic control problems, it is assumed that there exist random noise

and disturbances in the model and the controller, and the control design must take into account these random deviations.

- Energy-shaping control view the plant and the controller as energy-transformation devices. The control strategy is formulated in terms of interconnections (in a power-preserving manner) in order to achieve a desired behavior.

The aim of this chapter is to describe a control law that avoids longitudinal wheel slip or skid, independently of the driver's behavior (hard acceleration or emergency braking requirements) and of the conditions of the road surface (wet, dry or snow), using as unique actuator the torque provided by the electric motors. The electric motor that we dispose is an in-wheel electric motor, with a maximum power of 39 kW and a maximum torque of 34.2 Nm. The damping coefficient of the drive-line was also taken into account (R=17), giving a total braking/accelerating torque of 581.4 Nm per wheel. This torque is sufficient to brake the vehicle in emergency maneuvers, therefore no hydraulic brakes were considered. Nevertheless, in an actual vehicle the hydraulic braking should be considered, since a saturation of the battery charge that supplies the electric power to the motors could mean that no negative torque is produced by the motor. Therefore, a backup system should be taken into account in a possible vehicle design that includes in-wheel electric motors. In this work, this aspect was not considered, since the interest was focused on proving that with the braking/accelerating torques produced by the motors, one can achieve a stable wheel and vehicle behavior.

The first stage in the strategy is to estimate "on-line", using Dugoff tire model characteristics, the maximum friction between the wheel and the road which is described in Chapter 3. No actual model was implemented in the estimation routines and only estimations of different Dugoff parameters were conducted. Therefore, the advantages brought by the clarity of the maximum friction yielded from Dugoff model, were used to obtain a reliable estimation of the road conditions modeled by a more complex Pacejka model. The second stage in this approach is to apply the control that keeps the instantaneous longitudinal friction at its maximum value, therefore keeping the longitudinal slip of the wheels in the zone of the friction curves until the peak point.

The novelty of the present work consists in using the electric motor as the only actuator in acceleration and deceleration, in order to provide the necessary torques to accomplish both TCS and ABS functions. The in-wheel motors provide more possibilities for active safety and trajectory control. These motors have a very low latency and are able to provide a braking torque on the wheels faster than conventional hydraulic

brakes. In the classical ICE configuration, the estimation of the wheel friction forces is problematic, due to the lack of a reliable estimation of the torque generated by the engine. With the electric motor, due to a good knowledge of its output torque computed from the measured current, one can estimate the wheel friction forces starting from the wheel dynamics. Unlike the existing, rather conservative, control strategies, described in [13, 15, 36], which rely on a fixed threshold of the longitudinal slip, the electric motor allows to apply a control directly on the friction, while considering the road conditions. Keeping the friction at its peak in hard acceleration or braking maneuvers, not only will achieve a stable vehicle behavior, but also enables an energy regeneration strategy, since in braking phase the motor is functioning in generator mode.

4.2 Open-loop control

An open-loop controller, is a type of controller that uses only an input signal to actuate an output. A characteristic of the open-loop controller is that it does not use feedback to determine if its output has achieved the desired goal of the input. This means that the system does not observe the output of the processes that it is controlling. Consequently, a true open-loop system can not engage in machine learning and also cannot correct any errors that it could make. It may also not compensate for disturbances in the system. Open-loop control is useful for well-defined systems where the relationship between input and the resultant state can be accurately modeled by a mathematical formula.

The behavior of the open loop response of the vehicle is analyzed in this section. For this purpose, a torque input produced by the driver model will act on the overall vehicle system and will be saturated by an open loop control torque computed with the maximum friction taken into account. The longitudinal vehicle response will be analyzed in acceleration and braking phases in varying adherence conditions as well as in perturbation and/or noisy environments. The importance of the estimation of Dugoff parameters will be presented by comparing the case were these parameters are fixed with the one were they are estimated *on-line*. The advantages and limitations of the open loop control will be highlighted along the section.

4.2.1 Torque saturation control

In the vehicle model, longitudinal efforts are computed using the Pacejka model, described in Chapter 2. The curves peak introduced in the model will be estimated using the Dugoff model, as shown in Chapter 3. In other words, Dugoff model will be used to approximate the Pacejka model, in order to detect the maximum available friction. On one side, the driver model is used to simulate torque demands that are taken as input in the control strategy. On the other side, these torques will be saturated with a maximum value, computed with the knowledge of the maximum available friction.

The open-loop control will only saturate the demanded torque by a maximum torque value, which is computed starting from wheel dynamics equation (2.2) of the overall model:

$$I\dot{\omega} = T - r_e F_x - R_x. \tag{4.1}$$

Replacing F_x by equation (2.4), and extracting the torque T will yield:

$$T = I\dot{\omega} + r_e \mu_x F_z + R_x. \tag{4.2}$$

Therefore, the saturation torque taking into account the estimated maximum friction will be given by:

$$T_{sat} = I\dot{\omega} + r_e \mu_{x_{max}} F_z + R_x. \tag{4.3}$$

The torque obtained with the above formula will limit the torque demanded by the driver in the case were slip occurs, following an *activation algorithm* described as follows:

Here, T_{flat} is defined as in Equation (2.28):

$$T_{flat} = r_e(F_{aero} + \frac{1}{r_e}R_x + mPI_{out} + m\dot{V}_{x_{ref}}). \tag{4.4}$$

The output of the PI controller is described in the following algorithm:

Therefore, as long as we are in the linear zone of the friction curves, delimited by λ_{lim}, the torque applied at the wheel T_{wheel} is equal to the torque coming from the driver's requirements. Here, we are in the pseudo-sliding zone "a" as shown in Figure 1.5, therefore in the stable zone. Once the linear zone threshold λ_{lim} is exceeded, the

Table 4.1: Algorithm 4: Activation algorithm.

```
if |λ| ⩽ |λ_lim|
    T_wheel = T_flat
else
    if λ > 0
        T_wheel = min(T_flat, T_sat)
        else
            T_wheel = max(T_flat, T_sat)
```

Table 4.2: Algorithm 5: PI controller with anti-windup.

```
if ((ν ⩾ 0) and (PI_out ⩾ u_max)) or ((ν ⩽ 0) and (PI_out ⩽ u_min)
        PI_out_{t_k} = K_p ν_{t_k} + K_i (∫ ν)_{t_{k-1}} dt
else
        PI_out_{t_k} = K_p ν_{t_k} + K_i (∫ ν)_{t_k} dt,
```

minimum value between the saturated torque and the driver torque will be applied in acceleration, and the maximum value in deceleration. In this way, the saturated torque will always limit the bigger torque coming from the driver, which will avoid wheel slip or skid.

4.2.2 System behavior analysis with errors on the maximum friction estimation

Since the estimation strategy utilizes different derivatives of variables, it can affect the computation of various estimates used in the control strategy. This is the case of the maximum friction estimation, which can be affected by imprecise computations. Complex computations can induce inaccurate maximum values for the maximum friction available. In a first analysis, we will study the impact of an inaccurate value for the friction on the overall system behavior.

If the estimation of $\mu_{x_{max}}$ is precise, the control achieves a stable behavior, as seen in Figure 4.1. In this case, the maximum friction stays fixed, supposing all the other parameters estimated or adapted.

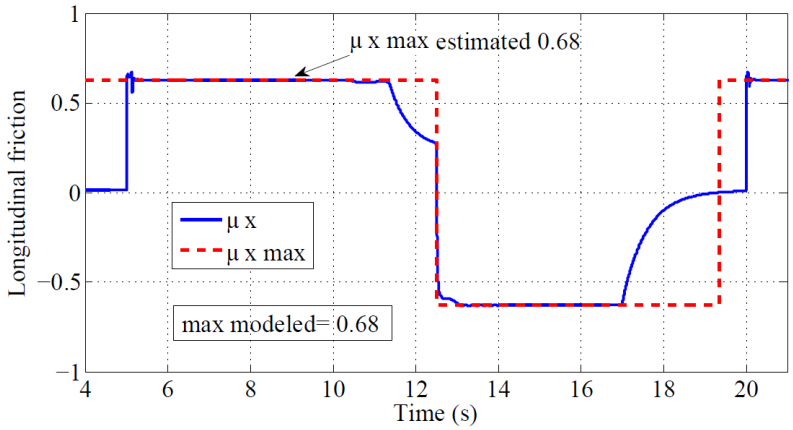

Figure 4.1: Unaffected maximum friction estimation.

In the case of underestimation of the maximum friction, the system response is as well stable, since the values of the maximum estimated friction are even farther from the peak, and therefore far from the unstable zone. The impact of the underestimation of the maximum friction can be seen in Figure 4.2. There are almost no oscillations in the transient phase, and a linear behavior is achieved in the stabilized phase.

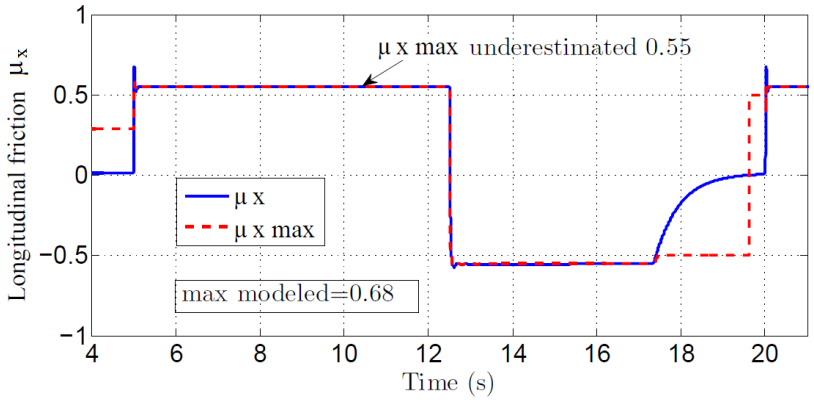

Figure 4.2: Underestimation of maximum friction.

The worst case scenario is when the maximum friction is overestimated and the results are shown in Figure 4.3, indicating the wheel excessive spin in acceleration and wheel lock-up in braking phase. So, once the peak of the friction characteristics is exceeded, the wheel spins faster and faster in acceleration, and blocks in braking phase. A torque controller has to limit the torque transmitted at the wheels in order

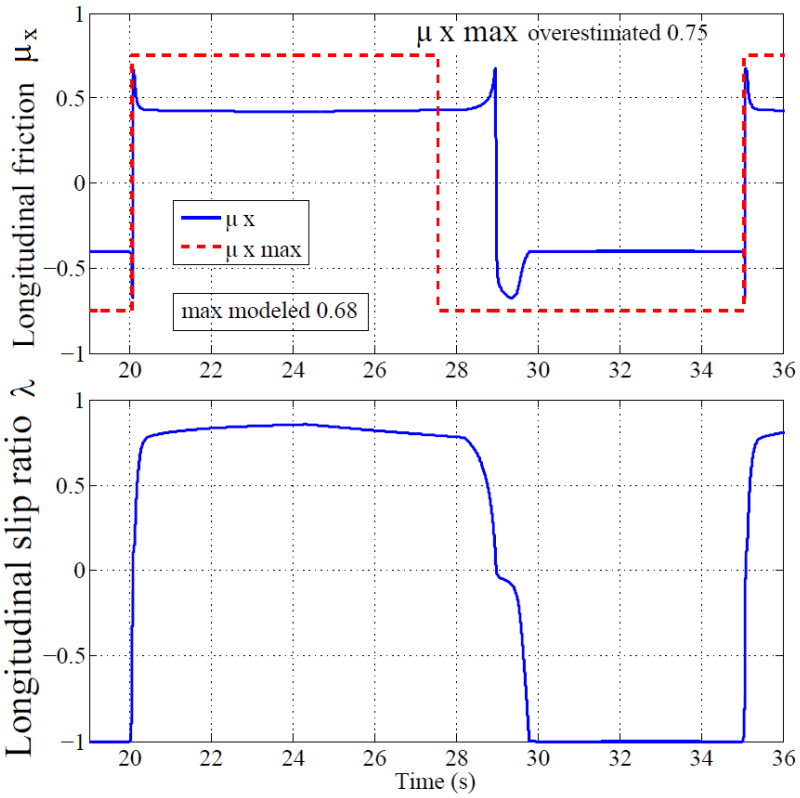

Figure 4.3: Overestimation of maximum friction.

to avoid the behavior shown in Figure 4.3.

4.2.3 Torque saturation control applied on "dynamic" Pacejka model

4.2.3.1 Noise-free environment

The state of the road X_r intervenes in the formulation of the dynamic Pacejka model, described in section 2.4.2.

$$F_x = \left(\frac{k_{d_1}}{X_r + k_{d_2}} + X_r k_{d_3} \right) \sin((X_r + k_c) \arctan(B\lambda - E(B\lambda - \arctan(B\lambda)))) \quad (4.5)$$

The input X_r profile and the speed profile used in the sequel are shown in Figure 4.4 and Figure 4.5, respectively. In Figure 4.5 we find hard acceleration and braking

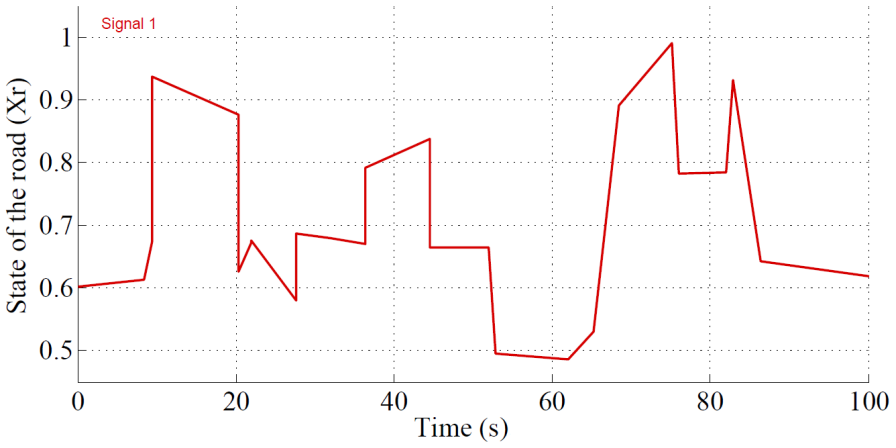

Figure 4.4: Time evolution of the state of the road X_r.

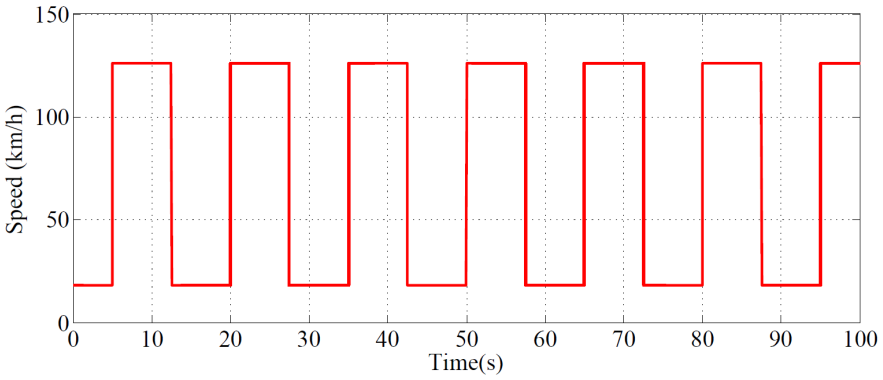

Figure 4.5: Speed profile used in the simulations.

phases, simulated to push the estimation and control strategies at their limits and to test the robustness of the proposed method.

Setting up the estimation of the maximum friction estimation as described in Section 3.4.3, along with the control strategy presented in Section 4.2.1, will yield the results in terms of maximum friction tracking shown in Figure 4.6.

One can be seen that even though the maximum friction changes in time, the estimation method provides a reliable value for $\mu_{x_{max}}$. The $\mu_{x_{controlled}}$ line in Figure 4.6 shows that the instantaneous friction never exceeds the maximum estimated value, therefore accomplishing the purpose of the control. At the same time, in Figure 4.6 one can see some low friction phases. These are in fact the moments where the reference speed to track is low, and no acceleration or braking maneuver is carried out, and therefore a low instantaneous friction value is obtained. A more closer look of the

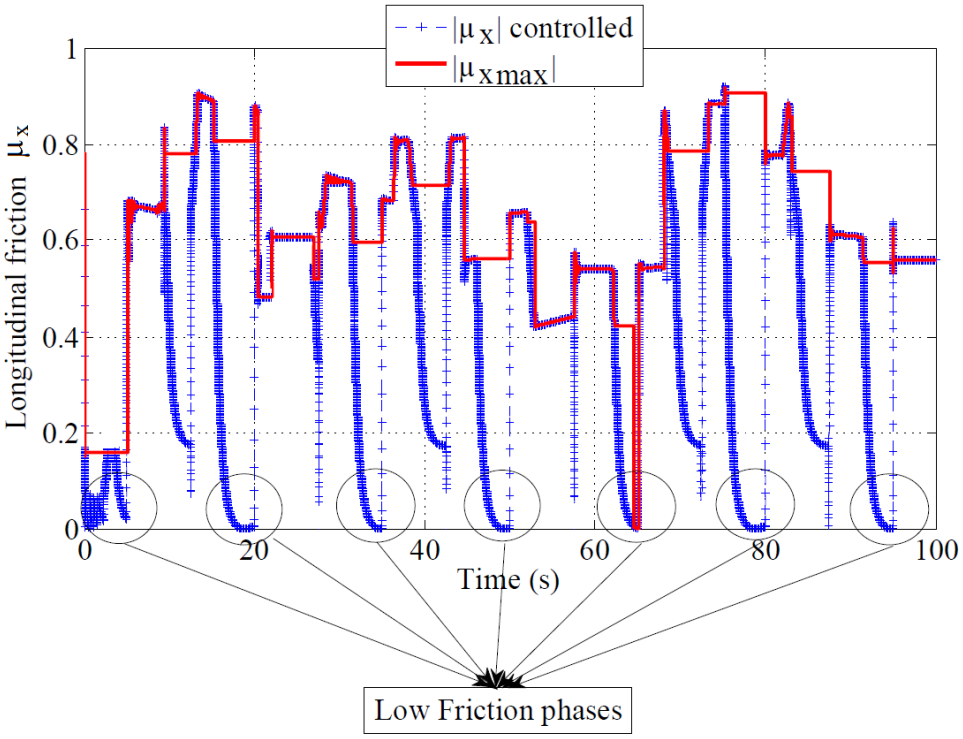

Figure 4.6: Maximum friction tracking.

friction tracking performed with the open loop control enabled is shown in Figure 4.7.

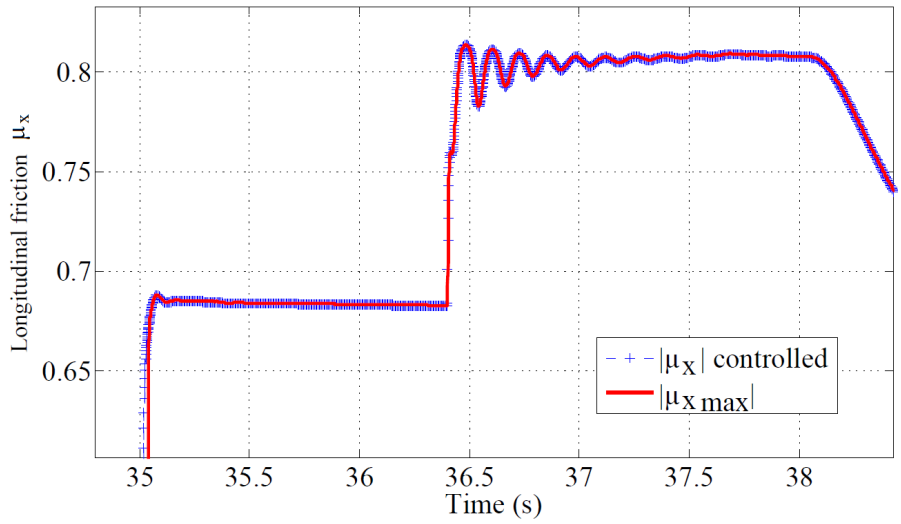

Figure 4.7: Zoomed-in maximum friction tracking.

An interesting fact happens at simulation time t=53s. Here the maximum friction

drops from approximately 0.7 to 0.4 during the acceleration phase. In other words we go from a rainy road to a snowy road. Nevertheless, the control tracks this variation of the maximum available friction, giving a stable wheel behavior, as shown in Figure 4.8.b.

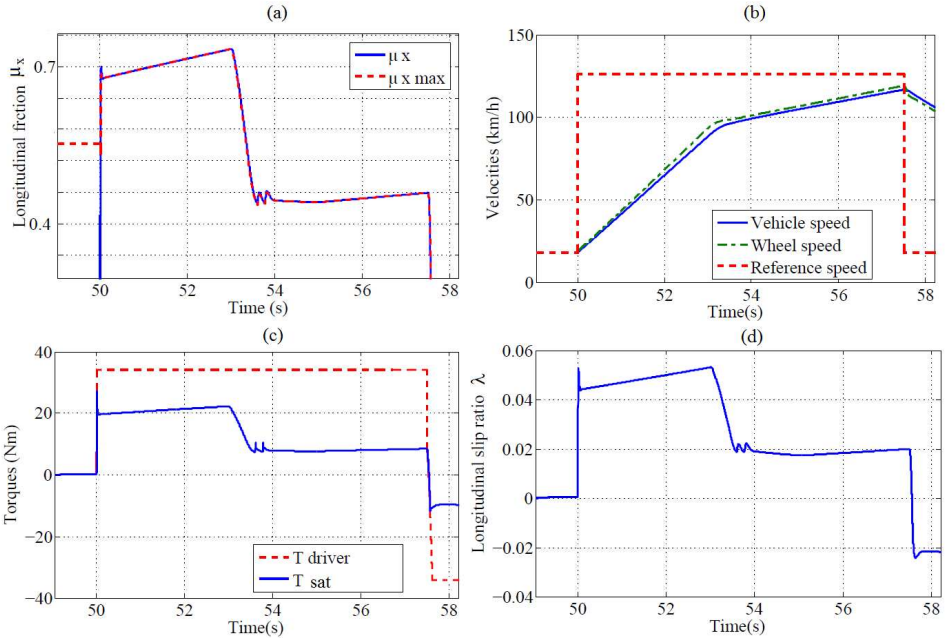

Figure 4.8: Maximum friction variation tracking.

Given the variation of parameter X_r which will also induce the variation of parameters C and D of Pacejka formula, the slope of the linear segment of the friction curves is continuously changing. In our strategy, the slope of the linear segment is defined by parameter K_x. We have computed its off-line values for the state of the road profile shown in Figure 4.4 to have a reference value to compare with its estimated value. Its evolution is shown in Figure 4.9 and one can see that the slope varies continuously, the estimation approximately follows the modeled value. Also, one has to take into account that K_x only updates when the values of the longitudinal slip are in the linear zone of the friction characteristics.

The adaptation parameter α will also be variable, depending on the state of the road. As in the case of K_x, off-line values for α were computed, for the same state of the road input X_r. Its evolution is shown in Figure 4.10. Note that the range of variation of α is reduced compared to the one of K_x. The estimation of the parameter α will compensate the errors that arise in the estimation of K_x, therefore its estimated

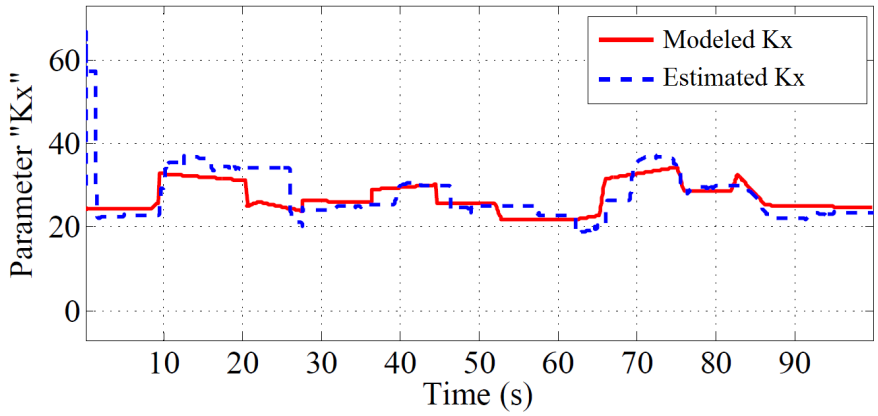

Figure 4.9: Reference and estimated value for K_x.

values differ from the the modeled values, yet they follow the modeled profile. The

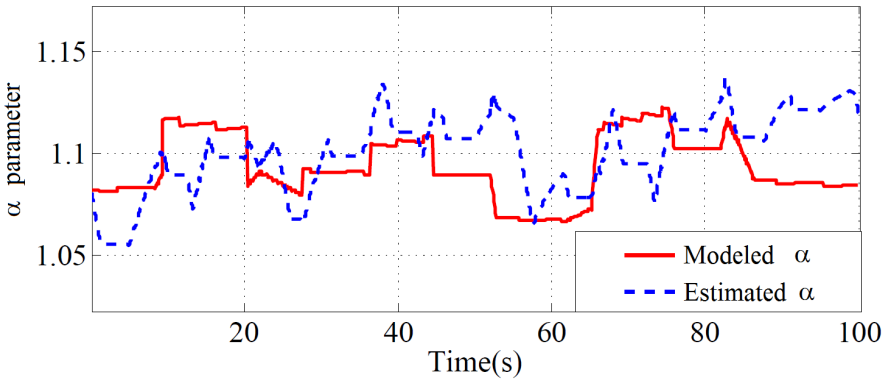

Figure 4.10: Reference and estimated value for α.

large variation of Pacejka parameters yields a model closer to real situations, giving estimations that no longer stay on one curve, but on multiple curves, as shown in Figure 4.11.

Even if the estimation points seem to be more dispersed than in a conventional modeling, it can be seen in Figure 4.11 that $\mu(\lambda)$ never exceeds the peak of the curves, showing good performance of the control scheme. The conditions vary from dry roads with $\mu_{x_{max}} = 0.9$ to snowy roads with $\mu_{x_{max}} = 0.3$. So, a large range of tire-road friction is ran through, testing the estimation and control methods and their limits, yielding good results in terms of friction tracking and vehicle behavior.

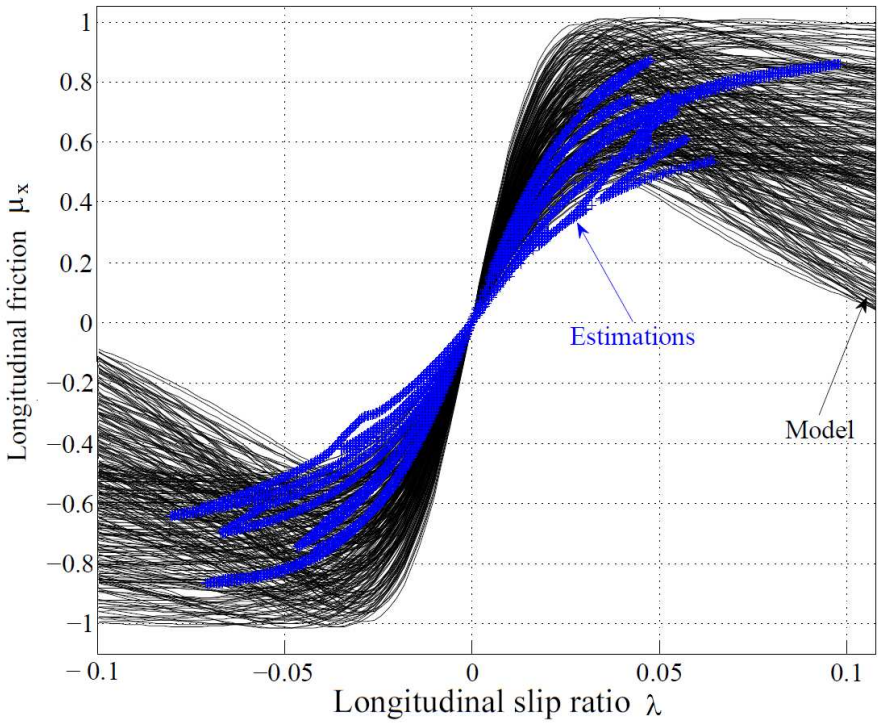

Figure 4.11: Friction estimation on time-varying road conditions.

4.2.3.2 Noise perturbation

In real systems, noise can affect the performances of the estimation strategy propagating to the control applied at the wheel. In the following, we take into account a random noise coming from wheel acceleration that affects the estimation of $\mu_{x_{max}}$.

As seen in Figure 4.13, the noise coming from the maximum friction estimation is propagated on the computation of the control. But, having taken into account the filtering provided by the electric motors, with their small delays, the final torque applied at the wheels is less affected by the noise (see Figure 4.13). Hence, even in noisy environment with continuous variation of Pacejka parameters, the control performs good tracking of the maximum friction, as seen in Figure 4.14.

As expected, the estimation of $\mu_{x_{max}}$ gives a larger dispersion of points in noisy environments (Figure 4.15), coming closer to the view seen in real experimental results (see Figure 2.11). This shows that our approach to modeling the road surface conditions comes closer to what is found in real environments. It can be seen in Figure 4.15 that even when the noise affects $\mu_{x_{max}}$, the parameter α compensates possible estimation errors, and therefore the peak of the curves is never exceeded, showing the

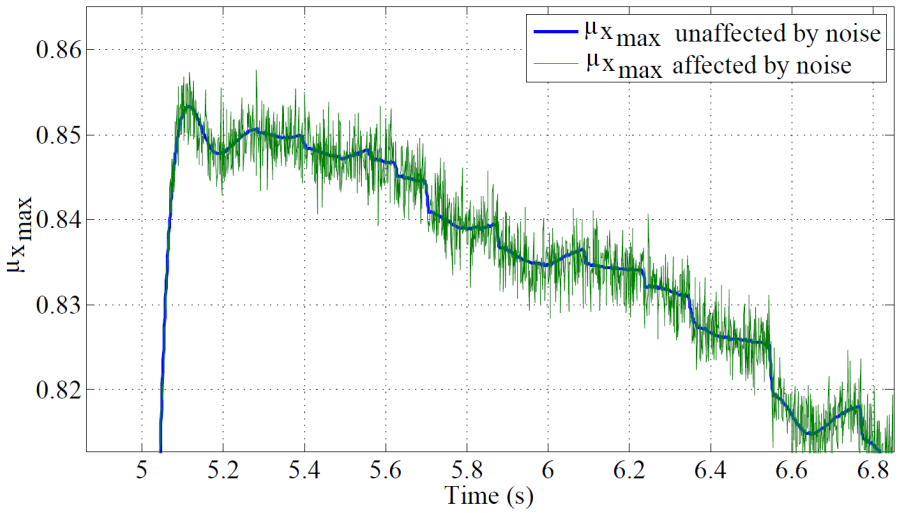

Figure 4.12: Noise affecting the estimation of $\mu_{x_{max}}$.

robustness of our method.

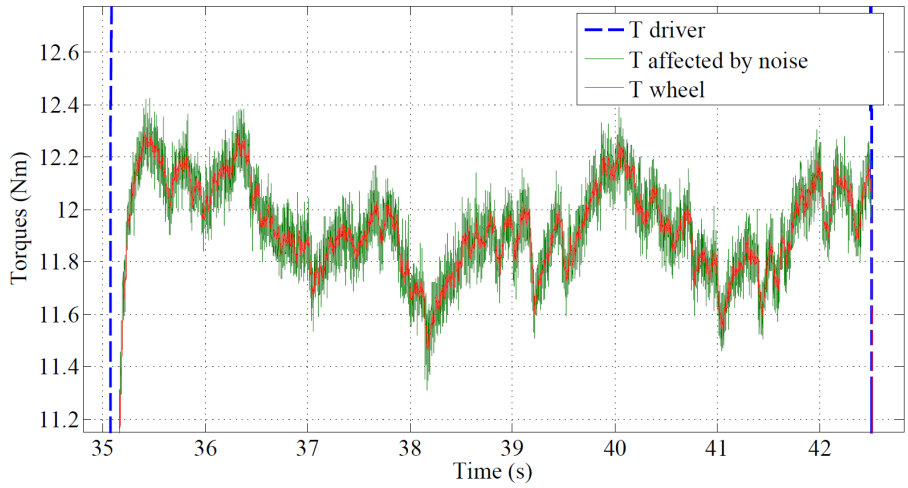

Figure 4.13: Noise affecting the computation of T_{sat}.

A closer look on the points shows the behavior of the estimation and control strategy. In Figure 4.16 it can be observed that the transition from one type of road surface to another is made in a continuous manner, as it is the case in actual tire-road environments.

The overall estimation process gives the expected results, detecting the variation of road conditions even when the estimation process is affected by noise. A part of the noise is attenuated by the electric motor [37] and the adaptation parameter α,

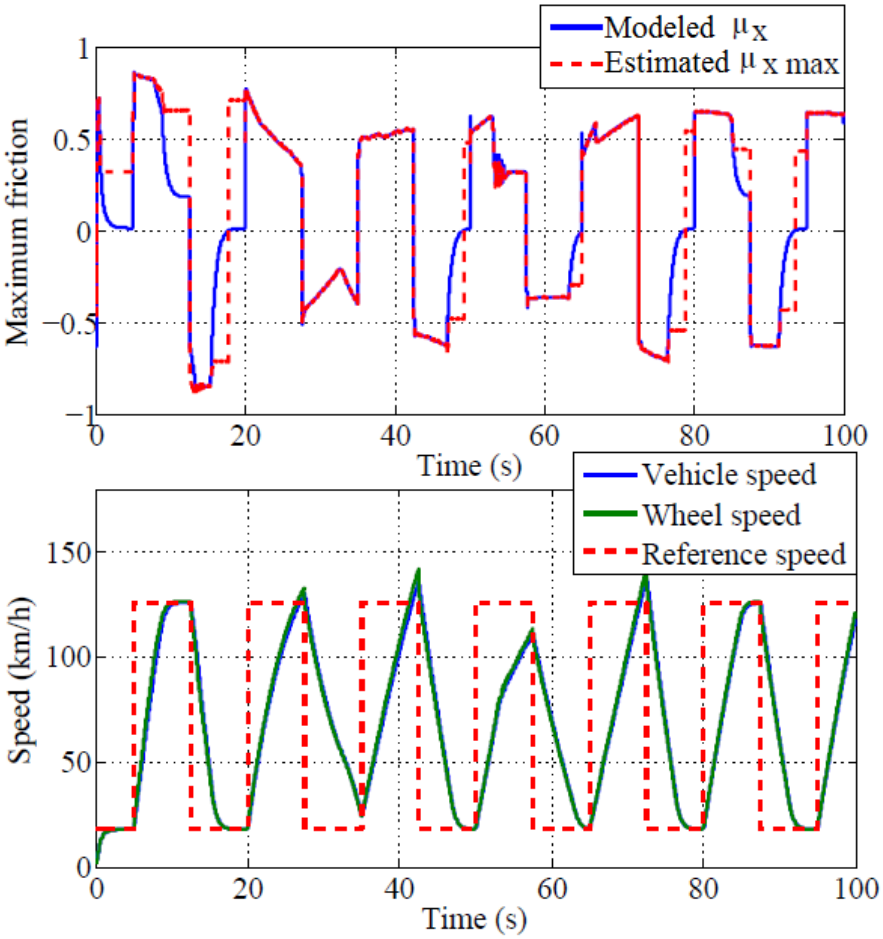

Figure 4.14: Speed and maximum friction tracking.

achieving the tracking of the maximum available friction in varying surface conditions.

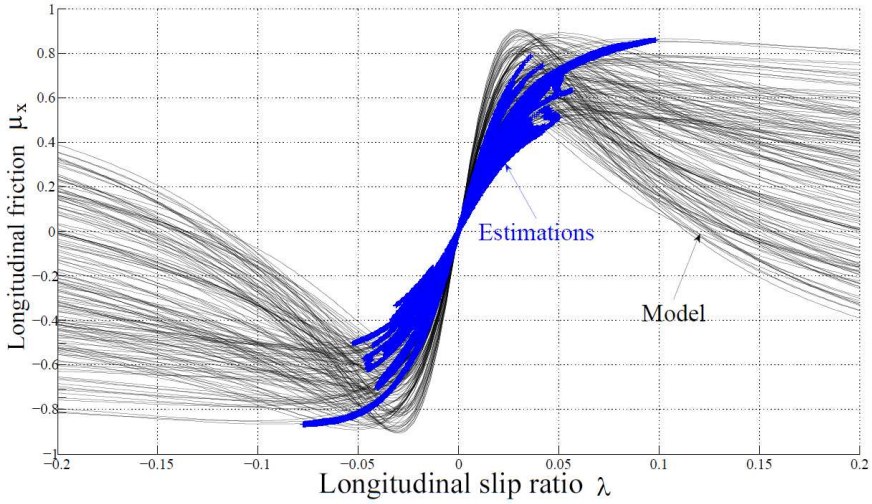

Figure 4.15: Maximum friction estimation in a noisy environment.

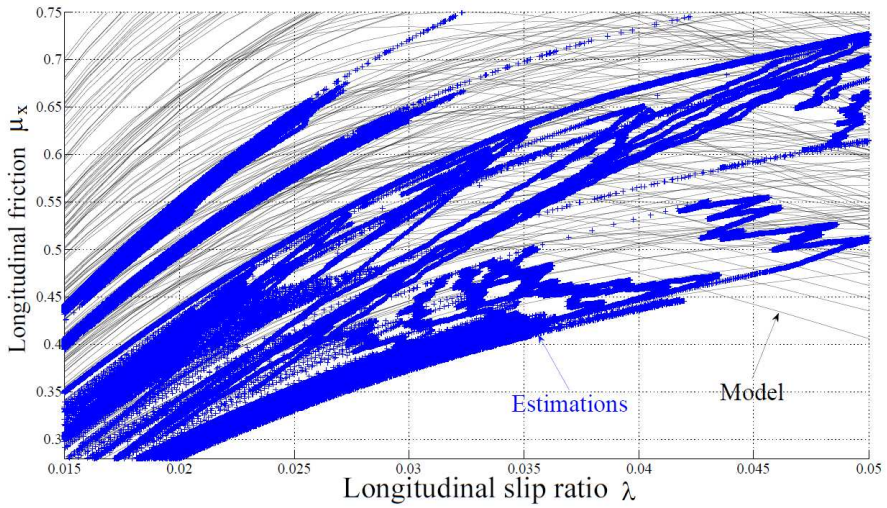

Figure 4.16: Maximum friction estimation in a noisy environment.

4.3 Closed-loop control

Generally, to obtain a more accurate tracking, it is necessary to feed the output of the system back to the inputs of the controller. A closed-loop controller uses feedback to control states or outputs of a dynamical system. Closed-loop controllers have the following advantages over open-loop controllers:

- disturbance rejection;
- guaranteed performance even with model uncertainties, when the model struc-

ture does not match perfectly the real process and the model parameters are not exact;

- unstable processes can be stabilized;
- reduced sensitivity to parameter variations;
- improved reference tracking performance.

In some systems, closed-loop and open-loop control are used simultaneously. In such systems, the open-loop control is termed "feed-forward" and serves to further improve reference tracking performance. A common closed-loop controller architecture is the PID controller.

4.3.1 Sliding-mode control

Sliding mode control strategy applied for vehicle dynamics control was, among others, proposed in [92, 100, 62]. In [92] the authors treat the design and sliding mode control of two structures with hybrid sources. The first structure uses super-capacitors, fuel cell and batteries and the second one is similar to the first but without batteries. In [100] the sliding mode control of an electric differential system for electric vehicles with two induction motor drives (one for each wheel) is described. In this case, the electric differential manages the speed difference between the two wheels when cornering.

The present control law is added in order to manage the case where the driver requirements induce slip or skid at the wheels. A feedback sliding control law is designed such that it will guarantee that the system trajectory moves towards the sliding surface and stays on it once hitting it. Since we dispose of the maximum friction and the instantaneous friction, the simplest control strategy consists in emergency situations (hard braking or hard acceleration), operating the vehicle at the maximum of the friction or close to it. The purpose of this control law is to keep the instantaneous friction at its maximum value (maximum friction estimated in Section 3.4), therefore an obvious sliding surface would be $S = \mu_{x_{max}} - \mu_x$.

Implementation of the control design requires the knowledge of the individual rotational wheel speeds and of the two variables obtained in Chapter 3, $\mu_{x_{max}}$ and μ_x. In order to take advantage of the previous $\mu_{x_{max}}$ estimation, a sliding surface $S = (\mu_{x_{max}} - \mu_x)sign(XBS)$ has been selected. This implies that when $S = 0$ the vehicle is operated at $\mu_x = \mu_{x_{max}}$.

Since the maximum friction $\mu_{x_{max}}$ is always greater than μ_x, we have to distinguish when the sliding surface becomes negative. This is the purpose of the the "$sign(XBS)$" term in the expression of the sliding surface, which is added to manage the case where the instantaneous friction crosses the peak of the friction curve at $\mu_{x_{max}}$. In this case, the XBS becomes negative and therefore the sliding surface becomes negative, allowing the control to bring back the values of μ_x to track $\mu_{x_{max}}$.

Taking the derivative of the sliding surface and substituting the expression of the friction obtained in equation (3.1), yields:

$$\dot{S} = -\dot{\mu}_x sign(XBS) = -\frac{1}{r_e F_z}(\dot{T} - I\ddot{\omega}) sign(XBS). \tag{4.6}$$

When $S = 0$, it is required that $\dot{S} = 0$. Next, $\dot{S} = 0$ implies that $\dot{T}_{eq_1} = I\ddot{\omega}$. Then :

$$T_{eq_1} = \int (I\ddot{\omega})\, dt = I\dot{\omega} + k_1. \tag{4.7}$$

Note that $S = 0$ implies that $\mu_x = \mu_{x_{max}}$. Substituting again the expression for μ_x and choosing $k_1 = r_e F_z \mu_{x_{max}} + R_x$ we obtain the equivalent torque in order to get $S = 0$ and $\dot{S} = 0$:

$$T_{eq} = I\dot{\omega} + r_e F_z \mu_{x_{max}} + R_x. \tag{4.8}$$

When $S \neq 0$, it is required that $S\dot{S} < 0$. Replacing the expression for $\dot{S}$, we obtain $Ssign(XBS)\dot{\mu}_x > 0$. We then get two possible cases :

- $Ssign(XBS) > 0$ (the zone of $\mu - \lambda$ curves before arriving at the peak). Then $\dot{\mu}_x > 0$. Therefore, from equation (4.6) we get $\dot{T}_{eq} > I\ddot{\omega}$. Replacing T_{eq} by its expression from equation (4.8) and calculating its first derivative will obtain $\dot{T}_{eq} = I\ddot{\omega}$. Taking $\dot{T}_{eq} = I\ddot{\omega} + \dot{T}_{sm_1}$, with $\dot{T}_{sm_1} = Sk_2 > 0$ will ensure that $\dot{T}_{eq} > I\ddot{\omega}$ is satisfied. Here, $k_2 > 0$ is a design parameter.

- $Ssign(XBS) < 0$ (the zone of $\mu - \lambda$ curves after crossing the peak). Then $\dot{\mu}_x < 0$. Now, the condition to verify becomes $\dot{T}_{eq} < I\ddot{\omega}$. Taking again $\dot{T}_{eq} = I\ddot{\omega} + \dot{T}_{sm_2}$, with $\dot{T}_{sm_2} = Sk_2 < 0$ will ensure that $\dot{T}_{eq} < I\ddot{\omega}$ is satisfied.

Putting together the two conditions we obtain:

$$T_{sm} = \int (Sk_2) dt. \tag{4.9}$$

The sliding control law is defined as:

$$T_{sliding} = T_{eq} + sign(S)T_{sm}, \tag{4.10}$$

leading to:

$$T_{sliding} = I\dot{\omega} + r_e F_z \mu_{x_{max}} + R_x + sign(S) \int (Sk_2)dt. \tag{4.11}$$

The presence of the *sign* function in the control law can induce chattering, therefore in the simulations presented in the sequel, it has been replaced by a *saturation* function, which allows the surface to remain in a tube with a desired width. As stated previously, the sliding mode control is added to manage the case where the slip or the skid of the wheels occurs. Hence, it has to be activated when this happens. We now have two control laws, one that tracks a reference speed (T_{flat}), and another one that tracks a reference adherence ($T_{sliding}$). In the next section the activation strategy of each control law is presented.

4.3.1.1 Activation of control

The purpose of the activation strategy is to achieve a control that has a double objective: to track a reference speed and in the same time to maintain grip of the wheels, regardless of drivers requirements and adherence variation. In the linear zone of the friction curve the applied control law is T_{flat}, while, when entering in the non linear zone, $T_{sliding}$ is applied. When the values for the longitudinal slip are below the values of λ_{lim} (computed as in Equation (3.10) p 92), then T_{flat} is applied. Otherwise, a switching between the two controls takes place, and it follows a "(min,max)" rule, as shown in algorithm 6.

This algorithm defines a "safety-zone" for all $|\lambda| \leqslant |\lambda_{lim}|$ in which we allow the torque coming from the driver requirement to be applied at the wheel of the vehicle, knowing that for these values of the slip we are at the beginning of the $\mu - \lambda$ curves and thus in the stable linear zone.

Once this threshold is exceeded, the switch between the sliding mode control and the flatness-based control is applied, limiting each time the greater torque, to avoid wheel slip or skid. In acceleration phases, the minimum value between the two torques is applied while in braking phases it is the maximum value that is applied.

Table 4.3: Algorithm 6: Switching algorithm.

---

if $|\lambda| \leqslant |\lambda_{lim}|$
  $T_{wheel} = T_{flat}$
else
  if $\lambda > 0$
    $T_{wheel} = \min(T_{flat}, T_{sliding})$
    else
      $T_{wheel} = \max(T_{flat}, T_{sliding})$

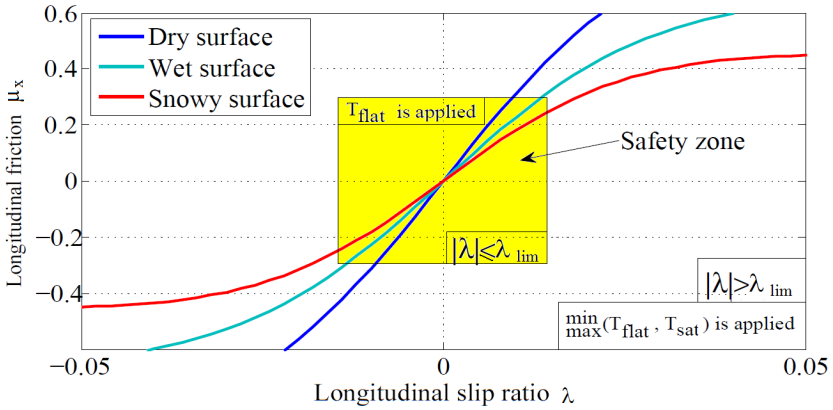

Figure 4.17: Safety zone (pseudo-linear zone of $\mu - \lambda$ curves).

4.3.2 Event driven model free control

Model-free control is associated with the corresponding "intelligent" PID controllers (iPIDs) [19], with many successful concrete applications. In the following, a brief recall of model free control is shown.

4.3.2.1 Brief model free control recall [96]

A finite dimensional SISO system can be implicitly described as:

$$A(y, \dot{y}, \ldots, y^{(a)}, u, \dot{u}, \ldots, u^{(b)}) = 0, \tag{4.12}$$

where $A : \mathbf{R}^{a+1} \times \mathbf{R}^{b+1} \to \mathbf{R}$ is a sufficient smooth function of its arguments. Assume that for integer ν, $0 < \nu \leqslant \iota$, $\partial A / \partial y^{(\nu)} \not\equiv 0$. The implicit function theorem [44] allows

to express $y^{(\nu)}$ locally:

$$y^{(\nu)} = E(t, y, \dot{y}, \ldots, y^{(\nu-1)}, y^{(\nu+1)}, \ldots, y^{(\iota)}, u, \dot{u}, \ldots, u^{(\kappa)}), \tag{4.13}$$

with the function $E : \mathbf{R} \times \mathbf{R}^{\iota} \times \mathbf{R}^{\kappa+1} \to \mathbf{R}$. No matter whether the system is linear or not, we can rewrite the system (4.12) as the following phenomenological model which is only valid in a very short time interval:

$$y^{(\nu)} = F + \beta u, \tag{4.14}$$

where $\beta \in \mathbb{R}$ is a non-physical constant parameter, which is chosen by the engineer in such a way that F and βu are of the same order of magnitude. The derivation order ν is also an engineer's choice.

Here, F stands for the neglected parts of the system. It can be determined by the knowledge of u, β and y. An estimate of F is obtained as follows:

$$\hat{F} = \hat{y}^{(\nu)} - \beta \tilde{u}, \tag{4.15}$$

where $\hat{y}^{(\nu)}$ is an estimate of the ν^{th} derivative of the measure y which is assumed available, and $\tilde{u}$ is an approximate value of u. Among the existing possibilities, $\tilde{u}$ can be chosen as a past value of the control variable u.

From above, we can see that F contains the real relationship between the inputs and the outputs, including all the unconsidered and neglected parts of the model as well as all the disturbances.

The resulting controller is then defined as:

$$u = \frac{1}{\beta} \left(y_r^{(\nu)} - \hat{F} + \Lambda(\mathbf{e}) \right), \tag{4.16}$$

where y_r is a reference trajectory which is selected as in flatness-based control [57]. The variable $\mathbf{e} = y_r - y$ is the tracking error and Λ is an appropriate function such that the closed loop error dynamics $e^{(\nu)} = \Lambda(\mathbf{e})$ is asymptotically stable.

From above, we can see that the derivation order ν is not necessarily equal to the derivation order a of y in equation (4.12). The derivation order ν is often taken equal to 1 or 2.

The estimate of $y^{(\nu)}$ in (4.15) can be obtained for example through a cascade of

first order filters as:

$$\mathscr{L}(\hat{\dot{y}}) = \frac{s}{1+T_f s}\,\mathscr{L}(y). \tag{4.17}$$

Typically, $1/T_f$ ranges from 8 to 20, and $\mathscr{L}$ denotes the transformation to the operational domain.

4.3.2.2 Application to vehicle dynamics

The model free control needs to keep instantaneous friction μ_x at its maximum value $\mu_{x_{max}}$. Here, we use the wheel torque T to control the instantaneous friction μ_x. The derivative of equation (2.5) yields:

$$\dot{\lambda} = \frac{r_e(\omega \dot{V}_x - V_x \dot{\omega})}{\max(r_e^2\omega^2, V_x^2)}. \tag{4.18}$$

The derivative of μ_x can be written as $\dot{\mu}_x = \frac{d\mu_x}{d\lambda}\dot{\lambda}$. In this equation we replace $\dot{\lambda}$ by the equation (4.18) and furthermore, we replace the expressions of $\dot{V}_x$ and $\dot{\omega}$ from equation (2.1) and equation (2.2) respectively. The following expression is obtained:

$$\dot{\mu}_x = \frac{r_e \frac{d\mu_x}{d\lambda}}{\max(r_e^2\omega^2, V_x^2)}\left[\left(\frac{\omega}{m} + \frac{r_e V_x}{I}\right)\mu_x F_x - \frac{\omega F_{aero}}{m} + \frac{V_x R_x}{I}\right] - \frac{r_e V_x \frac{d\mu_x}{d\lambda}}{I\max(r_e^2\omega^2, V_x^2)}T. \tag{4.19}$$

Now, $\dot{\mu}_x$ is expressed as in equation (4.14):

$$\dot{\mu}_x = F + \beta T. \tag{4.20}$$

where $\beta = -\dfrac{r_e V_x \frac{d\mu_x}{d\lambda}}{I\max(r_e^2\omega^2, V_x^2)}$ and F includes all the other parts. This leads to the following expression for the control input:

$$T = \frac{1}{\beta}\left[-\hat{F} - k_1 e - k_2 \int e\right], \qquad \hat{F} = \hat{\dot{\mu}}_x - \beta^- T^-, \qquad e = \mu_x - \mu_{x_{max}}. \tag{4.21}$$

with $\mu_{x_{max}}$ the reference friction, $\hat{\dot{\mu}}$ an estimate of the derivative of μ_x, β^- and T^- past values of β and T (approximations of β and T). Hence, we can rewrite the control

input as the following:

$$
\begin{aligned}
T(t_{k+1}) &= T(t_k) + \frac{1}{\beta(t_k)}\left[-\hat{\mu_x}(t_k) - k_1 e(t_k) - k_2 \sum e(t_k)\right], \\
e(t_k) &= \mu_x(t_k) - \mu_{x_{max}}(t_k). \\
\hat{\mu_x}(t_k) &= \frac{\mu_x(t_k) - \mu_x(t_{k-1})}{t_k - t_{k-1}}
\end{aligned} \tag{4.22}
$$

In the event driven model free control, we define $\varepsilon = |\mu_{x_{max}}| - |\mu_x| \geqslant k$ as our trigger law. The activation of the control law will follow the next algorithm:

Table 4.4: Algorithm 7: Control law activation.

---

if $|\varepsilon| \geqslant k$
  $T_{wheel} = T_{driver}$
else
  $T_{wheel} = T_{model\,free}$

4.4 Realistic case studies simulation and comparison of closed-loop strategies

4.4.1 Comparison between event driven model free and sliding mode control

In this case, a hard acceleration and a hard braking maneuver are simulated on a dry road ($\mu_{x_{max}} = 1$). Applying both control techniques on this scenario gives the results shown in comparison in Figures 4.18 and 4.19. In both cases the maximum friction is tracked when the trigger is activated, yet with almost no oscillations in the case of model free control (Figure 4.19.a compared to Figure 4.18.a). This results in a more stable torque response in the case of model free control (Figure 4.19.b) in comparison with the sliding mode control (Figure 4.18.b). Consequently, the transmitted torque gives a more stable wheel behavior in the case of model free control (Figure 4.19.c), improving vehicle stability and passenger comfort.

In realistic environments, perturbations can arise. These perturbations can be considered as a variation of the maximum friction. Indeed, friction is subject to variation,

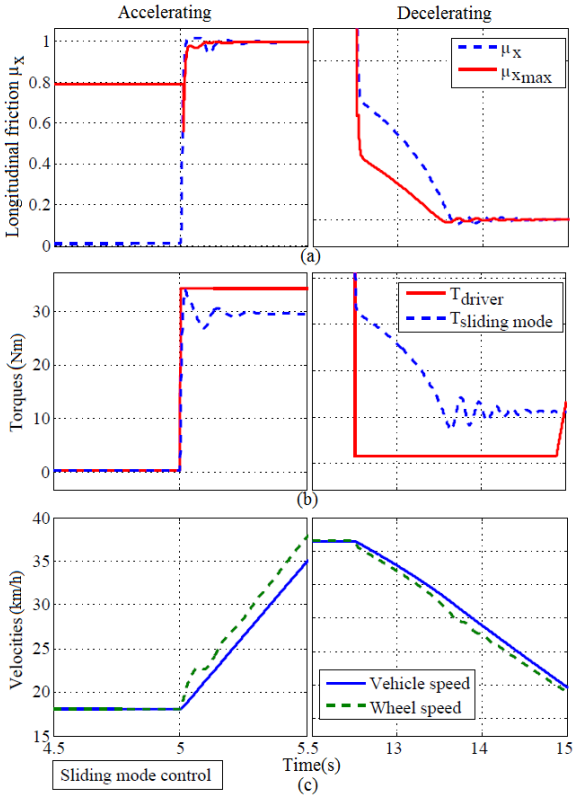

Figure 4.18: Sliding mode control without perturbation.

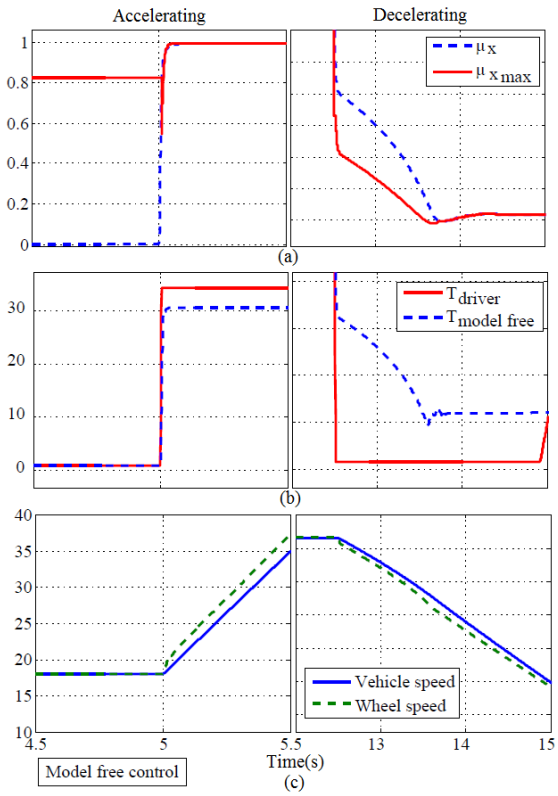

Figure 4.19: Model free control without perturbation.

its values changing due to numerous factors such as weather conditions (hot temperatures, rain, snow or ice), road maintenance and type of pavement (asphalt, concrete or cobblestone) among others. Therefore, modeling a perturbation as a change in the maximum friction is quite reasonable. In this second scenario, a perturbation is simulated to arise at simulation time t=21s, changing the maximum friction from its initial value of 1 to 0.85. In a realistic environment this could be regarded as a transition from a dry road to a wet one. Despite the perturbation, the control should be able to continuously track the reference maximum friction. The results are shown in Figure 4.20.

Once again, the model free control behaves smoother and achieves a quicker reference tracking in comparison to the sliding mode control, when a perturbation arises (Figure 4.20.a). This smoothness is transposed in the torque response computed with the model free technique (Figure 4.20.c). Consequently, the behavior of the wheel is more regular, giving a more stable behavior of the vehicle (Figure 4.20.b).

To show a detailed comparison, six criteria have been chosen to compare the per-

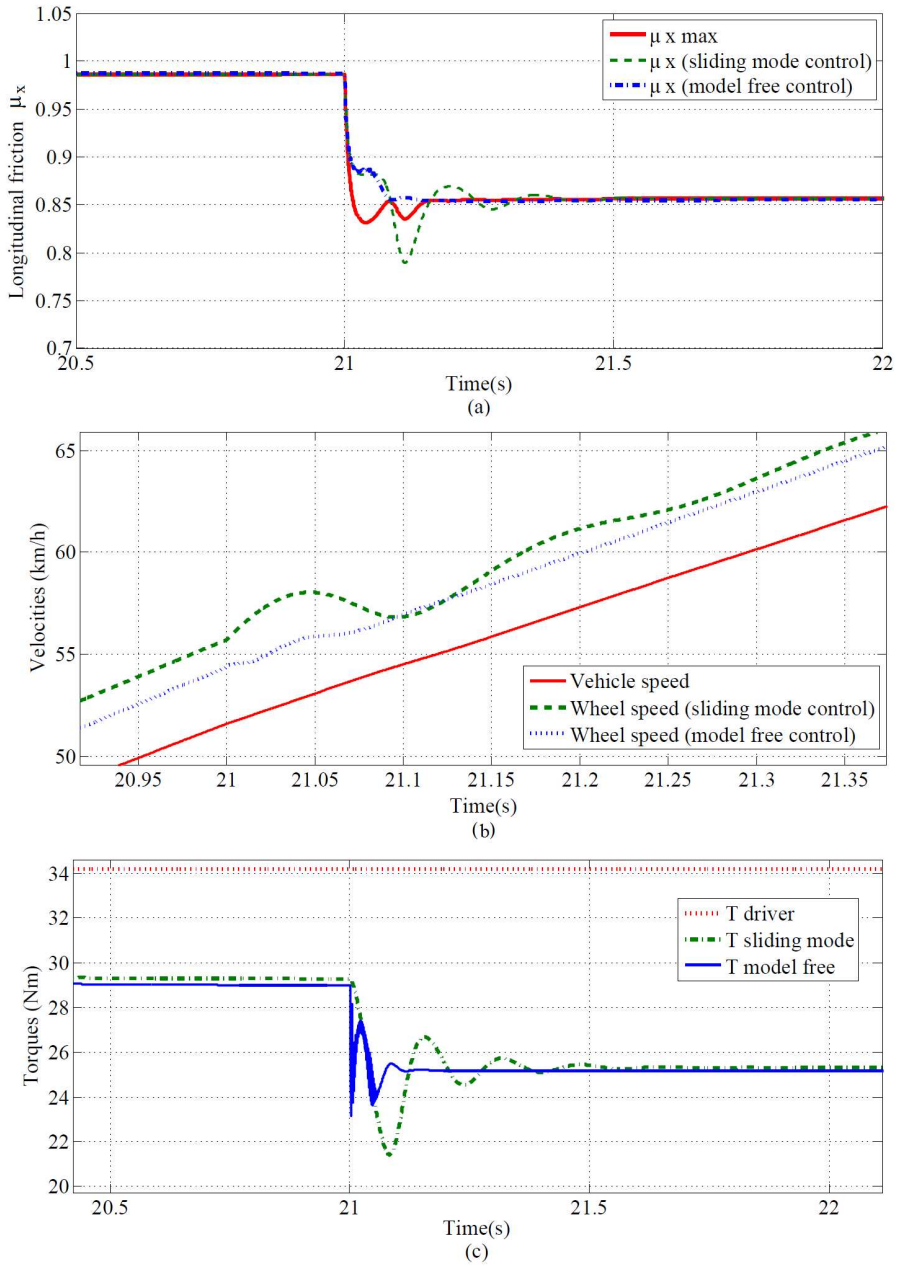

Figure 4.20: Comparison between control laws with perturbation.

formances of the two control techniques presented above:

- the response time in terms of reference friction tracking: ts being the time it takes for the instantaneous friction to track the maximum friction, i.e. the time it takes for $(\mu_{x_{max}} - \mu_x(\lambda)) \leqslant 0.005$.

- the absolute maximum tracking error: $\max(|\mu_{x_{max}} - \mu_x(\lambda)|)$, with $\lambda \varepsilon [-1, 1]$.
- the absolute mean tracking error: $\text{avg}(|\mu_{x_{max}} - \mu_x(\lambda)|)$, with $\lambda \varepsilon [-1, 1]$.
- the robustness in terms of the reference friction tracking when a perturbation arises, computed as the integral of the error: $\int_0^1 (\mu_{x_{max}} - \mu_x(\lambda) \mathrm{d}\lambda$.
- the robustness in terms of the reference friction tracking when a term of the model is poorly known: $\int_0^1 (\mu_{x_{max}} - \mu_x(\lambda)) \mathrm{d}\lambda$. In this case we chose the rolling resistance force R_x to be the poorly known term, since it is hard to estimate in real experimental tests.
- the robustness in terms of the reference friction tracking when the estimation of $\mu_{x_{max}}$ is affected by noise:$\int_0^1 (\mu_{x_{max}} - \mu_x(\lambda)) \mathrm{d}\lambda$.

For the six criteria described above, model free control and sliding mode control show the results presented in table 4.5.

Criteria	Model free control	Sliding mode control
Response time	0.2s	1.2s
Absolute maximum tracking error	0,0386	0,0729
Absolute mean tracking error	0,013	0,036
Robustness to perturbation	0,0242	0,22
Robustness to model errors	0,31	0,65
Robustness to noise	0,1148	0,234

Table 4.5: Comparison values for the chosen criteria.

In terms of response time, the model free control scheme achieves the tracking of the reference friction in 0.2 seconds, while the sliding mode scheme takes 1.2 seconds to track it (the time it takes for the tracking error $(\mu_{x_{max}} - \mu_x(\lambda)) \leqslant 0.005$). This is an important criteria, since the road conditions could rapidly change in a short amount of time, therefore, achieving a quick reference tracking is important for overall vehicular safety. As seen in Figure 4.20, a more oscillatory behavior of the computed control law is obtained when the sliding mode control is applied. This is the reason for the fact that absolute maximum tracking error in the case of model free technique is 0.0386, while the sliding mode technique achieves 0.0729. At the same time, the mean value for the tracking error is 0.0013 for the model free scheme and 0.036 for the sliding mode scheme. Another important criterion in terms of performance comparison, is the

robustness of the control when a perturbation arises. The perturbation was considered as a sudden change in the maximum available friction, passing from $\mu_{x_{max}} = 1$ to 0.8. Once again, the model free technique performs better than sliding mode control, giving $\int (\mu_{x_{max}} - \mu_x) = 0.0242$ compared to 0.22 obtained for the sliding mode control. Some terms in the vehicle model may be unknown or hard to estimate and possibly affected by noise, therefore the control should be also robust in these cases. Model free control applied on our vehicle model yields smaller errors than sliding mode control when one term is poorly known or when $\mu_{x_{max}}$ is affected by noise.

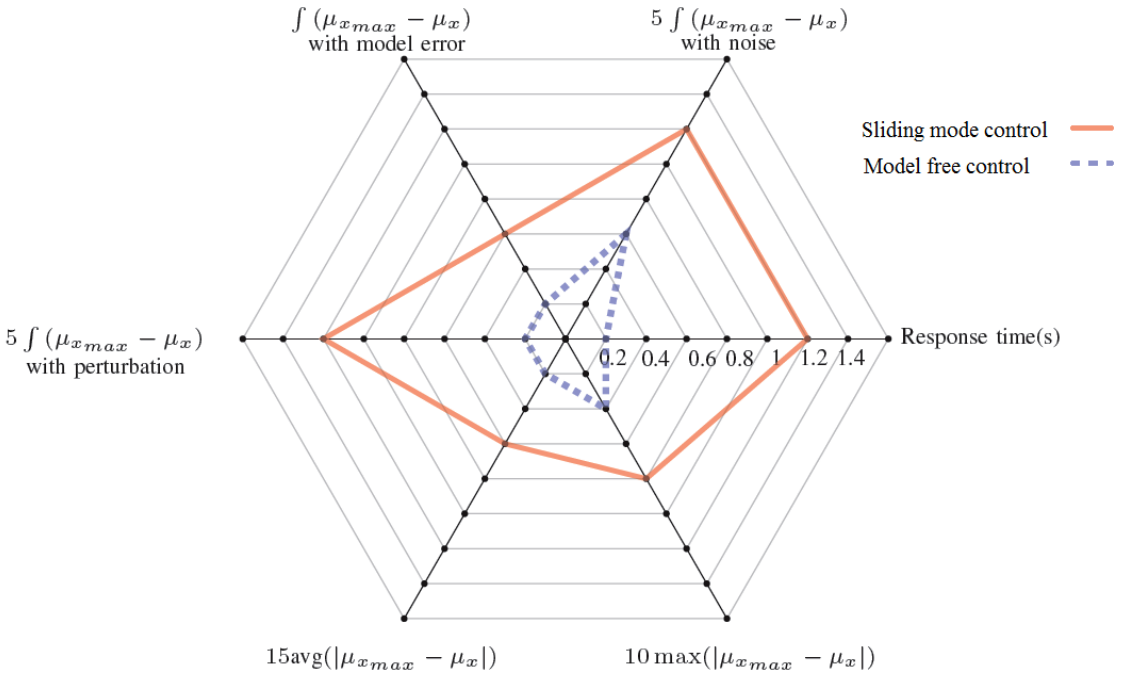

Figure 4.21: Criteria comparison between sliding mode control and model free control.

The radar diagram presented in Figure 4.21 shows the comparison of the six criteria described above. Since the criteria are different and give values that ar far apart one from another, different scale factors have been chosen to attain same levels of magnitude and, thereby, to show a proper visualization of the differences between the two methods. The diagram proves the better performances of the model free control compared to the sliding mode control.

4.4.2 Realistic simulation tests

In this section, three realistic case study scenarios are simulated, comparing sliding mode control with model free control. The preceding simulations were conducted in the extreme case of constant hard acceleration followed by hard braking phases, in order to test the limits of the estimation and control strategies. Of course, these scenarios are unlikely to arise in real situations. Therefore, closer to reality scenarios are simulated in this section.

In the sequel, the state of the road X_r is modeling the adherence as described in Section 2.4.2. The longitudinal force is expressed as function of the state of the road as follows:

$$F_x = \left(\frac{k_{d_1}}{X_r + k_{d_2}} + X_r k_{d_3} \right) \sin((X_r + k_c) \arctan(B\lambda - E(B\lambda - \arctan(B\lambda)))) \quad (4.23)$$

4.4.2.1 Acceleration phase from 5 to 30m/s: the state of the road X_r passes from 1 to 0.5, meaning a change from a dry road to a slippery road

The reference speed profile and the state of the road are shown in Figure 4.22:

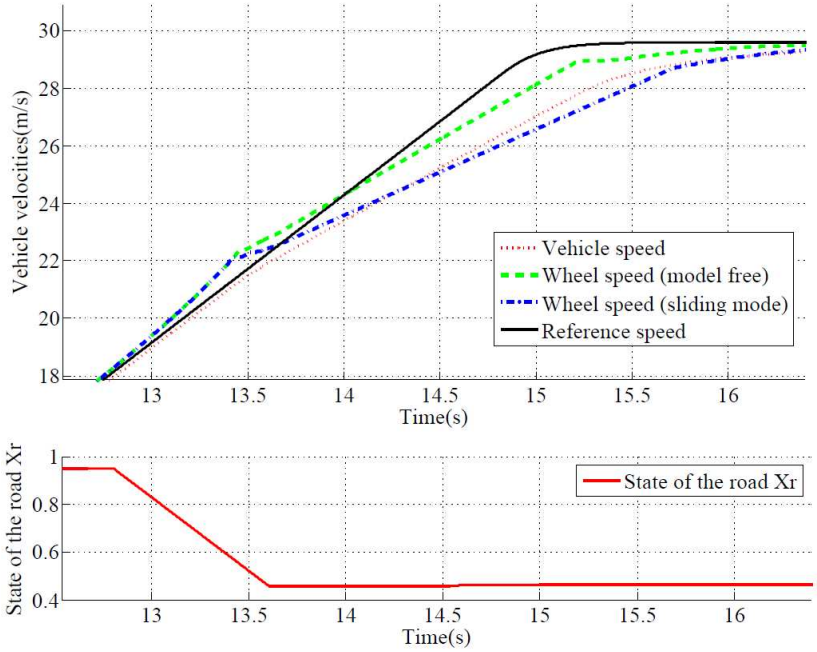

Figure 4.22: Vehicle and wheel velocities, and state of the road in acceleration.

As shown in Figure 4.23, the state of the road passes from 1 to approximately 0.5

during the acceleration maneuver. Nevertheless, both controls achieve wheel control. Because of the fact that the acceleration is not as hard as simulated before, the maximum of the state of the road is not attained by the maximum friction estimation strategy.

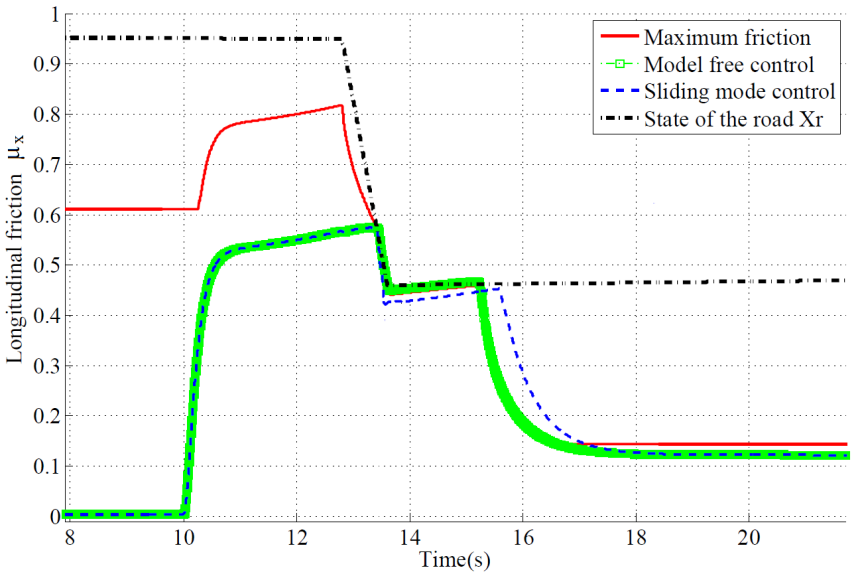

Figure 4.23: Instantaneous and maximum friction control in acceleration.

The demanded and computed torques for both control techniques are shown in Figure 4.24.

Since the acceleration maneuver is not hard, the values of the instantaneous friction are far from the peak of the curves, meaning that the estimation of parameter α is not precise as shown in Figure 4.25, its adaptation being computed only close to the peak of the curves. The estimation of K_x is computed in the linear zone of the friction curve, therefore its estimation follows the modeled value when the acceleration phase is finished and the values of μ_x return in the linear zone.

4.4.2.2 Braking from 30 to 5m/s: the state of the road X_r passes from 1 to 0.5 during braking maneuver

In this scenario we consider a braking maneuver from a constant speed of 30m/s to 5m/s. The maneuver is not hard, the reference speed taking 6 seconds to decrease from 30 to 5m/s. Once again, during the maneuver the state of the road is simulated to change from 1 to approximately 0.5, which can arise in a real driving case. The

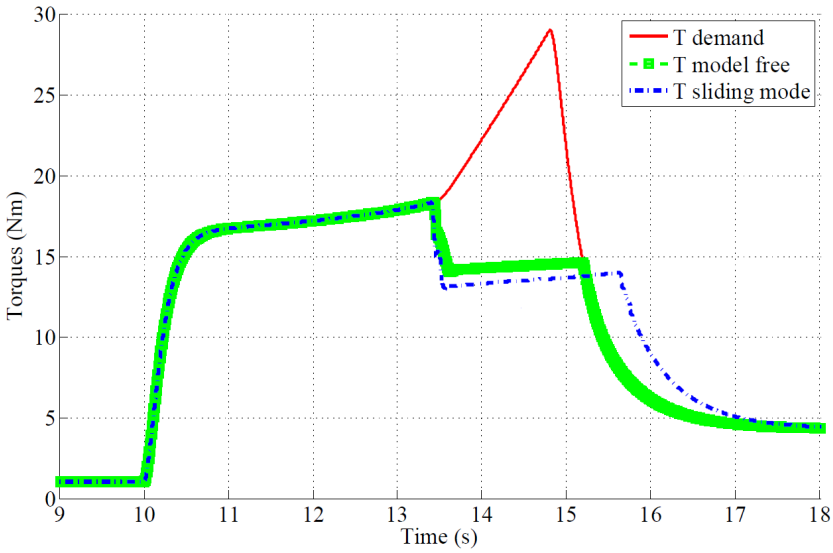

Figure 4.24: Demanded and computed torques in acceleration.

reference tracking speed, along with the vehicle velocities and the state of the road variation are shown in Figure 4.26. Here it can be seen that the wheel speed in the case of sliding mode control has a more oscillatory behavior than in the case of model free control, when the change in the state of the road arises.

These wheel oscillations are due to the computation of the sliding mode torque, shown in Figure 4.27, compared to a smoother behavior in the case of model free control.

The repercussions of the more oscillatory behavior in the case of sliding mode control is transmitted in the behavior of the control on the instantaneous friction, shown in Figure 4.28.

At the same time, the values for the longitudinal slip ratio show a smoother and more "peak free" behavior in the case of model free control, seen in Figure 4.29.

As can be observed in Figure 4.28, in this scenario, the values for the maximum friction attend the maximum modeled for the state of the road, meaning that the activation of the adaptation algorithm is enabled, as seen in Figure 4.30.

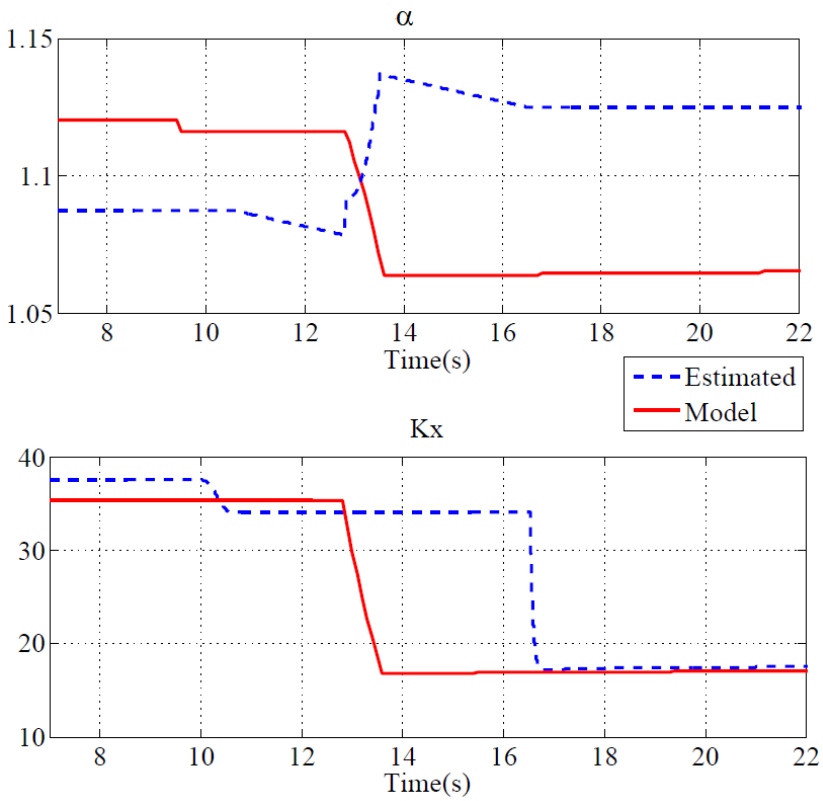

Figure 4.25: Evolution of estimated parameters K_x and α in acceleration.

4.4.2.3 At a constant vehicle speed, the state of the road X_r passes from 1 to 0.8, simulating the passage from a dry road to a wet road

Since this represents a smooth change on the state of the road, it does not affect the dynamic behavior of the wheel or of the vehicle. The only change that is observable is the speed of the wheels, since the friction drops, the wheels spin slightly faster, as observed in Figure 4.31.

In this chapter, sliding mode control technique and model free control technique were tested on various scenarios simulated in order to cover many of the possible realistic situations. Hard acceleration braking phases were simulated on varying road conditions, along with smoother reference speed scenarios. The closed-loop control achieves tracking of the reference friction even in extreme scenarios, when all variables are simulated to vary, but also in more "calm" situations, which are more likely to arise in real environments. The control task responds to the demanded specifications, using the in-wheel electric motor as the unique actuator in both situations, providing

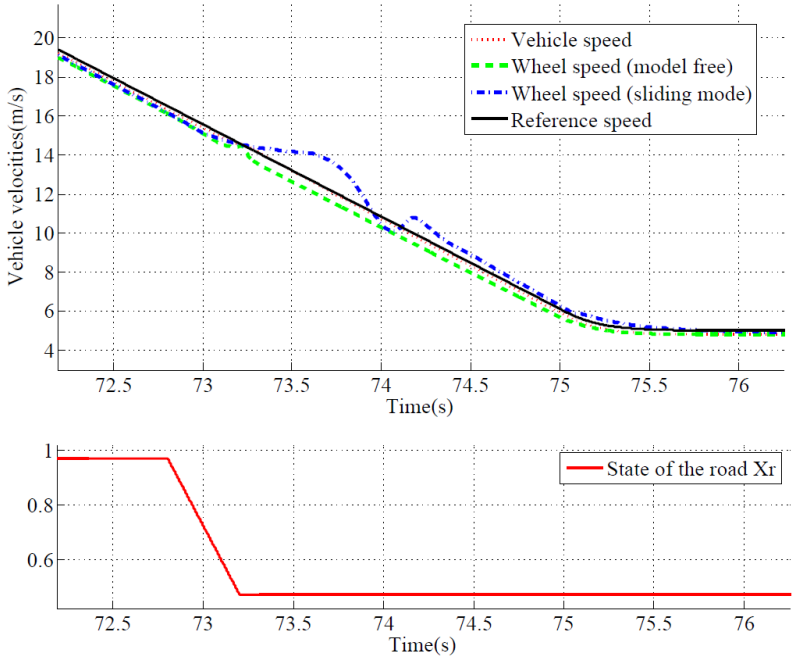

Figure 4.26: Vehicle and wheel velocities, and state of the road in braking.

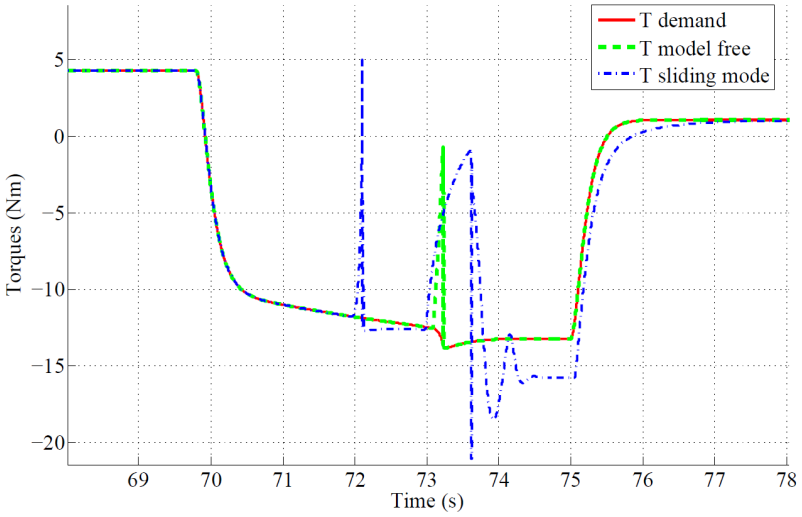

Figure 4.27: Demanded and computed torques in braking.

necessary torque to accomplish a stable wheel and vehicle behavior. The sliding mode control technique was compared to model free technique, and various criteria for comparison were described, showing the better performance of the model free control in the

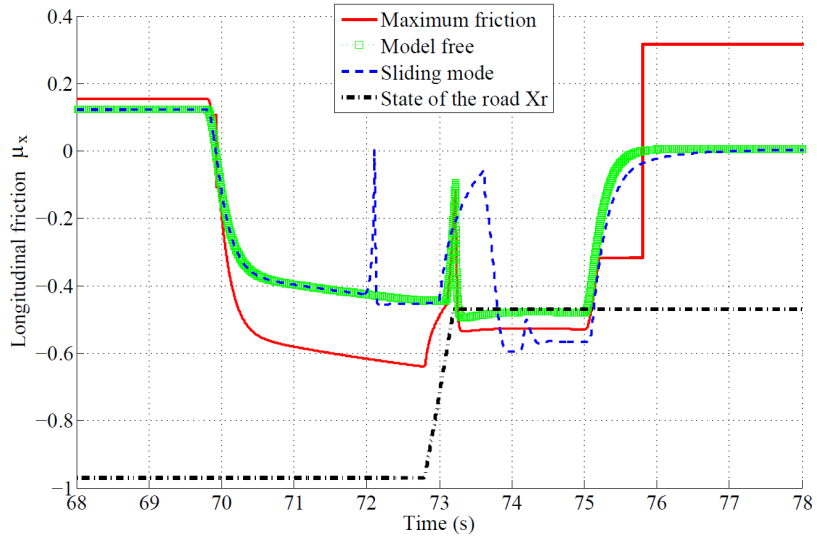

Figure 4.28: Instantaneous and maximum friction control in braking.

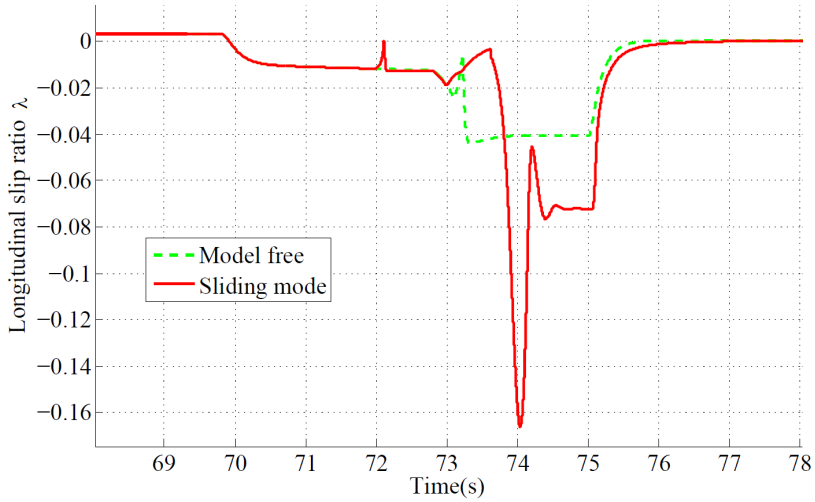

Figure 4.29: Longitudinal slip ratio evolution in comparison.

simulated situations. Nevertheless, both control techniques complete the control task even in noisy environments or ones affected by perturbations, proving the robustness of the proposed methods.

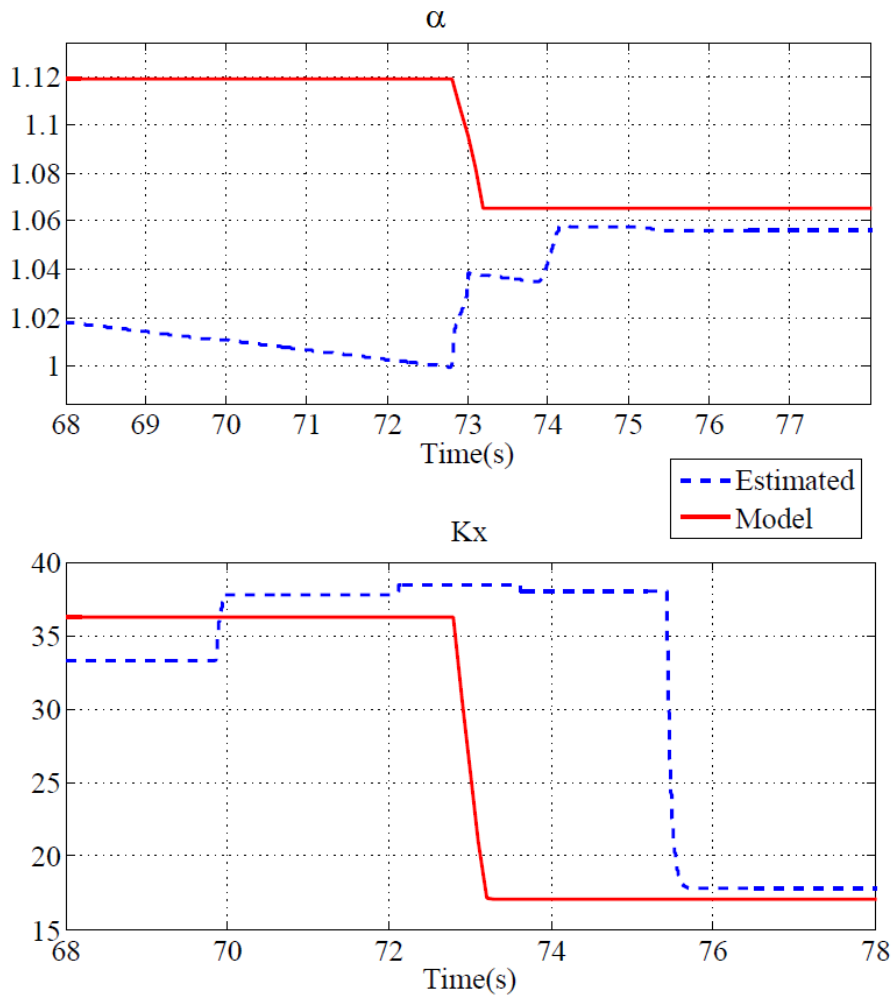

Figure 4.30: Evolution of estimated parameters K_x and α in braking.

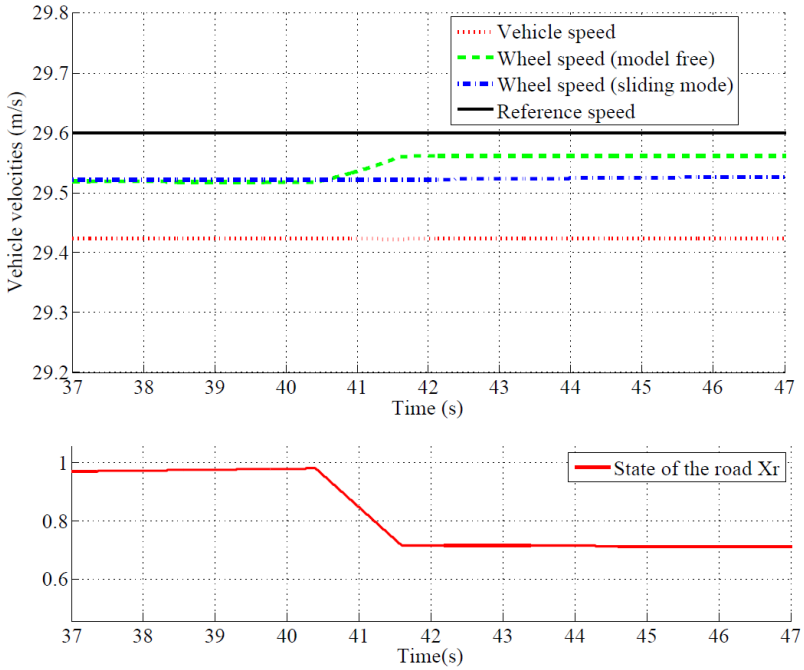

Figure 4.31: Vehicle and wheel velocities, and state of the road at constant speed.

Chapter 5

General conclusions and perspectives

Contents

5.1 Concluding remarks

This thesis summarizes the main contributions on the analysis, estimation and control of vehicle dynamics for a vehicle equipped with in-wheel electric motors. The attention is focused on the estimation of the maximum available friction between the tire and the road surface and on the control applied at the wheel in order to achieve a stable behavior of the wheel. Only longitudinal vehicular dynamics is discussed in this work.

Tire-road interaction represents the context in which the present work is placed. It represents the central problem in vehicular dynamics and therefore, different models were studied to achieve a better understanding of the phenomenon. Tire-road interaction influences vehicular safety in emergency braking situations or in hard acceleration maneuvers, having also an effect on to passenger comfort. The non-linearity of the friction curves gives the difficulty in estimating the maximum force that the tire can generate without losing grip on the road. Once the maximum is exceeded, applying more torque at the wheels will generate more wheel slip in acceleration and wheel block in braking maneuver.

One major problematic aspect in the classical vehicle configuration equipped with internal combustion engines is the lack of a reliable transmitted torque information. In order to estimate it, complex algorithms have to be set up, demanding high computational resources. In contrast, one of the advantages brought in by the in-wheel electric

motor is the information about the transmitted torque at the wheel. This information can be easily achieved by measuring the current that passes through the motor. This aspect was utilized along with the wheel dynamics equation in order to estimate the instantaneous longitudinal friction between the tire and the road. Other parameters of interest like the longitudinal slip ratio of the normal forces on the tires were easily estimated having the knowledge about the transmitted wheel torque. Nevertheless, instantaneous friction is not sufficient to achieve longitudinal control of the wheel. Therefore, a new approach on estimating the maximum available friction is introduced in this thesis. It is based on the reversibility of Dugoff tire model, making possible the computation of the maximum friction. Dugoff's model was utilized to estimate the maximum friction modeled by an empirical Pacejka model, with satisfactory results even in variable road conditions. With Dugoff's tire model, the difficulty resides in the estimation of two key parameters: one that yields the slope of the friction curves and the other that yields the peak of the friction curves. Different algorithms of adaptation and estimation were derived to accomplish reliable estimates of the parameters of interest.

After the estimation of the important parameters, different control techniques were set up to achieve longitudinal wheel control. Since estimates for the instantaneous friction and the maximum friction were derived in the estimation stage, one obvious way of controlling the wheel dynamics in emergency situations is to keep the instantaneous friction at its maximum available value. This new approach is called maximum friction tracking and is made possible by the use of the in-wheel electric motor. Standard control technique did not allow a direct control of the friction and they were based on fixed longitudinal slip ratio thresholds in order to accomplish wheel slip control. The new approach presented in this thesis is based on an activation algorithm that activates the maximum friction tracking only when needed, i.e. in emergency braking or acceleration maneuvers, when the instantaneous friction approaches the maximum available. Keeping the instantaneous friction to its maximum permits a stable and linear wheel dynamics in both acceleration and braking phases. Control techniques based on sliding-mode and model free design were tested in this thesis. One obvious disadvantage that also was visible along simulation results was the oscillations that arise in the case of sliding mode technique due to the non linearity of the sign function in the computation of the control law. Nevertheless, this can be reduced by applying a saturation function instead the usual sign function. Model free control proved to

be more efficient in terms of maximum friction tracking, achieving a faster reference tracking, along with less oscillations transmitted at the wheel. This yields a more stable behavior in acceleration and braking, giving a comfortable ride for the passengers. The novel idea introduced in this thesis is that the in-wheel electric motor can be used as single actuator in acceleration and braking phases, since it is powerful enough to provide necessary torques.

Perturbations and noise can affect both estimation process as well as the control process. Given that the vehicle operates in the outdoors environment, perturbations can arise easily. The road surface adherence is subject to variation, its values changing slowly or rapidly, depending also on the environment. A change in the road surface adherence was considered as a perturbation and simulation tests were conducted in order to show control and estimation strategies' behavior. Both tested control techniques proved to be efficient, with a slight advantage for the model free control, which achieves better results in terms of maximum friction tracking error and response time. Errors on the model and noise affecting the important parameters were also simulated. The results proved the robustness of both control techniques in the case where noise was simulated to affect the computation of the maximum friction. Even in such conditions, the maximum friction was well tracked, accomplishing the final objective of the control laws. These situations were pushed to the extreme intentionally in order to test the behavior of the estimation and control stages in limit situations. The estimation and the control strategies proved to be robust in changing road adherence conditions as well as in scenarios with perturbations and noise affecting the process. Some "realistic" scenarios were also tested in simulation, to complete all the possible scenarios that can arise in outdoors environments and responding to the specifications mentioned in the introductory chapter of the thesis.

5.2 Perspectives

The in-wheel electric motor provide more possibilities of wheel control, being places near the wheel. One of its key features is that it has low response time and almost instantaneous torque generation. Moreover, it can be independently controlled, enhancing the limits of vehicular control. For a vehicle equipped with four in-wheel electric motors, an advanced control strategy may be envisaged. Each wheel can be controlled and adequate torque is provided depending on the estimated maximum

friction. Therefore, lateral control in cornering maneuvers can be improved only by adjusting the torques transmitted at the wheels accordingly. Supervision techniques may also be set up to ensure that the correct torque distribution is achieved.

To meet the growing need for mobility of people and goods while massively reducing CO2 emissions, the electrification of vehicle becomes essential. The use of the in-wheel electric motor as a unique actuator in both acceleration and braking maneuvers permits the energy recovery in braking phases, but it has to be well coordinated with overall vehicle system and especially with the hydraulic brake system in order to achieve safety specifications and vehicle grip in overall conditions. Keeping the instantaneous friction to its maximum available when braking, means a maximum energy regeneration. Optimization algorithms correlated with an overall supervisor can be set up as already done in [48]. It shows the ability to control the wheel slip with accuracy on maximal friction point whatever the road adherence condition. The proposed algorithms enable the adaptation of the electric motors torque to varying friction limit, keeping braking optimal and safe without using classical hydraulic actuators for high dynamics correction.

Bibliography

[1] C.S. Ahn,"Robust Estimation of Road Friction Coefficient for Vehicle Active Safety Systems", *University of Michigan*, Phd. Dissertation, 2011. (Cited on page 79.)

[2] F. M. Atay, "Oscillation control in delayed feedback systems", *Dynamics, Bifurcations, and Control*, pp. 103-116, 2002. (Cited on page 46.)

[3] F. M. Atay, "Magnetic saturation and steady-state analysis of electrical motors", *Applied Mathematical Modelling*, vol. 24, pp. 827-842, 2000. (Cited on page 49.)

[4] F. M. Atay, E. Albas and V. Eldem "Modeling and Identification of saturation in electrical machinery", *Proceedings of the 1999 International Conference on the Integration of Dynamics, Monitoring, and Control*, pp. 343-347, United Kingdom, 1999. (Cited on page 50.)

[5] F. M. Atay, T. Durakbasa and A. Duyar, "A novel method for fault detection in electrical motors", *SV Sound and vibration*, vol. 35, pp. 26-29, 2001. (Cited on page 50.)

[6] F. M. Atay and J. Jost, "Qualitative Inference in Dynamical Systems", *Handbook of Statistical Systems Biology*, pp. 339-358, 20111. (Cited on page 56.)

[7] Automotive Engineering II, "*www.thecartech.com/subjects/auto_eng2/auto_b.htm*". (Cited on pages v and 44.)

[8] M. Burckhardt, "*Fahrwerktechnik: Radschlupfregelsysteme*", Vogel-Verlag, Germany, 1993. (Cited on page 37.)

[9] K. Cakir, A. Sabanovic,"In-wheel motor design for electric vehicles", *9th IEEE International Workshop on Advanced Motion Control*, Istanbul, 2006. (Cited on page 50.)

[10] C. Canudas-de-Wit, P. Tsiotras, E. Velenis, M. Basset, G. Gissinger "Dynamic friction models for road/tire longitudinal interaction", *Vehicle System Dynamics*, vol. 39, pp. 189-226, 2002. (Cited on page 86.)

[11] Y. K. Chin, W. C. Lin and D. Sidlosky, “Sliding-Mode ABS Wheel Slip Control,” *Proceedings of 1992 ACC*, Chicago, pp. 1-6, 1992. (Cited on page 47.)

[12] J. Dakhlallah, S. Glaser, S. Mammar, Y. Sebsadji, "Tire-road forces estimation using extended Kalman filter and sideslip angle evaluation", *Proc. American Control Conference*, pp. 4597-4602, Washington, USA, 2008. (Cited on page 86.)

[13] M. Denny, "The dynamics of anti-lock brake systems," *European Journal of Physics*, vol. 26, pp. 1007-1016, 2005. (Cited on pages 3, 20, 41, 79 and 108.)

[14] J. Diriwächter and R. Valsiner, , "Qualitative Developmental Research Methods in Their Historical and Epistemological Contexts," *FQS*, vol. 7, art. 8, 2006. (Cited on page 56.)

[15] D.A. Eichfeld, H. Klein, "Anti-lock braking system and vehicle speed estimation using fuzzy logic," *Proceedings of the 1st Embedded Computing Conference*, Paris, 1996. (Cited on pages 20, 79 and 108.)

[16] D. Fischer, M. Borner, J. Schmidt, R. Isermann, "Fault detection for lateral and vertical vehicle dynamics", *Control Engineering Practice* vol. 15, pp. 315-324, 2009. (Cited on page 86.)

[17] M. Fliess, H. Mounier, J. Villagra and B. d’Andrea-Novel, "A diagnosis-based approach for tire-road forces and maximum friction estimation". *Control Engineering Practice*, vol. 19, pp. 174-184, 2011. (Cited on pages v, vi, 15, 81, 84, 85 and 86.)

[18] M. Fliess, H. Mounier, J. Villagra and B. d’Andrea-Novel, “Estimation of longitudinal and lateral vehicle velocities: an algebraic approach," *Proceedings of American Control Conference*, Seatle, Washington, 2008. (Cited on page 82.)

[19] M. Fliess, C. Join, “Model-free control," *International Journal of Control*, pp. 1-25, 2013. (Cited on page 124.)

[20] M. Fliess, C. Join, H. Sira-Ramirez, “Non-linear estimation is easy," *International Journal of Modeling Identification and Control*, vol. 1, pp. 12-27, 2008. (Cited on page 79.)

[21] K. Forbus and D. Gentner, “Qualitative mental models: Simulations or memories?," *Proceedings of the Eleventh International Workshop on Qualitative Reasoning*, 1997. (Cited on page 56.)

[22] K. Forbus, K. Carney, B. Sherin, and L. Ureel, “VModel: A visual qualitative modeling environment for middle-school students", *Proceedings of the 16th Innovative Applications of Artificial Intelligence Conference*, San Jose, 2004. (Cited on page 56.)

[23] R. Freeman, “Robust Slip Control for a Single Wheel,” *University of California*, Santa Barbara, USA, 1995. (Cited on page 47.)

[24] H. Fujimoto, T. Saito, T. Noguchi, "Motion stabilization control of electric vehicle under snowy conditions based on yaw-moment observer", *Proceedings of IEEE International Workshop on Advanced Motion Control*, pp. 35-40, Kawasaki, Japan, 2004. (Cited on page 53.)

[25] M.S. Geamanu, A. Cela, H. Mounier, S.I. Niculescu, G. Le Solliec, "Adherence control for electric vehicles on varying road conditions", *Mediterranean Conference on Control and Automation*, Platanias-Chania, Crete, 2013. (Cited on page 33.)

[26] M.S. Geamanu, A. Cela, H. Mounier, S.I. Niculescu, G. Le Solliec, "Longitudinal Control for an All-Electric Vehicle", *International Electric Vehicle Conference*, Greenville, South Carolina, USA, 2012. (Cited on page 34.)

[27] M.S. Geamanu, A. Cela, H. Mounier, S.I. Niculescu, G. Le Solliec, "Maximum friction estimation and longitudinal control for a full in-wheel electric motor vehicle", *International Conference on Control, Automation and Systems*, Jeju, South Korea, 2012. (Cited on page 34.)

[28] M.S. Geamanu, A. Cela, H. Mounier, S.I. Niculescu, G. Le Solliec, "Road condition estimation and longitudinal control for electric vehicles", *International Conference on Control, Automation and Systems*, Gyeonggi-do, South Korea, 2011. (Cited on page 34.)

[29] M.S. Geamanu, A. Cela, H. Mounier, S.I. Niculescu, G. Le Solliec, "Tire-road friction estimation and longitudinal control for electric vehicles ", *International Journal on Control, Automation and Systems*, submitted, 2012. (Cited on page 34.)

[30] M. Gerard, W. Pasillas-Lepine., E. de Vries, M. Verhaegen, "Improvements to a five-phase ABS algorithm for experimental validation", *Vehicle System Dynamics*, vol. 50, pp. 1585-1611, 2012. (Cited on pages vi, 13, 73 and 74.)

[31] H.F. Grip, T.A. Johansen, T.I. Fossen, L. Imsland, J.C. Kalkkuhl and A. Suissa, "Nonlinear vehicle side-slip estimation with friction adaptation", *Automatica*, vol. 44, pp. 611-622, 2008. (Cited on page 86.)

[32] R. M. Hage, B. David, E. Le carpentier, F. Peyret and D. Meizel, "Link travel time estimation in urban areas by detectors and probe vehicles fusion", *2nd International Conference on Models and Technologies for Intelligent Transportation Systems*, Belgium, 2011. (Cited on pages 78 and 79.)

[33] B. Hassibi, A. H. Sayed, and T. Kailath, "Indefinite Quadratic Estimation and Control: A Unified Approach to H2 and Hoo Theories", *Society for Industrial and Applied Mathematics (SIAM)*, 1999. (Cited on pages 78 and 79.)

[34] P. He, Y. Hori, "Optimum Traction Force Distribution for Stability Improvement of 4WD EV in Critical Driving Condition", *Proceedings of IEEE International Workshop on Advanced Motion Control*, pp. 596-601, Istanbul, Turkey, 2006. (Cited on page 51.)

[35] Y. Hori. "Future Vehicle Driven by Electricity and Control-research on four-wheel motored UOT electric march II", *IEEE Transactions on Industrial Electronics*, vol. 51, pp. 954-962, 2001. (Cited on page 51.)

[36] R. Horowitz, L. Olmos and L. Alvarez, "Adaptive emergency braking control with observer-based dynamic tire-road friction model and underestimation of friction coefficient," *Proceedings of the 15th IFAC World Congress*, Barcelona, Spain, 2002. (Cited on pages 20, 79 and 108.)

[37] A. Hughes, "*Electric motors and drives: fundamentals, types, and applications*", *Elsevier*, United Kingdom, 2006. (Cited on page 118.)

[38] R.N. Jazar, "*Vehicle dynamics: theory and applications*", *Springer*, New York, USA, 2008. (Cited on pages 9, 60 and 83.)

[39] F. Jiang, “An Application of Nonlinear PID Control to a Class of Truck ABS Problems,” *Proceedings of the 40th IEEE Conference on Decision and Control*, Orlando, pp. 516-521, 2000. (Cited on page 46.)

[40] H. Jung, B. Kwak, Mando Corporation, "Slip controller design for traction control system" , *International journal of automotive technology*, vol.1, pp. 48-55, Kaist, Korea, 2000. (Cited on page 49.)

[41] T. Kailath, A.H. Sayed and B. Hassibi, “Linear Estimation,” *Prentice-Hall information and system sciences series*, 2000. (Cited on page 78.)

[42] E. Kayacan and O. Kaynak, “A Grey System Modeling Approach for Sliding Mode Control of Anti-lock Braking System,” *IEEE Transactions On Industrial Electronics*, vol. 56, pp. 3244-3252, 2009. (Cited on page 47.)

[43] A. Koita, D. Daucher and M. Fogli, “New probabilistic approach to estimate vehicle failure trajectories in curve driving,” *Probabilistic Engineering Mechanics*, vol. 34, pp. 73-82, 2013. (Cited on page 78.)

[44] S.G. Krantz and H.R. Parks, *The Implicit function theorem: history, theory, and applications*. Birkhäuser, Boston, Massachusetts, USA, 2002. (Cited on page 124.)

[45] J. R. Layne, K. M. Passino and S. Yurkovich, “Fuzzy Learning Control for Antiskid Braking Systems,” *IEEE Transactions on Control Systems Technology*, vol. 1, pp. 122-129, 1993. (Cited on page 47.)

[46] H., L. and E. Leahey, "Collaborative Research in Sociology: Trends and Contributing Factors", *American Sociologist*, vol. 39, pp. 290-306, 2008. (Cited on page 56.)

[47] M. Lisa, "The Sage encyclopedia of qualitative research methods", *Sage Publications*, Los Angeles, California, 2008. (Cited on page 56.)

[48] G. Le Solliec, A. Chasse, M.S. Geamanu, "Regenerative braking optimization and wheel slip control for a vehicle with in-wheel motors", *AAC* , Tokyo, Japan, 2013. (Cited on pages 30, 34 and 143.)

[49] H. Lee, M. Tomizuka, "Adaptive traction control" . *Department of mechanical engineering*, California PATH Research Report, University of California, Berkeley, 1995. (Cited on page 49.)

[50] C. Lee. K. Hedrick, K. Yi, "Real-time slip-based estimation of maximum tire-road friction coefficient", *IEEE/ASME Trans. Mechatronics*, vol. 9, pp. 454-458, 2004. (Cited on page 86.)

[51] W. K. Lennon and K. M. Passino, "Intelligent Control for Brake Systems," *IEEE Transactions on Control Systems Technology*, vol. 7, pp. 188-202, 1999. (Cited on page 48.)

[52] L. Li, S. Kodama, Y. Hori, "Anti-skid control for EV using dynamic model error based on back-EMF observer," *Industrial Electronics Society Annual Conference*, vol. 2, pp. 1700-1704, 2004. (Cited on page 52.)

[53] C.S Liu, H. Peng, "Road friction coefficient estimation for vehicle path prediction", *Vehicle system dynamics*, vol. 25, pp. 413-425, 1996. (Cited on page 86.)

[54] R. G. Longoria, "ME 390: Vehicle Dynamics and Controls," *Course*, Department of Mechanical Engineering, University of Texas, Austin, 2011. (Cited on pages vi and 46.)

[55] Massachusetts Institute of Technology, MIT, "Gateway to the Profession of Planning," *Course*, 2010. (Cited on page 56.)

[56] A. Maria, "Introduction to modeling and simulation", *Proceedings of the 29th conference on Winter simulation*, pp. 7-13, Washington DC, Maryland, USA, 1997. (Cited on pages 8 and 57.)

[57] Ph. Martin, M. Fliess, J. Levine and P. Rouchon, "Flatness and defect of nonlinear systems : introductory theory and examples," *Int. J. Control*, vol. 61, pp. 1327-1361, 1995. (Cited on pages 66, 69 and 125.)

[58] D. Meizel, S. Peyraud, J. Stephant and G. Mourioux, "A decoupled non-linear observer to estimate the 3D pose of a vehicle," *Proceedings 2nd International Conference on Communications, Computing and Control Applications (CCCA)*, France, 2012. (Cited on page 79.)

[59] D. Meizel, J. Stephant and M. Ouahi, "Evaluation of Torque Observer in Automotive Context," *Proceedings of the 18th IFAC World Congres*, Italy, 2011. (Cited on page 51.)

[60] D. Meizel, J. Stephant and M. Ouahi, “Redefining Automotive Supervision Using new sensor technology," *International Symposium on Advanced Vehicle Control (AVEC)*, United Kingdom, 2010. (Not cited.)

[61] D. Meizel, J. Stephant and M. Ouahi, “Simultaneous Observation of Inputs and State of Wheeled Vehicle Model," *7th IFAC Symposium on Intelligent Autonomous Vehicle (IAV)*, Italy, 2010. (Cited on page 50.)

[62] D. Meizel, J. Stephant and A. Charara, “Evaluation of a sliding mode observer for vehicle sideslip angle," *Control Engineering Practice*, vol. 15, 2007. (Cited on page 121.)

[63] D. Meizel, J. Stephant and M. Ouahi, “Simultaneous observation of the wheels' torques and the vehicle dynamic state," *Vehicle System Dynamics*, vol. 51, 2013. (Not cited.)

[64] D. Meizel, J. Stephant and G. Mourioux, “About the prediction of all-terrain vehicles rollover," *Proceedings of Mecatronics REM*, France, 2012. (Not cited.)

[65] D. Meizel and D. Grossoleil, “Practical design of minimal energy controls for an electric bicycle," *9th International Conference on Modeling, Optimization and SIMulation*, France, 2012. (Not cited.)

[66] L. Menhour, B. d'Andrea-Novel, C. Boussard, M. Fliess and H. Mounier, "Algebraic nonlinear estimation and flatness based lateral/longitudinal control for automotive vehicles", *ITSC 2011 - 14th International IEEE Conference on Intelligent Transportation Systems*, Washington DC, Maryland, USA, 2011. (Cited on pages 14 and 80.)

[67] "Michelin active wheel Press Kit" . *Michelin*, Paris, 2008. (Cited on pages vi and 50.)

[68] M. Milanese, C. Novara, L. Giarrao and B. Bamieh, “Learning complex systems from data: the Set Membership approach", *Multidisciplinary Research in Control*, vol. 289, pp. 195-206, 2003. (Cited on page 78.)

[69] C. Miyajima, Y. Nishiwaki,K. Ozawa, T. Wakita,K. Itou, K. Takeda,F. Itakura, “Driver Modeling Based on Driving Behavior and Its Evaluation in Driver Identification", *Proceedings of the IEEE* , vol. 95, pp. 427-437, 2007. (Cited on page 66.)

[70] H. Mounier, "Trajectory tracking and automotive real time framework", *Engineering Control Systems*, pp. 63-69, IEF Orsay, France, 2010. (Cited on page 67.)

[71] R. M. Murray, "Trajectory generation for a towed cable flight control system", *Proceedings of IFAC World Congress*, pp. 395-400, San Francisco, California, USA, 1996. (Cited on page 67.)

[72] K. Nam, Y. Hori, "Sliding mode controller design for optimal slip control of electric vehicles based on fuzzy vehicle velocity estimation logic", *FISITA 2010 Student Congress*, Budapest, 2010. (Cited on page 53.)

[73] W.R. Pasterkamp, H.B. Pacejka, "On line estimation of tire characteristics for vehicle control", *JSAE Review*, vol. 16, pp. 221-226, 1995. (Cited on pages v, 3, 12, 37, 41, 71 and 86.)

[74] Private communication, "Vehicle architectures", *IFPEN*, 2013. (Cited on pages v, 39 and 40.)

[75] R. Rajamani, F.Ling, *Vehicle Dynamics and Control*. Springer, New York, USA, 2006. (Cited on pages 9, 16, 37, 60 and 63.)

[76] P. Ratiroch-Anant, H. Hirata, M. Anabuki, M, S. Ouchi, "Adaptive Controller Design for Anti-Slip System of EV", *Robotics, Automation and Mechatronics, IEEE Conference*, pp. 1-6, Bangkok, Thailand, 2006. (Cited on page 54.)

[77] L. R. Raya, D. C. Brandea, J. H. Leverb, "Estimation of net traction for differential-steered wheeled robots," *Thayer School of Engineering, Dartmouth College, 8000 Cummings Hall, Hanover, NH 03755 and US Army Cold Regions Research and Engineering Laboratory, United States*. (Cited on pages 13 and 73.)

bibitemref145 J. Ryu, "State and parameter estimation for vehicle dynamics control using GPS," *Stanford University*, Phd. Dissertation, 2005.

[78] T. Saito, H. Fujimoto, T. Noguchi, "Yaw-moment stabilization control of small electric vehicle", *Proceedings of the IEEJ Technical Meeting on Industrial Instrumentation and Control*, Tokyo, Japan, 2002. (Cited on page 53.)

[79] S. Sakai, H. Sado, Y. Hori, "Anti-skid control with motor in electric vehicle", *Advanced Motion Control, Proceedings of the 6th International Workshop*, pp. 317-322, Nagoya, Japan, 2000. (Cited on page 53.)

[80] S. Sakai, Y. Hori, "Advantage of Electric Motor for Anti Skid Control of Electric Vehicle", *European Power Electronics Journal*, vol. 11, pp. 26-32, 2001. (Cited on page 53.)

[81] A. Sennaroglu, A. Askar and F. M. Atay, "Quantitative study of laser beam propagation in a thermally loaded absorber", *JOSA B*, vol. 14, pp. 356-363, 1997. (Cited on page 56.)

[82] S. Sekizawa, S. Inagaki,T. Suzuki, S. Hayakawa, N. Tsuchida, T. Tsuda, H. Fujinami, "*Modeling and Recognition of Driving Behavior Based on Stochastic Switched ARX Model*", *Intelligent Transportation Systems, IEEE Transactions on*, vol. 8, 2007. (Cited on page 66.)

[83] T. Shim, D. Margolis, "Model based road friction estimation", *Vehicle system dynamics*, vol. 41, pp. 241-276, 2004. (Cited on page 86.)

[84] J. Song, H. Kim and K. Boo, "A study on an Anti-Lock Braking System Controller and Rear-Wheel Controller to Enhance Vehicle Lateral Stability," *Proceedings of the Institution of Mechanical Engineers, Part D: Journal of Automobile Engineering*, vol. 221, pp. 777-787, 2007. (Cited on page 46.)

[85] J. Svendenius, "Tire modeling and friction estimation", *Phd Thesis*, Dept. Automatic Control, Lund University, 2007. (Cited on page 86.)

[86] H. S. Tan and M. Tomizuka, "An Adaptive Sliding Mode Vehicle Traction Controller Design," *Proceedings of the 1989 American Control Conference*, Pittsburgh, pp. 1053-1058, 1989. (Cited on page 49.)

[87] M. Tanelli, A. Astolfi and S. M. Savaresi, "Robust Nonlinear Output Feedback Control for Brake by Wire Control Systems," *Automatica*, vol. 44, pp. 1078-1087, 2008. (Cited on page 46.)

[88] M. Tanelli, A. Ferrara, P. Giani, "*Combined vehicle velocity and tire-road friction estimation via sliding mode observers*", *International conference on control applications CCA*, pp. 130-135, 2012. (Cited on page 80.)

[89] M. Tanelli, L.Piroddi, S.M. Savaresi, "Real time identification of tire-road friction conditions", *IET Control Theory Appl*, vol. 3, pp. 891-906, 2009. (Cited on page 86.)

[90] W. Ting and J. Lin, "Nonlinear Control Design of Anti-lock Braking Systems Combined with Active Sus-pensions," *Technical report of Department of Electrical Engineering*, National Chi Nan University, 2005. (Cited on page 47.)

[91] W. Ting and J. Lin, "Nonlinear Control Design of Anti-lock Braking Systems Combined with Active Sus-pensions," *Technical Report of Department of Electrical Engineering*, National Chi Nan University, 2005. (Cited on page 47.)

[92] C. Unsal and P. Kachroo, "Sliding Mode Measurement Feedback Control for Anti-lock Braking Systems," *IEEE Transactions on Control Systems Technology*, vol. 7, pp. 271-280, 1997. (Cited on pages 48 and 121.)

[93] F. van Harmelen, V. Lifschitz and R. Porter, "Handbook of KnowledgeRepresentation," *Elsevier,* 2008. (Cited on page 56.)

[94] M. van Nieuwstadt and R. M. Murray, "Real time trajectory generation for differentially flat systems," *Int. Journal of Robust and Nonlinear Control,* submitted for publication, 1997. (Cited on page 67.)

[95] E. Walter and L. Pronzato, "Identification of Parametric Models from Experimental Data", *Springer-Verlag*, London, 1997. (Cited on page 78.)

[96] J. Wang, M.S. Geamanu, A. Cela, H. Mounier, S.I. Niculescu, "Event driven model free control and comparison with standard approaches in motion controls", *IEEE Transatctions on Control System Technology*, submitted, 2013. (Cited on pages 34 and 124.)

[97] J. Wang, M.S. Geamanu, A. Cela, H. Mounier, S.I. Niculescu, "Event driven model free control of quad-rotor", *IEEE Multiconference on Systems and Control*, Hyderabad, India, 2013. (Not cited.)

[98] M. Widmer, G. Le Solliec, "Simulation and adhesion control of a vehicle with four in-wheel electric motors", *Internship report*, IFPEN, Rueil-Malmaison, 2010. (Cited on pages vi, 10, 60, 62, 63, 64 and 65.)

[99] A. B. Will and S. H. Zak, "Anti-lock Brake System Modeling and Fuzzy Control," *International Journal of Vehicle Design*, vol. 24, pp. 1-18, 2000. (Cited on page 47.)

[100] J. Yi, L. Alvarez, R. Horowitz and C. C. DeWit, “Adaptive Emergency Braking Control Using a Dynamical Tire/Road Friction Model,” *Proceedings of 39th IEEE Conference on Decision Control*, Sydney, pp. 456-461, 2000. (Cited on pages 47 and 121.)

[101] J. Yi, L. Alvarez, X. Claeys, R. Horowitz, "Emergency braking control with an observer-based dynamic tire/road friction model and wheel angular velocity measurement", *Vehicle system dynamics*, vol. 39, pp. 81-97, 2003. (Cited on page 86.)

[102] D. Yin,J. Hu, Y. Hori, "Robustness Analysis of Traction Control Based on Maximum Transmission Torque Estimation in Electric Vehicles", *Proceedings of the IEEE Technical Meeting on Industrial Instrumentation and Control*, Tokyo, Japan, 2009. (Cited on page 53.)

[103] J. S. Yu, “A Robust Adaptive Wheel-Slip Controller for Anti-lock Brake System,” *Proceedings of 36th IEEE Conference on Decision Control*, San Diego, pp. 2545-2546, 1997. (Cited on page 47.)

Appendix A

Appendix

The work of the author (Marcel-Stefan GEAMANU) is financially supported by the CNRS-IFPEN grant 186-654 (2010-2013).

Scientific training attended by the author:

- "Flatness and nonlinear estimation techniques" - Michel Fliess. 17/01/2011-21/01/2011.
- "Cooperative navigation and control of multiple robotic vehicles"- Antonio M. Pascoal/ Antonio P. Aiguar. 21/02/2011-25/02/2011.
- "An introduction to networked control systems"- Karl H. Johansson/ Vijay Gupta. 14/03/2011-18/03/2011.

Professional training attended by the author:

- "Micro-controller programming in C language" - 15/04/2013-19/04/2013.
- "Latex-Advanced level"-28/05/2013.

Road condition estimation and longitudinal control for electric vehicles

- **Authors**: M.S. Geamanu, A. Cela, H. Mounier, S.I. Niculescu, G. Le Solliec.
- **Conference**: International Conference on Control, Automation and Systems (ICCAS).
- **Venue**: Gyeonggi-do, South Korea.
- **Year**: 2011.

2011 11th International Conference on Control, Automation and Systems
Oct. 26-29, 2011 in KINTEX, Gyeonggi-do, Korea

Road condition estimation and longitudinal control for electric vehicles

Marcel Stefan Geamanu[1,3], Arben Cela[2], Guénaël LeSolliec[3], Hugues Mounier[1], Silviu-Iulian Niculescu[1]

[1]**Laboratoire des Signaux et Systemes (L2S, UMR 8506), CNRS-Supelec, 3 rue Joliot Curie, 91192 Gif-sur-Yvette, FRANCE**
(e-mails : marcel-stefan.geamanu@lss.supelec.fr, hugues.mounier@lss.supelec.fr, silviu.niculescu@lss.supelec.fr)
[2]**UPE ESIEE Paris, 2 boulevard Blaise Pascal, 93162 Noisy le Grand, FRANCE**
(e-mail : a.cela@esiee.fr)
[3]**IFPEN, 1 et 4 avenue de Bois-Préau, 92500 Rueil-Malmaison, FRANCE**
(e-mails : guenael.le-solliec@ifpen.fr, marcel-stefan.geamanu@ifpen.fr)

Abstract: This paper presents a road condition estimator based on the wheel acceleration and a torque controller for a vehicle equipped with an electric motor. In the first step, the instantaneous friction coefficient and the maximum friction coefficient between the wheel and the road are estimated, without knowing a priori the road conditions. Next, a longitudinal controller is set up to ensure the two main functions : braking with anti-skidding function and traction control using the electric motor torque as a unique actuator. Unlike the torque generated by classic internal combustion engines, the torque of electric motors is available almost instantaneously. In addition, it can be measured on-line which means that advanced control techniques can be applied. The approach presented in this paper relies on recent algebraic techniques for numerical differentiation and diagnosis, and a feedback sliding mode control scheme to ensure the vehicle is operated at the maximum friction zone in both acceleration and braking phases, along with a given reference speed to track.

Keywords: electric vehicles, tire-road friction estimation, sliding mode control, vehicle-dynamics control.

1. INTRODUCTION

Vehicle traction control and ABS systems are two of the most important components in providing safety and achieving desired vehicle motion [20]. Traction control system (TCS) is designed to use the maximum friction between the wheels and the road to provide a desirable longitudinal and lateral vehicle motion, ensuring in the same time passenger comfort. The ABS system is designed to prevent wheel block in case of sudden braking. Therefore, longitudinal control needs to achieve anti-spin acceleration and anti-skid braking, maintaining the fastest stable acceleration and deceleration.

In the field of active vehicle dynamics control systems, most of the available solutions are brake-based, see, e.g., [19,2,3]. Recently, [16] presented a five-state controller, where the threshold values are based on wheel deceleration. Others approaches are model-based, estimating either the wheel slip or the vehicle speed ([11,14]). Similar approaches, based on fuzzy logic are presented in [5,21,7]. In [17,18] a nine-degrees of freedom vehicle model is used, with an extended Kalman filter to estimate vehicle speed, braking forces, wheel slip and vehicle side-slip angle. Further, [13,10,1] propose to estimate the vehicle speed via nonlinear observers. The inconveniences of the approaches presented above are manifold, starting with the fact that some of them make use of different thresholds for the slip deceleration or the wheel slip, without taking into account the road condition variations. Others are estimating too many parameters like the vehicle speed, braking forces or friction coefficients via nonlinear observers, which can be difficult in view of real-time computations.

Starting from a simple, one wheel, modeling of a vehicle, the aim of this paper is to achieve no wheel slip nor skid, independently of the driver's behavior (hard acceleration or braking) and the conditions of the road surface (wet or dry), by estimating the least possible parameters. To represent driver's behavior, a simple approach was utilized, as the driver's commands result in a specific speed to track. For this purpose, a standard speed tracking scheme taking advantage of model's flatness was utilized. On the other hand, for the second unknown variable, the road condition, we took advantage of a diagnosis-based estimator [9].

The novelty of the present paper consists in using the electric motor torque as a unique actuator, in order to accomplish both TCS and ABS functions, taking advantage of the electric motor fast response time.

The remaining paper is organized as follows : in Section 2 the vehicle model equations are presented, along with a simple speed tracking scheme and the estimation of the road conditions ; Section 3 contains the control strategies in order to achieve no wheel slip nor skid in critical situations like hard braking or hard acceleration ; finally, in Section 4 the results of simulations are presented and in Section 5, some concluding remarks are given.

2. VEHICLE MODEL AND REPRESENTATION OF ITS DYNAMICS

2.1 Vehicle model

Let us consider the simplified one wheel model of a vehicle, neglecting the suspension dynamics :

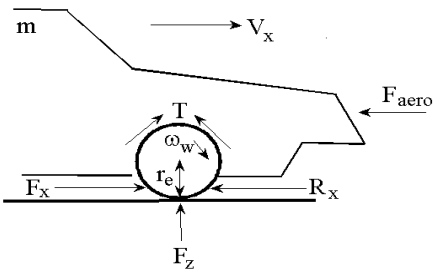

Fig. 1 Longitudinal model of the vehicle.

In Fig.1, we adopt the following notations : V_x- longitudinal speed of the vehicle, m- mass of the vehicle, F_{aero}- longitudinal aerodynamic drag force, R_x- force due to rolling resistance, F_z- normal force on the tire, r_e- effective tire radius, F_x- longitudinal tire force, T- wheel torque, ω_w- angular wheel speed, I_w - inertia moment of the wheel. The equations of the dynamics of the vehicle can be written as follows :

$$m\dot{V}_x = F_x - F_{aero} - R_x, \quad (1)$$

$$I_w\dot{\omega}_w = RT - r_eF_x, \quad (2)$$

$$F_x = \mu_x F_z, \quad (3)$$

$$\lambda = \frac{V_x - r_e\omega_w}{max(V_x, r_e\omega_w)}, \quad (4)$$

$\leftarrow$ where : $F_z = mg$, $F_{aero} = (\rho C_a A V_x^2)/2$, $R_x = mgC_r$ and R is the damping coefficient of the drive-line.

The model takes into account the longitudinal slip ratio : $-1 \leqslant \lambda \leqslant 1$ and the road surface friction coefficient between the road and the tire : $-1 \leqslant \mu_x(\lambda) = \frac{a\lambda}{b+c\lambda+\lambda^2} \leqslant 1$, where a, b, c are the shape parameters depending on the road conditions (dry or wet). In the model the torque limitations from the electric motor (Nm) are also considered : $-34.2 \leqslant T \leqslant 34.2$.

Driver's actions (acceleration or braking) can be translated in different speed tracking demands. This yields a traction or a braking torque, depending of the driver inputs, which has to be limited in order to avoid possible wheel slip or skid.

2.2 Flatness-Based Control

In order to track a reference speed V_x, a flatness-based trajectory tracking control law is implemented. The vehicle model is trivially flat, with V_x as a flat output [15]. This results in a PID controller with anti-windup and a feed-forward scheme, as shown in Fig. 2 :

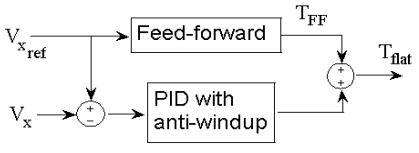

Fig. 2 Flatness-based speed tracking scheme with feed-forward and PID (proportional, integral, derivative) controller.

From the first equation of the vehicle's dynamics, Eq. (1), with no-slip assumption, we pull the expression for the feed-forward torque T_{FF} , which is an open-loop control :

$$T_{FF} = \frac{m}{R}\dot{V}_{x_{ref}} + \frac{F_{aero}}{R} + \frac{R_x}{R}. \quad (5)$$

To compensate the model mismatch, a PID controller with anti-windup has been added, yielding the necessary torque in order to track a reference speed $V_{x_{ref}}$ in low slip conditions.

$$PID_{out} = K_p\nu + K_i\int(\nu)dt + K_d\frac{d}{dt}\nu, \quad (6)$$

$\leftarrow$ with $\nu = V_{x_{ref}} - V_x$. The final expression for the flatness-based control law has the form :

$$T_{flat} = T_{FF} + \frac{m}{R}PID_{out} \quad (7)$$

The purpose of this control is to track the $V_{x_{ref}}$ trajectory, independently of the fact that the latter could induce slip or not. As seen in Fig. 3a, the flatness-based control does not suffice in *unknown* road conditions, resulting in a wheel spin in acceleration or a wheel block in braking. The flatness-based control tries to achieve the reference speed, not taking into account that the wheel spins or blocks, and therefore, it needs to be limited in order to accomplish proper TCS and ABS functions. The values of the longitudinal friction coefficient with respect to longitudinal slip with only the flatness-based control applied are in the non linear zone (shown in Fig. 3b).

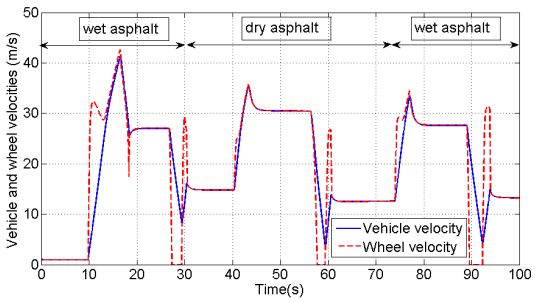

(a) V_x and ω_w

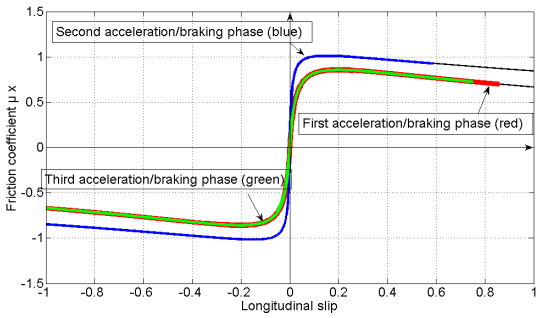

(b) $\mu - \lambda$ characteristics.

Fig. 3 Vehicle velocities and $\mu(\lambda)$ evolution with flatness-based control applied

A decisive and unknown factor is the changing road condition, which can often arise. So, an estimation of the road conditions is needed.

2.3 Road condition estimation

To estimate the type of the road surface on which a vehicle is moving, an approach presented in [9] has been used. In a first step, instantaneous friction will be computed, then the extended braking stiffness concept (XBS) is exploited to distinguish a road type from another. The XBS is defined as the derivative of the friction coefficient with respect to slip ratio [9] :

$$XBS(t) = \frac{d\mu_x}{d\lambda} = \frac{\hat{\dot{\mu}}_x}{\hat{\dot{\lambda}}} \tag{8}$$

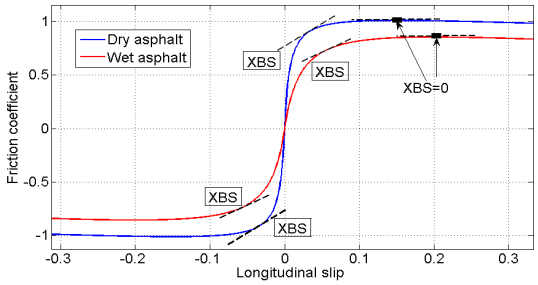

Fig. 4 Adhesion coefficient characteristic curve for dry and wet asphalt and XBS definition.

2.3.1 Longitudinal friction estimation

As stated in the previously mentioned paper, the friction coefficient μ_x turns out to be dependent solely on the longitudinal acceleration $\dot{V}_x$; thus the estimation requires a good knowledge of the vehicle longitudinal velocity coming from an accelerometer. Yet, the vehicle longitudinal speed isn't always available in standard equipped cars ; therefore we took advantage of Eq. (2) of the model, in order to estimate longitudinal friction. Replacing Eq. (3) in Eq. (2), the expression for μ_x is then :

$$\mu_x = \frac{1}{r_e mg}(RT - I_w \dot{\omega}_w) \tag{9}$$

Using the wheel acceleration to estimate the instantaneous friction is more reliable than using the vehicle speed estimation, knowing that in most cases signals coming from accelerometers can carry much more noise than odometers ($\dot{\omega}_w$ in Eq. (9)) and integration of noisy signals can be problematic. Also, using an electric motor as actuator

2.3.2 Maximum friction estimation

The last stage in the road surface estimation scheme is the most complicated one. The complexity of this estimation comes from the fact that most of the road surfaces have a similar characteristic curve $\mu_x - \lambda$ for standard situations. This approach tends to take advantage of the presented numerical algorithms to be able to detect danger zones in a reliable way. Once the failure is detected, a simple tire behavior model will help to obtain a good estimation of the maximum friction coefficient : $\mu_{x_{max}} = (F_x/F_z)\,|_{max}$.

As stated before, the extended braking stiffness, or XBS, will be used to detect the entrance in the danger zone (or, in other words, to signal the distinguishability between road surfaces). The algorithm for the maximum friction estimation can be written as follows [9] :

Algorithm 1 : $\mu_{x_{max}}$ computation [9]
if $(XBS(t_k) \leqslant XBS_{max})$
$\mu_{max}(t_k) = max(0, min(1, \mu^*_{x_{max}}(t_k)))$
$\mu^*_{x_{max}}(t_k) = \mu^D_{x_{max}}(t_k)(1 + \frac{XBS(t_k)}{XBS_{max}})$
if $XBS_{max} \leqslant XBS((tk))$
$\mu_{x_{max}}(t_k) = \mu_{x_{max}}(t_{k-1})$

where $\mu^D_{x_{max}}(t_k) = \frac{\alpha}{\hat{F}_z}(|K_x\hat{\lambda}(t_k)| - \sqrt{K_x\hat{\lambda}(t_k)(K_x\hat{\lambda}(t_k) - \hat{F}_x(t_k))})$ if $\tau < 1$, and $\mu^D_{x_{max}}(t_k) = \mu^D_{x_{max}}(t_{k-1})$ if $\tau > 1$. Here, α is a weighting factor between Pacejka and Dugoff tire models, K_x is the longitudinal stiffness coefficient and $\tau = (\mu_{x_{max}} F_z)/(2|K_x\lambda|)$.

In Fig. 5, a comparison between filtered XBS and μ_x evolution is shown for the profile speed in Fig. 3a. The first and the third phase are simulated on a wet road ($\mu_{x_{max}} = 0.8$) , while the second one is on a dry road ($\mu_{x_{max}} = 1$).

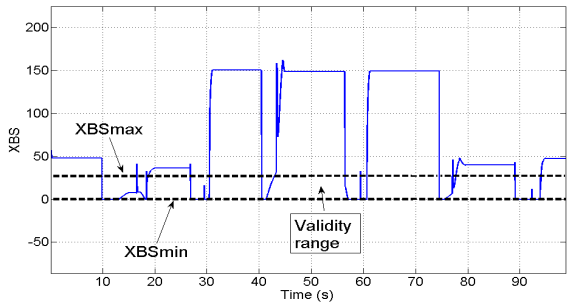

(a) XBS estimation, validity range and $\mu_{x_{max}}$ distinguishable zones.

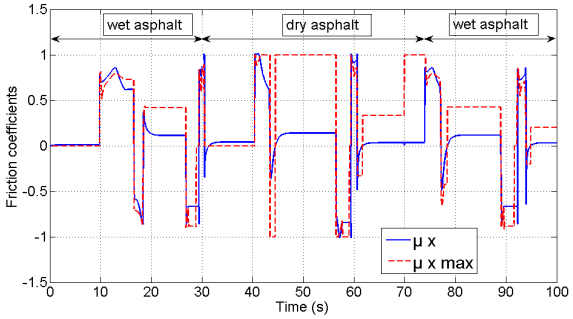

(b) Real μ_x and $\mu_{x_{max}}$ evolution.

Fig. 5 Extended braking stiffness estimation.

Similar trends can be appreciated in both graphs, i.e. when μ_x reaches a local peak, XBS is close to a local minima. Furthermore, the closest μ_x is to $\mu_{x_{max}}$, the lower value of XBS is obtained. As a result, an XBS validity range $[XBS_{min}, XBS_{max}]$ can be selected as significant for $\mu_{x_{max}}$ detection. Thus, when XBS values are greater than XBS_{max} or lower than XBS_{min}, it will be consi-

dered that μ_x remains equal to the last obtained value within the validity range. If μ_x falls into the validity range, a corrective factor will be applied to the $\mu_{x_{max}}$.

It can be seen that the estimation of $\mu_{x_{max}}$ is acceptably achieved, knowing that no a priori model for its evolution had been implemented in the simulation and in addition the road surface changes in time.

3. CONTROL STRATEGIES

3.1 Sliding mode control

Sliding mode control strategy applied for vehicle dynamics control was also utilized in [6,12]. A feedback sliding control law is designed such that it will guarantee that the system trajectory moves towards the sliding surface and stays on it. The present control law is added in order to manage the case where slip occurs. Implementation of the control design requires the knowledge of the rotational wheel speed and the two coefficients obtained in the previous section, $\mu_{x_{max}}$ and μ_x. In order to take advantage of the previous $\mu_{x_{max}}$ estimation, a sliding surface $S = \mu_{x_{max}} - \mu_x$ has been selected. This implies that when $S = 0$ the vehicle is operated at $\mu_x = \mu_{x_{max}}$.

Taking the derivative of the sliding surface and substituting the expression for the friction coefficient obtained in Eq. (9) yields :

$$\dot{S} = -\dot{\mu}_x = -\frac{1}{r_e mg}(R\dot{T} - I_w\ddot{\omega}) \tag{10}$$

When $S = 0$, it is required that $\dot{S} = 0$. Next, $\dot{S} = 0$ implies that $\dot{T}_{eq_1} = \ddot{\omega}(I_w/R)$. Then :

$$T_{eq_1} = \int (\frac{I_w}{R}\ddot{\omega})dt = \frac{I_w}{R}\dot{\omega} + k_1 \tag{11}$$

Note that $S = 0$ implies that $\mu_x = \mu_{x_{max}}$. Substituting again the expression for μ_x and choosing $k_1 = (r_e mg\mu_{max})/R$ we obtain the equivalent torque in order to get $S = 0$ and $\dot{S} = 0$:

$$T_{eq} = \frac{I_w}{R}\dot{\omega} + \frac{r_e mg\mu_{max}}{R} \tag{12}$$

When $S \neq 0$, it is required that $S\dot{S} < 0$. Replacing the expression for $\dot{S}$, we obtain $S\dot{\mu_x} > 0$. We then get two possible cases :
1) $S > 0$. Then $\dot{\mu}_x > 0$. Therefore, from Eq. (10) we get $\dot{T}_{eq} > \ddot{\omega}(I_w/R)$. Replacing T_{eq} by its expression from Eq. (12) and calculating its first derivative will obtain $\dot{T}_{eq} = \ddot{\omega}(I_w/R)$. Taking $\dot{T}_{eq} = \ddot{\omega}(I_w/R) + \dot{T}_{sm_1}$, with $\dot{T}_{sm_1} = Sk_2 > 0$ will ensure that $\dot{T}_{eq} > \ddot{\omega}(I_w/R)$ is satisfied. Here, $k_2 > 0$ is a design parameter.
2) $S < 0$. Now, the condition to verify becomes $\dot{T}_{eq} < \ddot{\omega}(I_w/R)$. Taking again $\dot{T}_{eq} = \ddot{\omega}(I_w/R) + \dot{T}_{sm_2}$, with $\dot{T}_{sm_2} = Sk_2 < 0$ will ensure that $\dot{T}_{eq} < \ddot{\omega}(I_w/R)$ is satisfied.
Putting together the two conditions we obtain :

$$T_{sm} = \int (Sk_2)dt \tag{13}$$

The sliding control law is defined as : $T_{sliding} = T_{eq} + sign(S)T_{sm}$, leading to :

$$T_{sliding} = \frac{I_w}{R}\dot{\omega} + \frac{r_e mg\mu_{max}}{R} + sign(S)\int (Sk_2)dt.$$

The presence of the $sign$ function in the control command can induce chattering, therefore in the simulations presented in the sequel, it has been replaced by a $saturation$ function, which allows the surface to remain in a tube with a desired width. This removes any possible oscillation which can arise due to the strong non linearity of the $sign$ function.

3.2 Hybrid control

In normal conditions (no-slip) the applied control law is T_{flat}, while, when slip occurs, $T_{sliding}$ is applied. When the values for the longitudinal slip are below a fixed threshold, chosen to be in the linear zone of $\mu - \lambda$ curves and far from the neighborhood of the maximum of the friction coefficient, then T_{flat} is applied. Otherwise, a switching between the two control commands takes place, and it follows a "(min,max)" rule, shown in the following algorithm :

Algorithm 2 : Switching algorithm
if $\|\lambda\| \leqslant \varepsilon$
$T_{hybrid} = T_{flat}$
else if $\lambda > 0$
$T_{hybrid} = min(T_{flat}, T_{sliding})$
else $T_{hybrid} = max(T_{flat}, T_{sliding})$

This algorithm defines a "safe-zone" for all $|\lambda| \leqslant \varepsilon$ in which we allow the torque coming from the driver demand to be applied at the wheel of the vehicle, knowing that for these values of the slip we are at the beginning of the $\mu - \lambda$ curves and thus in the stable linear zone.

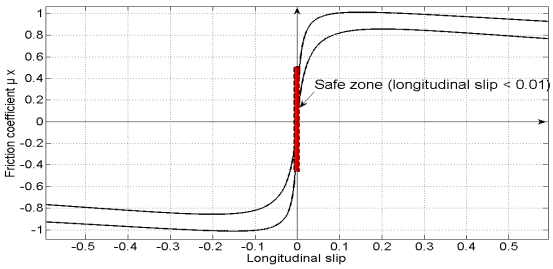

Fig. 6 Safe zone.

Once this threshold is exceeded, the switch between the sliding mode control and the flatness-based control is applied, limiting each time the greater torque, to avoid wheel slip or skid. In acceleration phase, the minimum value between the two torques is applied while in braking phase it is the maximum value that is applied.

4. RESULTS

Throughout the simulations, the values used for the various coefficients are : maximum engine torque : $T_{max} = 34.2Nm$, rolling resistance coefficient : $C_r = 0.01$, density of the air : $\rho = 1.3kg/m^3$, aerodynamic drag coefficient : $C_a = 0.32$, drag surface : $A = 1\,m^2$, the damping

coefficient of the drive-line : $R = 16$, mass of the vehicle : $m = 150kg$, effective wheel radius : $r_e = 0.3m$. The estimation and control methods have been tested in the SIMULINK environment for two types of road surfaces : one with $\mu_{x_{max}} = 0.8$, which corresponds to a wet road, and another one with $\mu_{x_{max}} = 1$, which corresponds to a dry road. Three alternatively accelerating and braking phases have been simulated on the two types of surfaces. The speed profile that was tested is shown in Fig. 7 :

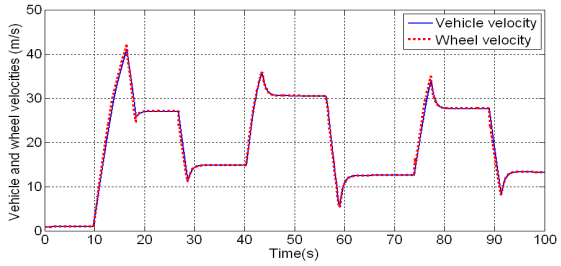

Fig. 7 Vehicle and wheel velocities.

As we can see, there is no noticeable difference of speed between the wheel and the chassis, showing that the control meets its attended requirements. In Fig. 8 the temporal evolutions of the calculated torques in order to track the speed profile shown in Fig. 7 are presented. The torque demand coming from the driver is represented by T_{flat} and the sliding mode control described in the above section is represented by $T_{sliding}$.

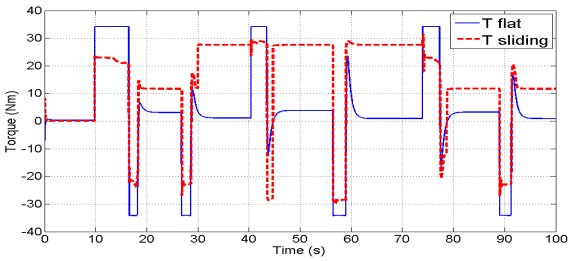

Fig. 8 Control laws.

As can be seen in Fig.8, the larger torque demanded by the driver T_{flat} is limited by the smaller torque computed with the sliding mode strategy $T_{sliding}$, in both the acceleration and braking phases, achieving satisfactory wheel slip control. The final hybrid torque applied at the wheel is shown in Fig. 9 :

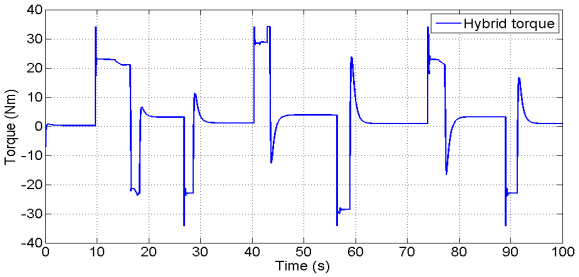

Fig. 9 Hybrid torque applied at the wheel.

The first braking/acceleration phase is simulated on a wet road with $\mu_{x_{max}} = 0.8$ (between simulation time 0 and 30s), then on a dry road with $\mu_{x_{max}} = 1$ (between simulation time 30 and 75s), and for the last part, again on a wet road with $\mu_{x_{max}} = 0.8$.

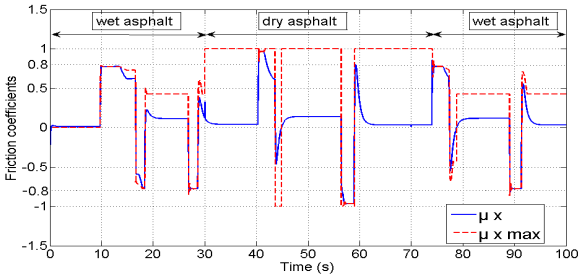

Fig. 10 $\mu_{x_{max}}$ and μ_x evolution with the hybrid control enabled.

From Fig. 10, one can easily notice that both the estimation stage and the control stage perform pretty well and cooperate without affecting one another. The estimation strategy gives good results, detecting the maximum friction coefficient for each type of surface, even when the control is enabled. The proposed control performs accurately, meaning that the instantaneous friction coefficient μ_x tracks the estimated maximum friction $\mu_{x_{max}}$ in a satisfactory manner. Therefore, the values of the longitudinal slip remain in the linear zone of the $\mu - \lambda$ curves.

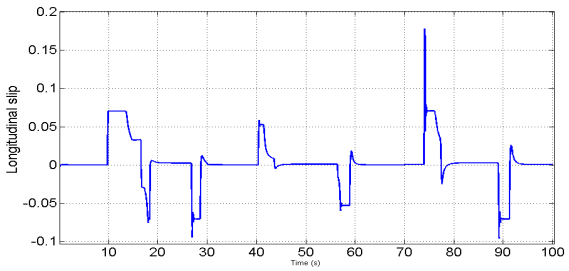

Fig. 11 Longitudinal slip values with the hybrid control enabled.

The values of estimated friction coefficient with respect to longitudinal slip are shown in Fig. 12. It proves that we remain in the linear zone and also close to the maximum adherence, performing adequate TCS and ABS functions, independently of the changing road conditions.

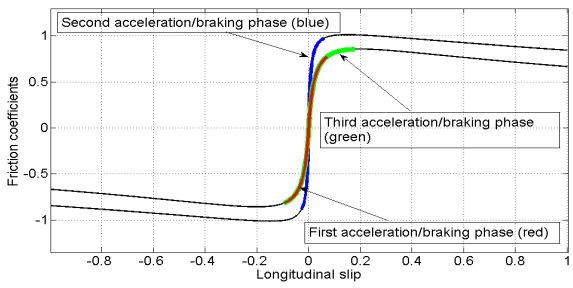

Fig. 12 $\mu - \lambda$ characteristics.

5. CONCLUDING REMARKS

A new approach to achieve longitudinal control of a vehicle equipped with an electric motor has been tested. It relies on the on-line estimation of the maximum and instantaneous friction coefficients, which are used in the implementation of a sliding-mode control law, along with a flatness-based control law. The final control applied to the vehicle is a hybrid control between flatness-based control simulating the driver behavior and a sliding mode control. The stability of the switching between the two controls is currently being studied and has not yet been proven, but along with the simulations in this paper no strange stability behavior was noticed. The motor torque is the unique control actuator to achieve anti-skid braking and anti-slip acceleration, with satisfactory results and therefore the goal of the paper is fulfilled. In a future work, other types of control laws will be tested along with new techniques of estimating the maximum friction coefficient.

REFERENCES

[1] L. Alvarez, X. Claeys, R. Horowitz and J. Yi, "Emergency braking control with an observer-based dynamic tire/road friction model and wheel angular velocity measurement," *Vehicle System Dynamics*, 39(2) : 81-97, 2003

[2] B. d'Andrea-Novel and H. Chou "Global vehicle control using differential braking torques and active suspension forces," *Vehicle System Dynamics*, 43(4) :261-284, 2005.

[3] M. Borrelli, F. Asgari, J. Tseng and H. Falcone, "A linear time varying model predictive control approach to the integrated vehicle dynamics control problem in autonomous systems," *46th IEEE Conference on Decision and Control, CDC 2007*, pages 2980-2985, 2007.

[4] M. Denny, " The dynamics of anti-lock brake systems," *European Journal of Physics*, 26 :1007-1016, 2005.

[5] D.A. Eichfeld and H. Klein, "Antilock braking system and vehicle speed estimation using fuzzy logic," *Proceedings of the 1st Embedded Computing Conference, Paris*, 1996.

[6] Q. Feng, S. Shuang, S. Jia, Z. Quanming "Sliding mode control design of active vehicle suspension systems with two-time scale submodels," *Advanced science letters*, 4(3) :953-957, 2011.

[7] D. Fischer, R. Isermann, R. Schwarz, P. Rieth and S. Semmler, "Estimation of vehicle velocity using brake-by-wire actuators," *Proceedings of the 15th IFAC World Congress, Barcelona*, Spain, 2002.

[8] M. Fliess, H. Mounier, J. Villagra and B. d'Andrea-Novel, "Estimation of longitudinal and lateral vehicle velocities : an algebraic approach," *American Control Conference, Seatle*, 2008.

[9] M. Fliess, H. Mounier, J. Villagra and B. d'Andrea-Novel, "A diagnosis-based approach for tire-road forces and maximum friction estimation," *Control Engineering Practice*, 19 :174- 184, 2011.

[10] J.T. Fossen, T. Fjær, H. Grip, J. Kalkkuhl, A. Suissa and L. Imsland, "Vehicle velocity estimation using nonlinear observers," *Automatica*, 42(12) :2091-2103, 2006.

[11] F. Gustafson, "Slip-based tire-road friction estimation," volume 33. *Automatica*, 1997.

[12] A. Haddoun, M. Benbouzid, D. Diallo, R. Abdessemed, J. Ghouili and K. Srairi, "Sliding mode control of EV electric differential system," *ICEM, Greece*, 2006.

[13] R. Horowitz, L. Olmos and L. Alvarez, "Adaptive emergency braking control with observer-based dynamic tire-road friction model and underestimation of friction coefficient," *Proceedings of the 15th IFAC World Congress. Barcelona, Spain*, 2002.

[14] K. Kinase, K. Kobayashi and K. Watanabe, "Absolute speed measurement of vehicles from noisy acceleration and erroneous wheel speed," *Proceedings of the Symposium on Intelligent Vehicles*, 1993.

[15] Ph. Martin, M. Fliess, J. Levine and P. Rouchon, "Flatness and defect of nonlinear systems : introductory theory and examples," *Int. J. Control*, 61(6) :1327-1361, 1995.

[16] W. Pasillas-Lepine, " Hybrid modeling and limit cycle analysis for a class of five-phase anti-lock brake algorithms," *Vehicle System Dynamics*, 44(2) :173-188, 2006.

[17] L. Ray, " Nonlinear state and tire force estimation for advanced vehicle control," *IEEE Transactions on Control Systems Technology*, 3(1) :117-124, 1995.

[18] L. Ray, " Nonlinear tire force estimation and road friction identification : simulation and experiments," *Automatica*, 33(10) :1819- 1833, 1997.

[19] Y. Sano and K. Sawase, "Application of active yaw control to vehicle dynamics by utilizing driving/braking force," *JSAE Review*, 20(2) :289-295, 1999.

[20] S. M. Savaresi and M. Tanelli, " Active Braking Control Systems Design for Vehicles," *Springer*, 2010.

[21] C. K. Watanabe and K. Kobayashi, "Estimation of absolute vehicle speed using fuzzy logic rule-based kalman filter," *Proceedings of the 1995 American Control Conference, Seattle, WA*, 1996.

Longitudinal Control for an All-Electric Vehicle

- **Authors**: M.S. Geamanu, A. Cela, H. Mounier, S.I. Niculescu, G. Le Solliec.
- **Conference**: International Electric Vehicle Conference (IEVC).
- **Venue**: Greenville, South Carolina, USA.
- **Year**: 2012.

Longitudinal Control for an All-Electric Vehicle

Marcel Stefan Geamanu,
Hugues Mounier and
Silviu-Iulian Niculescu
Laboratoire des Signaux et Systèmes (L2S)
UMR 8506 CNRS-Supelec,
3 rue Joliot Curie, 91192 Gif-sur-Yvette, FRANCE

Arben Cela
UPE ESIEE Paris,
2 boulevard Blaise Pascal,
93162 Noisy le Grand, FRANCE

Guénaël LeSolliec
and Marcel Stefan Geamanu
IFPEN, 1 et 4 avenue de Bois-Préau,
92500 Rueil-Malmaison, FRANCE

***Abstract*—The present paper describes a torque controller for a vehicle equipped with 4 electric motors, one at each wheel. The controller is set up to ensure two main functions: braking with anti-skidding and traction control using the electric motor torque as the unique actuator signal source. Unlike the torque generated by classic internal combustion engines, the torque of electric motors is available almost instantaneously. In addition, it can be measured on-line, which means that advanced control techniques can be applied. In order to generate the appropriate anti-skid or anti-slip torque for each wheel, one has to estimate the friction between the wheel and the road. In the first step, the instantaneous friction coefficient and the maximum friction coefficient between the wheel and the road are estimated, without prior knowledge of the road conditions. Next, the approach relies on a feedback sliding mode control scheme to ensure the vehicle is operated in the maximum friction zone in both hard acceleration and braking phases, along with a given reference speed to track. The only variables used in this strategy are the wheel acceleration, the instantaneous torque generated by the electric motors and the chassis acceleration.**

I. Introduction

Vehicle traction control system (TCS) and ABS (Antiblockiersystem) are two of the most important components in providing safety and achieving desired vehicle motion [1]. The TCS is designed to use the maximum friction between the wheels and the road to provide a desirable longitudinal and lateral vehicle motion, ensuring in the same time passenger comfort [12]. The ABS system is designed to prevent wheel lock in case of sudden hard braking, as described in [4], [5] and [14]. Therefore, longitudinal control needs to achieve anti-spin acceleration and anti-skid braking, maintaining the fastest stable acceleration and deceleration.

A critical factor in proper functioning of TCS and ABS is the friction between the wheels and the road, which is in addition an unknown variable and can induce unexpected vehicle and wheel behavior. Furthermore, the friction coefficient is subject to variation, its values changing due to numerous factors as the weather conditions (hot temperatures, rain, snow or ice), road maintenance and type of the pavement (asphalt, concrete or cobblestone). Therefore, estimating the friction coefficient becomes an important factor in achieving safety.

Emails: marcel-stefan.geamanu@lss.supelec.fr (corresponding author), hugues.mounier@lss.supelec.fr, silviu.niculescu@lss.supelec.fr, a.cela@esiee.fr, guenael.le-solliec@ifpen.fr, marcel-stefan.geamanu@ifpen.fr.

The aim of this work is to achieve a control law that avoids longitudinal wheel slip or skid, independently of the driver's behavior (hard acceleration or braking) and of the conditions of the road surface (wet or dry). The first stage in the strategy is to estimate "on-line" the maximum friction between the wheel and the road. The second one is to apply the control that allows the instantaneous friction to track the maximum friction in hard acceleration and braking phases. On one hand, to represent driver's behavior, a simple approach was used, as the driver's requirements result in a specific speed to track. To this purpose, a standard speed tracking scheme taking advantage of model's flatness was used. On the other hand, for the second unknown variable, the road condition, we took advantage of a diagnosis-based estimator [7].

In the conventional configuration of the majority of existing vehicles equipped with an internal combustion engine (ICE), there are two different actuators that accomplish ABS and TCS and hence, two solutions of control with different dynamics. The novelty of the present work consists in using the four electric motors as the only actuators in acceleration and deceleration, in order to provide the necessary torques to accomplish both TCS and ABS functions. New hub- or in-wheel motors provide more possibilities for active safety and trajectory control. These motors have a very low latency and are able to provide a torque on the wheels [11] faster than conventional brakes which are normally used for this purpose.

In the classical ICE configuration, the estimation of the wheel friction forces is problematic, due to the lack of a reliable estimation of the torque generated by the engine. With the electric motor, due to a good knowledge of its output torque, one can estimate the wheel friction forces. Unlike the existing, rather conservative, control strategies, described in [4], [15] and [10], which rely on the longitudinal slip and a fixed threshold, the electric motor allows to apply a control on the friction coefficient, while considering the road conditions.

The remaining paper is organized as follows, section 2 is devoted to introduce the vehicle model as well as the estimation of the parameters of interest. In section 3 are exposed the control strategies we are proposing: a flatness-based control in order to track a reference speed, and a sliding-mode control in order to track a maximum friction coefficient. Some illustrative examples and scenarios are detailed in section 4 and some concluding remarks are presented in section 5.

II. Vehicle Model and Representation of its Dynamics

A. Vehicle model

Let us consider the four wheeled model of a vehicle which consists of the main vehicle mass to which the four wheels are attached via a suspension system [16]. Since the present goal is to achieve longitudinal control of the vehicle, we are not interested in its lateral dynamics and therefore the full model can easily be taken as a bicycle model, as shown in Fig.1:

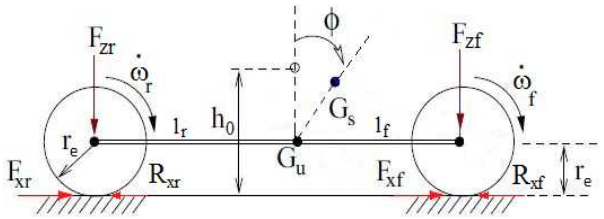

Fig. 1: Wheel forces

Here, G_s and G_u are respectively the centers of gravity of the suspended and unsuspended mass, l_f and l_r are the distances from the center of mass to the front and rear axle and ϕ is the pitch angle. The suspension dynamics are taken into account, with the associated load transfer that arises when the vehicle is accelerating or braking. The forces that act on each pair of wheels are shown in Fig.1.

The overall system equations including the vehicle, wheel and load transfer dynamics can be written as follows:

$$m\dot{V}_x = F_x - F_{aero}, \tag{1}$$

$$F_{z_i} = m_{w_i} g - k(l_i\phi - h_0) - cl_i\dot{\phi}, \tag{2}$$

$$F_{x_i} = \mu_{x_i} F_{z_i}, \tag{3}$$

$$I\dot{\omega}_i = T_i - r_e F_{x_i} - R_{x_i}, \tag{4}$$

$$F_x = \sum_{i=1}^{4} F_{xi}. \tag{5}$$

Here, r_e is the wheel radius, F_{aero} is the aerodynamic drag force, F_z is the normal force on the tire, F_x is the longitudinal tire force, μ_x is the longitudinal friction coefficient, ω is the wheel angular speed, R_x is the rolling resistance force, T is the wheel torque, l is distance from the center of gravity to the axle and the index $i = fl, fr, bl, br$ with the signification: fl=front left, fr=front right, bl=back left and br=back right.

The longitudinal friction coefficient between the road and the tire (μ_x) is modeled by a Pacejka function [3] of the longitudinal slip (λ), with two different curves for dry and wet road, as shown in Fig.2.

In order to apply the adequate control on the friction coefficient, our strategy follows four steps, starting with the estimation of the load transfer in acceleration and braking. Next, the longitudinal friction force is estimated which leads to the estimation of the instantaneous friction coefficient. This

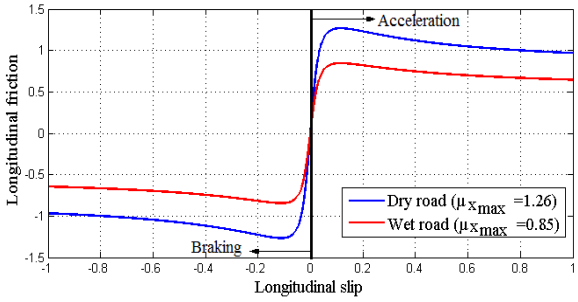

Fig. 2: Pacejka curves modeling the friction coefficient

will allow the computation of the maximum friction coefficient on which the sliding-mode control will be applied. These four steps are detailed in the next subsection.

B. Parameter estimation

1) Load transfer estimation: When a car is accelerating on a level road, the vertical forces under the front and rear wheels are [12]:

$$F_{zf} = \frac{1}{2}mg\frac{l_r}{l} - \frac{1}{2}mg\frac{h_0}{l}\frac{\dot{V}_x}{g}, \tag{6}$$

$$F_{zr} = \frac{1}{2}mg\frac{l_f}{l} + \frac{1}{2}mg\frac{h_0}{l}\frac{\dot{V}_x}{g}. \tag{7}$$

The first terms, $\frac{1}{2}mg\frac{l_r}{l}$ and $\frac{1}{2}mg\frac{l_f}{l}$, are called static parts, coming from the static weight distribution (static position of the center of gravity) and the second terms, $\pm\frac{1}{2}mg\frac{h_0}{l}\frac{\dot{V}_x}{g}$, are called dynamic parts of the normal forces, coming from the dynamic mass transfer in acceleration or deceleration (with $\dot{V}_x$ being the chassis longitudinal acceleration).

When the vehicle is braking, the dynamic part becomes significant in the front of the vehicle, giving a larger load in the front of the vehicle, and a smaller one in the back, and vice-versa in acceleration.

2) Longitudinal friction force estimation: As stated in [7], the friction coefficient μ_x turns out to be dependent solely on the longitudinal acceleration $\dot{V}_x$. Yet, the vehicle longitudinal acceleration can carry noise [8], so in order to estimate more accurately the longitudinal friction force, we took advantage of (4). The knowledge of the torque and the wheel dynamics allows the computation of the longitudinal force for each wheel. From (4), the expression for F_{x_i} is:

$$F_{x_i} = \frac{1}{r_e}(T_i - I\dot{\omega}_i - R_{x_i}). \tag{8}$$

3) Instantaneous friction coefficient and XBS estimation: Having computed the normal and longitudinal forces for each wheel, starting from (3), a good estimation of the instantaneous friction coefficient at each wheel is then:

$$\mu_{x_i} = \frac{F_{x_i}}{F_{z_i}}. \tag{9}$$

After estimating the individual instantaneous friction coefficients, the extended braking stiffness concept (XBS [7]) is exploited to distinguish a road type from another. The XBS is defined as the derivative of the friction coefficient with respect to longitudinal slip:

$$XBS(t) = \frac{d\mu_x}{d\lambda} = \frac{\dot{\hat{\mu}}_x}{\dot{\hat{\lambda}}}. \quad (10)$$

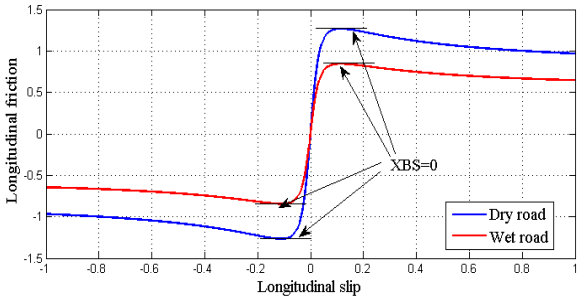

Fig. 3: Adhesion coefficient characteristic curve for dry and wet asphalt and XBS definition.

4) Maximum friction estimation: The last stage of the estimation strategy is the computation of the maximum friction coefficient and is the most complex one. The complexity of this estimation comes from the fact that most of the road surfaces have a similar characteristic curve $\mu_x - \lambda$ for standard situations. This approach tends to take advantage of numerical algorithms to be able to detect dangerous zones (the non linear zones of the curves before arriving at the peak as shown in Fig.3) in a reliable way. Once the entrance in the non linear zone is detected, a simple tire behavior model will help in deriving a good estimation of the maximum friction coefficient.

As stated before, the extended braking stiffness, or XBS, will be used to detect the entrance in the non linear zone of the friction curves. The algorithm for the maximum friction estimation can be written as follows:

Algorithm 1 : $\mu_{x_{max}}$ computation [7]

if $(XBS(t_k) \leqslant XBS_{max}$)

$\mu_{max}(t_k) = max(0, min(1, \mu^*_{x_{max}}(t_k)))$

$\mu^*_{x_{max}}(t_k) = \mu^D_{x_{max}}(t_k)(1 + \frac{XBS(t_k)}{XBS_{max}})$

if $XBS_{max} \leqslant XBS((tk))$

$\mu_{x_{max}}(t_k) = \mu_{x_{max}}(t_{k-1})$,

where $\mu^D_{x_{max}}(t_k) = \frac{\alpha}{\hat{F}_z}(|K_x\hat{\lambda}(t_k)| - \sqrt{K_x\hat{\lambda}(t_k)(K_x\hat{\lambda}(t_k) - \hat{F}_x(t_k))})$ if $\tau < 1$, and $\mu^D_{x_{max}}(t_k) = \mu^D_{x_{max}}(t_{k-1})$ if $\tau > 1$.

Here, the parameter α is a weighting factor between Pacejka and Dugoff tire models, K_x is the longitudinal stiffness coefficient and $\tau = (\mu_{x_{max}} F_z)/(2|K_x\lambda|)$.

For the sake of uniformity, all the graphs have as time range [0, 80].

In Fig.4 is shown the evolution of filtered XBS and in Fig.5, the evolution of the instantaneous and maximum friction coefficient.

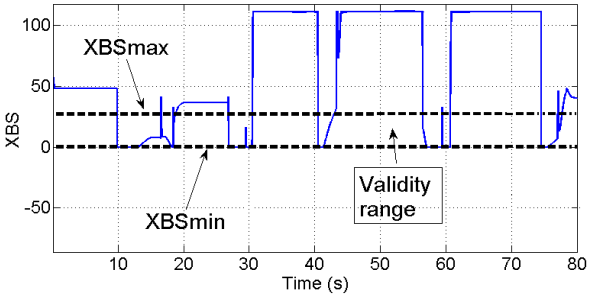

Fig. 4: XBS estimation and validity range.

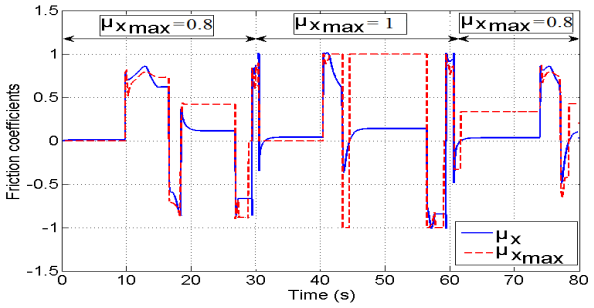

Fig. 5: Instantaneous μ_x evolution and $\mu_{x_{max}}$ estimation.

Similar trends can be observed in both graphs, i.e. when μ_x reaches a local peak, XBS is close to a local minimum. A validity range $[XBS_{min}, XBS_{max}]$ can be selected as significant for $\mu_{x_{max}}$ detection. Thus, when XBS values are greater than XBS_{max} or lower than XBS_{min}, it will be considered that μ_x remains equal to the last obtained value within the validity range. If μ_x falls into the validity range, a corrective factor will be applied to the $\mu_{x_{max}}$, as seen in the algorithm 1.

The estimation of $\mu_{x_{max}}$ is achieved, having a mean detection time of 0.1 seconds, knowing that no a priori model for its evolution had been implemented in the simulation and in addition the adherence of the road surface changes in time. The first and the third phase of the estimation are simulated on a wet road (with a $\mu_{x_{max}} = 0.8$) , while the second one is on a dry road (with a $\mu_{x_{max}} = 1$).

We dispose now of all the necessary parameter estimations in order to apply a control on the vehicle's longitudinal dynamics. Yet, the longitudinal dynamics are influenced by the "actions" of the driver (acceleration or braking), which can be translated in different speed requirements. Depending on the driver inputs, this yields a traction or a braking torque, which has to be limited in order to avoid possible wheel slip or skid.

In the next section is presented the flatness-based control strategy for the tracking of a reference speed (as a result of driver's inputs), along with a sliding-mode control strategy that activates when the wheel slip or skid occurs (ensuring the TCS and ABS functions).

III. Control Strategies

A. Flatness-Based Control

In order to track a reference speed V_x, a flatness-based trajectory tracking control is implemented. The vehicle model is trivially flat [13], which means, roughly speaking, that there exists an output, called a flat output, which can be expressed as a function of all the inputs and system variables and their derivatives. Here, V_x is a flat output.

Making the (physically sound) assumption that the wheel dynamics is fast compared to the car body one, the model (1)-(4) reduces to:

$$m\dot{V}_x = \frac{1}{r_e}T - F_{aero}. \tag{11}$$

A linearizing transformation with new input u is given by $T = r_e(F_{aero} + mu)$, yielding the trivial dynamics $\dot{V}_x = u$. An anti-windup controller is then chosen for u:

$$u = PI_{out} + \dot{V}_{x_{ref}}. \tag{12}$$

The final expression for the flatness-based controller is:

$$T_{flat} = r_e(F_{aero} + mPI_{out} + m\dot{V}_{x_{ref}}). \tag{13}$$

The "anti-windup" reacts when the control reaches the limits of the actuator, thereupon the integral term could increase indefinitely. A combination of conditional integration and calculation of the output of the integrator as a function of the controller output PI is used here. When the PI output goes out of the electric motor torque limitations range, the integral term stops charging. The output of the PI controller is shown in the following algorithm:

Algorithm 2 : PI controller with anti-windup

if $(PI_{out} > u_{min})$ or $(PI_{out} < u_{max})$

$$PI_{out_{t_k}} = K_p\nu_{t_k} + K_i(\int \nu)_{t_k}dt$$

else

$$PI_{out_{t_k}} = K_p\nu_{t_k} + K_i(\int \nu)_{t_{k-1}}dt,$$

with $\nu = V_{x_{ref}} - V_x$ and u_{min}, u_{max} being the torque ranges of the electric motor.

The purpose of this control is to track the $V_{x_{ref}}$ trajectory, independently of the fact that the latter could induce slip or not. As seen in Fig.6, when driver's inputs are significant (hard acceleration; hard braking), the flatness-based control does not suffice in *unknown* road conditions, resulting in a wheel spin in acceleration or a wheel block in braking. The flatness-based control tries to achieve the reference speed, not taking into account that the wheel spins or blocks, and therefore, the its output torque needs to be limited in order to accomplish adequate TCS and ABS functions.

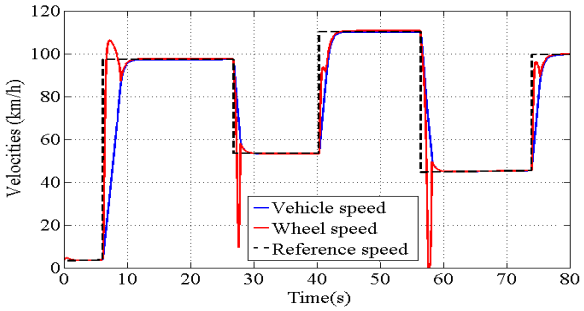

Fig. 6: Vehicle velocities evolution with flatness-based control applied.

In the next subsection is presented the control strategy that is activated to prevent the wheel slip or skid.

B. Sliding mode control

Sliding mode control strategy applied for vehicle dynamics control was also proposed in [2] and [9]. In [2] the authors treat the design and sliding mode control of two structures with hybrid sources. The first structure uses super-capacitors, fuel cell and batteries and the second one is similar to the first but without batteries. In [9] is described the sliding mode control of an electric differential system for electric vehicles with two induction motor drives (one for each wheel). In this case, the electric differential will manage the speed difference between the two wheels when cornering.

The present control law is added in order to manage the case where the driver requirements induce slip or skid of the wheels. A feedback sliding control law is designed such that it will guarantee that the system trajectory moves towards the sliding surface and stays on it once hitting it. The purpose of this control law is to keep the instantaneous friction coefficient at its maximum value (maximum friction estimated in the previous section), therefore an obvious sliding surface would be $S = \mu_{x_{max}} - \mu_x$.

Implementation of the control design requires the knowledge of the individual rotational wheel speeds and of the two coefficients obtained in the previous section, $\mu_{x_{max}}$ and μ_x. In order to take advantage of the previous $\mu_{x_{max}}$ estimation, a sliding surface $S = (\mu_{x_{max}} - \mu_x)sign(XBS)$ has been selected. This implies that when $S = 0$ the vehicle is operated at $\mu_x = \mu_{x_{max}}$.

Since the maximum friction coefficient $\mu_{x_{max}}$ is always greater than μ_x, we have to distinguish when the sliding surface becomes negative. This is the purpose of the the term "$sign(XBS)$" in the expression of the sliding surface, which is added to manage the case where the instantaneous friction crosses the peak of the friction curve at $\mu_{x_{max}}$. In this case, the XBS becomes negative and therefore the sliding surface becomes negative, allowing the control to bring back the values of μ_x to track $\mu_{x_{max}}$.

Taking the derivative of the sliding surface and substituting the expression for the friction coefficient obtained in (9),

yields:

$$\dot{S} = -\dot{\mu}_x sign(XBS) = -\frac{1}{r_e F_z}(\dot{T} - I_w\ddot{\omega})sign(XBS). \quad (14)$$

When $S = 0$, it is required that $\dot{S} = 0$. Next, $\dot{S} = 0$ implies that $\dot{T}_{eq_1} = I_w\ddot{\omega}$. Then :

$$T_{eq_1} = \int (I_w\ddot{\omega})\, dt = I_w\dot{\omega} + k_1. \quad (15)$$

Note that $S = 0$ implies that $\mu_x = \mu_{x_{max}}$. Substituting again the expression for μ_x and choosing $k_1 = r_e F_z \mu_{x_{max}} + R_x$ we obtain the equivalent torque in order to get $S = 0$ and $\dot{S} = 0$:

$$T_{eq} = I_w\dot{\omega} + r_e F_z \mu_{x_{max}} + R_x. \quad (16)$$

When $S \neq 0$, it is required that $S\dot{S} < 0$. Replacing the expression for $\dot{S}$, we obtain $Ssign(XBS)\dot{\mu}_x > 0$. We then get two possible cases :
1) $Ssign(XBS) > 0$ (the zone of $\mu - \lambda$ curves before arriving at the peak). Then $\dot{\mu}_x > 0$. Therefore, from Eq. (14) we get $\dot{T}_{eq} > I_w\ddot{\omega}$. Replacing T_{eq} by its expression from Eq. (16) and calculating its first derivative will obtain $\dot{T}_{eq} = I_w\ddot{\omega}$. Taking $\dot{T}_{eq} = I_w\ddot{\omega} + \dot{T}_{sm_1}$, with $\dot{T}_{sm_1} = Sk_2 > 0$ will ensure that $\dot{T}_{eq} > I_w\ddot{\omega}$ is satisfied. Here, $k_2 > 0$ is a design parameter.
2) $Ssign(XBS) < 0$ (the zone of $\mu - \lambda$ curves after crossing the peak). Then $\dot{\mu}_x < 0$. Now, the condition to verify becomes $\dot{T}_{eq} < I_w\ddot{\omega}$. Taking again $\dot{T}_{eq} = I_w\ddot{\omega} + \dot{T}_{sm_2}$, with $\dot{T}_{sm_2} = Sk_2 < 0$ will ensure that $\dot{T}_{eq} < I_w\ddot{\omega}$ is satisfied.
Putting together the two conditions we obtain:

$$T_{sm} = \int (Sk_2)dt. \quad (17)$$

The sliding control law is defined as:

$$T_{sliding} = T_{eq} + sign(S)T_{sm}, \quad (18)$$

leading to:

$$T_{sliding} = I_w\dot{\omega} + r_e F_z \mu_{x_{max}} + R_x + sign(S)\int (Sk_2)dt. \quad (19)$$

The presence of the $sign$ function in the control law can induce chattering, therefore in the simulations presented in the sequel, it has been replaced by a $saturation$ function, which allows the surface to remain in a tube with a desired width. As stated previously, the sliding mode control is added to manage the case where the slip or the skid of the wheels occurs. Hence, it has to be activated when this happens. We have now two control laws, one that tracks a reference speed (T_{flat}), and another one that tracks a reference adherence ($T_{sliding}$) . In the next section is presented the strategy of activation of each control law.

C. Activation of control

The purpose of the activation strategy is to achieve a control that has a double objective: to track a reference speed and in the same time to maintain grip of the wheels, regardless of drivers requirements and adherence variation. In the linear zone of the friction curve the applied control law is T_{flat}, while, when entering in the non linear zone, $T_{sliding}$ is applied. When the values for the longitudinal slip are below a fixed threshold, chosen to be in the linear zone of $\mu - \lambda$ curves and far from the neighborhood of the maximum of the friction coefficient, then T_{flat} is applied. Otherwise, a switching between the two controls takes place, and it follows a "(min,max)" rule, shown in algorithm 3.

Algorithm 3: Switching algorithm

if $|\lambda| \leqslant \varepsilon$
$T_{hybrid} = T_{flat}$,
else if $\lambda > 0$
$T_{hybrid} = min(T_{flat}, T_{sliding})$,
else $T_{hybrid} = max(T_{flat}, T_{sliding})$.

This algorithm defines a "safety-zone" for all $|\lambda| \leqslant \varepsilon$ in which we allow the torque coming from the driver requirement to be applied at the wheel of the vehicle, knowing that for these values of the slip we are at the beginning of the $\mu - \lambda$ curves and thus in the stable linear zone. Once this threshold is exceeded, the switch between the sliding mode control and the flatness-based control is applied, limiting each time the greater torque, to avoid wheel slip or skid.

IV. Results

To show the behavior of the chosen strategy, we have simulated a scenario with the vehicle in a hard acceleration and a hard braking phases on a road that changes of adherence conditions. The simulation starts on a dry road ($\mu_{x_{max}} = 1$ between simulation time 0 and 40s), and it finishes on a wet road ($\mu_{x_{max}} = 0.8$ between simulation time 40 and 80s).

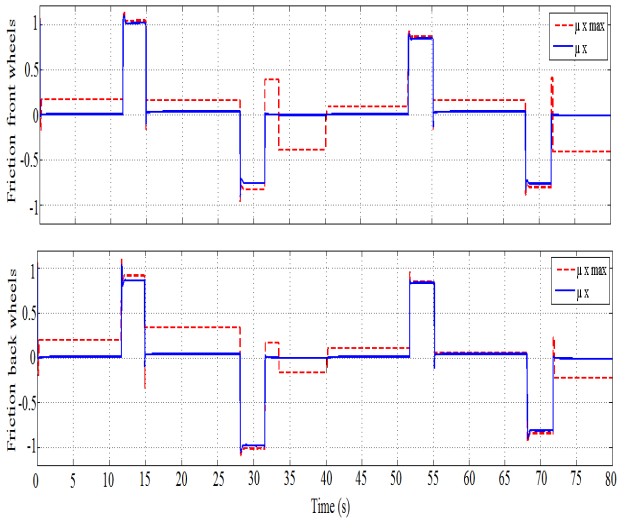

Fig. 7: Instantaneous and maximum friction coefficients.

The estimation stage detects the maximum friction coefficient for both types of roads as shown in Fig.7, while the control achieves to track this values when needed. The profile speed on which the scenario was simulated is shown in Fig.8. On the same figure one can observe that the longitudinal slip

remains at low values and the reference speed is also well tracked.

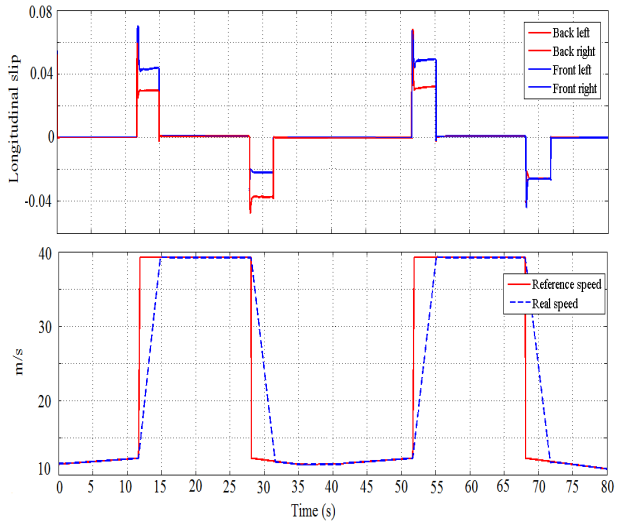

Fig. 8: Slip values and reference speed tracking.

The effect of load transfer can be seen in the torques applied at the front and back wheels, giving a larger torque applied on the front wheels in braking when the normal force is larger, and a smaller one applied on the back. The same phenomenon arises in acceleration, with a smaller normal force in the front and consequently a smaller torque applied, and a bigger one in the back of the vehicle, as shown in Fig.9.

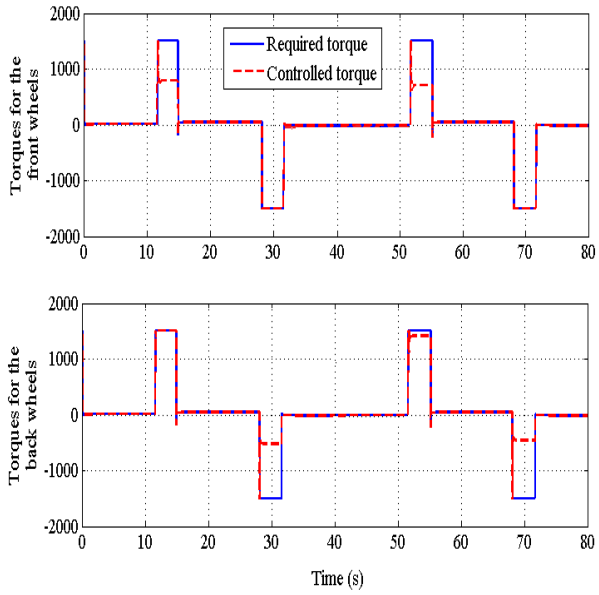

Fig. 9: Required and controlled torques.

The control tracks the reference speed and, when needed, the maximum friction, achieving a stable behavior of the vehicle in hard acceleration and emergency braking maneuvers on time-varying adherence.

V. Concluding Remarks

A new approach to achieve longitudinal control of a vehicle equipped with four electric motors has been tested. It relies on the on-line estimation of the maximum and instantaneous friction coefficients, which are used in the implementation of a sliding-mode based control. The motor torques are the unique control actuators to achieve anti-skid braking and anti-slip acceleration, with satisfactory results. The final control applied to the vehicle tracks a reference speed, using a flatness-based control, and a reference adherence, using a sliding mode control. The later activates only when the values of the instantaneous friction are in the non linear zone of $\mu - \lambda$ characteristics, achieving a stable behavior of the vehicle in acceleration and braking phases.

Acknowledgment

The work of the first author (M.S.G) is financially supported by the CNRS-IFPEN grant 186-654 (2010-2013).

References

[1] L. Alvarez, X. Claeys, R. Horowitz and J. Yi, "Emergency braking control with an observer-based dynamic tire/road friction model and wheel angular velocity measurement," *Vehicle System Dynamics*, 39(2): 81-97, 2003

[2] M.Y. Ayad, M. Becherif, A. Henni, M. Wack and A. Aboubou, "Sliding mode control applied to fuel cell, super-capacitors and batteries for vehicle hybridizations," *IEEE International Energy Conference and Exhibition (EnergyCon)*, pp:478-483, Manama, Bahrain, 2011.

[3] C. Canudas de Wit and P. Tsiotras "Dynamic tire friction models for vehicle traction control," *Proceedings of the 38th IEEE Conference on Decision and Control, Phoenix, AZ , USA* ,4 : 3746 - 3751, 1999.

[4] M. Denny, "The dynamics of anti-lock brake systems," *European Journal of Physics*, 26 :1007-1016, 2005.

[5] D.A. Eichfeld and H. Klein, "Antilock braking system and vehicle speed estimation using fuzzy logic," *Proceedings of the 1st Embedded Computing Conference, Paris*, 1996.

[6] Q. Feng, S. Shuang, S. Jia and Z. Quanming "Sliding mode control design of active vehicle suspension systems with two-time scale sub-models," *Advanced science letters*, 4(3):953-957, 2011.

[7] M. Fliess, H. Mounier, J. Villagra and B. d'Andrea-Novel, "A diagnosis-based approach for tire-road forces and maximum friction estimation," *Control Engineering Practice*, 19 :174- 184, 2011.

[8] J.T. Fossen, T. Fjær, H. Grip, J. Kalkkuhl, A. Suissa and L. Imsland, "Vehicle velocity estimation using nonlinear observers," *Automatica*, 42(12) :2091-2103, 2006.

[9] A. Haddoun, M. Benbouzid, D. Diallo, R. Abdessemed, J. Ghouili and K. Srairi, "Sliding mode control of EV electric differential system," *ICEM, Greece*, 2006.

[10] R. Horowitz, L. Olmos and L. Alvarez, "Adaptive emergency braking control with observer-based dynamic tire-road friction model and under-estimation of friction coefficient," *Proceedings of the 15th IFAC World Congress. Barcelona, Spain*, 2002.

[11] A. Hughes, "*Electric motors and drives: fundamentals, types, and applications*", *Elsevier* 2006.

[12] R.N. Jazar, "*Vehicle dynamics: theory and applications*", *Springer* 2008.

[13] Ph. Martin, M. Fliess, J. Levine and P. Rouchon, "Flatness and defect of nonlinear systems : introductory theory and examples," *Int. J. Control*, 61(6) :1327-1361, 1995.

[14] W. Pasillas-Lepine, "Hybrid modeling and limit cycle analysis for a class of five-phase anti-lock brake algorithms," *Vehicle System Dynamics*, 44(2) :173-188, 2006.

[15] S. M. Savaresi and M. Tanelli, "*Active braking control systems design for vehicles*," *Springer*, 2010.

[16] M. Widmer and G. Le Solliec, "Internship report: simulation and traction control of a vehicle with four in-wheel electric motors", 2010.

Maximum friction estimation and longitudinal control for a full in-wheel electric motor vehicle

- **Authors**: M.S. Geamanu, A. Cela, H. Mounier, S.I. Niculescu, G. Le Solliec.
- **Conference**: International Conference on Control, Automation and Systems (ICCAS).
- **Venue**: Jeju, South Korea.
- **Year**: 2012.

2012 12th International Conference on Control, Automation and Systems
Oct. 17-21, 2012 in ICC, Jeju Island, Korea

Maximum friction estimation and longitudinal control for a full in-wheel electric motor vehicle

Marcel Stefan Geamanu[1,3,*], Arben Cela[2], Guénaël LeSolliec[3], Hugues Mounier[1], Silviu-Iulian Niculescu[1]

[1]**Laboratoire des Signaux et Systemes (L2S, UMR 8506), CNRS-Supelec, 3 rue Joliot Curie, 91192 Gif-sur-Yvette, FRANCE**
(e-mails : marcel-stefan.geamanu@lss.supelec.fr, hugues.mounier@lss.supelec.fr, silviu.niculescu@lss.supelec.fr)
[2]**UPE ESIEE Paris, 2 boulevard Blaise Pascal, 93162 Noisy le Grand, FRANCE**
(e-mail : a.cela@esiee.fr)
[3]**IFPEN, 1 et 4 avenue de Bois-Préau, 92500 Rueil-Malmaison, FRANCE**
(e-mails : guenael.le-solliec@ifpen.fr, marcel-stefan.geamanu@ifpen.fr)
[*]**Corresponding author**

Abstract: The present paper describes a longitudinal control strategy in time-varying road surface adhesion coefficient conditions, for a vehicle equipped with 4 in-wheel electric motors. The controller task is to ensure two main functions : braking (achieving an ABS-like function, i.e. no wheel skid), and traction control (TCS-like function, i.e. low wheel slip) using the electric motor torques as the unique actuators signal sources. The torque of electric motors is available almost instantaneously, unlike the torque generated by classic internal combustion engines. In addition, information about its values can be measured, starting from the current that passes through the motor, which means that advanced control techniques can be applied directly on the transmitted torque. In order to generate the appropriate anti-skid or anti-slip torque for each wheel, firstly an estimation of the instantaneous friction between the wheel and the road has to be made. Next, the maximum friction coefficient between the wheel and the road is computed with the help of an algorithm based on Dugoff tire model, without prior knowledge of the road conditions. Ultimately, the control strategy will compute a maximum torque that is allowed to be transmitted at the wheels in order to achieve TCS and ABS functions, along with a given reference speed to track. The only variables used in this strategy are the wheel acceleration, the instantaneous torque generated by the electric motors and the chassis acceleration.

Keywords: vehicle dynamics control, electric vehicles, tire-road friction estimation.

1. INTRODUCTION

Two of the most important components in providing safety and achieving desired vehicle motion [1], are the traction control system (TCS) and ABS (Antiblockiersystem) . The TCS is designed to use the maximum friction between the wheels and the road to provide a desirable longitudinal and lateral vehicle motion, ensuring in the same time passenger comfort [10]. The ABS system is designed to prevent wheel lock in case of hard braking, as described in [3], [5], [12]. Therefore, longitudinal control needs to achieve anti-spin acceleration and anti-skid braking, maintaining the fastest stable acceleration and deceleration.

The interaction between the vehicle and the surface of the road on which is moving has a crucial influence on vehicle's behavior during acceleration, braking or cornering maneuvers. The vehicle response to the driver's inputs (steering, acceleration or braking) depends on a critical factor that is the adherence between the tire and the road surface. The friction between the wheels and the road is subject to variation, its values changing due to numerous factors as the weather conditions (hot temperatures, rain, snow or ice), road maintenance and type of the pavement (asphalt, concrete or cobblestone). This is the most important parameter in the functioning of TCS and ABS systems, therefore estimating it becomes main factor in achieving proper proper behavior of these two systems.

The aim of this work is to achieve a control law that avoids longitudinal wheel slip or skid, independently of the driver's behavior (hard acceleration or braking) and of the conditions of the road surface (wet, dry or snow). The first step in the strategy is to estimate "on-line" the maximum friction between the wheel and the road, starting from Dugoff's tire model [4]. The second one is to apply the control that does not allow the instantaneous friction to exceed the maximum available in hard acceleration and braking phases. Driver's requirements (acceleration, braking) result in a specific speed to track. To this purpose, a standard speed tracking scheme taking advantage of model's flatness property was used.

Conventional configuration of the majority of existing vehicles equipped with an internal combustion engine (ICE) includes two different actuators that accomplish ABS and TCS and hence, two control solutions with different dynamics. The novelty of the present work consists in using the four in-wheel electric motors as the only actuators in acceleration and deceleration, in order to provide the necessary torques to accomplish both TCS and ABS functions. These motors are powerful (39 kW each), they have a very low latency and are able to provide a braking torque on the wheels [9] faster than conventional

brakes which are normally used for this purpose.

Estimating wheel forces is problematic in the classical ICE configuration, due to the lack of a reliable estimation of the torque generated by the engine. With the electric motor, due to a good knowledge of its output torque calculated from the current intensity that passes through the motor, one can estimate the wheel friction forces. Unlike the existing, rather conservative, control strategies, described in [3], [5], [8], which rely on the longitudinal slip and a fixed threshold, the electric motor allows to apply a control on the friction coefficient, while considering the road conditions.

The remaining paper is organized as follows, section 2 is devoted to introduce the vehicle model as well as the estimation of the parameters of interest. In section 3 are exposed the control strategies we are proposing : a flatness-based control in order to track a reference speed, and a torque limiter control in order to achieve an instantaneous friction that does not exceed the estimated maximum friction. Some illustrative examples and scenarios are detailed in section 4 and some concluding remarks are presented in section 5.

2. VEHICLE MODEL AND REPRESENTATION OF ITS DYNAMICS

2.1 Vehicle model

Let us consider the four wheeled model of a vehicle which consists of the main vehicle mass to which the four wheels are attached via a suspension system [14]. Since the present goal is to achieve longitudinal control of the vehicle, we are not interested in its lateral dynamics and therefore the full model can easily be taken as a bicycle model, as shown in Fig.1 :

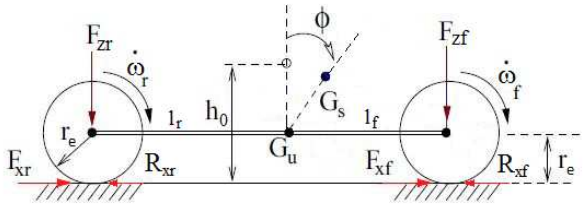

Fig. 1 Bicycle view of the vehicle model.

Here, G_s and G_u are respectively the centers of gravity of the suspended and unsuspended mass, l_f and l_r are the distances from the center of mass to the front and rear axle and ϕ is the pitch angle. The suspension dynamics are taken into account, with the associated load transfer that arises when the vehicle is accelerating or braking. The forces that act on each axle are shown in Fig.1. The overall system equations including the vehicle, wheel and load transfer dynamics can be written as follows :

$$m\dot{V}_x = F_x - F_{aero}, \tag{1}$$

$$F_{z_i} = m_{w_i} g - k(l_i\phi - h_0) - cl_i\dot{\phi}, \tag{2}$$

$$F_{x_i} = \mu_{x_i} F_{z_i}, \tag{3}$$

$$I\dot{\omega}_i = T_i - r_e F_{x_i} - R_{x_i}, \tag{4}$$

$$F_x = \sum_{i=1}^{4} F_{xi}. \tag{5}$$

Here, r_e is the wheel radius, F_{aero} is the aerodynamic drag force, F_z is the normal force on the tire, F_x is the longitudinal tire force, μ_x is the longitudinal friction coefficient, ω is the wheel angular speed, R_x is the rolling resistance force, T is the wheel torque, l is distance from the center of gravity to the axle and the index $i = fl, fr, bl, br$ with the signification : fl=front left, fr=front right, bl=back left and br=back right.

The longitudinal friction coefficient between the road and the tire (μ_x) is modeled by a Pacejka function [2] of the longitudinal slip (λ), with two different curves for dry and wet road, as shown in Fig.2.

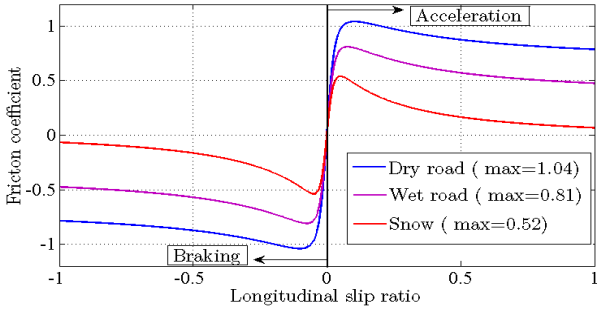

Fig. 2 Pacejka curves modeling the friction coefficient.

In order to apply the adequate control on the friction coefficient, our strategy follows four steps, starting with the estimation of the load transfer in acceleration and braking. Next, the longitudinal friction force is estimated which leads to the estimation of the instantaneous friction coefficient. This will allow the computation of the maximum friction coefficient which will be used in the control strategy. These four steps are detailed in the next subsection.

2.2 Parameter estimation

2.2.1 Load transfer estimation

The vertical forces under the front and rear axles when a car is accelerating on a level road, are [13] :

$$F_{zf} = \frac{1}{2}mg\frac{l_r}{l} - \frac{1}{2}mg\frac{h_0}{l}\frac{\dot{V}_x}{g}, \tag{6}$$

$$F_{zr} = \frac{1}{2}mg\frac{l_f}{l} + \frac{1}{2}mg\frac{h_0}{l}\frac{\dot{V}_x}{g}. \tag{7}$$

The first terms, $\frac{1}{2}mg\frac{l_r}{l}$ and $\frac{1}{2}mg\frac{l_f}{l}$, are called static parts, coming from the static weight distribution (static position of the center of gravity) and the second terms,

$\pm\frac{1}{2}mg\frac{h_0}{l}\frac{\dot{V}_x}{g}$, are called dynamic parts of the normal forces, coming from the dynamic mass transfer in acceleration or deceleration (with $\dot{V}_x$ being the chassis longitudinal acceleration). When the vehicle is braking, the dynamic part becomes significant in the front of the vehicle, giving a larger load in the front of the vehicle, and a smaller one in the back, and vice-versa in acceleration.

2.2.2 Longitudinal friction force estimation

As stated in [6], the friction coefficient μ_x turns out to be dependent solely on the longitudinal acceleration $\dot{V}_x$. Yet, the vehicle longitudinal acceleration can carry noise [7], so in order to estimate more accurately the longitudinal friction force, we took advantage of (4). The knowledge of the torque and the wheel dynamics allows the computation of the longitudinal force for each wheel. From (4), the expression for F_{x_i} is :

$$F_{x_i} = \frac{1}{r_e}(T_i - I\dot{\omega}_i - R_{x_i}). \tag{8}$$

2.2.3 Instantaneous friction coefficient estimation

Having computed the normal and longitudinal forces for each wheel, starting from Eq.(3), a good estimation of the instantaneous friction coefficient at each wheel is then :

$$\mu_{x_i} = \frac{F_{x_i}}{F_{z_i}}. \tag{9}$$

2.2.4 Maximum friction estimation using Dugoff tire model

Dugoff tire model has an interesting feature, assuming a uniform vertical pressure distribution on the tire contact patch. This is a simplification compared to the more realistic parabolic pressure assumed in Pacejka model. However, the longitudinal forces are directly related to the maximum friction coefficient in more transparent equations than in Pacejka model, hence the interest to estimate Dugoff parameters in order to obtain a maximum friction coefficient estimation.

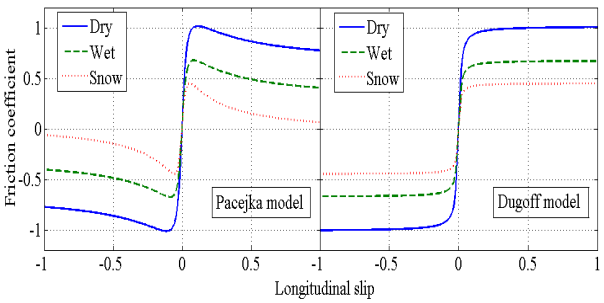

Fig. 3 Friction coefficients compared on Pacejka and Dugoff curves.

In Dugoff's tire-model, longitudinal efforts are modeled as follows :

$$F_x^D = f(\tau)K_x\lambda. \tag{10}$$

where $f(\tau)$ is a piecewise function :

$$f(\tau) = \begin{cases} (2-\tau)\tau & , \tau < 1 \\ 1 & , \tau \geqslant 1 \end{cases}, \quad \tau = \frac{\mu_{x_{max}}F_z}{2|K_x\lambda|} \tag{11}$$

It is not difficult to see that $\mu_{x_{max}}$ can be expressed in terms of four a priori known variables F_x, F_z, λ, K_x. The $\mu - \lambda$ characteristics have two specific regions. The first one is linear and its limit is given by $\tau = 1$, therefore, when its values are below 1, we are in the non linear region. In the linear region, the longitudinal efforts are calculated as $F_x^D = K_x\lambda$. Therefore, the values for K_x can be derived in the linear region of the friction curves ($f(\tau) = 1$), applying a first order filter on the following equation :

$$K_x = \frac{F_x}{\lambda}. \tag{12}$$

The filter permits to keep a historical of the precedent values of the parameter as the friction coefficient changes. The longitudinal stiffness parameter K_x is in fact the slope of the $\mu - \lambda$ curves (or $F_x - \lambda$ curves) in the linear region and impacts on the shape of the curves, as observed in Fig.4 :

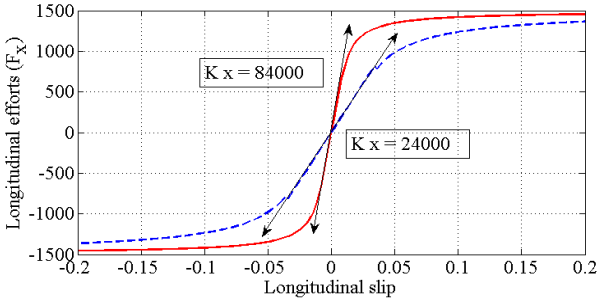

Fig. 4 Longitudinal stiffness parameter K_x and its impact on the friction curves based on Dugoff model.

In the non linear region of the curves, longitudinal efforts are calculated as $F_x^D = (2-\tau)\tau K_x\lambda$. Knowing that $\tau = (\mu_{x_{max}}F_z)/(2|K_x\lambda|)$, we can calculate the limit value for the longitudinal slip after which we enter in the non linear region :

$$|\lambda_{lim}| = \frac{\mu_{x_{max}}F_z}{2|K_x|}. \tag{13}$$

Hence, if $|\lambda| \leqslant \lambda_{lim}$, we are in the linear region of the curves, otherwise we are in the non linear one. This parameter has a certain importance in the following development of the estimation strategy and is as well used later in the control strategy.

Next, let us take the non linear region case of the $f(\tau)$ function, i.e. $f(\tau) = (2-\tau)\tau$. Then, the longitudinal efforts can be expressed as follows :

$$F_x^D = \left(2 - \frac{\mu_{x_{max}}F_z}{2|K_x\lambda|}\right)\frac{\mu_{x_{max}}F_z}{2|K_x\lambda|}K_x\lambda. \tag{14}$$

This expression can be rewritten as a second algebraic equation of the maximum friction coefficient :

$$\mu_{x_{max}}^2F_z^2 - 4\mu_{x_{max}}|K_x\lambda|F_z + 4|K_x\lambda|F_x^D = 0, \tag{15}$$

whose two solutions are :

$$\mu_{x_{max}} = \frac{2(|K_x\lambda| \pm \sqrt{K_x\lambda(K_x\lambda - F_x^D)})}{F_z}. \tag{16}$$

The sign between the two terms of the numerator is '+' when $\lambda \geqslant 0$ and '-' when $\lambda < 0$.

As observed in "off-line" calculations, Dugoff tire model saturates at a different level than Pacejka tire model. It is in fact a weighting factor between Dugoff and Pacejka models that drives Dugoff model to cross through Pacejka model exactly in the peak of the curve (Fig.5). Its values can be calculated only close to the peak of the $\mu - \lambda$ curve.

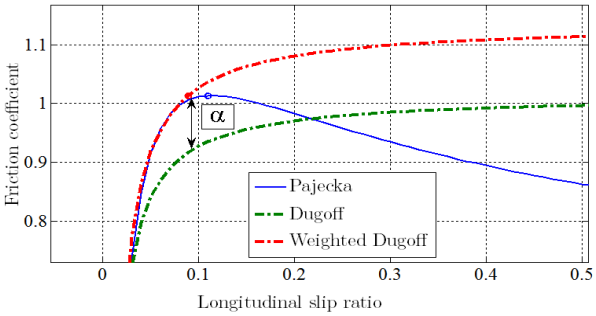

Fig. 5 Weighting parameter α at the peak of longitudinal efforts built with Pacejka and Dugoff models.

The two key parameters, K_x and α are used in the obtainment of the maximum friction coefficient. For the longitudinal stiffness coefficient K_x we have calculated "off-line" its different values for different types of road surface conditions and we have obtained K_x=47000 for a dry road ($\mu_{x_{max}} = 1$), K_x=34500 for a wet road ($\mu_{x_{max}} = 0.8$) and K_x=27600 for a snowy road ($\mu_{x_{max}} = 0.5$). The evolution for the estimated values and the model values is shown in Fig.6.

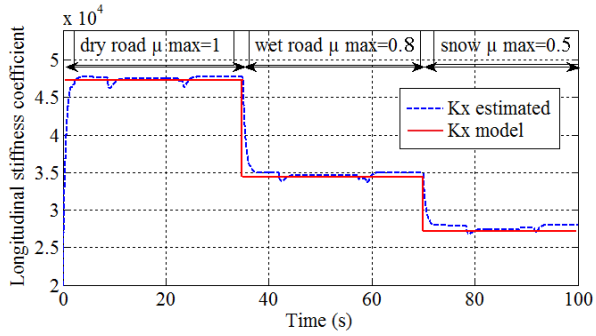

Fig. 6 Longitudinal stiffness parameter K_x and its values for different adherences.

For the second parameter, α, we have also derived "off-line" its different values for different types of adherence and we have obtained α=1.12 for a dry road ($\mu_{x_{max}} = 1$), α=1.16 for a wet road ($\mu_{x_{max}} = 0.8$) and α=1.2 for a snowy road ($\mu_{x_{max}} = 0.5$). As it can be observed, α hardly varies from one type of road to another. An algorithm that takes advantage of the estimation of the slope of the friction curves (S) is designed to adapt α as the friction curve changes. The initial value of α starts with an "off-line" initial value of $\alpha_{init} = 1.1$. Next, as the friction curve changes, the parameter adapts its value following the next algorithm :

Algorithm 1 : α adaptation algorithm

if $(|\lambda| \geqslant \lambda_{lim})$
  i=1 (ADAPT ON)
    if $S_{min} - S_{[min;max]} \geqslant 0$
      $\alpha = \int (S_{min} - S)_{[min;max]} k_{up} i$
    else
      $\alpha = \int (S_{min} - S)_{[min;max]} k_{down} i$
else
  i=0 (ADAPT OFF)

Here, S is defined as the derivative of the friction coefficient with respect to longitudinal slip :

$$S(t) = \frac{d\mu_x}{d\lambda} = \frac{\hat{\mu}_x}{\hat{\lambda}}. \tag{17}$$

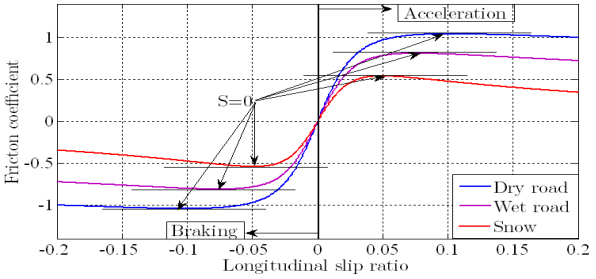

Fig. 7 Adhesion coefficient characteristic curve for dry, wet and snowy road and S definition.

In algorithm 1, α adapts only when S is close to 0, between limits $S_{min} = 1$ and $S_{max} = 5$. We proposed an algorithm that calculates the estimation of α and Fig.8 shows that it reaches the values calculated "off-line" as the friction coefficient changes.

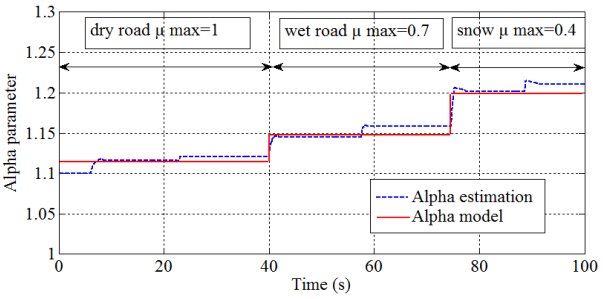

Fig. 8 Estimation of parameter α following the adaptation algorithm 1.

Having the estimates of K_x and α, we propose an algorithm that computes the maximum friction coefficient as follows :

Algorithm 2 : $\mu_{x_{max}}$ computation

if $(|\lambda| > \lambda_{lim})$

$$\mu^D_{x_{max}}(t_k) = \alpha \frac{2(|K_x \lambda(t_k)| \pm \sqrt{K_x \lambda(t_k)(K_x \lambda(t_k) - F_x(t_k))})}{F_z}$$

else

$$\mu^D_{x_{max}}(t_k) = \mu^D_{x_{max}}(t_{k-1})$$

3. CONTROL STRATEGIES

3.1 Flatness-Based Control

In order to track a reference speed V_x, a flatness-based trajectory tracking control is implemented. The vehicle model is trivially flat [11], which means, roughly speaking, that there exists an output, called a flat output, which can be expressed as a function of all the inputs and system variables and their derivatives. Here, V_x is a flat output. Making the (physically sound) assumption that the wheel dynamics is fast compared to the car body one, the model (1)-(4) reduces to :

$$m\dot{V}_x = \frac{1}{r_e}T - F_{aero}. \tag{18}$$

A linearizing transformation with new input u is given by $T = r_e(F_{aero} + mu)$, yielding the trivial dynamics $\dot{V}_x = u$. An anti-windup controller is then chosen for u :

$$u = PI_{out} + \dot{V}_{x_{ref}}. \tag{19}$$

The final expression for the flatness-based controller is :

$$T_{flat} = r_e(F_{aero} + mPI_{out} + m\dot{V}_{x_{ref}}). \tag{20}$$

The ”anti-windup” reacts when the control reaches the limits of the actuator, thereupon the integral term could increase indefinitely. A combination of conditional integration and calculation of the output of the integrator as a function of the controller output PI is used here. When the PI output goes out of the electric motor torque limitations range, the integral term stops charging. The purpose of this control is to track the $V_{x_{ref}}$ trajectory, independently of the fact that the latter could induce slip or not. Nevertheless, when driver’s inputs are significant (hard acceleration ; hard braking), the flatness-based control does not suffice in *unknown* road conditions, resulting in a wheel spin in acceleration or a wheel block in braking. Therefore, a control that limits the output torque needs to be introduced.

3.2 Torque saturation

This control will only saturate the demanded torque by a maximum torque value, which is calculated starting from wheel dynamics equation 4 of the overall model : $I\dot{\omega}_i = T_i - r_eF_{x_i} - R_{x_i}$. Replacing F_{x_i} by equation 3, and extracting the torque T_i will yield : $T_i = I\dot{\omega}_i + r_e\mu_{x_i}F_{z_i} + R_{x_i}$. Therefore, the saturation torque will be given by :

$$T_{sat_i} = I\dot{\omega}_i + r_e\mu_{x_{max}}F_{z_i} + R_{x_i}. \tag{21}$$

The maximum friction coefficient $\mu_{x_{max}}$ will be calculated for each axle, front and rear, since due to the load transfer that arises in acceleration and braking maneuvers, the friction at the front axle is different from the one at the rear axle.

3.3 Activation of control

The purpose of the activation strategy is to achieve a control that has a double objective : to track a reference speed and in the same time to maintain grip of the wheels, regardless of drivers requirements and adherence variation. In the linear zone of the friction curve the applied control law is T_{flat}, while, when entering in the non linear zone, T_{sat} is applied. When the values for the longitudinal slip are below λ_{lim}, then T_{flat} is applied. Otherwise, a switching between the two controls takes place, and it follows a "(min,max)" rule, shown in algorithm 3.

Algorithm 3 : Switching algorithm

if $|\lambda| \leqslant \lambda_{lim}$
  $T_{wheel} = T_{flat}$,
else if $\lambda > 0$
  $T_{wheel} = min(T_{flat}, T_{sat})$,
  else $T_{wheel} = max(T_{flat}, T_{sat})$.

This algorithm defines a "safety-zone" for all $|\lambda| \leqslant \lambda_{lim}$ in which we allow the torque coming from the driver requirement to be applied at the wheel of the vehicle, knowing that for these values of the slip we are at the beginning of the $\mu - \lambda$ curves and thus in the stable linear zone. Once this variable threshold is exceeded, the switch between the saturation control and the flatness-based control is applied, limiting each time the greater torque, to avoid wheel slip or skid.

4. RESULTS

To test both estimation and control strategy efficiencies, a scenario with three acceleration/braking phases was simulated. It starts on a wet road surface ($\mu_{x_{max}} = 0.81$ between simulation time 0 and 15s), it continues on a dry road surface ($\mu_{x_{max}} = 1.04$ between simulation time 16 and 30s), and it finishes on a snowy road surface ($\mu_{x_{max}} = 0.52$ between simulation time 31 and 45s). Even if such a scenario does not seem completely realistic, it covers a good range of friction values that can change during driving. The reference profile speed along with front and back wheels velocities is shown in Fig.9.

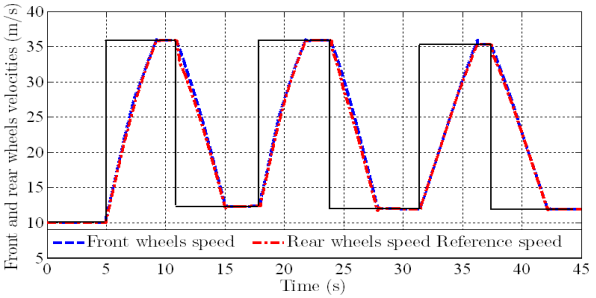

Fig. 9 Reference speed tracking results.

In Fig.9 can be observed that no uncontrollable wheel spin or wheel block is accomplished, resulting in a stable acceleration and deceleration of the wheels. The control law keeps the instantaneous friction values at maximum values when needed (i.e. in hard acceleration or braking

phases), achieving good grip of the wheels on the road. Friction coefficients evolution is shown in Fig.10.

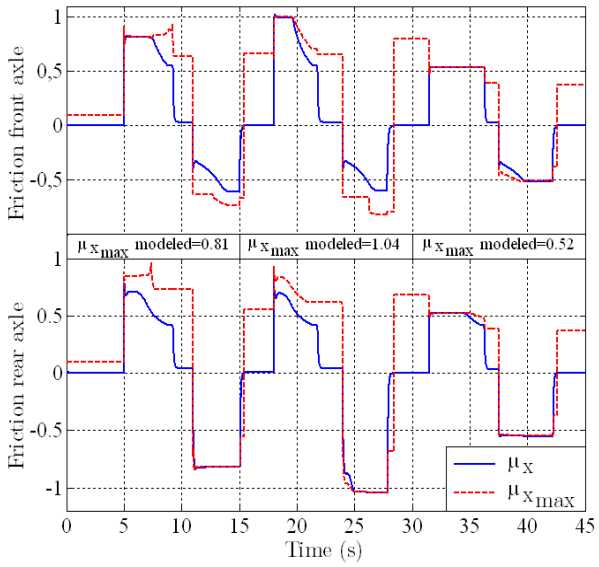

Fig. 10 Instantaneous and maximum friction estimation evolutions.

Another noticeable phenomenon that can be observed in Fig.10 is that, due to load transfer, at the front axle the instantaneous friction achieves the maximum value, while at the back is still far from it. This happens because at the front of the vehicle, in acceleration, the normal force on the wheels is smaller than at the back of the vehicle. A smaller F_z means a greater μ_x (Eq. 4). The exact same phenomenon occurs in braking maneuvers, when the load transfers at the front of the vehicle, giving a smaller normal force at the back and consequently a greater μ_x. It can also be observed that the estimation strategy detects the maximum friction available, even if it changes its values, and the control law limits the torque to avoid that $\mu_x$does not exceed the maximum.

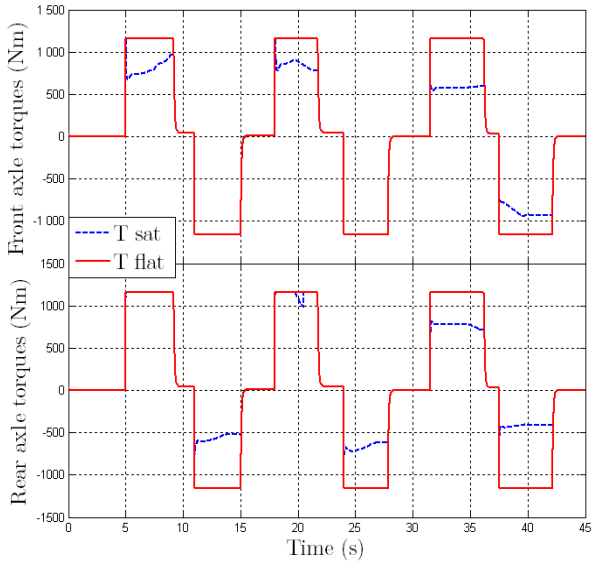

Fig. 11 Flatness based torque and saturated torque evolutions.

The limitation of the flatness based generated torque (T_{flat} for the reference speed tracking), by the saturation generated torque (T_{sat} for the friction limitation) is shown in Fig.11.

5. CONCLUDING REMARKS

A new approach based on Dugoff tire model is proposed along with a torque saturation control law. This method detects the maximum friction available, estimating "on-line" two parameters in order to match the more realistic Pacejka model, which is considered to simulate real tire friction behavior. Next, the control that takes the latter estimation and saturates the transmitted torque at the wheels, achieves stable wheel acceleration and deceleration in emergency braking situations or hard acceleration maneuvers.

ACKNOWLEDGMENT

The work of the first author (M.S.G) is financially supported by the CNRS-IFPEN grant 186-654 (2010-2013).

REFERENCES

[1] L. Alvarez, X. Claeys, R. Horowitz and J. Yi, "Emergency braking control with an observer-based dynamic tire/road friction model and wheel angular velocity measurement," *Vehicle System Dynamics*, 39(2) : 81-97, 2003.

[2] C. Canudas de Wit and P. Tsiotras "Dynamic tire friction models for vehicle traction control," *Proceedings of the 38th IEEE Conference on Decision and Control, Phoenix, AZ , USA* ,4 : 3746 - 3751, 1999.

[3] M. Denny, "The dynamics of anti-lock brake systems," *European Journal of Physics*, 26 :1007-1016, 2005.

[4] H. Dugoff, P.S. Fancher, L. Segel " Tire performance characteristics affecting vehicle response to steering and braking control inputs," Technical report, *Highway Safety Research Institute*, Ann Arbor, MI, 1969.

[5] D.A. Eichfeld and H. Klein, "Anti-lock braking system and vehicle speed estimation using fuzzy logic," *Proceedings of the 1st Embedded Computing Conference, Paris*, 1996.

[6] M. Fliess, H. Mounier, J. Villagra and B. d'Andrea-Novel, "A diagnosis-based approach for tire-road forces and maximum friction estimation," *Control Engineering Practice*, 19 :174-184, 2011.

[7] J.T. Fossen, T. Fjær, H. Grip, J. Kalkkuhl, A. Suissa and L. Imsland, "Vehicle velocity estimation using nonlinear observers," *Automatica*, 42(12) :2091-2103, 2006.

[8] R. Horowitz, L. Olmos and L. Alvarez, "Adaptive emergency braking control with observer-based dynamic tire-road friction model and underestimation of friction coefficient," *Proceedings of the 15th IFAC World Congress. Barcelona, Spain*, 2002.

[9] A. Hughes, "*Electric motors and drives : fundamentals, types, and applications*", *Elsevier* 2006.

[10] R.N. Jazar, "*Vehicle dynamics : theory and applications*", *Springer* 2008.

[11] Ph. Martin, M. Fliess, J. Levine and P. Rouchon, "Flatness and defect of nonlinear systems : introductory theory and examples," *Int. J. Control*, 61(6) :1327-1361, 1995.

[12] W. Pasillas-Lepine, "Hybrid modeling and limit cycle analysis for a class of five-phase anti-lock brake algorithms," *Vehicle System Dynamics*, 44(2) :173-188, 2006.

[13] S. M. Savaresi and M. Tanelli, "*Active braking control systems design for vehicles*," *Springer*, 2010.

[14] M. Widmer and G. Le Solliec, "Internship report : simulation and traction control of a vehicle with four in-wheel electric motors", 2010.

Adherence control for electric vehicles on varying road conditions

- **Authors**: M.S. Geamanu, A. Cela, H. Mounier, S.I. Niculescu, G. Le Solliec.
- **Conference**: Mediterranean Conference on Control and Automation (MED).
- **Venue**: Platanias-Chania, Crete.
- **Year**: 2013.

Adherence control for electric vehicles on varying road conditions

Marcel Stefan Geamanu,
Hugues Mounier and
Silviu-Iulian Niculescu
Laboratoire des Signaux et Systèmes (L2S)
UMR 8506 CNRS-Supelec,
3 rue Joliot Curie, 91192 Gif-sur-Yvette, FRANCE

Arben Cela
UPE ESIEE Paris,
2 boulevard Blaise Pascal,
93162 Noisy le Grand, FRANCE

Guénaël LeSolliec
and Marcel Stefan Geamanu
IFPEN, 1 et 4 avenue de Bois-Préau,
92500 Rueil-Malmaison, FRANCE

***Abstract*—The present paper describes a torque saturation control technique applied on vehicular control, operating on time-varying tire-road adherence conditions and with noise perturbation. The method is based on an instantaneous estimation of the maximum available friction using the Dugoff tire model [3]. The novelty lies in the modeling of the road conditions, which are regarded as continuous variables. A "dynamic" Pacejka model is built around the classical Pacejka model, giving a more realistic approach of the tire-road interaction. The implemented estimation method has to adapt to all the parameter changes, to produce a reliable maximum friction on which the control will be applied. The complex modeling of the road conditions will be enlarged with a noise perturbation, to test our method's robustness, which represents the objective of the present work. At the same time, the vehicle is considered to be equipped with "in-wheel" electrical motors, which provide a quick transmission of the torque directly at the wheel.**

I. Introduction

In vehicular safety, two embedded systems are crucial in good behavior of the vehicle. The first one is the ABS (Anti-blockier System) which prevents the wheel from blocking in case of hard braking maneuver as described in [2], [4], [13]. The second one is the TCS (Traction Control System) which prevents the wheel from spinning in case of hard accelerating maneuver [11]. Both of these systems are based on the friction between the tire and the road and depending on it, they act on the appropriate sub-systems of the vehicle which act on the brakes or the acceleration respectively. Hence, the tire-road friction plays an important role in the good functioning of ABS and TCS and so, a good estimation of the friction is needed. Nevertheless, the influence of the friction on the longitudinal dynamics is hard to quantify since it depends on numerous factors which are not easily separable.

For a better understanding of this phenomena it is helpful to look closer at the Pacejka formula [14], which is an empirical formula whose results are usually close to the reality. Nevertheless, the curves remain at theoretical level, since a slight change in the parameters yield different shapes of the curves.

Emails: marcel-stefan.geamanu@lss.supelec.fr (corresponding author), hugues.mounier@lss.supelec.fr, silviu.niculescu@lss.supelec.fr, a.cela@esiee.fr, guenael.le-solliec@ifpen.fr,

Instead of the curves modeled by Pacejka, in real environments we find a cloud of points whose position can vary from a sample time to another for the same road conditions [8], [15], as shown in figure 1. In addition, perturbations and noise can easily affect the estimation process with possible influence on the final control applied at the wheels.

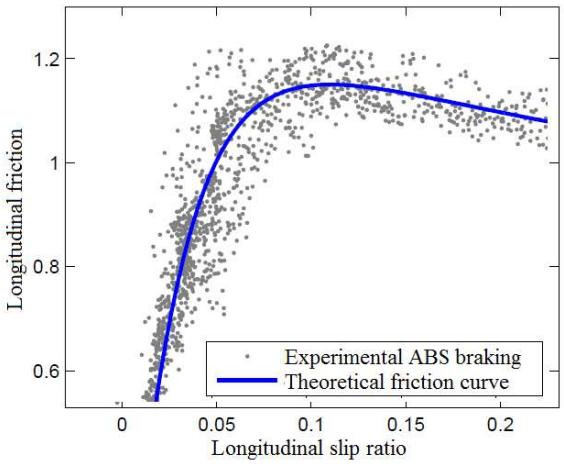

Fig. 1: Experimental friction estimation

In this paper, a different approach regarding the Pacejka model is presented. Here, instead of considering only three theoretical curves modeling the main types of road surfaces (dry, wet and snowy), we interpret them as continuously varying during the driving maneuver. This approach will give a more realistic modeling of the road surface conditions and will allow to have a better view of the results of the proposed method in this environment. At the same time, adding noise on the measurement variables will bring even more realism to the model, allowing in addition to test the robustness of our method. Another innovation of the present work consists in using the in-wheel electric motor as the only actuator in acceleration and deceleration, in order to provide the necessary torque to accomplish both TCS and ABS functions. The in-wheel motor used here is powerful (39 kW), it has a very low latency and is able to provide a braking torque on the wheels

[10] faster than conventional brakes which are normally used for this purpose. With the electric motor, due to a good knowledge of its output torque computed from the current intensity that passes through the motor, one can envisage the estimation of the tire-road friction forces. Unlike the existing, rather conservative, control strategies, described in [2], [4], [5], [9], [12], which rely on the longitudinal slip and on a fixed threshold, the electric motor allows to apply a control on the friction coefficient, while considering the road conditions.

The remaining of the paper is organized as follows: in section 2, a new approach into modeling the road conditions is presented; in section 3, the vehicle model, the estimation method and the control strategy are described; section 4 shows the results of the proposed control method; some concluding remarks are presented in section 5.

II. Continuous variation of the road conditions

Classical Pacejka formula is expressed as follows [14]:

$$F_x = D\,\sin(C\,\arctan(B\lambda - E(B\lambda - \arctan(B\lambda)))) \quad (1)$$

with F_x being the longitudinal force and λ the longitudinal slip ratio. The B, C, D and E parameters are calculated as follows:

- $C = b_0$
- $D = (b_1 F_z + b_2) F_z$
- $B = ((b_3 F_z^2 + b_4 F_z) e^{-b_5 F_z})/CD$
- $E = b_6 F_z^2 + b_7 F_z + b_8$

with F_z being the normal force on the tire. The constant parameters $b_0 - b_8$ have fixed values depending on the type of the utilized tire. Here, $b_0 = 1.5699, b_1 = -25.63, b_2 = 1305, b_3 = 6.825, b_4 = 395.69, b_5 = 0, b_6 = 0.0034, b_7 = -0.0082, b_8 = 0.6565$. In this formula, parameters C and D have the most noticeable influence on the curves. One interpretation of the Pacejka coefficients is the following:

- C represents the behavior of the curves once the maximum value is exceeded . A small C will be translated in a small slope of the curve after its peak. This parameter has also an influence on the slope of the pseudo-linear segment of the curves.

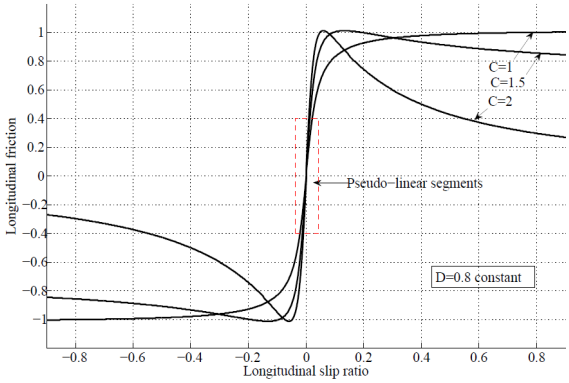

Fig. 2: Parameter C influence on the friction curves

- D is the maximum force the tire can generate, at its peak performance, influencing also the slope of the curves as shown in figure 3.

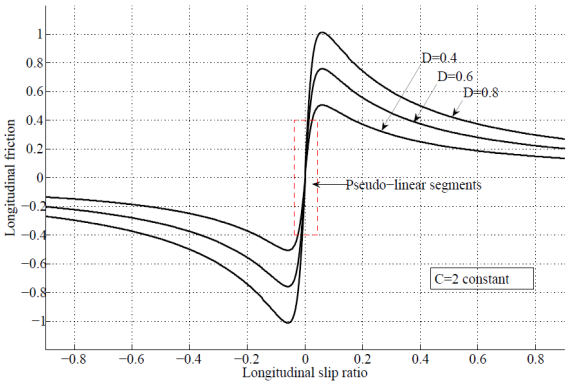

Fig. 3: Parameter D influence on the friction curves

The effect of parameters C and D on the friction curves is shown in figure 2 and 3. So, instead of using fixed parameters in the computation of C and D, we can consider them as time-varying in order to model the variation of road conditions in real situations. In these situations estimation can be problematic, as the road conditions change continuously. To model this variation, we have summed up parameters C and D into one single variable which gives the state of the road, called X_r. Modeling C and D into one single variable represents the realistic case of the friction variation. The friction between the wheels and the road is subject to variation, its values changing due to numerous factors as the weather conditions (hot temperatures, rain, snow or ice), road maintenance and type of the pavement (asphalt, concrete or cobblestone). Therefore, X_r will vary between $[0..1]$, giving a maximum adherence when is close to value 1 (simulating a dry asphalt road for example), and a small adherence when is close to value 0 (simulating a snowy or icy road), but will take into account all the other adherences in between, modeled as a continuous variation of C and D. Parameters C and D will have the following expressions:

$$C = X_r + k_c \quad (2)$$

$$D = \frac{k_{d_1}}{X_r + k_{d_2}} + X_r k_{d_3} \quad (3)$$

with $k_c, k_{d_1}, k_{d_2}, k_{d_3}$ being design parameters. Therefore, Pacejka formula will be rewritten as follows:

$$F_x = \left(\frac{k_{d_1}}{X_r + k_{d_2}} + X_r k_{d_3}\right) \sin((X_r + k_c)\arctan(B\lambda - E(B\lambda - \arctan(B\lambda)))) \quad (4)$$

Therefore, we have the variable X_r which will give us the state of the road surface and we can use this input variable to model a continuous variation of the road surface condition. This will yield a more realistic approach of Pacejka curves, regarded as multiple time-varying curves, as shown in figure

4. Here we pass through snowy roads with $\mu_{x_{max}} = 0.4 \sim 0.5$ and rainy roads with $\mu_{x_{max}} = 0.7 \sim 0.8$ towards dry roads with $\mu_{x_{max}} = 0.9 \sim 1$. Nevertheless, the curves between these values are also taken into account, giving an approach to model road conditions closer to reality. To model the continuous

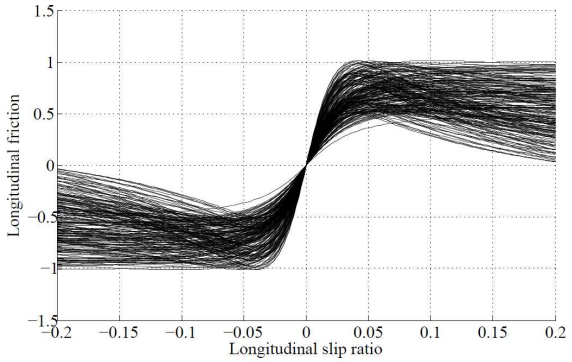

Fig. 4: Realistic modeling of Pacejka curves

change of Pacejka parameters, in the simulation we used the following time evolution of the variable X_r arbitrary chosen, which gives us the state of the road surface, as shown in figure 5: This profile passes from dry road surface (simulation time

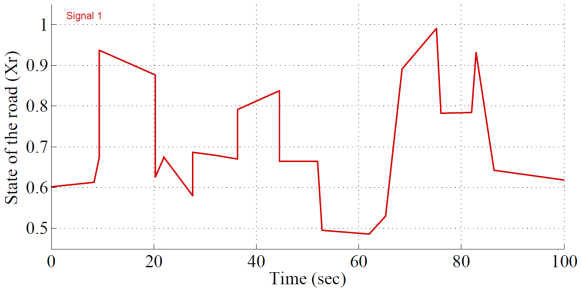

Fig. 5: Time evolution of the state of the road

70s-80s), through rainy road surface (simulation time 10s-20s, 35s-45s) and snowy road surface (simulation time 54s-65s). In this way, we model variation of the parameters via a more realistic approach, testing the performances of our Dugoff-based maximum friction estimation.

III. Vehicle Dynamics and Control

A. Vehicle model

To test our estimation method along with the control applied on it, we have chosen a simple vehicle model as shown in [7]. Even though it is a simple model, it will allow us to test the efficiency and robustness of our approach. The equations of the dynamics of the vehicle and of the wheel can be written as follows:

$$m\dot{V}_x = F_x - F_{aero}, \tag{5}$$

$$I\dot{\omega} = T - rF_x - R_x, \tag{6}$$

$$F_x = \mu_x F_z, \tag{7}$$

$$\lambda = \frac{r\omega - V_x}{\max(V_x, r\omega)}, \tag{8}$$

where: m is the quarter vehicle mass (kg), V_x is the chassis speed (m/s), $F_z = mg$ is the normal force on the tire (N), $F_{aero} = (\rho C_a A V_x^2)/2$ is the aerodynamic drag force (N), $R_x = mgC_r$ is the rolling resistance force (N), F_x is the longitudinal force (N), T is the driving/braking torque (Nm), λ is the longitudinal slip ratio, ω is the wheel velocity (rad/s) and r is the effective tire radius (m).

In the model we have considered a Pacejka modeling of the friction, as presented in section 2, which will give an approach closer to a realistic tire-road friction environment. Driver's actions (acceleration or braking) can be translated in different torque inputs, depending of the driver requirements. The driver model is described in [6].

Once the driver torque is computed, it will have to be limited as function of the maximum available friction, in order to avoid wheel slip in acceleration or wheel skid in braking maneuver.

B. Maximum friction estimation using Dugoff tire-model [6]

Dugoff tire model [3] has an interesting feature, assuming a uniform vertical pressure distribution on the tire contact patch. This is a simplification compared to the more realistic parabolic pressure assumed in Pacejka model (figure 6). However, the longitudinal forces are directly related to the maximum friction coefficient in more simple equations than in Pacejka model, hence the interest to estimate Dugoff parameters in order to obtain a maximum friction coefficient estimation.

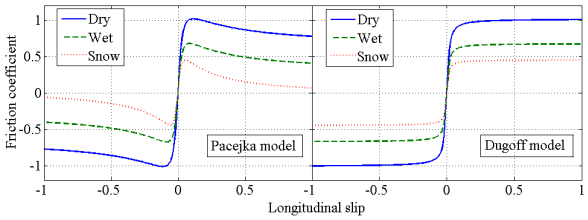

Fig. 6: Friction coefficients compared on Pacejka and Dugoff curves.

In Dugoff's tire-model, longitudinal efforts are modeled as follows:

$$F_x^D = f(\tau) K_x \lambda. \tag{9}$$

where $f(\tau)$ is a piecewise function:

$$f(\tau) = \begin{cases} (2-\tau)\tau, & \tau < 1 \\ 1, & \tau \geqslant 1 \end{cases}, \quad \tau = \frac{\mu_{x_{max}} F_z}{2|K_x \lambda|} \tag{10}$$

It is not difficult to see that $\mu_{x_{max}}$ can be expressed in terms of four a priori known variables F_x, F_z, λ, K_x.

The $\mu - \lambda$ characteristics have two specific regions. The first one is linear corresponding to a single value $\tau = 1$. The second is nonlinear defined for all values of τ inferior to 1. In the linear region, the longitudinal efforts are calculated as $F_x^D = K_x\lambda$. Therefore, the values for K_x can be derived in the linear region of the friction curves ($f(\tau) = 1$), as shown in [6].

Next, let us take the non linear region case of the $f(\tau)$ function, i.e. $f(\tau) = (2 - \tau)\tau$. Then, the longitudinal efforts can be expressed as follows:

$$F_x^D = \left(2 - \frac{\mu_{x_{max}} F_z}{2|K_x\lambda|}\right) \frac{\mu_{x_{max}} F_z}{2|K_x\lambda|} K_x\lambda. \tag{11}$$

This expression can be rewritten as a second algebraic equation of the maximum friction coefficient:

$$\mu_{x_{max}}^2 F_z^2 - 4\mu_{x_{max}}|K_x\lambda|F_z + 4|K_x\lambda|F_x^D = 0, \tag{12}$$

whose two solutions are:

$$\mu_{x_{max}} = \frac{2(|K_x\lambda| \pm \sqrt{K_x\lambda(K_x\lambda - F_x^D)})}{F_z}. \tag{13}$$

As observed in "off-line" calculations, Dugoff tire model saturates at a different peak value than Pacejka tire model. It is in fact a weighting factor (called α) between Dugoff and Pacejka models that drives Dugoff model to cross through Pacejka model exactly in the peak of the curve (figure 7). Its values can be calculated only close to the peak of the $\mu - \lambda$ curve. The two key parameters, K_x and α are used in the computation of the maximum friction coefficient and their estimation is presented in [6]. Hence, we are using a simple Dugoff tire model in order to achieve an on-line estimation of a more complex Pacejka tire model which is closer to a realistic friction environment.

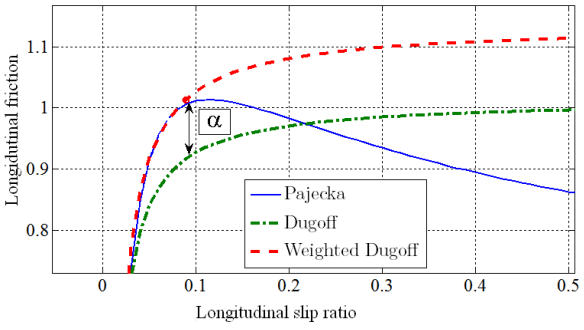

Fig. 7: Weighting parameter α at the peak of longitudinal efforts built with Pacejka and Dugoff models.

C. Torque saturation control

A high value of the torque computed from driver's actions will induce wheel slip in acceleration or wheel skid in braking maneuver. Therefore, its value has to be limited with a computed torque that takes into account the state of the road and its maximum available friction. The proposed control method will saturate the demanded torque, coming from driver's requirements, with a maximum torque value, which is computed starting from wheel dynamics Eq.(6) of the overall model. Replacing F_x by Eq.(7), and extracting the torque T will yield:

$$T = I\dot{\omega} + r\mu_x F_z + R_x. \tag{14}$$

Therefore, the saturation torque will be given by:

$$T_{sat} = I\dot{\omega} + r\mu_{x_{max}} F_z + R_x. \tag{15}$$

The maximum friction coefficient $\mu_{x_{max}}$ will be calculated following the estimation strategy presented in subsection B.

IV. Simulation Results

A. Noise-free environment

Along with the state of the road profile input shown in figure 5, the following speed profile was used in simulation. In figure 8 we find hard acceleration and braking phases, simulated to push the estimation and control strategies at their limits and to test the robustness of the proposed method.

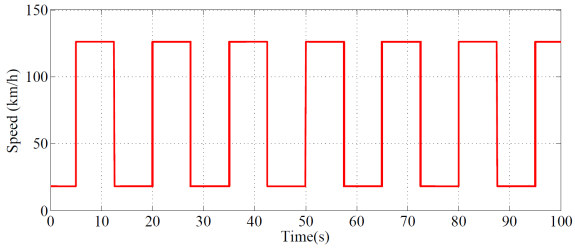

Fig. 8: Speed profile used in the simulations

Having set up the estimation of the maximum friction estimation as described in section 2.B, along with the control strategy presented in section 2.C, will yield the following result in terms of maximum friction tracking.

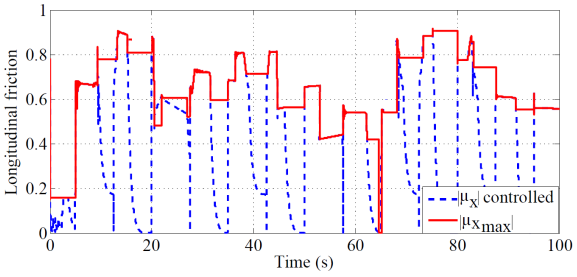

Fig. 9: Maximum friction tracking

In figure 9 can be seen that even though the maximum friction changes in time, the estimation method provides a reliable value for $\mu_{x_{max}}$. The $\mu_{x_{controlled}}$ line in figure 9 shows that the instantaneous friction never exceeds the maximum estimated value, therefore accomplishing the purpose of the

control. An interesting fact happens at simulation time t=53s. Here the maximum friction drops from approximately 0.7 to 0.4 during the acceleration phase. In other words we go from a rainy road to a snowy road. Nevertheless, the control tracks this variation of the maximum available friction, giving a stable wheel behavior, as shown in figure 10.b. Given the variation of parameter X_r which will also induce the variation of parameters C and D of Pacejka formula, the slope of the linear segment of the friction curves is continuously changing. In our strategy, the slope of the linear segment is defined by parameter K_x. We have computed its off-line values for the state of the road profile shown in figure 5 to have a reference value to compare with its estimated value. Its evolution is shown in figure 11 and one can see that even if the slope varies continuously, the estimation follows the modeled value. Also, one has to take into account that K_x updates only when the values of the longitudinal slip are in the linear zone of the friction characteristics.

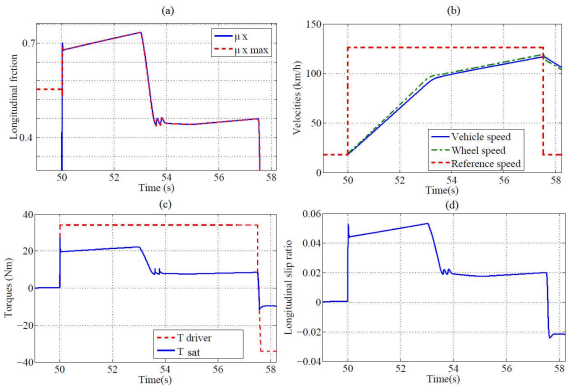

Fig. 10: Maximum friction variation tracking

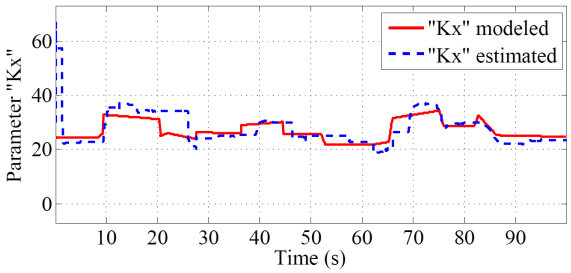

Fig. 11: Reference and estimated value for K_x

The adaptation parameter α will also be variable, depending on the state of the road. As in the case of K_x, off-line values for α were computed, for the same state of the road input X_r. Its evolution is shown in figure 12. The range of variation of α is reduced compared to the one of K_x. The estimation of parameter α will compensate the errors that arise in the estimation of K_x, therefore its estimated values differ from the the modeled values, yet they follow the modeled profile. The large variation of Pacejka parameters brings a modeling

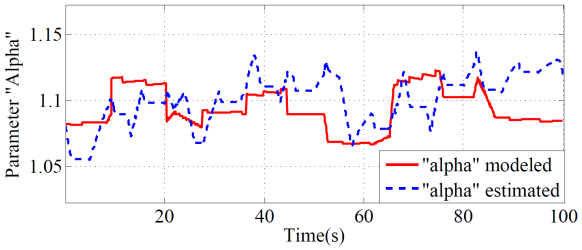

Fig. 12: Reference and estimated value for α

closer to real situations, giving estimations that no longer stay only one curve, but on multiple curves, as shown in figure 13.

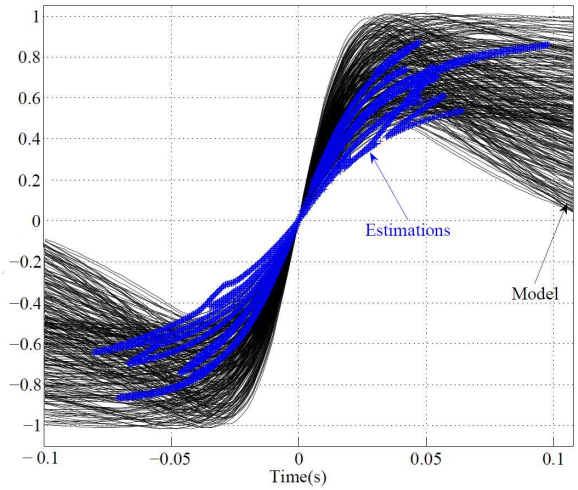

Fig. 13: Friction estimation on time-varying road conditions

Even if the estimation points seem to be more dispersed than in a conventional modeling, it can be seen in figure 13 that $\mu(\lambda)$ never exceeds the peak of the curves, showing good performance of the control scheme. The conditions vary from rainy roads with $\mu_{x_{max}} = 0.9$ to snowy roads with $\mu_{x_{max}} = 0.3$. So, a large range of tire-road friction is ran through, testing the estimation and control methods and their limits, yielding good results in terms of friction tracking and vehicle behavior.

B. Noise perturbation

In real systems, noise can affect the performances of the estimation strategy propagating to the control that is applied at the wheel. In the following we take into account a random noise coming from wheel acceleration that affects the estimation of $\mu_{x_{max}}$.

Adding noise will increase the complexity of the problem, since it can propagate at the final control applied at the wheels. As seen in figure 15, the noise coming from the maximum friction estimation is propagated on the computation of the control. But, having taken into account the filtering provided by the electric motors, with their small delays, the final

torque applied at the wheels is less affected by the noise (see figure 15). Hence, even in noisy environment with continuous

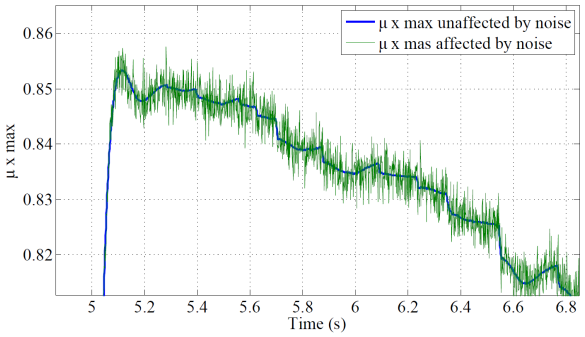

Fig. 14: Noise affecting the estimation of $\mu_{x_{max}}$

variation of Pacejka parameters, the control performs good tracking of the maximum friction, as seen in figure 16.

As expected, the estimation of $\mu_{x_{max}}$ gives a larger dispersion of points in noisy environment (figure 17), coming closer to the view seen in real experimental results (see figure 1). This shows that our approach into modeling the road surface conditions comes closer to what is found in real environments. It can be seen in figure 17 that even when the noise affects $\mu_{x_{max}}$, the parameter α compensates possible estimation errors, therefore, the peak of the curves is never exceeded, showing the robustness of our method.

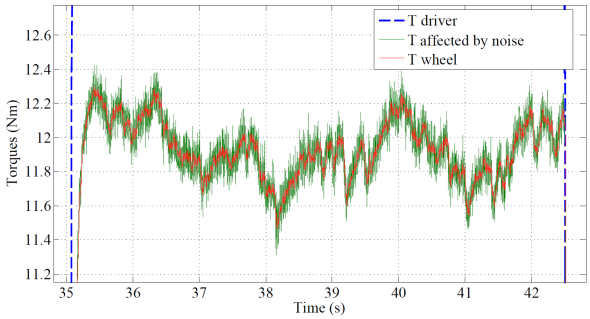

Fig. 15: Noise affecting the computation of T_{sat}

A closer look on the points shows the behavior of the estimation and control strategy. In figure 18 can be observed that the transition from one type of road surface to another is made in a continuous manner, as it arrives in actual tire-road environments.

The overall estimation process, gives the expected results, detecting the variation of road conditions even when the estimation process is affected by noise. Some of the noise is attenuated by the electric motor [10] and the adaptation parameter α, achieving the tracking of the maximum available friction in varying surface conditions.

V. Concluding Remarks

In this paper, a new approach regarding the modeling of road surface conditions has been presented. It considers a

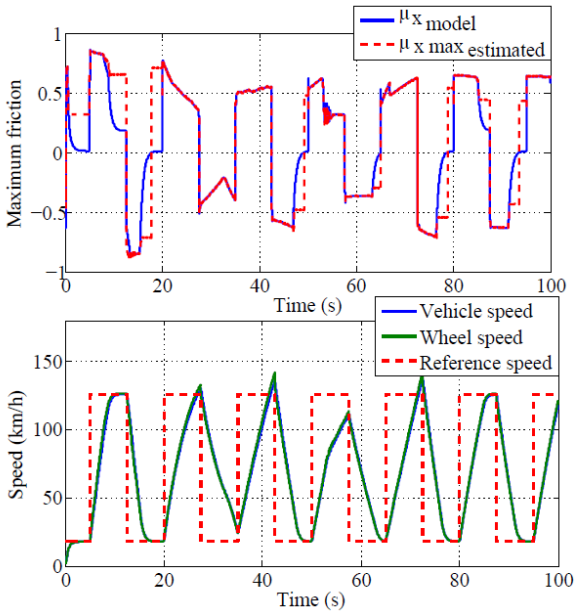

Fig. 16: Speed and maximum friction tracking

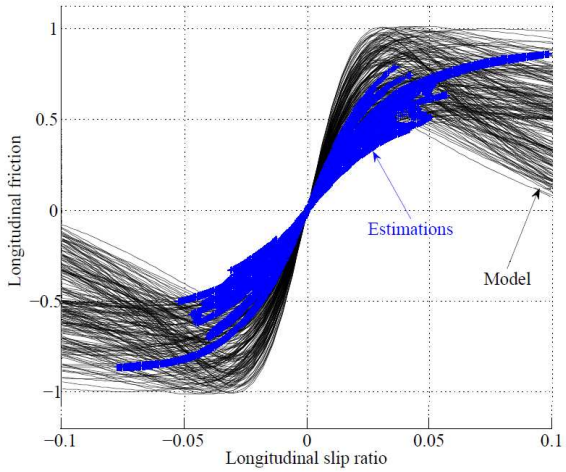

Fig. 17: Maximum friction estimation in noisy environment

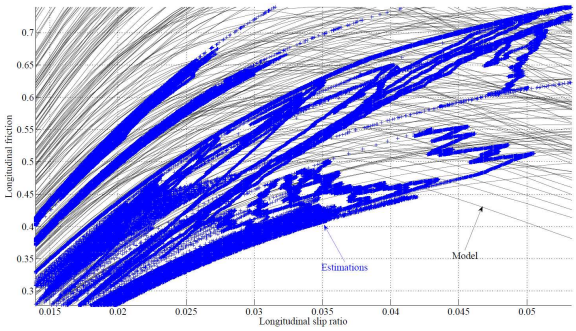

Fig. 18: Maximum friction estimation in noisy environment

continuous variation of the friction curves, as it arrives in true environments. A "dynamic" behavior of Pacejka parameters is considered in order to model a state of the road variable, X_r. On this new approach of tire-road model, a maximum friction estimation method based on Dugoff model has been tested in noise-free and noisy conditions, giving promising results in terms of adaptation to operating conditions. Even though the estimation process is computed on a time-varying road conditions, and in addition affected by noise, it provides maximum friction values that do not exceed the peak of the friction curves. The results show that the estimation and control strategies perform well in complex circumstances, providing robustness to the proposed method. All the accomplishments were "facilitated" by the use of the electric motor and its consideration as an unique actuator. The electric motor provided the knowledge of the instantaneous torque transmitted at the wheels. In a conventional ICE vehicle, the complexity of the approach increases, since an on-line torque estimator has to be set up and the response times of the actuators in ICE vehicle configuration are greater than in an EV configuration.

ACKNOWLEDGMENT

The work of the first author (Marcel Stefan Geamanu) is financially supported by the CNRS-IFPEN grant 186-654 (2010-2013).

REFERENCES

[1] L. Alvarez, X. Claeys, R. Horowitz and J. Yi, "Emergency braking control with an observer-based dynamic tire/road friction model and wheel angular velocity measurement," *Vehicle System Dynamics*, 39(2): 81-97, 2003

[2] M. Denny, "The dynamics of anti-lock brake systems," *European Journal of Physics*, 26:1007-1016, 2005.

[3] H. Dugoff, P.S. Fancher, L. Segel " Tire performance characteristics affecting vehicle response to steering and braking control inputs," Technical report, *Highway Safety Research Institute*, Ann Arbor, MI, 1969.

[4] D.A. Eichfeld and H. Klein, "Anti-lock braking system and vehicle speed estimation using fuzzy logic," *Proceedings of the 1st Embedded Computing Conference, Paris*, 1996.

[5] R. Freeman, "Robust Slip Control for a Single Wheel," *University of California*, Santa Barbara, 1995.

[6] M.S. Geamanu, A. Cela, G. LeSolliec, H. Mounier, and S.I Niculescu: *Maximum friction estimation and longitudinal control for a full in-wheel electric motor vehicle*. Proceedings of 12th International Conference on Control, Automation and Systems, Korea, 2012.

[7] M.S. Geamanu, A. Cela, G. LeSolliec, H. Mounier, and S.I Niculescu: *Road condition estimation and longitudinal control for electric vehicles*. Proceedings of 11th International Conference on Control, Automation and Systems, Korea, 2011.

[8] M. Gerard, W. Pasillas-Lepine., E. de Vries, M. Verhaegen, "Improvements to a five-phase ABS algorithm for experimental validation", *Vehicle System Dynamics*, 2010.

[9] R. Horowitz, L. Olmos and L. Alvarez, "Adaptive emergency braking control with observer-based dynamic tire-road friction model and underestimation of friction coefficient," *Proceedings of the 15th IFAC World Congress. Barcelona, Spain*, 2002.

[10] A. Hughes, "*Electric motors and drives: fundamentals, types, and applications*", *Elsevier* 2006.

[11] R.N. Jazar, "*Vehicle dynamics: theory and applications*", *Springer* 2008.

[12] G. F. Mauer, "A Fuzzy Logic Controller for an ABS Braking System," *IEEE Transactions on Fuzzy Systems*, Vol. 3, No. 4, 1995, pp. 381-388.

[13] W. Pasillas-Lepine, "Hybrid modeling and limit cycle analysis for a class of five-phase anti-lock brake algorithms," *Vehicle System Dynamics*, 44(2):173-188, 2006.

[14] W.R. Pasterkamp, H.B. Pacejka, "On line estimation of tire characteristics for vehicle control", *JSAE Review*, vol 16, p.221 - 226, 1995.

[15] L. R. Raya, D. C. Brandea, J. H. Leverb, "Estimation of net traction for differential-steered wheeled robots," *Thayer School of Engineering, Dartmouth College, 8000 Cummings Hall, Hanover, NH 03755 and US Army Cold Regions Research and Engineering Laboratory, United States*.

Regenerative braking optimization and wheel slip control for a vehicle with in-wheel motors

- **Authors**: G. Le Solliec, A. Chasse, M.S. Geamanu.
- **Conference**: 7th Symposium on Advances in Automotive Control (AAC).
- **Venue**: Tokyo, Japan.
- **Year**: 2013.

Regenerative braking optimization and wheel slip control for a vehicle with in-wheel motors

G. Le Solliec*, A. Chasse, M. Geamanu *****

*IFP Energies Nouvelles, Rueil-Malmaison, France (e-mail:guenael.le-solliec@ifpen.fr).
**IFP Energies Nouvelles, Rueil-Malmaison, France (e-mail:alexandre.chasse@ifpen.fr).
*** Laboratoire des Signaux et Systèmes, CNRS-Supelec, France (e-mail: marcel-stefan.geamanu@lss.supelec.fr).

Abstract: To meet the growing need for mobility of people and goods while massively reducing CO_2 emissions, the electrification of vehicle becomes essential. One solution is the use of in-wheel motors on the rear wheels of a conventional vehicle with a thermal powertrain on front axle. It provides new opportunities to control the torque to the wheel with a fast response time. One knows that electric motors on hybrid vehicles enable energy recovery during braking, but it has to be well coordinated with overall system and especially hydraulic brake system in order to achieve safety behavior and vehicle grip in overall conditions. Furthermore, the knowledge of motor torque able to prospect new solutions to estimate and control the longitudinal friction between the road and the tires and operate efficient slip control while optimizing regenerative braking. It could then be used as the main actuator for traction control and ABS systems in both acceleration and deceleration.

1. INTRODUCTION

In the context of a massive reduction in CO_2 emissions related to the mobility of persons and goods, vehicle electrification is one of the most effective solutions. This breakthrough technology can be deployed in different ways, from a micro hybrid to full electric vehicles. This variation of architectures is justified by a proper adaptation of vehicles to different societal uses as well as infrastructure. One solution is the use of in-wheel motors on the rear wheels of a conventional vehicle with a thermal powertrain on front axle. This dedicated dual mode architecture combines the advantages of an electric vehicle in urban conditions (zero emission and no noise), with a significant preservation of the range autonomy. Many technological issues related to the use of in-wheel motors had to be addressed, such as their integration and impact on vehicle dynamics.

Control and supervision of both powertrains had to be developed taking into account performances (energy management, dynamic) and safety operation. We will here focus on one valuable feature of the use of in-wheel motors: the new prospects of regenerative braking optimization and wheel slip control due to the proximity of the electrical motors to the wheel. Electric motors on hybrid vehicles enable energy recovery during braking, but it has to be well coordinated with overall system and especially hydraulic brake system. The vehicle supervisor has then to integrate all the constraints to optimize the use of all the actuators.

Traction control and ABS systems are main components in providing safety behaviour and achieving desired vehicle grip in overall conditions. In conventional vehicles, two main actuators accomplish those functions, the combustion engine and the hydraulic brake system. It means different solutions of control adapted to actuators dynamics *(Denny, Savaresi et al.)*. Using in-wheel motors provides new opportunities to control the torque to the wheel with a fast response time *(Hori et al.)*. The knowledge of motor torque, by measuring its output current, able to prospect new solutions to estimate the longitudinal friction between the road and the tires and operate efficient slip control while optimizing regenerative braking. It could then be used as the main actuator to ensure safety vehicle motion in both acceleration and deceleration.

2. VEHICLE DYNAMICS MODEL

The vehicle model consists of the main vehicle mass to which the four wheels are attached via a suspension system. Only the longitudinal and pitch dynamics are represented which is sufficient to validate supervision strategies and the optimal use of in-wheel motors for regenerative braking and traction control as discussed in the next sections. Therefore, this model can easily be represented as a bicycle model (Fig. 1).

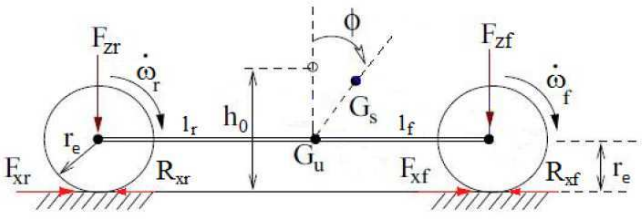

Fig. 1. Vehicle dynamics model

The pitch angle (Φ) is computed considering position of both centers of gravity of the suspended and unsuspended mass (G_u and G_s), suspension dynamics and load transfer that arises when the vehicle is accelerating or braking. Simplified system equations for longitudinal dynamics can be written as follow for each wheel i :

$$
\begin{aligned}
&I_w\dot{\omega}_i = T_{wi} - r_e F_{xi} - c_r F_{zi} \\
&F_{zi} = mg/4 - k(l_k\phi - h_0) - cl_k\dot{\phi} \\
&F_{xi} = \mu_{xi} F_{zi}
\end{aligned}
\qquad (1)
$$

where I_w is wheel inertia, ω_i its angular speed, T_{wi} the torque applied (coming from motor, engine, and/or brake), r_e the wheel radius, F_{xi} and F_{zi} the longitudinal and normal forces on the wheel i, $l_{k(f\ or\ r)}$ and h_0 defining the position of center of gravity position and c_r the rolling resistance parameter.

The equation for longitudinal vehicle dynamic is :

$$
\begin{aligned}
&m\dot{V}_x = F_x - F_{aero} \\
&F_x = \Sigma F_{xi} \\
&F_z = mg
\end{aligned}
\qquad (2)
$$

where m is the vehicle mass, V_x the vehicle speed, F_x and F_z the longitudinal and normal total force on vehicle, and F_{aero} the aerodynamic drag force.

The longitudinal tire friction coefficient between the road and the tire (μ_x) is function of the road conditions and the longitudinal slip (λ) of the wheel defines as follow :

$$
\lambda = \frac{V_x - r_e\omega}{max(V_x, r_e\omega)} \qquad (3)
$$

A Pacejka formula *(Pacejka et al.)* is classically used to model this friction coefficient (Fig. 2). It should be noted that limits of grip are known as maximum and minimum of this curve respectively in acceleration and deceleration, and those limits are varying with road conditions.

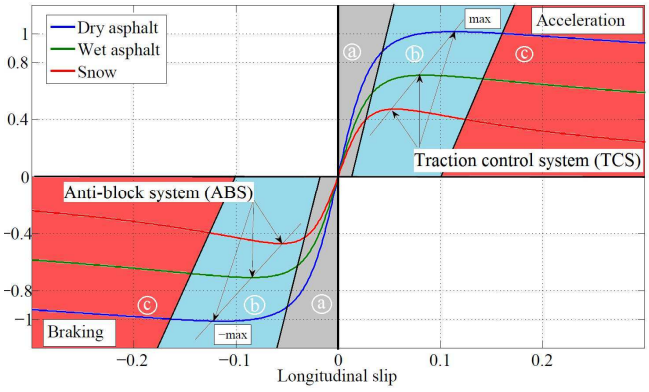

Fig. 2. Pacejka models for longitudinal friction coefficient

3. TORQUE DISTRIBUTION DURING BRAKING

The stability of the trajectory of a vehicle is strongly related to the behaviour of the rear axle when accelerating or braking. In addition, the objective of an electric device which participates in the reduction of CO_2 emissions is to optimize energy recovery from the rear wheels during deceleration. Therefore, maintaining vehicle stability will not only affect the in-wheel motor but the entire system : the motor and the hydraulic brake, which will require an upstream supervision.

During braking, the total wheels torque is decomposed as follows, where $T_{wheel\ sp}$ is the total driver torque request, $T_{mi\ sp}$ is the torque setpoint for the motor i (on rear wheels), $T_{brake\ f}$ and $T_{brake\ r}$ are the hydraulic braking torques on each axles :

$$
T_{wheel\ sp} = \sum T_{mi\ sp} + T_{brake\ \ f} + T_{brake\ \ r} \qquad (4)
$$

The engine torque has been neglected since during braking phases the engine should be declutched to maximize energy recovery. We first compute the torque splitting between both axles and in a second one, depending on the communication with the ABS system control, we distribute the rear axle torque to the electric motors and the hydraulic brakes.

3.1 Axles torque splitting

From the total braking torque requested to the wheel, the static weight distribution of the car and the dynamic mass transfer in deceleration, we can compute the normal forces applied on the front and the rear axles *(Jazar)* :

$$
\begin{aligned}
F_{zf} &= \frac{m\cdot g\cdot l_r}{2l} - \frac{h_0\cdot T_{wheel\ sp}}{2l\cdot r_e} \\
F_{zr} &= \frac{m\cdot g\cdot l_f}{2l} + \frac{h_0\cdot T_{wheel\ sp}}{2l\cdot r_e}
\end{aligned}
\qquad (5)
$$

To maintain the vehicle stability, the friction on the rear wheels must be kept higher than on the front wheels. But, on our specific case, we have interest to apply a maximum braking torque on the rear axle to maximize the energy recovery. We will then try to maintain the same friction on the rear and the front axle :

$$
-\mu_{\max} < \left(\frac{F_x}{F_z}\right)_{front} = \left(\frac{F_x}{F_z}\right)_{rear} < 0 \qquad (6)
$$

Neglecting rolling resistance force, the requested axle torque considering iso-friction and steady-state conditions are :

$$
\begin{aligned}
T_{f\ sp} &= T_{wheel\ sp}\frac{F_{zf}}{mg} \\
T_{r\ sp} &= T_{wheel\ sp}\frac{F_{zr}}{mg}
\end{aligned}
\qquad (7)
$$

Then, from previous equations and the value of the maximum braking torque on the front axle, we compute a static map providing the axle torques splitting function of the maximum friction coefficient μ_{max} and the requested total wheel torque.

Figure 3 shows the axle torque distribution for different values of this requested total wheel torque during braking. The maximum friction coefficient used in this case is 0.8. One can notice that the minimum total wheel torque fitted to this application is then near to -3000 Nm. Indeed, the two hydraulic brakes on the front axle have reached their maximum values (-1000 Nm) and the rear brake torque is saturated to keep the same friction according to (6). In this condition the minimum value of the tire friction isn't reached, the front brakes are saturated before.

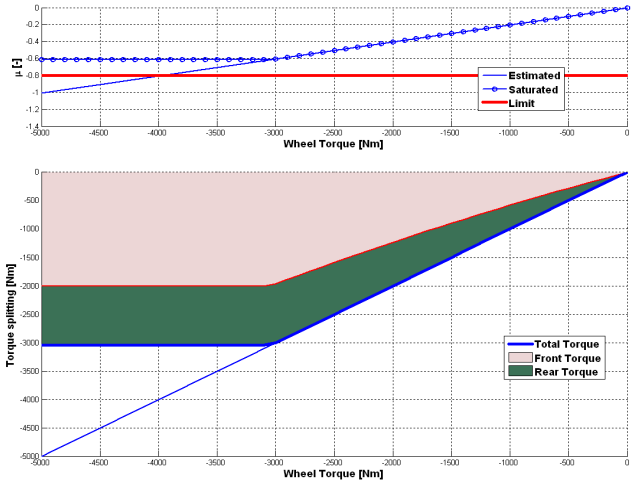

Fig. 3. Axle torque distribution for braking

3.2 Rear torque distribution between the wheel motors and the hydraulic brakes

Once computed the requested rear torque, we have the possibility to fulfil it with two actuators : the hydraulic brakes and the in-wheel motors. The solution depends on the possibility to decouple the position of the brake pedal to the hydraulic brakes pressure. The simplest one without any modifications on the ABS system is to apply a constant negative torque to the wheel motors during a deceleration. This braking torque should represent the engine braking torque witch is declutched. Figure 4 shows a deceleration obtained with this strategy. The wheel motors apply a constant torque which is widely lower than its maximum. A lot of energy is dispersed as heat by the rear hydraulic brakes (in gray) and could be recovered by the in-wheel motors. On the other hand, the tire frictions are well maintained equal on the rear and front axle.

An interesting use of the wheel motors is to recovery the maximum electric energy during braking phases while control the friction on the rear axle. Figure 5 shows the same braking phase but with a maximum use of the electric motors to fulfil the requested rear torque. We can see on this specific braking, that the wheel motors quite realize the rear torque request. The rear brakes are then only slightly used at the beginning of the braking since the rear torque setpoint is lower than the maximum wheel motor torque.

3.3 Behaviour in low friction conditions

As seen previously, the axles torque splitting strategy can use an estimation of friction limit during braking to limit the torque on each axle according to (6). Figure 6 shows results of this strategy in low friction conditions. This ensures vehicle stability by meeting the two constraints : keeping the same friction coefficient on both axles while remaining bellow the road limit. Furthermore, one can notice that the rear torque distribution strategy able to optimize energy recovery using only the in-wheel motors.

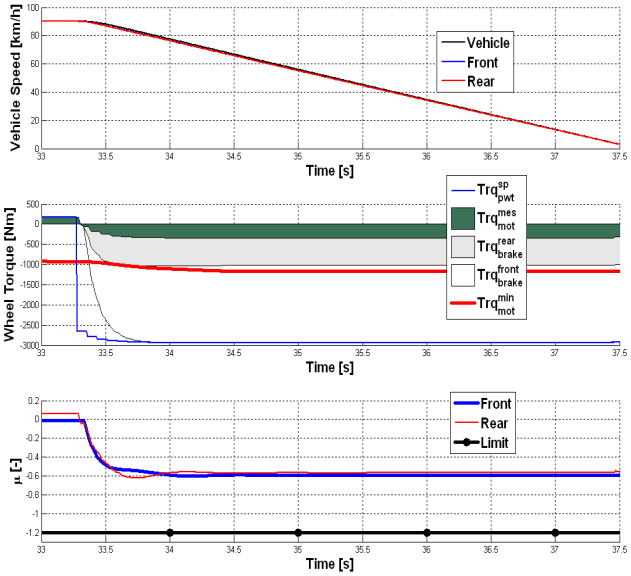

Fig. 4. Torque distribution during braking on a dry road with a constant wheel motor torque

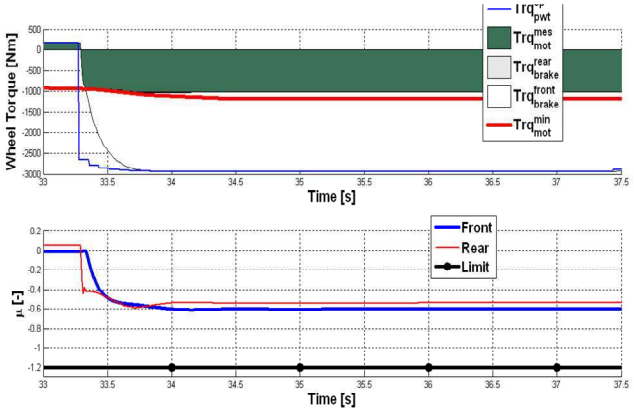

Fig. 5. Torque distribution during braking on a dry road with full control of the braking system

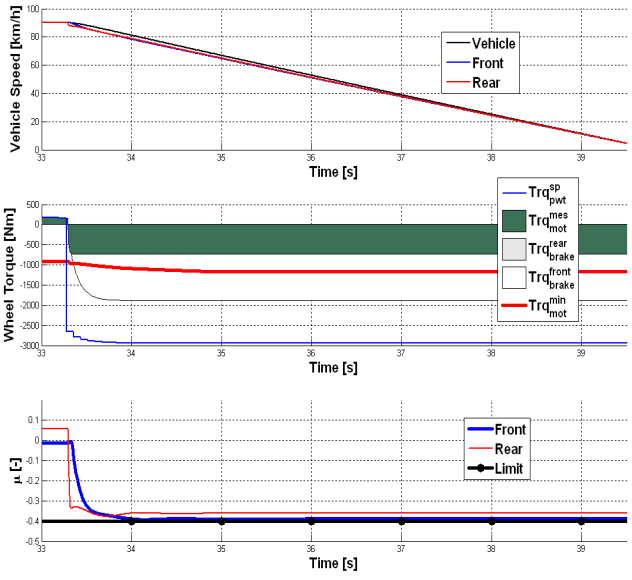

Fig. 6. Torque distribution during braking on a wet road with full control of the braking system

4. FRICTION ESTIMATION

With a classical architecture, the estimation of the friction force is complex because of immeasurable parameters, as the torque applied to the wheel, and need complex observers *(Ono et al., Alvarez et al.).* The torque output of the motor can be easily calculated from its current. This merit makes it easier to estimate the driving and braking force between the tire and the road surface, and then the maximum friction coefficient according to varying road conditions.

4.1. Longitudinal friction estimation

As seen in equation (5), the normal forces applied to the wheels may be pretty well approached by considering pitch rate and static weight distribution *(Jazar).* With in-wheel motors, the torque and the wheel velocities are measured. The longitudinal friction force for a wheel can then be directly estimated from the motion equation (1) :

$$F_{xi} = \frac{1}{r_e}\left(T_i - I\dot{\omega}_i - c_r F_{zi}\right) \qquad (9)$$

The instantaneous friction coefficient μ_x can then be directly estimated for each wheel according to equation (1).

4.2. Maximum friction estimation

As seen in section 2, the limit of friction to prevent wheel slip during driving or braking is the maximum of the curve $\mu_x - \lambda$ depending on road surface conditions. To optimize slip control strategies, it is helpful to get a relevant estimation of this limit. As Pacejka model is highly complex and nonlinear, a simpler Dugoff tire model *(Dugoff et al.)* will be used. It has the advantage to represent longitudinal friction coefficient related to its maximum and Dugoff model is very close to the Pacejka model up to the peak of the curves (Figure 7). It depends only of two parameters, K_x the longitudinal stiffness coefficient, and α a weight factor :

$$\mu_x = f(\varphi) K_x \lambda$$
$$f(\varphi) = \begin{cases} (2-\varphi)\varphi & \varphi < 1 \\ 1 & \varphi \geq 1 \end{cases} \quad \varphi = \alpha \frac{\mu_{x\,max}}{2|K_x \lambda|} \qquad (10)$$

Considering the nonlinear zone case, μ_{xmax} can be expressed as the solution of a second order equation, the sign in expression depending of the sign of longitudinal slip λ :

$$\mu_{x\max} = \frac{2}{\alpha}\left(K_x\lambda \pm \sqrt{K_x\lambda\left(K_x\lambda - \mu_x\right)}\right) \qquad (11)$$

The parameter Kx is estimated on-line from instantaneous estimation of friction coefficient and longitudinal slip when longitudinal friction is in its linear part of the curve :

$$K_x = \frac{\mu_x}{\lambda} \qquad (12)$$

To estimate the parameter α, an approach is to use the extended braking stiffness XBS, defined as the derivative of the friction coefficient *(Fliess et al., Geamanu et al.)*. It needs to be close to this limit to adapt accurately. We applied a least-squares method minimizing error between Dugoff model and instantaneous estimation of friction coefficient when XBS is under a threshold (e.g. friction coefficient closed to its maximum). It's behave as an integral controller during nonlinear parts of the curve minimizing estimation error with α parameter.

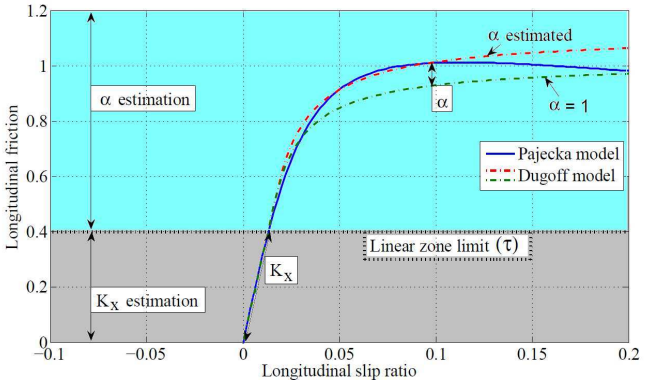

Fig. 7. Pajecka and Dugoff models comparaison

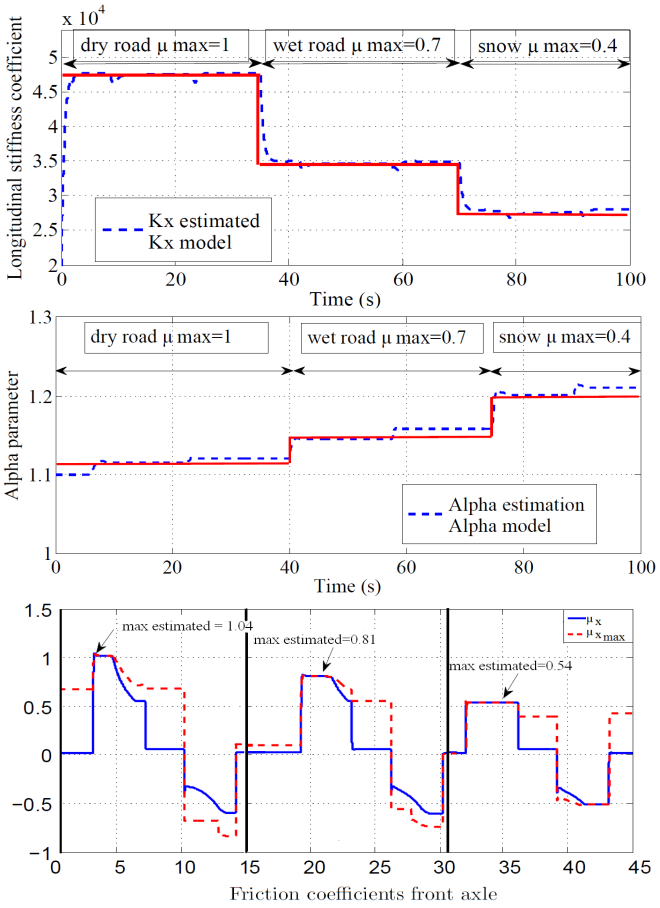

Fig. 8. On-line estimation of parameters K_x and α *in varying road conditions.*

The figure 8 presents results for Dugoff model parameters estimation during three successive acceleration and braking phases with different road conditions (dry, wet, snow). On a wide range of road conditions the α parameter range is low,

from 1.1 to 1.2, while the K_x parameter range is large, from 2.5e4 to 5e4. This is the most important parameter for a relevant maximum friction estimation and its estimation is done during normal driving conditions far from the grip limit.

One must notice different values for α parameter during acceleration and braking phases. This is mainly due to simplification of mass transfer (5) resulting in error in F_z and μ_x estimation. But it demonstrates the interest in on-line adaptation of α parameter in order to compensate model simplification and/or friction estimation error.

Those results show an accurate maximum value on the limit as far as parameters are well adapted and invoke a good robustness to road variations and the dynamic behaviour is considered to be on the safe side in an emergency situation.

4. WHEEL SLIP CONTROL

With a classical ABS system, because of highly nonlinear behaviour of friction curves and the latency of the hydraulic actuators, the existing control strategies are often based on sliding-mode control, as it guarantees the robustness of the system against changing working conditions *(Chin et al., Kayacan et al.)* and rely directly on the longitudinal slip with often a conservative fixed threshold.

Taking advantage of their fast response time and the knowledge of their output torque, the electric motors allow applying a control on the friction coefficient μ_x instead of slip λ, while considering varying road conditions. Considering the maximum friction μ_{xmax} estimation and its on-line adaptation algorithm, the proposed control law will only saturate the requested wheel torque coming from driver with a maximum torque estimated from wheel dynamic equation (2) :

$$T_{\max_i} = I_{wi}\dot{\omega}_i + F_{zi}\left(r_e\mu_{x\max} + c_r\right) \qquad (13)$$

One must notice that μ_{xmax} estimation assumed here closed-loop for wheel slip control with α parameter adaptation. Indeed minimizing Dugoff model on direct estimation with least-squares method able to keep on limit when torque request is too high. Adding a proportional controller on α parameter enables to tune fast dynamic correction in transient independently of adaptation algorithm.

5. RESULTS

Next section presents results of friction estimation, wheel slip control and torque supervision in two characteristic cases : varying low friction conditions and emergency braking.

5.1 Low friction conditions

In electric driving mode and in both driving and braking case, the wheel slip controller aims to limit in-wheel motors torque to assume both TCS (traction control) and ABS functions, while taking in account changing road conditions. To validate the behaviour of friction estimation and control, successive acceleration and braking have been simulated while changing road adherence conditions (Figure 9).

The maximum friction coefficient μ_{xmax} is switched from 0.6 to 0.4 and vice versa at 16, 26 and 30s. One can first notice the relevant dynamic estimation of maximum friction coefficient from Dugoff model (10) in transient and during slip control in both acceleration and braking case. Particularly when the road condition is changing during transient (at 16 and 26s) this estimation fits in real time. Then, the control achieves to track this value when needed (if estimated friction coefficient μ_x tends to exceed this limit) by limiting the requested torque. The wheel slip is then limited to get optimal grip to the road while preventing wheel lock.

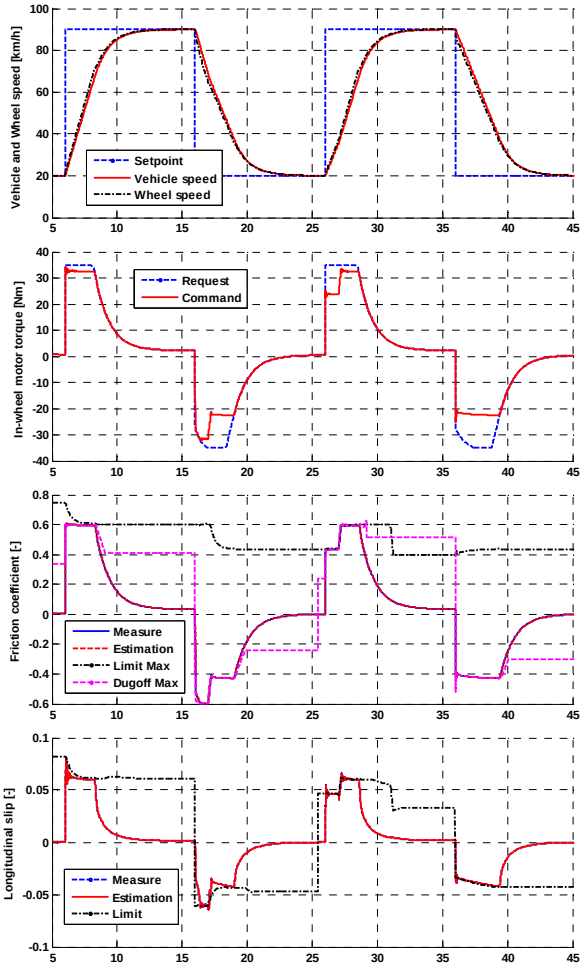

Fig. 9. Wheel slip control in both driving and braking case while changing road adherence conditions.

5.2 Emergency braking

During emergency braking, the ABS system is triggered to prevent wheels from blocking. The latency of the hydraulic actuators causes a bang-bang behaviour of the controller with an oscillation around the optimal grip. As presented before, one valuable feature of the use of in-wheel motors is to improve wheel slip control while optimizing regenerative braking. Next results show how this wheel slip controller using in-wheel motors can also prevent wheels from blocking with deactivated ABS system on the rear wheels.

An emergency braking on dry road has been simulated in three different cases (Figure 10) :

1. The supervisor computes maximum braking torque for both electric and hydraulic actuators and wheel slip controller is deactivated. In this case, the wheel blocks and the slip is not controlled anymore.

2. The supervisor computes maximum braking torque for both actuators and wheel slip saturation torque control is applied fully on the electric motor. The longitudinal slip is well controlled with a limited oscillation but the regenerative braking is not optimal anymore. In some case, in-wheel motor torque could even reach the actuator saturation.

3. The supervisor uses maximum friction coefficient estimation to compute feedback torque distribution between electric and hydraulic actuators (section 3). It reduces the hydraulic brake torque to keep in-wheel motor torque close to its maximum and optimize regenerative brake while keeping longitudinal slip control. In this case the supervisor acts as a preventive control, improving transient behaviour.

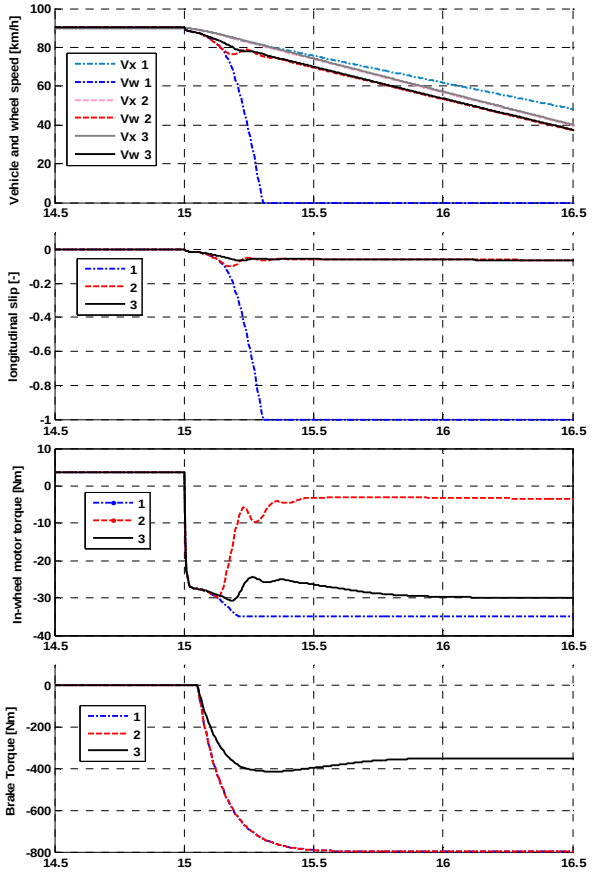

Fig. 10. Wheel slip control during an emergency braking with both electric and hydraulic actuators.

6. CONCLUSION

In this paper, control issues related to the use of in-wheel motors during braking have been addressed. The proximity of electric motors to the wheels and the knowledge of their output torque help in regenerative braking optimization and wheel slip control.

During braking, being intrusive on hydraulic brake system able the supervisor to manage torque distribution between axles to maintain vehicle stability, and between both electric and hydraulic actuators on rear axle in order to optimize the use of in-wheel motors for energy recovery while keeping wheel grip under road limit.

Finally, we show the ability to control the wheel slip with accuracy on maximal friction point whatever the road adherence condition. The proposed algorithms able to adapt electric motors torque to varying friction limit keeping braking optimal and safe without using classical hydraulic actuators for high dynamics correction.

REFERENCES

M. Denny (2005). *The Dynamics of Anti-lock Brake Systems,* European Journal of Physics, vol. 26.

S. M. Savaresi and M. Tanelli (2010). *Active Braking Control Systems Design for Vehicles.* Springer.

Y. Hori, Y. Toyoda and Y. Tsuruoka (2009). *A Novel Traction Control without Chassis Velocity for Electric Vehicles.* EVS24, International Electric Vehicle Symposium.

H. Pacejka and E. Baker (1991). *The magic formula tyre model.* 1st International Coll. Tyre Models Vehicle System Analysis.

R.N. Jazar (2008). *Vehicle dynamics: Theory and Applications.* Springer.

E. Ono, K. Asano, M. Sugai, S. Ito, M. yamamoto, M. Sawada, and Y. Yasui (2003). *Estimation of automotive tire force characteristics using wheel velocity.* Control Engineering Practice, vol. 11.

L. Alvarez, X. Claeys, R. Horowitz and J. Yi (2003). *Emergency braking control with an observer-based dynamic tire/road friction model and wheel angular velocity measurement.* Vehicle System Dynamics. vol. 39

H. Dugoff, P. S. Fancher, and L. Segel (1969). *Tire performance characteristics affecting vehicle response to steering and braking control inputs*. Technical Report, Highway Safety Research Institute, Ann Arbor, MI.

M. Fliess, H. Mounier, J. Villagra and B. d'Andrea-Novel (2011). *A diagnosis based approach for tire-road forces and maximum friction estimation.* Control Engineering Practice. vol. 19

M. Geamanu, A. Cela, G. Le Solliec, H. Mounier, S. Niculescu (2011). *Road condition estimation and longitudinal control for electric vehicles.* 11th ICCAS

Y. K. Chin,W. C. Lin, D.M. Sidlosky, and M. S. Sparschu (1992). *Sliding-mode ABS wheel slip control.* American Control Conference.

E. Kayacan, Y. Oniz and O. Kaynak (2009). *A Grey System Modelling Approach for Sliding-mode Control of Antilock Braking system*. IEEE, vol. 56

Event driven model free control of quad-rotor

- **Authors**: J. Wang, M.S. Geamanu, A. Cela, H. Mounier, S.I. Niculescu.
- **Conference**: IEEE Multiconference on Systems and Control.
- **Venue**: Hyderabad, India.
- **Year**: 2013.

Event driven model free control of quadrotor

Jing Wang, Marcel-Stefan Geamanu, Arben Cela, Hugues Mounier and Silviu-Iulian Niculescu

***Abstract*— In this paper we propose a new control approach, *event driven model free control*, which deals with the "trade-off" between computational cost and system performance. The model free control scheme demands low computational resources and has high robustness, which is especially suitable for systems with complex dynamics and/or affected by disturbances. Particularly for the embedded systems, the event driven model free control demands even fewer computational resources, since the actuation is allowed only when an event is triggered. The proposed method is implemented on a quadrotor model in different realistic scenarios with disturbances and uncertainties. Under the time and event triggered schemes, the model free control is compared with the backstepping and sliding mode controls in these scenarios.**

I. Introduction

Quadrotors are vertical take-off and landing (VTOL) aircrafts with four rotors, which have embedded microprocessors, micro-electro-mechanical (MEMS) sensors and Lithium Polymer (LiPo) batteries. Due to the simplicity in the design and maneuver, quadrotors have many applications, such as border patrol, surveillance, aerial photography, etc. The quadrotor system is nonlinear, which has twelve states highly coupled with the inputs (see eq. (14)). Its aerodynamics is complex and difficult to include all the parts in the modeling, which makes it a partially known system. In the applications, quadrotors are often affected by disturbances, such as wind, weather conditions, etc. Therefore, the quadrotor control systems bring out many challenges: control algorithm complexity reduction; energy consumption reduction; robustness to perturbations; fast response to environmental and system changes, etc.

Many control methods are proposed in literature: Castillo et al. have proposed a Lyapunov controller using a nested saturation algorithm [1]; S. Bouabdallah has implemented a backstepping control and a sliding mode control [2]; Mistler et al. have used a dynamic feedback control [3]; Mokhtari et al. have applied a mixed feedback linearization with linear GH_∞ controller. However, to the best of authors' knowledge, these methods are tested in the ideal cases without disturbances, and the comparison of the control methods have never been proposed on quadrotor in realistic scenarios.

The recently introduced model free control is proposed for the challenges in the control of quadrotor. A preliminary work can be found in [4]. It is a simple but efficient technique for the nonlinear, unknown or partially known dynamics [5]. While retaining the PID reduced computational cost, it is able to cope with general types of nonlinearities. The comparison between the model free control and traditional PID controllers is given in d'Andréa-Novel et al. [6]. Model free control has been implemented in some academic SISO systems [5], joint motion control in humanoid locomotion [7], non-minimum phase systems [8], etc.

In order to further save the computational resources and energy consumption, the event triggered scheme is proposed on the model free control. Contrarily to the time triggered control scheme, in the event based scheme the control signals are sent only upon the triggering of an event. The event driven control was firstly proposed by Årzén [9]. The comparisons of the time driven and event driven control scheme for first order stochastic and nonlinear systems are proposed in [10] and [11] respectively.

The paper is organized as follows: In section II the event driven model free is presented; In section III the scenarios without and with wind disturbance are firstly presented. The model of quadrotor is then given. The model free control, backstepping control and sliding mode control laws are presented; In section IV the simulation results of the control laws in two scenarios are presented in both time and event driven schemes. The comparisons results in other realistic scenarios are also given.

II. Event driven model free control

A finite dimensional SISO system can be described implicitly as

$$E(y, \dot{y}, \ldots, y^{(a)}, u, \dot{u}, \ldots, u^{(b)}) = 0, \tag{1}$$

where $E : \mathbf{R}^{a+1} \times \mathbf{R}^{b+1} \to \mathbf{R}$ is a sufficient smooth function of its arguments. Assume that for integer ν, $0 < \nu \leqslant \iota$, $\partial E / \partial y^{(\nu)} \not\equiv 0$. The implicit function theorem [**?**] allows to express $y^{(\nu)}$ locally

$$y^{(\nu)} = E(t, y, \dot{y}, \ldots, y^{(\nu-1)}, y^{(\nu+1)}, \ldots, y^{(\iota)}, u, \dot{u}, \ldots, u^{(\kappa)}), \tag{2}$$

with the function $E : \mathbf{R} \times \mathbf{R}^{\iota} \times \mathbf{R}^{\kappa+1} \to \mathbf{R}$. No matter the system is linear or not, we can rewrite the system (1) as following phenomenological model which is only valid in a very short time interval:

$$y^{(\nu)} = F + \alpha u, \tag{3}$$

J. Wang, M.S. Geamanu, H. Mounier and S.I. Niculescu are with the Laboratory of Signals and Systems (L2S), CNRS, Supélec, Université Paris Sud 11, Supélec, 3, rue Joliot Curie, 91192 Gif sur Yvette Cedex (e-mails: {jing.wang, marcel.geamanu, hugues.mounier, silviu.niculescu}@lss.supelec.fr).

A. Cela is with Computer Science and Telecommunication Department, UPE, ESIEE Paris, 2 Bd Blaise Pascal, 93162 Noisy Le Grand Cedex (e-mail: celaa@esiee.fr).

J. Wang is also with Institut Polytechnique des Sciences avancées (IPSA), 7-9 rue Maurice Grandcoing 94200 Ivry-sur-Seine.

M.S. Geamanu is also with Institut Francais du Petrole et Energies Nouvelles (IFPEN), 4 avenue du Bois Preau, 92500 Rueil-Malmaison.

where $\alpha \in \mathbb{R}$ is a non-physical constant parameter, which is chosen by the engineer in such a way that F and αu are of the same order of magnitude. The derivation order ν is also an engineer's choice.

Here, F stands for the neglected parts of the system. It can be determined by the knowledge of u, α and y. An estimate of F is obtained as follows:

$$\hat{F} = \hat{y}^{(\nu)} - \alpha\tilde{u}, \tag{4}$$

where $\hat{y}^{(\nu)}$ is an estimate of the ν^{th} derivative of the measure y which is assumed available, and $\tilde{u}$ is an approximate value of u. Among the existing possibilities, $\tilde{u}$ can be chosen as a past value of the control variable u.

The resulting controller is then defined as:

$$u = \frac{1}{\alpha}\left(y_r^{(\nu)} - \hat{F} + \Lambda(\mathbf{e})\right), \tag{5}$$

where y_r is a reference trajectory. The variable $\mathbf{e} = y_r - y$ is the tracking error and Λ is an appropriate function such that the closed loop error dynamics $e^{(\nu)} = \Lambda(\mathbf{e})$ is asymptotically stable.

From above, we can see that the derivation order ν is not necessarily equal to the derivation order a of y in eq. (1). The derivation order ν is often taken equal to 1 or 2.

The estimate of $y^{(v)}$ in (4) can be obtained for example through a cascade of first order filter as:

$$\mathscr{L}(\hat{\dot{y}}) = \frac{s}{1 + T_f s}\mathscr{L}(y). \tag{6}$$

Typically, $1/T_f$ ranges from 8 to 20, and $\mathscr{L}$ denotes the transformation to the operational domain.

Here, we choose the function $\Lambda(\mathbf{e})$ as PID controller. The desired behavior is obtained by implementing the so-called intelligent PID controller (for instance $\nu = 2$):

$$u = -\frac{\hat{F}}{\alpha} + \frac{\ddot{y}_r}{\alpha} + K_P e + K_I \int e + K_D \dot{e}, \tag{7}$$

where K_P, K_I, K_D are the usual tuning gains.

The basic Årzén's event based controller consists of two parts: a time triggered event detector $\mathcal{C}_t$ and an event triggered PID controller $\mathcal{C}_e$ [9]. The latter computes the control signal to be delivered to the actuators. The former $\mathcal{C}_t$ runs at a fixed sampling period h_e, and upon fulfillment of a certain event triggering law L_e, sends events to $\mathcal{C}_e$. Upon reception of the event, $\mathcal{C}_e$ computes the control signal and sends it to the actuators.

Usual event triggering laws L_e include:

(1) Error threshold law:

$$|e(t_k)| > e_{lim}, \tag{8}$$

where $e = y_r - y$ is the tracking error, t_k is the current discrete sensing time by $\mathcal{C}_e$, and e_{lim} is a fixed limit.

(2) Error difference threshold:

$$|e(t_k) - e(t_{k-1})| > e_{lim}. \tag{9}$$

(3) ISS based law:

$$e(t_k) = \sigma\frac{a}{b}|y(t_k)|, \tag{10}$$

assuming the system can be rendered ISS (Input to State Stable) through static feedback [12]. Here, σ is chosen less than one to ensure an associated Lyapounov function decreases, a and b are chosen according to the Lipschitz constants of $\mathcal{K}_\infty$ [12]).

In order to ensure the stability of the system, a maximum sampling period h_M is defined in [10]. The time interval between two events must then be smaller than h_M:

$$t_k - t_{k-1} < h_M. \tag{11}$$

Other conditions ensuring the stability of the system have also proposed, such as the forgetting factor used in event driven PID control [11].

III. The Quadrotor Model: Scenario and Control

A. Scenario

The task is the photo shooting in an outdoor garden. An autonomous quadrotor with limited energy is used. The quadrotor needs to follow a square path with length of 2m while hovering at the altitude of 10m, which is given in Figure 1. At each corner, the quadrotor will hover about 15s to take photos. The total simulation time is 150s. The reference trajectory is expressed as:

$$\sigma(t) = \begin{cases} 0 & 0\text{s} \leqslant t \leqslant t_1, \\ h_d \frac{(t-t_1)^5}{(t-t_1)^5 + (T_f - t + t_1)^5} & t_1 < t \leqslant t_2 \\ 2 & t_2 < t \leqslant t_3 \\ h_d - h_d \frac{(t-t_3)^5}{(t-t_3)^5 + (T_f - t + t_3)^5} & t_3 < t \leqslant t_4 \\ 0 & t_4 < t \leqslant 150\text{s} \end{cases}$$

$$\begin{aligned} &h_d = 2\text{m}, \quad T_f = 6\text{s}. \\ &x = \sigma(t), \quad \text{with } t_1 = 10\text{s}, t_2 = 16\text{s}, t_3 = 90\text{s}, t_4 = 96\text{s}. \\ &y = \sigma(t), \quad \text{with } t_1 = 40\text{s}, t_2 = 46\text{s}, t_3 = 120\text{s}, t_4 = 126\text{s}. \\ &z = 10\text{m}. \end{aligned} \tag{12}$$

As the shooting takes place at an outdoor garden, there may

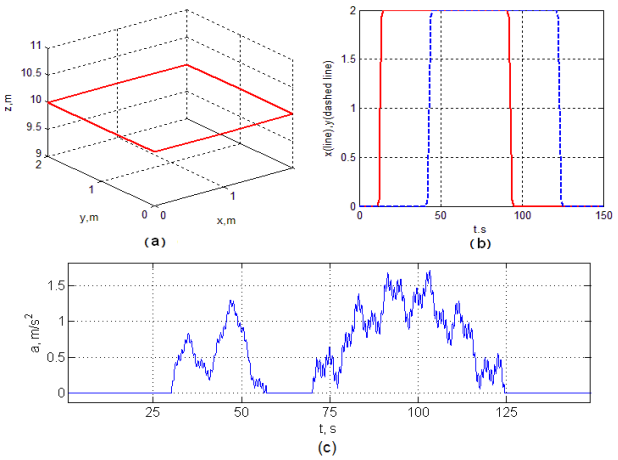

Fig. 1. (a) and (b) Reference trajectory for the quadrotor. (c) The wind disturbance w.r.t time.

be wind during the shooting. The wind is represented as the extra acceleration and affects all x, y and z axis, which is depicted in Figure 1.

$$a(t)=\begin{cases}0 & 0\leqslant t\leqslant 30,\\ 0.8\sin(\frac{\pi(t-30)}{31})+0.056\sin(\frac{24\pi(t-30)}{11}) & \\ +0.4\sin(\frac{\pi(t-30)}{7})+0.08\sin(\frac{\pi(t-30)}{2}) & 30<t\leqslant 57,\\ 0 & 57<t\leqslant 70,\\ 1.35\sin(\frac{\pi(t-70)}{55})+0.105\sin(\frac{24\pi(t-70)}{11}) & \\ +0.15\sin(\frac{\pi(t-70)}{2})+0.225\sin(\frac{\pi(t-70)}{5}) & 70<t\leqslant 124,\\ 0 & 124\leqslant t\leqslant 150.\end{cases} \tag{13}$$

B. Model

The model of the quadrotor is a six d.o.f. system with twelve states and four inputs which is depicted in eq. (14). The notations c and s represent cos and sin respectively. The rotation angles ϕ, θ and ψ are along the x, y and z axis respectively, namely roll, pitch and yaw. The parameters in the system can be found in the footnote.[1]

$$\begin{aligned}
I_{xx}\ddot{\phi} =&\dot{\theta}\dot{\psi}(I_{yy}-I_{zz})+J_r\dot{\theta}\Omega_r+l(-T_2+T_4)+(-1)^{i+1}\sum_{i=1}^{4}R_{mxi},\\
I_{yy}\ddot{\theta} =&\dot{\phi}\dot{\psi}(I_{zz}-I_{xx})-J_r\dot{\phi}\Omega_r+l(T_1-T_3)+(-1)^{i+1}\sum_{i=1}^{4}R_{myi},\\
I_{zz}\ddot{\psi} =&\dot{\theta}\dot{\phi}(I_{xx}-I_{yy})+(-1)^{i}\sum_{i=1}^{4}Q_i\\
m\ddot{z} =&\mathrm{s}\theta\sum_{i=1}^{4}H_{xi}-\mathrm{s}\phi\,\mathrm{c}\theta\sum_{i=1}^{4}H_{yi}+\mathrm{c}\phi\,\mathrm{c}\theta\sum_{i=1}^{4}T_i-mg+\rho gV_{vol},\\
m\ddot{x} =&-\mathrm{c}\theta\,\mathrm{c}\psi\sum_{i=1}^{4}H_{xi}-(\mathrm{s}\phi\,\mathrm{s}\theta\,\mathrm{c}\psi-\mathrm{c}\phi\,\mathrm{s}\psi)\sum_{i=1}^{4}H_{yi},\\
m\ddot{y} =&-\mathrm{c}\theta\,\mathrm{s}\psi\sum_{i=1}^{4}H_{xi}-(\mathrm{s}\phi\,\mathrm{s}\theta\,\mathrm{s}\psi+\mathrm{c}\phi\,\mathrm{c}\psi)\sum_{i=1}^{4}H_{yi}.
\end{aligned} \tag{14}$$

Here, T_i and H_i are the thrusts and hub forces of each motor; Q_i and R_i are the drag and rolling moments; ω_i are the rotational speeds of the four motors.

$$\begin{aligned}
T_i &= C_T\rho A\omega_i^2R_{rad}^2, \quad & H_i &= C_H\rho A\omega_i^2R_{rad}^2,\\
Q_i &= C_Q\rho A\omega_i^2R_{rad}^3, \quad & R_i &= C_R\rho A\omega_i^2R_{rad}^3,\ \ i=1,\ldots,4.
\end{aligned}$$

In eq. (14), $\dot{\phi}\dot{\psi}(I_{zz}-I_{xx})$, $\dot{\theta}\dot{\psi}(I_{yy}-I_{zz})$, $\dot{\theta}\dot{\phi}(I_{xx}-I_{yy})$ are the body gyro effect moments; $J_r\dot{\theta}\Omega_r$, $J_r\dot{\phi}\Omega_r$ ($\Omega_r=\omega_1-\omega_2+\omega_3-\omega_4$) are the propeller gyro effect moments; $(-1)^{i+1}\sum_{i=1}^{4}R_{mxi}$, $(-1)^{i+1}\sum_{i=1}^{4}R_{myi}$ are the rolling moments due to the sideward flight; $(-1)^{i}\sum_{i=1}^{4}Q_i$ is the unbalanced counter torque; ρgV_{vol} is Archimedes' force;

[1] $I_{xx}, I_{yy} = 6.228\times10^{-3}\mathrm{kg}\cdot\mathrm{m}^2$, $I_{zz} = 1.121\times10^{-2}\mathrm{kg}\cdot\mathrm{m}^2$, $J_r = 6.01\times10^{-5}\mathrm{kg}\cdot\mathrm{m}^2$, $l = 0.232\mathrm{m}$, $h = 0.058\mathrm{m}$, $m = 0.53\mathrm{kg}$, $C_x, C_y, C_z = 1.32$, $A_c = 0.005\mathrm{m}^2$, $\rho = 1.293\mathrm{kg/m}^2$, $b = 3.13\times10^{-5}\mathrm{N}\cdot\mathrm{s}^2$, $d = 7.5\times10^{-7}\mathrm{N}\cdot\mathrm{s}^2$, $A = 0.0707\mathrm{m}^2$, $V_{vol} = 3.04\times10^{-4}$.

The system is controlled by the rotational speeds of the four motors ω_i. In the control system, we define

$$\begin{aligned}
u_1 &= \sum_{i=1}^{4}T_i, \qquad & u_2 &= l(T_2-T_4),\\
u_3 &= l(-T_1+T_3), \qquad & u_4 &= (-1)^{i+1}\sum_{i=1}^{4}Q_i.
\end{aligned} \tag{15}$$

Then, the rotational speeds ω_i can be computed using u_i through:

$$\begin{aligned}
u_1 &= b\sum_{i=1}^{4}\omega_i^2, \qquad & u_2 &= bl(-\omega_2^2+\omega_4^2),\\
u_3 &= bl(\omega_1^2-\omega_3^2), \qquad & u_4 &= (-1)^{i+1}d\sum_{i=1}^{4}\omega_i^2.
\end{aligned} \tag{16}$$

Further details about the model can be found in [13].

C. Model free control

Firstly, we control the altitude z. We rewrite the vertical dynamics in (14) as:

$$m\ddot{z} = (c\theta c\phi)u_1 + F_z. \tag{17}$$

where F_z includes the neglected vertical dynamics in eq. (14). In discrete time, the unknown part F_z can be expressed as following, where $\hat{\ddot{z}}(k)$ is an estimate of $\ddot{z}(k)$:

$$\hat{F}_z = m\hat{\ddot{z}}(t_k) - (c\theta c\phi)u_1(t_{k-1}). \tag{18}$$

Thus, the chosen control law is:

$$\begin{aligned}
u_1(t_k) =& u_1(t_{k-1})+\frac{m}{c\theta c\phi}\Big(\hat{e}_{2d}^z(t_k)+k_1^ze_d^z(t_k)+k_0^ze^z(t_k)\Big),\\
\hat{e}_{2d}^z(t_k) =& \ddot{z}_r(t_k)-\hat{\ddot{z}}(t_k), \quad e_d^z(t_k)=\dot{z}_r(t_k)-\hat{\dot{z}}(t_k),\\
e^z(t_k) =& z_r(t_k)-z(t_k),\\
\hat{\ddot{z}}(t_k) =& \frac{T_f}{T_f+h}\hat{\ddot{z}}(t_{k-1})+\frac{1}{T_f+h}\Big(\dot{z}(t_k)-\dot{z}(t_{k-1})\Big),\\
\hat{\dot{z}}(t_k) =& \frac{T_f}{T_f+h}\hat{\dot{z}}(t_{k-1})+\frac{1}{T_f+h}\Big(z(t_k)-z(t_{k-1})\Big),
\end{aligned} \tag{19}$$

where $\ddot{z}_r$, $\dot{z}_r$, z_r are the reference acceleration, velocity and position of z. The variable h is the sampling period, $h = t_k - t_{k-1}$.

Then we control the position x and y. As the input u_1 is already used in the control of the altitude z, we now use u_2 and u_3 to control the positions x and y. Therefore, we need to differentiate twice the equations related to x and y in eq. (14) in order to get the control inputs u_2 and u_3. Then, we obtain:

$$\begin{aligned}
x^{(4)} =& \frac{u_1}{mI_{xx}}(s\psi c\phi - c\psi s\theta s\phi)u_2+\frac{u_1}{mI_{yy}}(c\psi c\theta c\phi)u_3+F_x,\\
y^{(4)} =& -\frac{u_1}{mI_{xx}}(c\psi c\phi+s\psi s\theta s\phi)u_2+\frac{u_1}{mI_{yy}}(s\psi c\theta c\phi)u_3+F_y,
\end{aligned} \tag{20}$$

where F_x, F_y are the remaining parts of the horizontal and lateral system. For further simplicity, here we define

$A = \frac{u_1}{mI_{xx}}(s\psi c\phi - c\psi s\theta s\phi)$, $B = \frac{u_1}{mI_{yy}}(c\psi c\theta c\phi)$, $C = -\frac{u_1}{mI_{xx}}(c\psi c\phi + s\psi s\theta s\phi)$ and $D = \frac{u_1}{mI_{yy}}(s\psi c\theta c\phi)$.

We implement the model free control scheme in a similar manner as previous:

$$\begin{pmatrix} u_2(t_k) \\ u_3(t_k) \end{pmatrix} = \begin{pmatrix} u_2(t_{k-1}) \\ u_3(t_{k-1}) \end{pmatrix} + \begin{pmatrix} A & B \\ C & D \end{pmatrix}^{-1} \begin{pmatrix} \hat{e}^x_{4d} + \sum k^x_i e^x_{id} \\ \hat{e}^y_{4d} + \sum k^y_i e^y_{id} \end{pmatrix}, \tag{21}$$

where $\hat{e}^x_{4d}, \hat{e}^y_{4d}$ are the errors between the references $x^{(4)}_r, y^{(4)}_r$ and the estimates of $x^{(4)}, y^{(4)}$, $i = 0, ..., 3$.

For the yaw control, we consider the equation of ψ as:

$$I_{zz}\ddot{\psi} = u_4 + F_\psi. \tag{22}$$

Then the needed control law is:

$$u_4(t_k) = u_4(t_{k-1}) + I_{zz}\Big(\hat{e}^\psi_{2d}(t_k) + k^\psi_1 e^\psi_d(t_k) + k^\psi_0 e^\psi(t_k)\Big), \tag{23}$$

where $\hat{e}^\psi_{2d}$ is the error between the reference $\ddot{\psi}_r$ and the estimate of $\ddot{\psi}$.

D. Backstepping control

For the purpose of comparison, a backstepping control proposed by S. Bouabdallah et al. [2] is also used on the quadrotor system. In order to simplify the control laws, some parts in the model in eq. (14) are neglected, such as the rolling moments and the hub forces. The system is written into the state space form using the state vector $(x_1, \ldots, x_{12})$ with $x_1 = \phi$, $x_2 = \dot{\phi}$, $x_3 = \theta$, $x_4 = \dot{\theta}$, $x_5 = \psi$, $x_6 = \dot{\psi}$, $x_7 = z$, $x_8 = \dot{z}$, $x_9 = x$, $x_{10} = \dot{x}$, $x_{11} = y$, $x_{12} = \dot{y}$.

The system is separated into the angular and position subsystems. The angular subsystem is thus firstly controlled, and then the position subsystem is controlled by using the angles from the angular subsystem.

In the angle subsystem, the control laws are defined as:

$$\begin{aligned} u_2 &= \frac{1}{b_1}\Big(z_1 - a_1x_4x_6 - a_2x_4\omega - \alpha_1(z_2 + \alpha_1 z_1) - \alpha_2 z_2\Big), \\ u_3 &= \frac{1}{b_2}\Big(z_3 - a_3x_2x_6 - a_4x_2\omega - \alpha_3(z_4 + \alpha_3 z_3) - \alpha_4 z_4\Big), \\ u_4 &= \frac{1}{b_3}\Big(z_5 - a_5x_2x_4 - \alpha_5(z_6 + \alpha_5 z_5) - \alpha_6 z_6\Big), \end{aligned} \tag{24}$$

with $z_1 = x_{1d} - x_1$, $z_2 = x_2 - \dot{x}_{1d} - \alpha_1 z_1$, $z_3 = x_{3d} - x_3$, $z_4 = x_4 - \dot{x}_{3d} - \alpha_3 z_3$, $z_5 = x_{5d} - x_5$, $z_6 = x_6 - \dot{x}_{5d} - \alpha_5 z_5$ and $a_1 = (I_{yy} - I_{zz})/I_{xx}$, $a_2 = J_r/I_{xx}$, $a_3 = (I_{zz} - I_{xx})/I_{yy}$, $a_4 = J_r/I_{yy}$, $a_5 = (I_{xx} - I_{yy})/I_{zz}$, $b_1 = 1/I_{xx}$, $b_2 = 1/I_{yy}$, $b_3 = 1/I_{zz}$. All the $\alpha_i (i = 1, \ldots, 12.)$ are the control gains.

In the position subsystem, the control laws are defined as:

$$\begin{aligned} u_1 &= \frac{m}{cx_1cx_3}\Big(z_7 + g - \alpha_7(z_8 + \alpha_7 z_7) - \alpha_8 z_8\Big), \\ u_x &= \frac{m}{u_1}\Big(z_9 - \alpha_9(z_{10} + \alpha_9 z_9) - \alpha_{10} z_{10}\Big), \\ u_y &= \frac{m}{u_1}\Big(z_{11} - \alpha_{11}(z_{12} + \alpha_{11} z_{11}) - \alpha_{12} z_{12}\Big), \end{aligned} \tag{25}$$

with $z_7 = x_{7d} - x_7$, $z_8 = x_8 - \dot{x}_{7d} - \alpha_7 z_7$, $z_9 = x_{9d} - x_9$, $z_{10} = x_{10} - \dot{x}_{9d} - \alpha_9 z_9$, $z_{11} = x_{11d} - x_{11}$, $z_{12} = x_{12} - \dot{x}_{11d} - \alpha_{11} z_{11}$ and $u_x = s\psi s\phi + c\psi s\theta c\phi$, $u_y = -c\psi s\phi + s\psi s\theta c\phi$.

E. Sliding mode control

For comparison, a sliding mode control proposed by S. Bouabdallah et al. [2] is also proposed. The state variables are defined in the backstepping control. The sliding surfaces are chosen as:

$$\begin{aligned} S_\phi &= z_2 = x_2 - \dot{x}_{1d} - \alpha_1 z_1, & z_1 &= x_{1d} - x_1, \\ S_\theta &= z_4 = x_4 - \dot{x}_{3d} - \alpha_3 z_3, & z_3 &= x_{3d} - x_3, \\ S_\psi &= z_6 = x_6 - \dot{x}_{5d} - \alpha_5 z_5, & z_5 &= x_{5d} - x_5, \\ S_x &= z_8 = x_8 - \dot{x}_{7d} - \alpha_7 z_7, & z_7 &= x_{7d} - x_7, \\ S_y &= z_{10} = x_{10} - \dot{x}_{9d} - \alpha_9 z_9, & z_9 &= x_{9d} - x_9, \\ S_z &= z_{12} = x_{11} - \dot{x}_{11d} - \alpha_{11} z_{11}, & z_{11} &= x_{11d} - x_{11}, \end{aligned} \tag{26}$$

where $\dot{x}_{id} (i = 1, 3, 4, 5, 7, 9, 11.)$ are the references. The control laws are:

$$\begin{aligned} u_2 &= \frac{1}{b_1}\Big(-k_1 sign(S_\phi) - k_2 S_\phi - a_1x_4x_6 - a_2x_4\omega + \ddot{\phi}_d - \alpha_1^2 z_1\Big), \\ u_3 &= \frac{1}{b_2}\Big(-k_3 sign(S_\theta) - k_4 S_\theta - a_3x_2x_6 - a_4x_2\omega + \ddot{\theta}_d - \alpha_2^2 z_3\Big), \\ u_4 &= \frac{1}{b_3}\Big(-k_5 sign(S_\psi) - k_6 S_\psi - a_5x_2x_4 + \ddot{\psi}_d - \alpha_3^2 z_5\Big), \\ u_1 &= \frac{m}{cx_1cx_3}\Big(-k_7 sign(S_z) - k_8 S_z + g + \ddot{z}_d - \alpha_7^2 z_7\Big), \\ u_x &= \frac{m}{u_1}\Big(-k_9 sign(S_z) - k_{10} S_z + \ddot{x}_d - \alpha_9^2 z_9\Big), \\ u_y &= \frac{m}{u_1}\Big(-k_{11} sign(S_z) - k_{12} S_z + \ddot{y}_d - \alpha_{11}^2 z_{11}\Big). \end{aligned} \tag{27}$$

The definition of all the parameters can be found in the previous backstepping control section III-D.

IV. Comparison of the control laws

A. Basic scenario: time and event triggered schemes

In the time triggered scheme, the sampling period is 10ms, and it yields 15000 actuation steps. The simulation results of the three control methods are given in Figure 2. Three methods have followed the reference trajectory nicely. The maximum absolute tracking errors are 0.042m, 0.09m and 0.08m for the model free, backstepping and sliding mode control respectively, which are 2.1%, 4.5% and 4% of the desired length 2m.

In the event triggered scheme, the chosen event triggering law is the error difference threshold as in eq. (9). Here, we set the error difference threshold of z 0.02m, yaw angle 0.1rad, x and y 0.001m. Every 10ms, the control system verifies the tracking error differences, and decides the corresponding actions. The simulation results are shown in Figure 2. The event triggered model free control, backstepping control and sliding mode control yield 9008, 9987 and 8493 actuation steps, which are 60%, 66.6% and 56.6% of 15000 actuation steps in the time driven scheme. The maximum absolute tracking errors are 0.06m, 0.1m and 0.1m in the three control methods, which increased 0.43%, 0.11% and 0.25% with respect to their results in the time triggered scheme.

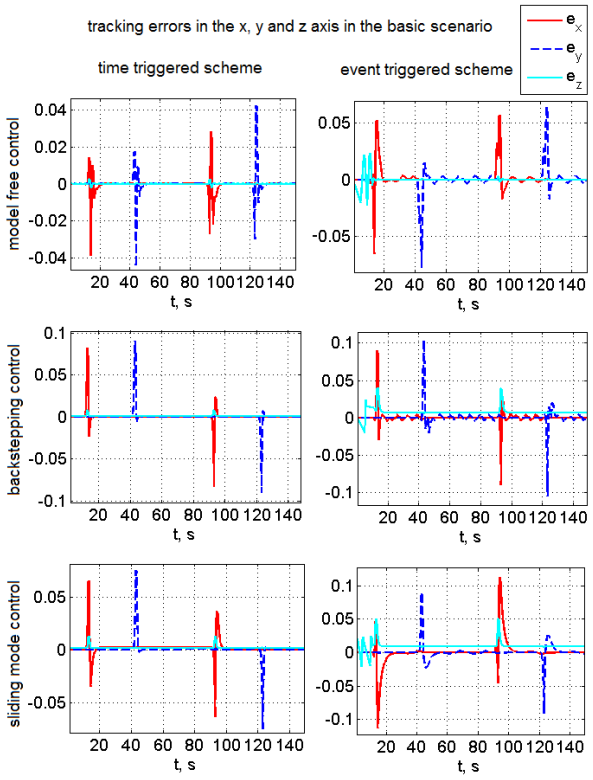

Fig. 2. The tracking errors along the x, y and z axis in the basic scenario. The first row: the model free control. The second row: the backstepping control. The third row: the sliding mode control. The first column: the time triggered scheme. The second column: the event triggered scheme.

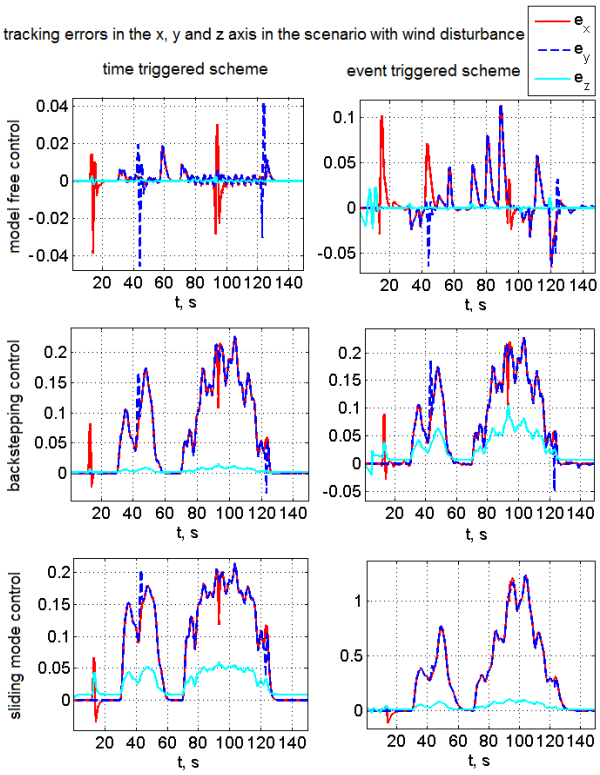

Fig. 3. The tracking errors along the x, y and z axis in the scenario with wind disturbance. The first row: the model free control. The second row: the backstepping control. The third row: the sliding mode control. The first column: the time triggered scheme. The second column: the event triggered scheme.

B. Scenario with wind disturbance: time and event triggered schemes

All the control methods are simulated in the scenario with wind disturbance. The simulation results are in Figure 3. The chosen event triggering law is the same as in the basic scenario.

In the time triggered scheme, the maximum absolute tracking errors are 0.042m, 0.23m and 0.21m in three control methods, which increased 0%, 155.6% and 162.5% with respect to the time triggered controls in the basic scenario. The wind does not have great influence in the model free control, however it has highly affected the backstepping and sliding mode controls.

In the event triggered scheme, the model free, backstepping and sliding mode controls yield 12110, 12116 and 12445 actuation steps, which are 80.7%, 80.8% and 83.0% of 15000 actuation steps. The maximum absolute tracking errors are 0.11m, 0.22m and 1.25m respectively in three control methods, which increased 83.3%, 120% and 1150% with respect to the event triggered controls in the basic scenario.

C. Discussion

In order to get a comprehensive evaluation, all the methods are implemented in other realistic scenarios with parameter uncertainties, with sensor noises and with actuator faults. Further details can be found in [13]. The maximum absolute tracking errors, the sum of the error variances and the actuation steps of all the control methods in all scenarios can be found in Table I and Figure 4.

In different realistic scenarios, the model free control has the smallest tracking errors than other control methods, and the event triggered model free control has the smallest errors than other event triggered methods. In the model free control, the part F is evaluated at each actuation step using the system measurement $\hat{y}$ and the last time input $\tilde{u}$. The model free control avoids the time-consuming computation of the full control model and has an algorithm complexity $O(5n^2+3n)$, while the backstepping and sliding mode controls have to compute the full model and have an algorithm complexity $O(6n^2+4n)$. The disturbances and uncertainties are also considered into F in the real time control, and that is why the model free control compensate them well.

The event triggered scheme matches the model free control. While the maximum tracking errors are bounded in desirable limits, the actuation steps are reduced more than one third. The event triggered model free control works well in the realistic scenarios with disturbances. The sliding mode control does not match with the event triggered scheme. The tracking errors are too high to be accepted in the scenarios with disturbances.

TABLE I

THE MAXIMUM ABSOLUTE TRACKING ERRORS, THE SUM OF THE ERROR VARIANCES AND THE ACTUATION STEPS OF ALL THE CONTROL METHODS IN ALL SCENARIOS. MF: MODEL FREE CONTROL. BS: BACKSTEPPING CONTROL. SM: SLIDING MODE CONTROL.

max absolute errors	time triggered			event triggered		
	MF	BS	SM	MF	BS	SM
basic scenario	0,042	0,09	0,08	0,06	0,1	0,1
wind	0,042	0,23	0,21	0,11	0,22	1,25
parameter uncertainties	0,075	0,11	0,11	0,19	0,22	0,41
sensor noise	0,08	0,09	0,08	0,08	0,09	0,08
actuator faults	0,04	0,06	0,07	0,13	0,2	0,35
error variance						
basic scenario	0,0049	0,0028	0,0058	0,2	0,2	0,077
wind	0,0052	2,4723	3,5238	0,0635	2,6679	65.4849
parameter uncertainties	0,0212	0,0468	0,2805	0,1281	1,8675	3,5517
sensor noise	0,2309	0,0029	0,0088	0,2309	0,0029	0,0088
actuator faults	0,0327	0,0167	0,0188	0,0918	0,0661	0,554
actuation steps						
basic scenario	15000			9008	9987	8493
wind	15000			12110	12116	12445
parameter uncertainties	15000			10803	14976	14983
sensor noise	15000			15000	15000	15000
actuator faults	15000			9298	10020	8297

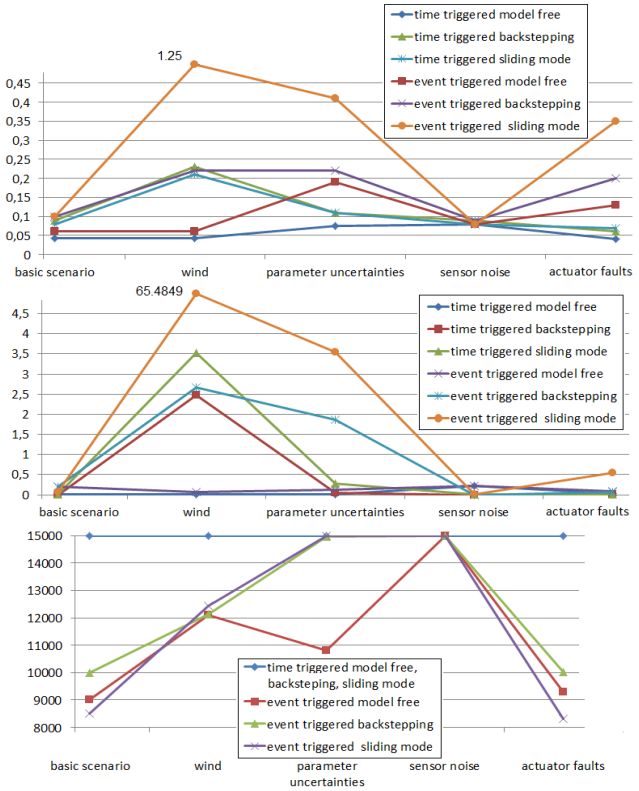

Fig. 4. The First figure: the maximum absolute tracking error. The second figure: the sum of the error variances$\times 10^7$. The third figure: the actuation steps.

V. CONCLUSION

In this paper, event driven model free controllers have been proposed and applied on quadrotor system in different realistic scenarios. The proposed method avoids the time-consuming computation of the full control model by evaluating the part F at each actuation step using the system measurement $\hat{y}$ and the last time input $\tilde{u}$. The part F can also take the disturbances and uncertainties into account in the real time control, therefore the model free control has a better performance in the realistic scenarios with disturbances.

Under the event driven scheme, the model free control has smaller tracking errors and lower actuation steps than backstepping and sliding mode control. In the realistic scenarios with disturbances and uncertainties, the event driven model free control has achieved almost the same results as in the scenarios without disturbance, which proves its robustness to perturbations. In the same scenarios, the backstepping and sliding mode controls have higher tracking errors.

The proposed method gives promising results in terms of control algorithm complexity reduction, computational resources reduction and robustness to perturbations, which is appropriate for implementation in embedded systems.

REFERENCES

[1] P. Castillo, A. Dzul and R. Lozano. *Real-time stabilization and tracking of a four-rotor mini rotorcraft.* IEEE Transactions on Control Systems Technology, vol. 12, no 4, p. 510-516, 2004.

[2] S. Bouabdallah, *Design and control of quadrotors with application to autonomous flying.* PhD thesis, Ecole Polytechnique Federale De Lausanne, 2007.

[3] V. Mistler, A. Benallegue and N.K. M'Sirdi. *Exact linearization and noninteracting control of a 4 rotors helicopter via dynamic feedback.* 10th IEEE International Workshop on Robot and Human Interactive Communication, p. 586-593, 2001.

[4] J. Wang, H. Mounier, A.Cela and S.I. Niculescu, *Event driven intelligent PID controllers with applications to motion control.* Proc. of 18th IFAC World Congress, Milan, Italy, 2011.

[5] M. Fliess, C. Join and H. Sira-Ramirez, *Complex continuous nonlinear systems: their black box identification and their control.* Proc. of 14th IFAC Symp. System Identif. (SYSID-2006), Newcastle, Australia, 2006.

[6] B. d'Andréa-Novel, M. Fliess, C. Join, H. Mounier and B. Steux, *A mathematical explanation via "intelligent" PID controllers of the strange ubiquity of PIDs.* Proc. of 18th Mediterranean Conference on Control and Automation, Marrakech, Morroco, 2010.

[7] L. Villagra and C. Balaguer, *A model-free approach for accurate joint motion control in humanoid locomotion.* International Journal of Humanoid Robotics, Vol. 8, No. 1 (2011).

[8] S. Andary and A. Chemori, *A dual model-free control of non-minimum phase systems for generation of stable limit cycles.* 50th IEEE Conference on Decision and Control and European Control Conference (CDC-ECC), Orlando, FL, USA, December 12-15, 2011.

[9] K.E. Årzén, *A simple event-based PID controller.* Proc. of 14th IFAC World Congress, Beijing, PR China, 1999.

[10] K.E. Årzén and B. Bernhardsson, *Comparison of Riemann and Lebesque sampling for first order stochastic systems.* Proc. of 41st IEEE Conference on Decision and Control, 2002.

[11] S. Durand and N. Marchand, *Further results on event-based PID controller.* Proc. of the European Control Conference, Hongrie, 2009.

[12] E.D. Sontag, *Input to state stability: basic concepts and results.* Nonlinear and Optimal Control Theory, pp. 163-220, Springer-Verlag, Berlin, 2007.

[13] J. Wang, *Analysis and control of quadrotor.* PhD thesis, Laboratory of signals and systems (L2S), CNRS, Supélec, University of Paris 11, 2013.